GAS CHROMATOGRAPHIC METHODS DEVELOPED ON THE BCR TWO-STAGE SUPER-PRESSURE GASIFICATION PROGRAM

Ta-Chuang Lo Chang
Richard A. Glenn

Bituminous Coal Research, Inc.
350 Hochberg Road
Monroeville, Pennsylvania

INTRODUCTION

Under a project sponsored by the Office of Coal Research, Bituminous Coal Research, Inc., (BCR) has been developing a two-stage super-pressure process for coal gasification.(1) The development work began with a small high-pressure rocking autoclave, then was transferred to a 5 lb/hr externally-heated continuous flow reactor (1), and now is being scaled up to a 100 lb/hr internally-fired process and equipment development unit.

Fixed gases plus some light hydrocarbons comprise the principal products of interest from this coal gasification process. Their composition varies with the experimental conditions and upon the kind and amount of inert gas used. For rigorous interpretation of results of the gasification experiments, accurate determination of the product gas composition is a prerequisite. The analytical methods employed have to be not only accurate but also rapid and simple to meet the desired time schedule.

At the outset, a search of the technical literature for suitable methods revealed several procedures using gas-solid or/and gas-liquid chromatography which might be suitable.(2,3,4) Unfortunately, they were found to be either too complicated and time consuming, or did not determine all the desired components. This paper describes the three gas chromatographic methods and two sampling devices which have been developed for the analysis of the various product gases obtained on the coal gasification program.

EXPERIMENTAL

A. Methods for Batch Autoclave Tests

In the batch autoclave experiments, small quantities of a coal slurry were injected into a preheated autoclave that was partially pressurized with nitrogen. At the end of the reaction period, the product gas was exhausted at atmospheric pressure and room temperature to an all-glass gas holder using additional nitrogen as a purge gas.(1)

The nature of this product gas was thoroughly studied by both gas-solid and gas-liquid chromatography. It was found to be composed of H_2 (major), CO_2 (major), CH_4 (major), CO (minor), C_2H_6 (minor to trace), C_2H_4 (trace to 0), C_3H_8 (trace to 0), and H_2S (trace). Because nitrogen was used to purge the autoclave before and after gasification, it was also present in the product in varying quantities.

Based on the composition of the product gas, a G.C. method, using an 11.5-ft silica gel column, was developed to determine all components except H_2S. The trace quantity of H_2S was determined separately by conventional iodometric titration.

1. Sample Collection: For the batch autoclave tests, gas samples were taken from the gas holder at normal pressure and collected in 500 ml glass tubes using 15 percent H_2SO_4 in saturated Na_2SO_4 solution as the confining liquid.

2. Analytical Method: After being conditioned by removal of H_2S by absorption in $CdCl_2$ and of H_2O by adsorption on Drierite, the gas sample (0.5 ml) is injected into an 11.5-ft silica gel column operated at 50 C, with 50 ml/min of helium carrier gas. Changes in composition of the column effluent as detected by a thermoconductivity cell are automatically recorded. From the resultant chromatogram, the amounts of the individual components are calculated.(5) A chromatogram of a synthetic mixture produced on such a column is shown in Figure 1.

The analysis of a single sample required about 35 minutes, including the conditioning of the sample. Six samples or more can be analyzed in duplicate during a normal working day.

3. Discussion of Results: The composition of a number of gaseous products collected at room temperature from the autoclave experiments, as determined by this G.C. method is listed in Table 1 together with similar data by Orsat method for comparison. The results obtained with the two methods for CH_4, C_2H_6, and H_2 are not in agreement. By the Orsat method, CO_2, O_2, total olefins, and CO were determined by absorption; H_2 and CH_4 by slow combustion and absorption; and, lastly, N_2 was determined by difference. The H_2 and CH_4 values by this Orsat method were accurate only when the sample contained no other saturated hydrocarbons. If C_2H_6 or any other saturates were present, they were combusted and estimated together with CH_4, making the observed values for CH_4 high and those for H_2 low. Thus, when a significant amount of C_2H_6 was present as in these samples, the CH_4 and H_2 values were not as accurate as those determined by the G.C. method.

Precision of the G.C. method using the 11.5-ft silica gel column in an F & M Model 720 gas chromatograph was determined by replicate analyses of a mixture containing 15 percent H_2, 1.0 percent CO, 20 percent CO_2, 35 percent CH_4, 2 percent C_2H_6, and 0.5 percent C_2H_4 (balance helium). From six analyses, the absolute standard deviations were estimated as 0.420 (H_2), 0.042 (CO), 0.212 (CO_2), 0.230 (CH_4), 0.234 (C_2H_6), and 0.030 (C_2H_4). These deviations are small; therefore, the precision of the G.C. method is high.

B. Methods for 5 lb/hr Continuous Flow Reactor (CFR) Tests

In the 5 lb/hr continuous reactor, coal is gasified under conditions simulating those that prevail in Stage 2 of the two-stage super-pressure gasifier. In these experiments, coal entrained in a simulated Stage 1 gas (CO, H_2, CO_2, H_2O) is partially gasified by passage through an externally-heated metal reactor at elevated pressures.(1)

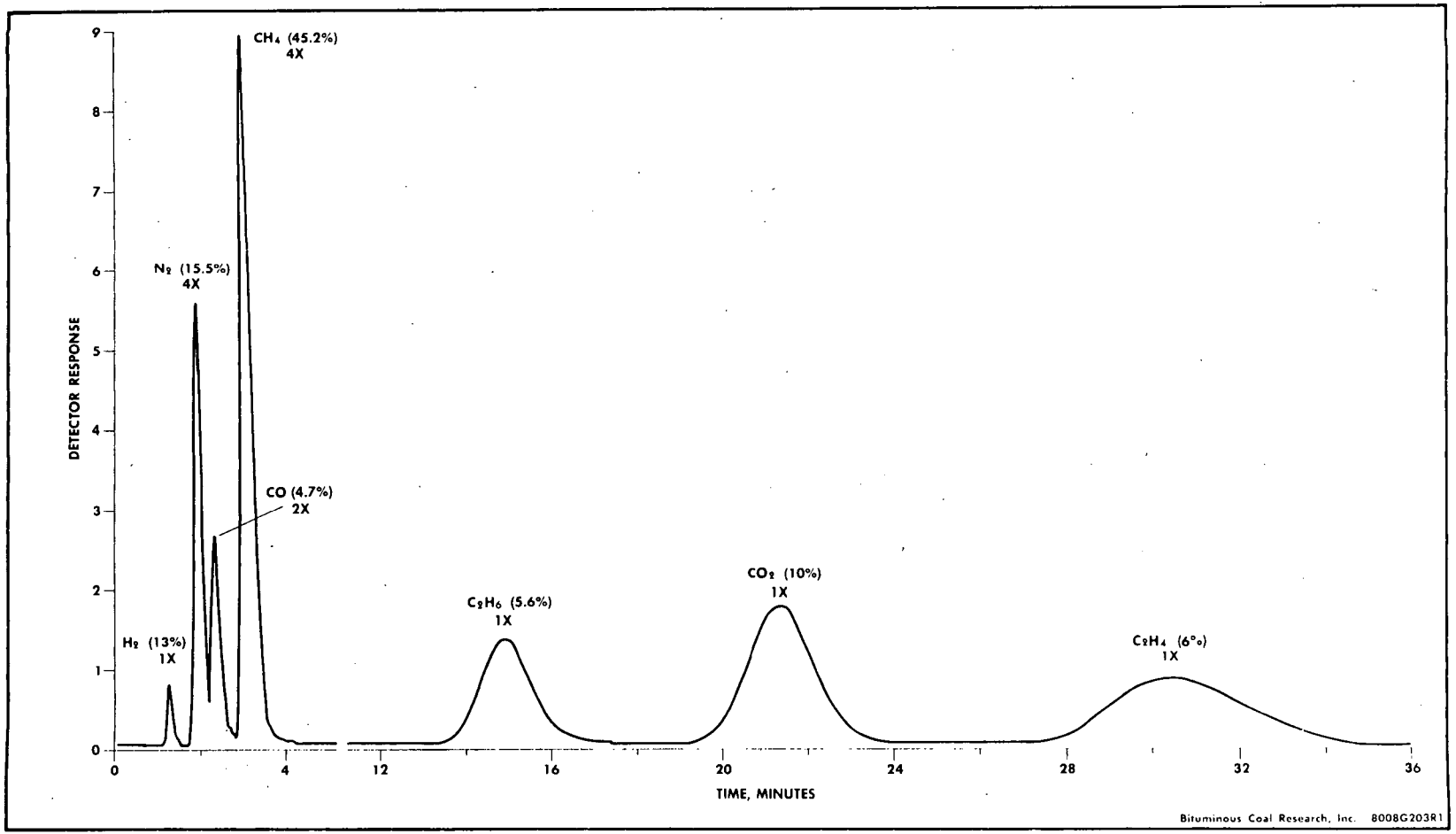

Figure 1. Chromatogram of a Mixture on the 11.5 ft Silica Gel Column

TABLE 1. COMPARISON OF G.C. ANALYSIS AND ORSAT ANALYSIS OF COAL GAS SAMPLES FROM AUTOCLAVE EXPERIMENTS

Sample No.	COMPONENT, VOLUME PERCENT																	
	H_2		O_2		CO		CO_2		CH_4		C_2H_6		C_2H_4		C_3H_8		N_2	
	GC	Orsat	GC	Orsat	GC	Orsat	GC	Orsat	GC	Orsat	GC	Orsat	GC	Orsat*	GC	Orsat	GC	Orsat
202	22.2	23.3	0.3	0.4	1.7	1.9	22.4	22.0	48.4	47.6	0.5	-	0.5	0.6	tr	-	4.0	4.2
212	31.2	33.0	0.4	0.5	1.5	1.8	24.2	25.2	38.1	33.4	tr	-	tr	0.3	0	-	4.6	5.8
222	32.0	36.0	0.2	0.2	2.8	3.5	17.1	18.0	40.5	35.7	0.1	-	0.5	0.6	0	-	6.8	6.0
342A	7.1	5.3	-	0	4.1	4.0	3.4	3.7	21.2	26.4	3.1	-	1.1	1.3	<0.05	-	60.0	59.3
342B	21.2	23.8	0	0.2	1.2	1.3	17.3	19.7	42.5	41.5	0.3	-	tr	0.3	0	-	17.5	13.2
382A	14.9	13.3	0	0.1	3.0	2.9	10.4	11.7	41.5	47.3	2.9	-	0.5	0.5	<0.05	-	26.8	24.2
382B	22.9	25.5	0	0	1.6	1.6	21.6	21.2	40.7	38.2	0.2	-	tr	0.4	0	-	13.0	13.1
382C	23.9	26.9	0	0.2	1.3	1.4	21.9	21.0	39.8	37.7	tr	-	0	0.2	0	-	13.1	12.6
392A	12.8	8.4	0	0.2	0.3	0.3	12.4	15.0	30.1	37.8	4.6	-	1.0	0.8	tr	-	38.8	37.5
392B	29.0	30.0	0	0.2	2.1	2.0	21.4	25.0	33.0	29.6	0.2	-	tr	0.4	0	-	14.3	12.8
412A	16.9	15.7	0	0.1	0.5	0.6	17.6	19.2	36.6	38.5	2.5	-	0.1	0.3	0	-	25.8	25.6
412B	19.3	11.2	0	0.1	0.6	0.7	15.9	18.8	32.2	39.0	3.5	-	tr	0.6	0	-	28.5	29.6
412C	23.9	25.5	0	0.2	1.2	1.2	22.8	24.5	36.9	33.3	0.4	-	0	0.3	0	-	14.8	15.0

tr = trace
* as olefin

To enable calculation of material balances, argon gas was added to the simulated Stage 1 gas as an internal reference and thus constituted a major component of the product gas. Other major components of the dry product gas were H_2, CO, CO_2, CH_4, and sometimes N_2 from the purge gas. Minor to trace components were C_2H_6, C_2H_4, and H_2S. The trace amounts of H_2S were determined by the conventional iodometric titration, as in the analysis of the autoclave products. As the 11.5-ft silica gel column does not resolve mixtures of A, N_2, and O_2, the presence of argon precluded the procedure for batch autoclave samples from being applied to samples from the 5 lb/hr flow reactor tests. New procedures, therefore, were developed.

1. Sampling System: At the sampling point of the flow reactor, the product gas was already quenched with water and reduced in pressure from about 1000 psi down to 10 to 40 inches of water.

The sampling method for the 5 lb/hr reactor was essentially the same as for the autoclave, except that several glass sampling bulbs were connected in parallel to a common manifold in such a way that several samples could be collected at two minute intervals during each test. This system was found very satisfactory at this pressure range.

2. Analytical Methods: Under normal operating conditions, there was no O_2 in the product gas from the 5 lb/hr CFR tests. However, at times air becomes admixed with the sample and an accurate method for determining O_2 as well as A was required. A molecular sieve column separates A and N_2 at room temperature, but not A and O_2. To solve this problem, a method using a differential technique was developed for the determination of these two components using only the 6-ft molecular sieve 5A column.(6) The overall G.C. method as finally developed for analysis of the product gas involved two columns: a 3-ft silica gel column and a 6-ft molecular sieve 5A column. On the silica gel column, CO_2, C_2H_6, and C_2H_4 were measured, and on the molecular sieve, using the differential technique, H_2, A, O_2, N_2, CH_4, and CO.

However later, significant loss of CO_2 to the confining liquid in the sampling system was observed whenever the CO_2 concentration in the sample was higher than 20 percent; this was found to occur even when the confining liquid was 15 percent H_2SO_4 saturated with Na_2SO_4. It was found that for samples containing 25 percent CO_2, the observed value was only 22-23 percent, and for those having 35 percent CO_2, the observed value was 31-32 percent. To avoid this error, CO_2 was determined separately by the Orsat apparatus before gas chromatography on dual columns in an F & M Model 700-231 gas chromatograph.(5)

a. Determination of CO_2: Prior to gas chromatography, a separate analysis of CO_2 is made by conventional Orsat procedures.

Immediately after sampling, the sampling tube contains gas at a pressure slightly higher than 1 atmosphere with less than 5 ml confining liquid saturated with CO_2 from the sample left inside. The first portions of the sample are released for CO_2 determination without admitting additional confining liquid into the tube. The observed CO_2 result so obtained represents the true concentration in the sample.

b. Preconditioning of sample for gas chromatography: Prior to gas chromatography, the sample is preconditioned by passage through a $CdCl_2$ absorbent to remove H_2S and then through a Drierite tube to remove H_2O.(5)

The sample is not processed to remove CO_2 prior to being measured for chromatography as a CO_2 absorption unit (Indicarb cartridge) may be connected to the system between the inlet valve and the column as desired.

c. Determination of C_2H_6 and C_2H_4: A portion (0.5 ml) of the preconditioned dry, H_2S-free gas sample is analyzed for C_2H_6 and C_2H_4 using the 3-ft silica gel column operated at 50 C with 50 ml/min helium carrier gas and with automatic recording of changes in composition of the column effluent. A typical chromatogram is shown in Figure 2A.

d. Determination of H_2, A, O_2, N_2, CH_4, and CO: Another portion (0.5 ml) of the preconditioned gas sample is analyzed for H_2, A (or O_2), N_2, CH_4, and CO using the 6-ft molecular sieve 5A column located in the same oven and operated under the same conditions as for the silica gel column in (c) above. A typical chromatogram is shown in Figure 2B.

e. Calculation of sample composition: The overall composition of the sample on a dry, H_2S-free basis is calculated as follows:

(1) Percent CO_2 as determined by Orsat
(2) Percent of other components by normalization of the values from gas chromatography to the CO_2-containing basis, using the formula:

$$f_n = \frac{100 - CO_2\% \text{ (from Orsat)}}{(H_2{}^{Rd}\% + N_2{}^{Rd}\% + CH_4{}^{Rd}\% + \text{-----})}$$

where

f_n = normalization factor

$H_2\% = f_n\ (H_2{}^{Rd}\%)$

$N_2\% = f_n\ (N_2{}^{Rd}\%)$

$CH_4\% = f_n\ (CH_4{}^{Rd}\%)$, and

$H_2{}^{Rd}\%$, $N_2{}^{Rd}\%$, $CH_4{}^{Rd}\%$---are observed values from the G.C. chromatogram

Time required for a complete analysis in duplicate is about one hour including calculation. During a normal working day seven samples can be analyzed by one operator.

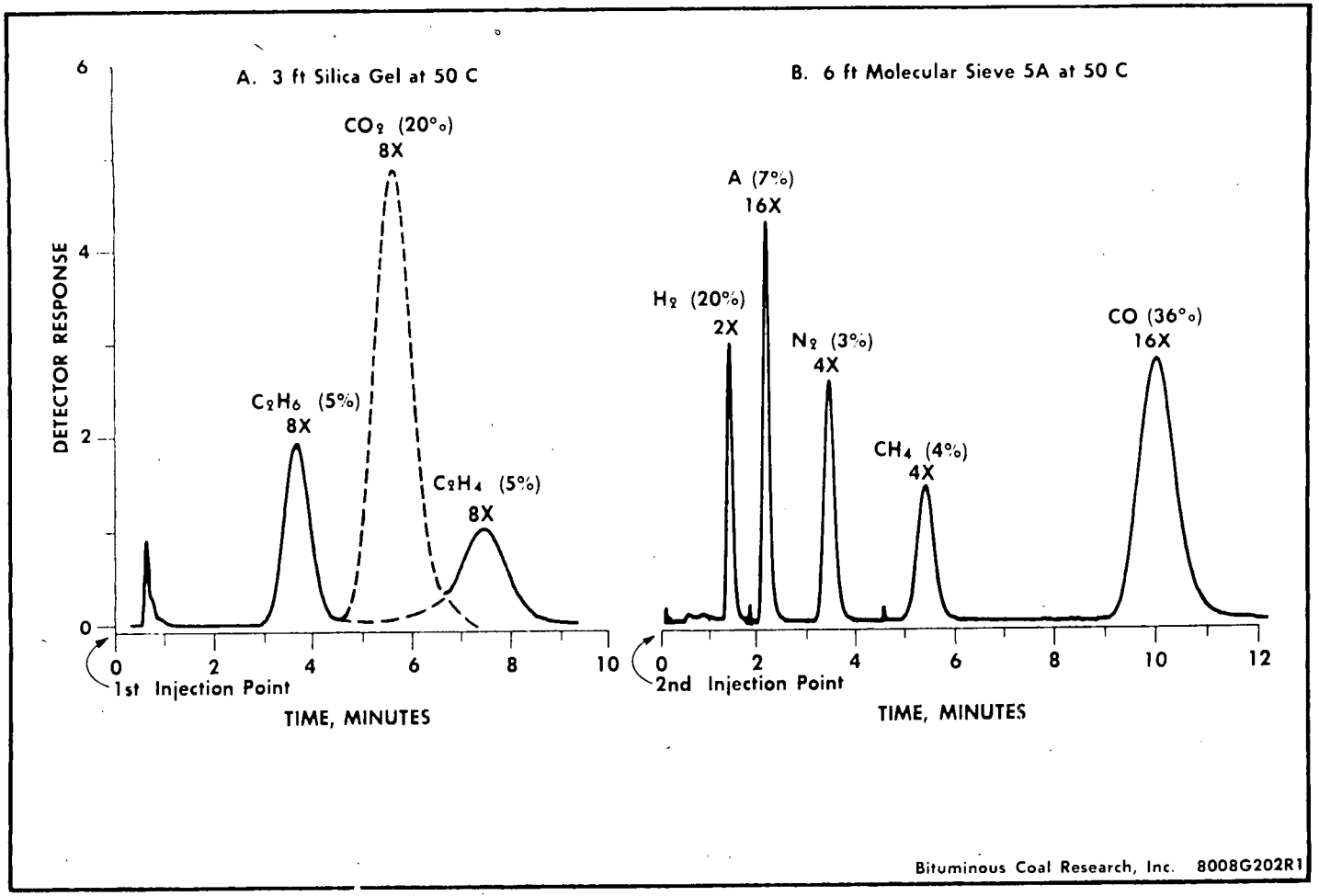

Figure 2. Chromatograms Produced on the 3 Ft Silica Gel and the 6 Ft Molecular Sieve Columns

3. Results and Discussion: Precision of this method, using the Orsat CO_2 analyzer and the F & M gas chromatograph Model 700-231, may be expressed as standard deviations of the components in a gas sample. The observed precision, as shown in Table 2, is considered high and quite satisfactory.

The product gases from more than 100 CFR experiments have been collected by the glass sampling system and analyzed by this combined method. Tables 3, 4, and 5 show the composition of several samples collected during experiments using three different coals.

In all three tables, sample "S" represents the simulated Stage 1 gas as purchased for use in the experiments. The three samples of Stage 1 gas were fairly consistent in composition showing only slight deviations. Sample "1" represents the composition of the product gas before introduction of coal feed. It is apparent that CO in the feed gas reacted with H_2O by the water gas shift reaction to form H_2 and CO_2, thus making the product gas higher in CO_2 and H_2 and lower in CO than the original feed gas. A small amount of CH_4 was also detected in the product gas, possibly due to the reaction of CO and H_2.

After coal feeding began, two or more samples were collected, each over a period of 2 minutes. These, designated as Sample 2, Sample 3, etc., contained CH_4 in amounts consistent with the operating conditions. Only trace amounts (less than 0.02%) of C_2H_6, and even less C_2H_4 were found in these samples.

The last sample shown in the tables is the total composite product gas as accumulated in a gas holder during the total period of each CFR test. This sample, naturally, contained less CH_4, as the gas holder also accumulated the N_2 used to purge the reactor system before and after the test and an extra amount of the Stage 1 feed gas used to establish equilibrium with steam at the start of the test.

C. Methods for 100 lb/hr Process and Equipment Development Unit

Construction of a 100 lb/hr internally-fired process and equipment development unit (PEDU) is nearing completion. Except for use of an ash-free fuel in Stage 1, this PEDU will simulate closely the conditions expected in both Stage 1 and Stage 2 of a full-scale two-stage super-pressure pilot plant. In the main zone (Stage 2) of the 100 lb/hr reactor, steam and fresh coal will react with Stage 1 gas to form a second stage product gas relatively rich in CH_4 and will leave a residue of partially reacted coal.

It is expected that the final product gas of the PEDU may deviate in composition from that produced in the 5 lb/hr CFR unit by possible presence of C_2 and C_3 hydrocarbons. In view of this possibility, a rapid G.C. column capable of separating CO_2 and minute quantities of C_2 to C_3 hydrocarbons has been developed.

A stainless steel sampling system, eliminating the use of a confining liquid, has also been developed for the taking of samples directly from the PEDU system.

TABLE 2. REPLICATE ANALYSES OF A GAS SAMPLE BY COMBINED ORSAT AND DIFFERENTIAL G.C. METHOD

Run No.	Component, Percent by Volume						
	CO_2*	C_2H_6	H_2	A	N_2	CH_4	CO
1	18.6	1.8	24.8	11.9	1.9	10.5	30.5
2	18.5	1.9	24.6	11.9	2.0	10.7	30.4
3	18.5	1.8	24.8	11.9	1.9	10.7	30.4
4	18.3	1.3	25.9	11.8	1.8	10.7	30.2
5	18.6	1.5	25.9	11.8	1.9	10.2	30.1
6	18.5	1.5	25.1	11.7	1.9	10.8	30.5
Mean	18.50	1.63	25.18	11.84	1.90	10.60	30.35
Std. Dev. (σ)	0.110	0.233	0.577	0.082	0.100	0.219	0.164

* CO_2 by Orsat Method

TABLE 3. COMPOSITION OF GAS PRODUCTS IN GASIFICATION OF PITTSBURGH SEAM COAL IN 5 LB/HR CFR, TEST NO. 79

Sample No.		Component, Percent Volume						
		CO_2	H_2	A	N_2	CH_4	CO	C_2H_6
S	Simulated Stage 1 gas	15.7	18.5	9.9	0	0	55.9	0
1	Product gas without coal	29.8	31.8	8.3	0	T	30.1	0
2	First sample with coal feeding	26.4	28.1	7.7	0	7.2	30.6	T
3	Second sample with coal feeding	25.5	26.7	7.6	0	8.0	32.2	0
4	Third sample with coal feeding	24.2	25.4	7.6	0	8.9	33.9	0
5	Total accumulated product	17.7	20.8	5.8	29.6	2.6	23.5	0

TABLE 4. COMPOSITION OF GAS PRODUCTS IN GASIFICATION OF LIGNITE IN 5 LB/HR CFR, TEST NO. 82

Sample No.	Sampling	Component, Percent Volume						
		CO_2	H_2	A	N_2	CH_4	CO	C_2H_6
S	Simulated first stage gas	15.5	18.5	9.9	0	0	56.1	0
1	Product gas without coal	29.7	31.6	8.4	0	0.1	30.2	0
2	First sample with coal feeding	29.0	28.0	6.2	0	9.6	27.2	T
3	Second sample with coal feeding	29.0	28.6	6.3	0	9.6	26.5	T
4	Third sample with coal feeding	28.7	28.8	5.6	0	11.3	25.6	T
5	Total accumulated product	23.8	25.6	6.5	14.3	3.5	26.3	-

TABLE 5. COMPOSITION OF GAS PRODUCTS IN GASIFICATION OF ELKOL COAL IN 5 LB/HR CFR, TEST NO. 93

Sample No.	Sampling	Component, Percent Volume						
		CO_2	H_2	A	N_2	CH_4	CO	C_2H_6
S	Simulated first stage gas	15.6	20.1	10.1	0	0	54.2	0
1	Product gas without coal	26.6	30.2	8.7	0	0.1	34.4	0
2	First sample with coal feeding	30.5	28.2	6.9	0	11.6	22.8	0.02
3	Second sample with coal feeding	30.1	28.3	6.9	0	11.5	23.2	T
4	Third sample with coal feeding	30.0	28.1	6.8	0	11.8	23.3	T
5	Fourth sample with coal feeding	30.5	27.9	6.9	0	11.7	23.0	T
6	Total accumulated product	22.6	24.6	6.5	16.5	4.2	25.6	T

1. Sampling System: To eliminate the use of a confining liquid in the sampling system, an evacuated stainless steel (s.s.) device, as shown in Figure 3, was developed. It consists of eight 1500 ml s.s. sampling bulbs (A.C. Tank Co.) each equipped with a Hoke packless valve and connected in parallel to a common 1/4-inch OD manifold. For sampling prefiltered gas, the inlet of the system is provided with a single-stage, corrosion-resistant regulator and a 0-30 psi gauge. For sampling unfiltered gas, an MSA filter cartridge is inserted between the regulator and the sampling point. At the outlet of the manifold, a control valve is installed, together with a trap and a flow indicator flask containing silicon fluid.

After the fully evacuated system is connected to the sampling point, the manifold is purged at a regulated pressure of 4 psi. The outlet of the manifold is closed and bulb No. 1 is immediately opened. The pressure of gas in the bulb is then gradually increased at a constant rate to about 20 psi during the period of operation to be sampled, usually one to two minutes. At the end of the sampling period, bulb No. 1 is closed and the outlet of the manifold is again opened; the manifold gas pressure is immediately reduced to 4 psi and purging is continued.

The procedure is repeated for collection of the next sample using bulb No. 2.

2. An Improved G.C. Method for the 100 lb/hr PEDU Tests: Recently, a new column packing known as Porapak Q was reported to be better than silica gel for resolving many types of organic compounds and gases (7, 8). So an investigation of Porapak Q for resolution of CO_2, H_2S, and light hydrocarbons was made. In experiments with an 8-ft Porapak Q column, it was found that mixtures of C_1-C_3, CO_2, and H_2S could be completely separated in a shorter time and eluted in much sharper peaks than on a 3-ft silica gel column.

Figure 4 shows a chromatogram produced by a synthetic mixture on the 8-ft Porapak Q column operated at 50 C with 50 ml/min of helium carrier gas. The elution sequence of the components is as follows: Composite (N_2, H_2, O_2, CO), CH_4, CO_2, C_2H_4, C_2H_6, H_2S, and C_3H_8. Good precision on the analysis of C_1-C_3 hydrocarbons and H_2S has been achieved on this column. Standard deviations of these components in a synthetic mixture are shown in Table 6. Since H_2S can be rapidly and accurately determined on this Porapak Q column, the iodometric titration of H_2S as used for the 5 lb/hr CFR tests can be eliminated.

Therefore, in the future an 8-ft Porapak Q will be used in combination with a 6-ft molecular sieve 5A for product gas analysis. Time required for a complete analysis of inorganic gases and C_1-C_3 hydrocarbons, in duplicate, is about 2 hours.

CONCLUSION

Each of the three phases encountered so far in the development of the BCR two-stage super-pressure gasification process has presented some specific analytical problems. By development of three G.C. methods and two sampling devices, these analytical problems have been satisfactorily solved.

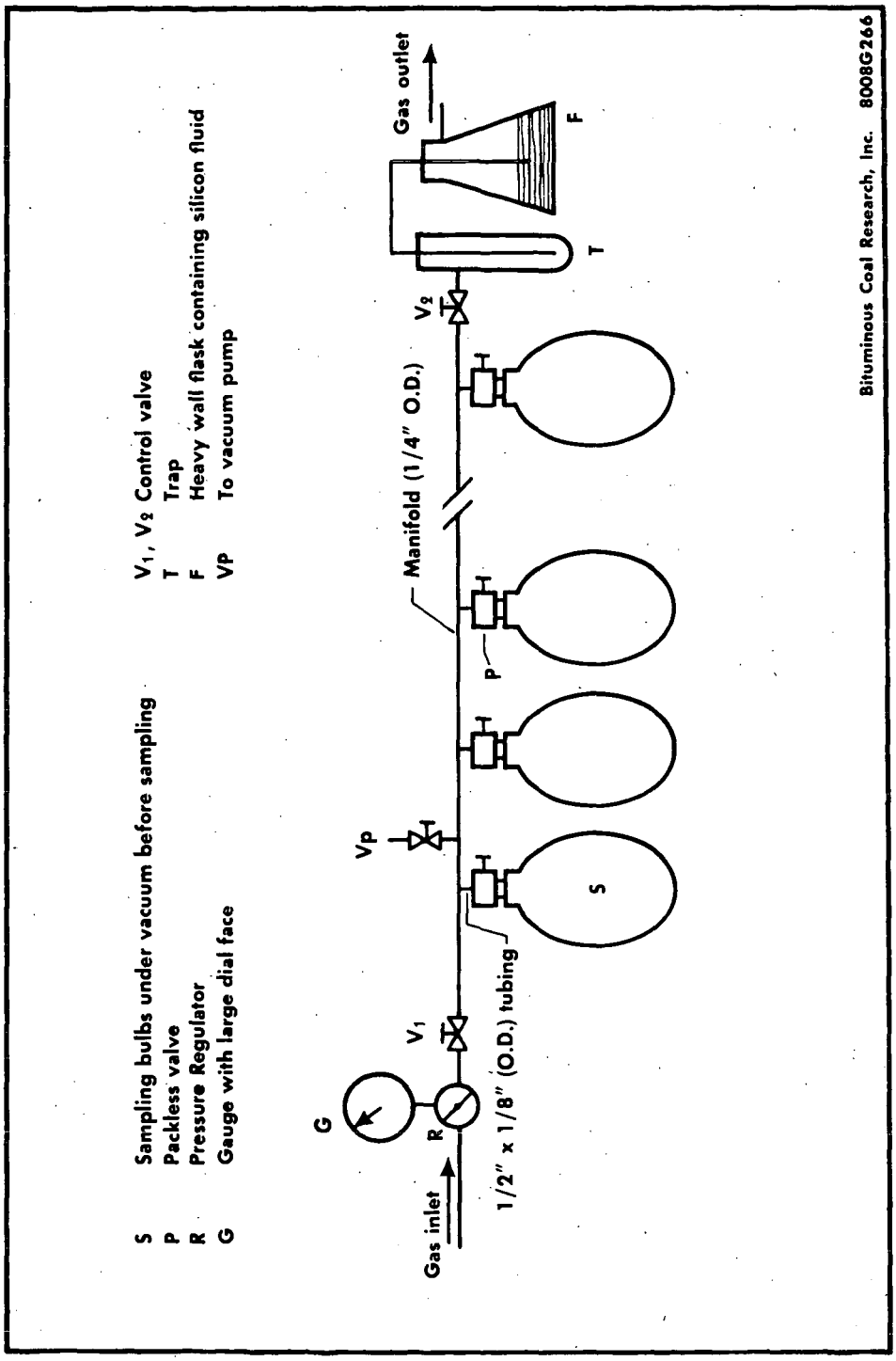

Figure 3. Stainless Steel Sampling System

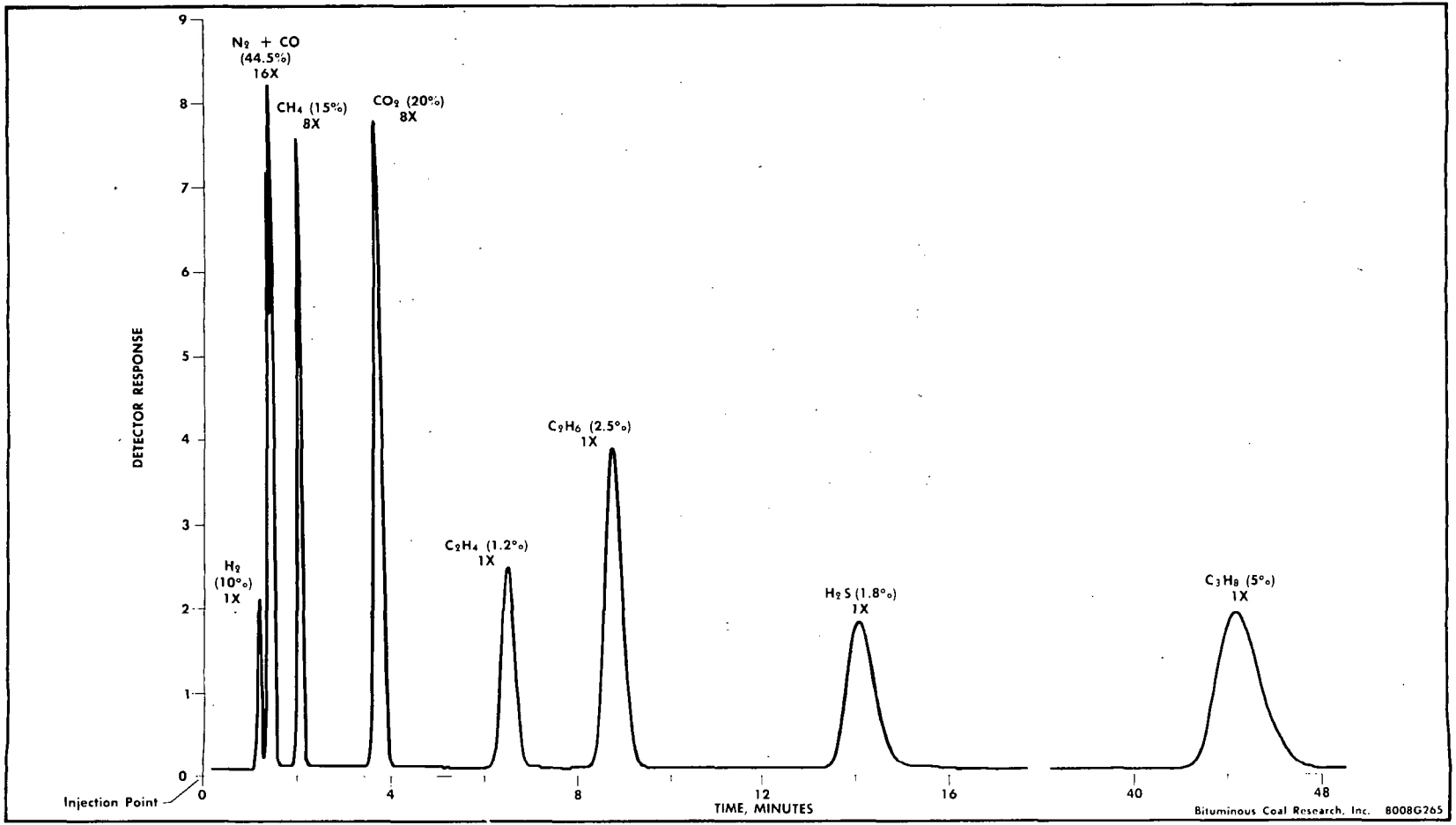

Figure 4. Chromatogram Produced on the 8 Ft Porapak Q Column

TABLE 6. REPLICATE ANALYSES OF A SYNTHETIC MIXTURE* ON THE 8-FT PORAPAK Q COLUMN

	Component, Percent by Volume					
Run No.	CH_4	CO_2	C_2H_4	C_2H_6	H_2S	C_3H_6
1	10.1	30.5	0.48	0.49	0.21	0.47
2	10.0	30.8	0.50	0.50	0.18	0.48
3	10.1	30.6	0.50	0.50	0.18	0.50
4	9.8	30.4	0.52	0.48	0.20	0.46
5	10.0	30.5	0.50	0.49	0.21	0.47
6	9.9	30.8	0.49	0.49	0.21	0.50
Mean	9.983	30.600	0.498	0.492	0.198	0.480
Absolute σ	0.117	0.168	0.013	0.022	0.015	0.167

* Balance of the mixture was nitrogen.

ACKNOWLEDGMENT

This paper is based on work conducted by Bituminous Coal Research, Inc., for the Office of Coal Research, U.S. Department of the Interior, under Contract No. 14-01-0001-324. The authors wish to thank the Office of Coal Research for permission to publish this paper.

LITERATURE REFERENCES

1. Glenn, R. A., Donath, E. E., and Grace, R. J., "Gasification of coal under conditions simulating stage 2 of the BCR two-stage super-pressure gasifier," Chapter from "Fuel Gasification," Washington: American Chemical Society, 1967. pp 81-103.

2. Cvejanovich, G. J., "Separation and analysis of mixtures of hydrocarbon and inorganic gases by gas chromatography," Anal. Chem. 34 (6), 654-7 (1962).

3. Swinnerton, J. W., Linnenbom, V. J., and Cheek, C. H., "Determination of dissolved gases in aqueous solutions by gas chromatography," Anal. Chem. 34 (4), 483-5 (1962).

4. Manka, D. P., "Complete gas chromatographic analysis of fixed gases with one detector using argon as gas carrier," Anal. Chem. 36 (3), 480-2 (1964).

5. Chang, T. L., "Gas chromatographic methods for mixtures of inorganic gases and C_1-C_2 hydrocarbons," to be published in J. Chromatog.

6. Chang, T. L., "Gas chromatographic analysis of mixtures containing oxygen and argon by elimination of oxygen," J. Gas Chromatog. 4 (10), 371-5 (1966).

7. Hollis, O. L., "Separation of gaseous mixtures using porous poly-aromatic polymer beads," Anal. Chem. 38 (2), 309-16 (1966).

8. Wilhite, W. F. and Hollis, O. L., "The use of porous-polymer beads for analysis of the Martian atmosphere," J. Gas Chromatog. 6 (2), 84-8 (1968).

HEAT CAPACITY OF COAL

Anthony L. Lee

Institute of Gas Technology
3424 South State Street
Chicago, Illinois 60616

INTRODUCTION

Although many authors have reported the heat capacity of coal and the experimental methods used (1-6,8,11,13,15-18), few of their investigations were conducted above 300°C (572°F). Because of the difficulties of determining the heat capacity of coal experimentally, especially during heating and at high temperatures, disagreements have arisen among research workers. Some authors have found that the heat capacity of coal increases with temperature (3,5), while others have found that it decreases. (1,2) This disagreement could be the result of the methods used to obtain the heat capacity. Since coal contains up to 50% volatile matter, the weight of coal changes considerably during heating as the volatile matter escapes. To further complicate the matter, if the coal were allowed to oxidize during heating, one can be sure that the results would not be the same. Even if one takes the escaped volatile matter into consideration, the precision of the measurement will suffer because the treatment of experimental data depends on the material balance, the analytical methods, and the assumptions.

The decrease of C_p as the temperature increases above 300°C could be explained by the endothermic reaction of so-called "pyrolysis," "decarbonization," or "coking." (7,14,18) Coal starts devolatilization quickly at temperatures above 700°F. So, at 700°F or above, the experimentally measured value is —

$$a = C_p + \Delta H_e \qquad (1)$$

where:

a = the measured value and is called the pyro-heat capacity in this paper

C_p = the heat capacity of coal

ΔH_e = the heat of the endothermic reaction

To determine the true heat capacity of coal, the ΔH_e must be known accurately. Since coal is complicated in nature, it is experimentally difficult to determine ΔH_e accurately. As an example, Agroskin and Goncharov (1,2) proposed to determine C_p directly as follows:

1. Heat the coal to the decarbonizing temperature until coking stops
2. Measure the C_p of the residue

Obviously, as this residue is no longer the coal one started with, the measured C_p is not the C_p of the coal but the C_p of the coke.

This author proposes to determine the ΔH_e as follows:

1. Drop the cold coal into the hot calorimeter to determine the C_p and ΔH_e.

2. Drop the coke from the previous run to determine the C_p of the coke.

The analyses of volatile matter, coal, and char must be very accurate so that a close material balance can be achieved. If the heat capacities of all the volatile matter are known, the heat capacity of coal can be deduced, the difference between these two runs being the ΔH_e. However, since there is no common base for these two runs, this method has the same flaw as Agroskin's; that is, the C_p of the coke is not the same as that of the coal. From an engineering point of view, the "$C_p + \Delta H_e$" term is the one that is needed in actual cases. Since the temperatures are all above decarbonizing temperature, the effect to worry about is "$C_p + \Delta H_e$."

The reported C_{pm} values at temperatures above 700°F include the value of the endothermic reaction; therefore, it is called the "pyro-heat capacity of coal.

EXPERIMENTAL WORK

In this work, two calorimeters(12) were used to measure the heat capacities of coal at temperatures from 600° to 1500°F and pressures from 0 to 1500 psia. Figure 1 presents a schematic drawing of the standard drop calorimeter, which is suitable for operation at temperatures lower than the decarbonization temperature. Figure 2 is a schematic drawing of the reaction calorimeter used at high temperatures.

The coal sample is contained in a basket that is suspended in the cold neck zone of the calorimeter. The calorimeter body is inside the furnace and is maintained at a constant temperature. An inert gas is used to achieve the desired pressure in the calorimeter. The sample is lowered into the calorimeter body after the temperature and pressure of the calorimeter have been stabilized for 2 hours. The cooling rate of the calorimeter is measured by four thermocouples and two resistance thermometers distributed around the calorimeter body. The coal is analyzed before and after the experiment. A gas sample is also taken to check for the volatile matter that escaped from the coal. Because the volatile matter is contained within the calorimeter at all times, if one knows the composition, weight, and other variables of the gas and solid, the total material and energy balance can be determined.

Establishing an energy balance around the calorimeter, we have –

$$(mC_p\Delta T)_{\text{calorimeter}} = (mC_p\Delta T)_{\text{baskets}} + (mC_p\Delta T)_{\text{coal}} \qquad (2)$$

The mC_p (mass X heat capacity) of the calorimeter was determined by using pure alumina, for which the heat capacity is well established for a wide temperature range.(9) The results of calorimeter constants are presented in Figure 3.

The ΔT of the calorimeter is measured, the mC_p of the baskets is calibrated as a function of temperature, the initial temperature of the coal

ınd the basket is measured, and the final temperature of the coal and ;he basket is assumed to be the same as that of the calorimeter final ;emperature. Therefore, the only unknown remaining in Equation 2 is ;he C_p – the pyro-heat capacity of the coal.

The composition of the coal and chars investigated is presented in Table 1.

Table 1. ANALYSIS OF COAL AND COAL CHARS

	Raw Coal	Pretreated Coal	Low-Temp Residue	High-Temp Residue	N.D. Lignite
Proximate Analysis, wt %					
Moisture	1.3	0.5	0.6	0.6	34.0
Volatile Matter	34.6	23.3	4.6	3.3	28.4
Fixed Carbon	52.0	63.5	77.6	71.6	31.3
Ash	12.1	12.7	17.2	24.5	6.3
Total	100.0	100.0	100.0	100.0	100.0
Ultimate Analysis, wt %					
Carbon	71.2	70.1	76.9	72.6	64.8
Hydrogen	5.14	3.70	2.05	1.08	0.78
Nitrogen	1.23	1.37	1.01	0.54	0.91
Oxygen	6.03	8.30	0.65	0.00	20.85
Sulfur	4.19	3.80	2.09	1.24	3.20
Ash	12.21	12.73	17.30	24.62	9.46
Total	100.00	100.00	100.00	100.00	100.00

. typical experimental run is presented in Figure 4. The results of this ;tudy are presented in Table 2 and Figure 5. The general trend of the ıeat capacity of coal is that it increases as temperature, the amount of ;olatile matter, and the moisture content increase, and decreases as the ısh content increases. This behavior agrees with other investigators' ;ork.(3,5,6, ,10,11) The heat capacity of the coal behaves this way ıecause the heat capacities of the volatile matter (CH_4, H_2, etc.) and ;he moisture (H_2O) are higher than graphite's and the heat capacity of ;sh is lower than graphite's. Detailed discussion may be found else-;here.(5,6,10)

The temperature of the calorimeter is measured to within ± 0.02°F, the ;ressure is measured to within ± 2 psi for above atmospheric pressure ıeasurements and to within 10 microns for vacuum measurements, the weight ;f a sample is measured to within ± 0.0005 gram, the coal analysis is ac-urate to within ± 0.7%, and the gas analysis is accurate to ± 2.0%. The stimated precision of the results is about ± 10% because of the thermal ag of the calorimeter(12), the distribution of the volatile matter ;ithin the calorimeter, and the calibration results.(12)

OMPARISON OF DATA

The U.S. Bureau of Mines reported the heat contents of various coals (1) ;r temperatures up to 2000°F. The heat capacities deduced from this ;rk range from 0.2 to 0.5 Btu/lb-°F; the general trend is that the C_p ncreases with increasing temperature.

For comparison purposes, the literature values of the heat capacity f coal are presented in Figure 5 with the data obtained from this work. ach curve is preceded by a reference number and a numerical number. ne reference number indicates the source of information, which is listed

Table 2, Part 1. HEAT CAPACITY OF COAL (Analysis of Coal After Measurement)

Run No.	TL-81	TL-82	TL-83	TL-88	TL-89	TL-90	TL-91	TL-92	TL-94
Starting Coal		High Temp				Low Temp		High Temp	Pretreated
Proximate Analysis, wt %									
Moisture	1.2	1.3	1.2	3.3	0.6	0.6	0.6	0.5	1.1
Volatile Matter	1.2	1.0	1.3	0.6	0.7	1.1	1.5	0.5	1.9
Fixed Carbon	78.3	77.8	81.4	65.4	76.9	83.1	80.9	78.2	83.3
Ash	19.3	19.9	16.1	30.7	21.8	15.2	17.0	20.8	13.7
Ultimate Analysis, wt %									
C	73.1	71.6	78.8	64.3	73.6	81.7	80.5	72.6	87.7
H_2	0.81	0.84	1.10	0.76	0.88	0.88	0.88	0.74	0.75
N_2	0.59	0.56	0.57	0.46	0.67	0.76	0.79	0.56	0.87
O_2	4.86	5.65	2.16	1.55	1.02	--	--	4.04	--
S	1.13	1.22	1.06	1.19	1.89	1.70	1.97	1.17	2.25
Ash	19.51	20.13	16.31	31.74	21.94	15.32	17.08	20.89	13.83
Temperature, °F	1488.40	1531.33	1494.25	1568.65	1568.73	1566.63	1531.67	1532.30	1566.65
Pressure, psia	1036	524	1008	0	0	0	508	504	0
C_p, Btu/lb-°F	0.297	0.320	0.385	0.384	0.374	0.478	0.334	0.351	0.487

Table 2, Part 2. HEAT CAPACITY OF COAL (Analysis of Coal After Measurement)

Run No.	TL-95	TL-97	TL-98	TL-100	TL-102	TL-103	TL-104	TL-107	TL-108
Starting Coal	Raw		Pretreated	High Temp	Low Temp	Pretreated	Raw	High Temp	Low Temp
Proximate Analysis, wt %									
Moisture	0.5	0.9	0.7	1.2	2.0	2.4	1.8	1.0	1.1
Volatile Matter	1.1	1.1	1.4	1.8	3.2	4.7	4.1	1.2	2.4
Fixed Carbon	79.8	79.4	80.9	75.6	71.1	77.3	75.2	81.3	76.5
Ash	18.6	18.6	17.0	21.4	23.7	15.6	18.9	16.5	20.0
Ultimate Analysis, wt %									
C	79.1	69.1	78.8	72.0	71.8	70.7	76.1	79.3	74.2
H_2	0.65	0.83	0.88	1.36	1.31	1.54	1.44	1.38	1.60
N_2	0.49	0.90	0.86	0.6	0.83	0.77	1.15	0.67	0.88
O_2	--	7.31	0.09	2.91	--	8.50	--	0.80	1.09
S	3.24	3.09	2.21	1.42	2.35	2.49	4.05	1.16	2.05
Ash	18.70	18.77	17.16	21.71	24.20	16.00	19.21	16.69	20.18
Temperature, °F	1568.55	1535.60	1534.45	1337.54	1335.48	1335.66	1334.21	1292.03	1292.68
Pressure, psia	0	49E	508	0	0	0	0	500	500
c_p, Btu/lb-°F	0.569	0.546	0.489	0.340	0.324	0.554	0.577	0.250	0.320

Table 2, Part 3. HEAT CAPACITY OF COAL (Analysis of Coal After Measurement)

Run No.	TL-109	TL-110	TL-112	TL-113	TL-114	TL-115	TL-117	TL-118	TL-119	TL-120
Starting Coal	Pretreated	High Temp	Lignite Partly Gasfd.	Raw	Lignite Partly Gasfd.	Lignite	High Temp (Ireland Mine)	Low Temp	Pretreated	Lignite
Proximate Analysis, wt %										
Moisture	1.7	2.2	5.4	0.8	1.5	2.5	1.8	2.2	2.5	2.0
Volatile Matter	3.1	1.8	6.7	3.1	5.9	5.2	2.0	4.1	9.4	11.8
Fixed Carbon	78.0	70.4	72.3	79.3	74.9	80.2	77.9	72.8	74.4	75.4
Ash	17.2	25.6	15.6	16.8	17.7	12.1	18.3	20.9	13.7	10.8
Ultimate Analysis, wt %										
C	72.6	69.6	77.7	75.1	77.1	82.9	78.6	73.7	73.6	80.2
H_2	1.90	1.06	1.09	1.74	1.21	1.66	1.90	1.76	2.63	2.57
N_2	1.15	0.60	0.36	1.15	0.44	1.02	0.60	0.93	1.44	1.10
O_2	3.90	1.37	4.17	1.81	2.44	1.10	--	0.29	5.46	4.43
S	2.92	1.24	0.22	3.31	0.84	0.88	1.09	1.95	2.82	0.72
Ash	17.53	26.13	16.46	16.89	17.97	12.44	18.60	21.37	14.05	10.98
Temperature, °F	1293.67	1292.49	1334.94	1294.35	1334.72	1335.33	1081.18	1077.12	1076.59	1074.34
Pressure, psia	498	496	496	500	0	0	0	0	0	0
C_p, Btu/lb-°F	0.462	0.261	0.348	0.517	0.545	0.607	0.300	0.322	0.377	0.592

Table 2, Part 4. HEAT CAPACITY OF COAL
(Analysis of Coal After Measurement)

Run No.	TL-121	TL-124	TL-125	TL-126	TL-127	TL-128	TL-131	TL-132	TL-133	TL-134	TL-135
Starting Coal	Raw Ireland Mine Coal	High Temp	Low Temp	Pretreated	Lignite	Raw	High Temp	Low Temp	Pretreated	Lignite	Raw Ireland Mine Coal
Proximate Analysis, wt %											
Moisture	2.5	3.6	2.1	2.6	3.6	1.0	1.7	1.3	1.8	3.1	0.7
Volatile Matter	8.2	2.4	3.8	18.2	26.0	18.4	2.2	4.0	20.3	37.5	32.0
Fixed Carbon	73.5	74.7	73.8	65.9	61.1	66.1	63.5	76.7	59.3	52.4	55.9
Ash	15.8	19.3	20.3	13.3	9.3	14.5	32.6	18.0	18.6	7.0	11.4
Ultimate Analysis, wt %											
C	74.6	76.3	74.0	70.9	72.7	71.4	62.6	74.9	63.7	66.8	70.4
H_2	2.56	1.25	1.82	3.33	3.89	4.10	1.11	1.93	3.41	4.45	4.85
N_2	1.25	0.55	0.83	1.24	1.16	1.28	0.52	0.88	1.08	0.99	1.17
O_2	2.44	0.83	0.64	7.50	11.82	4.94	1.25	1.99	9.40	19.75	8.82
S	2.94	1.04	1.99	3.35	0.77	3.63	1.34	2.05	3.52	0.80	3.29
Ash	16.21	20.03	20.72	13.68	9.66	14.65	33.18	18.25	18.89	7.21	11.47
Temperature, °F	1077.03	810.62	811.56	811.48	811.35	810.43	615.94	616.43	615.95	--	616.31
Pressure, psia	0	0	0	0	0	0	0	0	0	0	0
C_p, Btu/lb-°F	0.448	0.268	0.326	0.369	0.531	0.505	0.249	0.271	0.265	--	0.418

in the section "LITERATURE CITED," and the numerical number indicates the volatile matter content.

As can be seen from Figure 5, the agreement among authors is not too good, although the general trend is that the heat capacity of coal increases with increasing volatile matter content and temperature.

CORRELATION

Based on the data obtained from this work and that available in the literature, the heat capacity of coal is assumed to be a function of the volatile matter content and the temperature. The change of heat capacity with volatile matter content at a constant temperature, $(\partial C_p/\partial V_m)_T$, is nearly constant for every temperature. The heat capacity and temperature, $(\partial C_p/\partial T)_{V_m}$, are also nearly constant for every constant volatile matter content within the accuracy of the data. The $(\partial C_p/\partial V_m)_T$ was plotted against temperature. The intercepts of the V_m vs. T plot were also plotted against temperature. When an equation is fitted to each of these two plots, the following generalized correlation results –

$$C_{pm} = 0.17 + 1.1 \times 10^{-4}\, T + (3.2 \times 10^{-3} + 3.05 \times 10^{-6}\, T)V_m \qquad (3)$$

where:

C_{pm} = mean pyro-heat capacity in Btu/lb-°F; base temperature is 70°F

T = temperature in °F

V_m = volatile matter, dry basis, in weight percent

Equation 3 can predict all the heat capacity data of coal within the experimental accuracy of the data. The largest deviation is about 10%, while the average deviation is about ± 5%. A comparison of the predicted values with the experimental data is shown in Figure 6. To avoid overcrowding, not all of the literature values are presented.

ACKNOWLEDGMENT

This work is jointly sponsored by the American Gas Association, Research and Development, and the U.S. Department of the Interior, Office of Coal Research. Their support is gratefully acknowledged. Valuable advice and discussions were provided by B. S. Lee, H. L. Feldkirchner, F. C. Schora, S. A. Weil, and Alan Kardas of the Institute of Gas Technology. J. R. DeSando assisted in the experimental work.

LITERATURE CITED

1. Agroskin, A. A. and Goncharov, E. I., "The Specific Heat of Coal," Coke Chem. U.S.S.R. 7, 9-14 (1965).

2. Agroskin, A. A. and Goncharov, E. I., "Determination of the Specific Heat of Coals During Carbonization," Coke Chem. U.S.S.R. 11, 16-20 (1965).

3. Batchelor, J. D., Yavorsky, R. M. and Gorin, E., "Measurement of the Thermal Properties of Carbonaceous Materials," J. Chem. Eng. Data 4, 241-46 (1959).

4. Binford, J. S., Jr., Strohmenger, J. M. and Hebert, T. H., "A Modified Drop Calorimeter. The Heat Content of Aluminum Carbide and Cobalt (II) Fluoride Above 25°," J. Phys. Chem. 71, 2404-08 (1967).

5. Clendenin, J. D. et al., "Thermal and Electrical Properties of Anthracite and Bituminous Coals," Trans. 7th Annual Anthracite Conference of Lehigh Univ. Bethlehem, Pa., 1949.

6. Coles, G., "The Specific Heat of Coal and Its Relation to Composition," J. Soc. Chem. Ind. XLII, 435-39 (1923).

7. Dewey, P. H. and Harper, D. R., 3rd, "Heats of Combustion of Anthracite Cokes and of Artificial and Natural Graphites," Carnegie Inst. Tech. and Nat. Bur. Stand. 21, Contribution 71 (1938) October.

8. Fritz, V. W. and Moser, H., "Specific Heat, Thermal Conductivity and Thermal Diffusivity of Mineral Coal, Charcoal and Coke," Feuerungstechnik 5, 97-107 (1940).

9. Furukawa, G. T. et al., "Thermal Properties of Aluminum Oxide From 0° to 1200°K," J. Res. Nat. Bur. Stand. 57, 67-82 (1956).

10. Gomez, M., Gagle, J. B. and Taylor, A. R., Jr., "Heat Content and Specific Heat of Coals and Related Products," U.S. Bur. Mines Report 6607. University: Univ. of Alabama Press, 1964.

11. Kazmina, V. V., "Determination of the Specific Heat of Cokes," Coke Chem. U.S.S.R. 11, 26-29 (1965).

12. Lee, A. L., Feldkirchner, H. L., Schora, F. C. and Henry, J. J., "Heat of Reaction of Hydrogen and Coal," ACS Div. Fuel Chem. Preprints 11, No. 2, Pt. 2, 393-401 (1967).

13. Mantell, C. L., Industrial Carbon, 2nd Ed., 432. New York: D. Van Nostrand, 1947.

14. Morlock, R. J., Naso, A. C. and Cameron, J. R., "Heat Requirements for Coking." Presented at the Canadian Coal Conferences, Ottawa, March 30, 1967.

15. Porter, H. C. and Taylor, G. B., "The Specific Heat of Coal and Its Relation to the Presence of Combined Water in the Coal Substance," Ind. Eng. Chem. 5, 289-93 (1913).

16. Terres, V. E. et al., "The Solution of the Problem of the Origination of Fibre Coal on the Ground of Its Specific Heats," Brennstoff-Chemie 37, 366-70 (1956) June.

17. Terres, V. E. et al., "The Solution of the Problem of the Origination of Fibre Coal on the Ground of Its Specific Heats," Brennstoff-Chemie 37, 269-73 (1956) June.

18. Voloshin, A. I. et al., "Determination of the Heat of Coking Under Laboratory Conditions," Coke Chem. U.S.S.R. 3, 17-20 (1962).

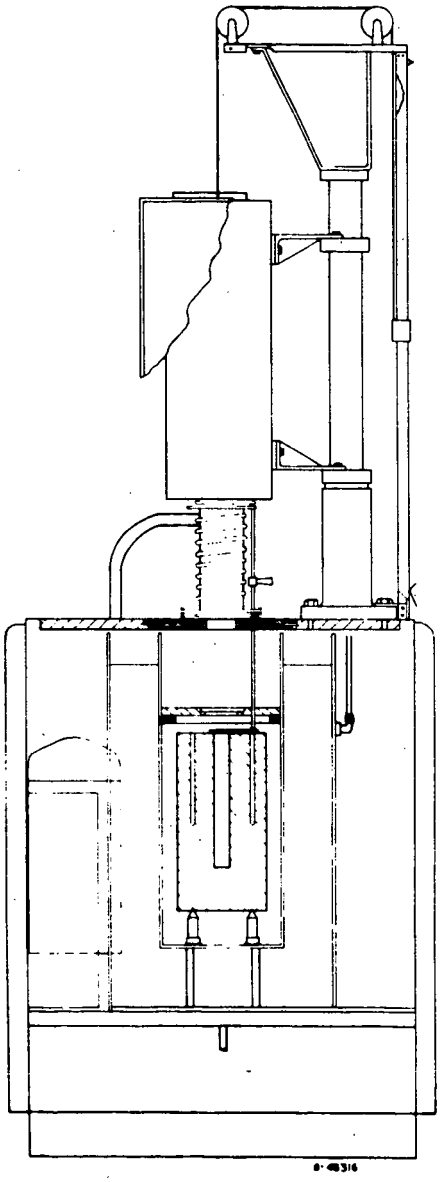

Figure 1. DROP CALORIMETER

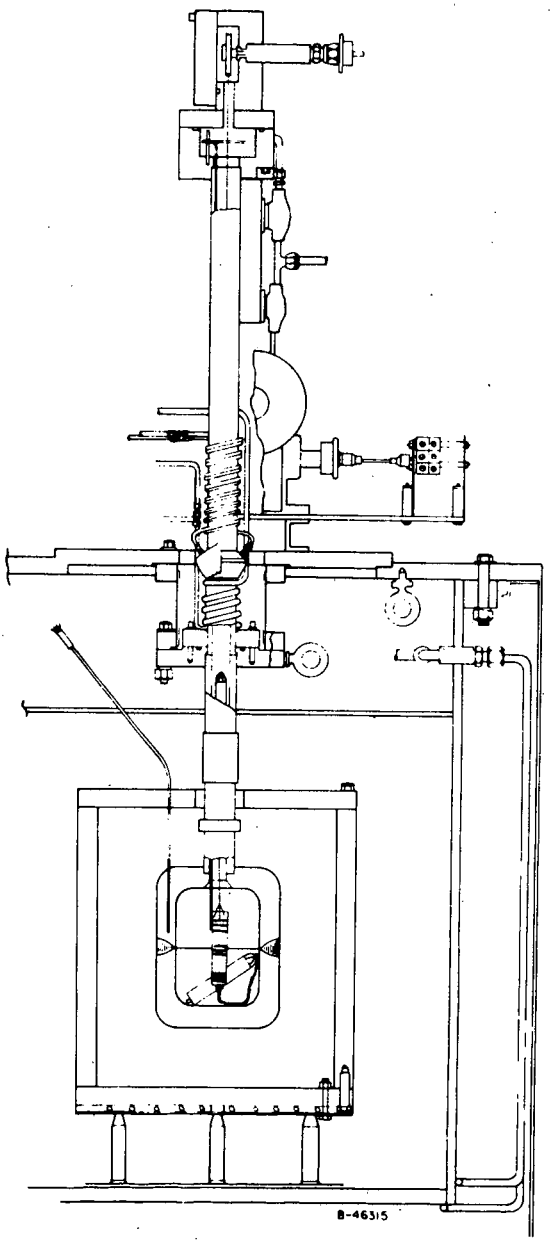

Figure 2. HEAT-OF-REACTION CALORIMETER

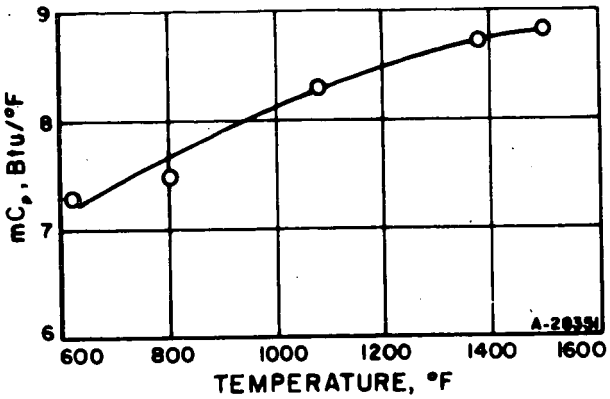

Figure 3. CALORIMETER CONSTANTS CALIBRATED BY USING ALUMINUM OXIDE

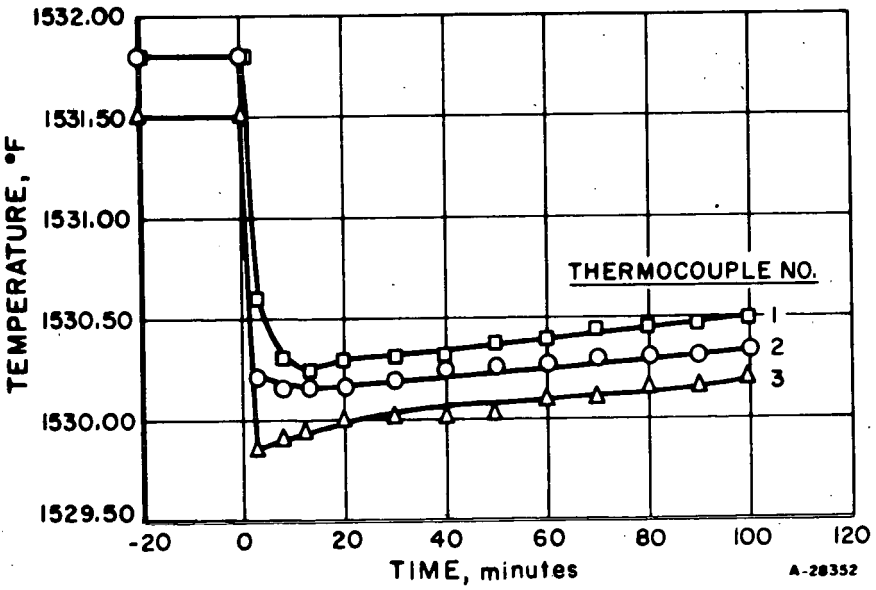

Figure 4. TIME-TEMPERATURE COOLING CURVE FOR RUN NO. 92

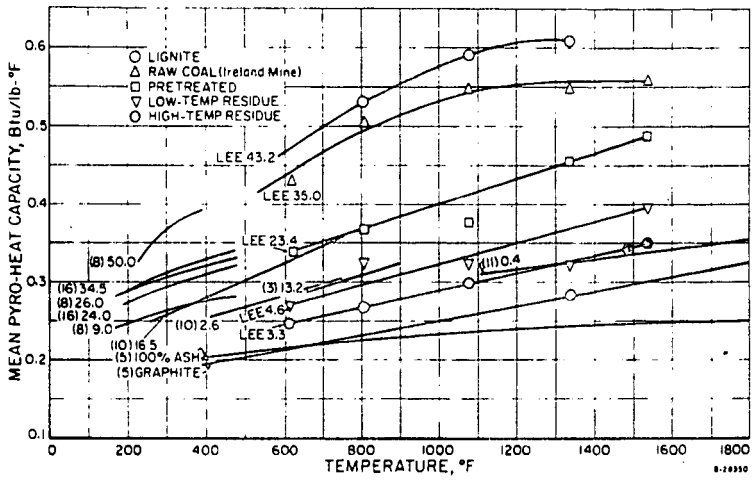

Figure 5. MEAN PYRO-HEAT CAPACITY OF COAL
(Base Temperature = 70°F)

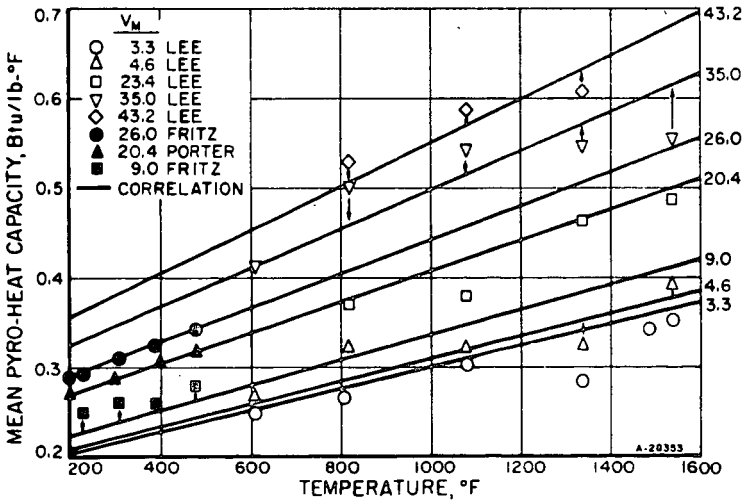

Figure 6. COMPARISON OF CORRELATION WITH EXPERIMENTAL DATA

FLUID-BED GASIFICATION OF PITTSBURGH-SEAM COAL WITH OXYGEN AND WITH AIR

A. J. Forney, R. F. Kenny, and J. H. Field

U. S. Bureau of Mines, Pittsburgh Coal Research Center
4800 Forbes Avenue, Pittsburgh, Pennsylvania 15213

Introduction

Most processes for producing either high-Btu gas or gasoline from coal include a gasification step to make hydrogen or synthesis gas. For high-Btu gas or gasoline pressure gasification is preferred because of its greater yield of methane and higher rate of gasification. The fluid-bed gasification system has the advantage over other systems of better control, better heat transfer, faster reaction time, and the utilization of fine coals. However, oxygen is an expensive item in the process. If air can be substituted for oxygen, significant savings in coal conversion costs may be realized. Some experimenters have operated gasifiers without oxygen: The British with the ICI moving burden technique (7)[1], the Australians with a similar system except for the substitution of sand for the hot ash (1), Consolidation Coal with the CO_2-acceptor process (2), Rummel with the slag bath (8), and Kellogg with a molten salt bath (6). The Bureau of Mines is now trying steam plus oxygen in gasification of coal under pressure and steam plus air at pressures below 7 atmospheres.

Pressure Gasification

The Bureau's work in fluidized gasification has been directed mainly to gasifying caking coals, specifically Pittsburgh-seam coal (3). The first system tried involved two fluid beds in series (figure 1)--the first pretreating the raw coal at about 400° C with steam plus air or oxygen; the second gasifying the coal plus the gases and tars with additional steam and oxygen at 850° to 900° C. Due to the cocurrent flow in the two reactors, the methane yield was less than expected. In the second system tried (figure 2) the coal, 70 pct through 200 mesh, was fed into the top of the reactor where it dropped through the pretreating oxygen and steam which mixed with the rising gases from a 3-inch-diameter fluid-bed gasifier. Again the pretreating-carbonizing section was operated at 400° C and the gasifier at 900° C. At 20 atmospheres pressure the gas production was 28 SCF/lb coal, the dry gas composition approximately 36 pct H_2, 19 pct CO, 31 pct CO_2, and 14 pct CH_4, with traces of C_2H_6 and C_3H_8. The throughput of the gasifier was 140 lb/hr-sq ft. This high methane yield (14 pct) means that in the production of high-Btu gas from gasification plus methanation, as much methane can be made in the gasification as in the methanation.

---

[1] Underlined numbers in parentheses in the text indicate items in the list of references at the end of this paper.

By increasing the pressure of the gasifier to 40 atmospheres, we estimate that we can reduce the cost of the high-Btu gas about 5¢/1,000 SCF. This 40-atmosphere gasifier is now under construction.

Since almost one-third of the cost of high-Btu gas from gasification plus methanation is due to the cost of oxygen, we have also undertaken to develope a system in which air is substituted for oxygen.

Atmospheric Gasification With Steam Plus Air

A sketch of the apparatus is shown in figure 3, and a photograph of the unit is shown in figure 4. The concept is to feed air and steam through separate ports into a fluid-bed gasifier. The 8-inch diameter by 5-foot high reactor is baffled so the products of combustion can be separated from the products of steam gasification. The system is based on the flow characteristics of a fluidized bed; namely, that while the solids mix thoroughly, the upward flowing gases have little lateral motion. Thus it is possible to keep two dissimilar gas streams separate in a fluid bed (4, 5). The bottom of the reactor is not baffled for the first foot of reactor height; above that a solid baffle is used. The coal, which has been pretreated in a combined entrained and free-fall section, drops into the steam side of the gasifier so that its carbonization gases will be part of the product stream. Figure 5 shows a flowsheet of the system.

The gas produced at present indicates that the gas streams can be kept partially isolated. The gas produced is not suitable for high-Btu gas as the nitrogen content--14-20 pct--is too high. It could, however, be used as a synthesis gas in making liquid fuels, ammonia, or as a rich producer gas. Analyses of the product and combustion gases, and the temperature profile on the air-coal and the steam-coal side are shown in table 1. The process is equally applicable to both caking and non-caking coals. With caking coal, such as our Pittsburgh-seam, pretreatment with steam and oxygen was included in our experiments, but this should not be considered an essential part of the process.

At total flows of 90 cu ft/hr of steam and 60 cu ft/hr of air, and at coal feed rates of 3 lb/hr, the least nitrogen in the product stream is 14 pct (test 14-3). The flows are regulated by controlling the quantity of combustion product gas leaving the combustion side. Any gas in excess of the set flow passes through the back pressure regulator on the product gas side. The nitrogen percentage is recorded by an on-stream chromatograph on the product side and the controller varied to keep it to a minimum. The composition of the two gas streams thus depend both on the efficiency of the baffle configuration and on the setting of the flow controller on the combustion side.

Temperature profiles (test 12-5) show 905° C on the combustion side compared with 870° C on the product side at the level 19 inches above the base of the reactor. Since the electric heaters which heat up the reactor shut off at temperatures exceeding 800° C, these temperatures indicate good solids mixing and heat transfer from the combustion side to the product side.

TABLE 1.- Tests in a fluid-bed gasifier using air in place of oxygen

Test No.	11-6	12-5	14-3	14-9	15-9	17-2
Coal feed, lb/hr	2.8	3.0	3.18	3.18	3.08	3.86
Steam, SCF/lb	30	30	30	30	30	20
Air, SCF/lb	20	20	20	20	20	20
Pretreater oxygen, SCF/lb	1	1	1	1	1	1
Pretreater steam, SCF/lb	5	5	5	5	5	5
Pressure, atm	2.5	2.5	4	4	4	4
Combustion side temperature, °C:						
2 in. from base	970	880	780	945	760	760
11 in. from base	830	920	900	935	880	900
19 in. from base	840	905	880	940	882	900
31 in. from base	725	740	710	760	740	700
Product side temperature, °C:						
2 in. from base	772	480	443	425	410	440
11 in. from base	825	821	850	640	740	860
19 in. from base	835	870	850	890	850	885
31 in. from base	715	710	680	790	720	690
Product gas analysis, pct:						
H_2	35	43	45	38	43	35
N_2	28	22	14	27	19	34
CO	9	12	12	11	13	13
CH_4	7	6	10	7	9	3
C_2+	4	3	2	1	1	1
CO_2	17	14	17	16	15	14
Heating value, Btu/cu ft	284	292	322	246	290	203
Combustion gas analysis, pct:						
H_2	14	5	13	12	8	9
N_2	62	74	62	62	71	71
CO	8	8	9	12	8	7
CH_4	1	1	2	1	--	--
CO_2	15	12	14	13	13	13
Heating value, Btu/cu ft	78	51	91	88	50	50
Yield product gas, SCF/lb	14	17	10	20	15	16
Yield combustion gas, SCF/lb	20	20	26	20	19	15
Total yield,[1] SCF/lb	13	14	13	16	14	10
Product gas H_2+CO+HC, pct	63	79	54	69	79	80
Total H_2+CO+HC						
Pct HV in product gas	72	85	58	74	82	80
Carbon conversion, pct	60	56	50	50	52	--

[1] H_2+CO+HC.

Analyses of gas made on the product side indicate a maximum of 322 Btu/cu ft or twice the producer gas value, and analyses of gas made on the combustion side, 50 to 90 Btu. A maximum of 79 pct of the H_2+CO+HC, made in the reactor, is on the product side; a maximum of 85 pct of the heating value is on the product side. The large percentage of CO on the combustion side probably results from CO_2 from coal-air combustion reacting with hot carbon. As is seen in table 1, the CO on the combustion side is almost as great as on the product side. When the steam flow was lowered from 30 to 20 cu ft/lb coal feed, the percentage nitrogen increased considerably (17-2) to 34 pct. Further tests are being made to try to lower this nitrogen concentration.

The scheme shown in figure 6 will be tested in the future. This design may not give as good gas separation as the first design, but with air in the annulus, it should give better heat transfer.

Conclusion

Pittsburgh-seam coal can be gasified satisfactorily in a free-fall, fluid-bed reactor to give a product gas of high methane content--20 pct (on a CO_2-free basis). This yield of methane means that in the production of a high-Btu gas from gasification plus methanation as much methane can be made in the gasification as in the methanation step.

Substituting air for oxygen, we tried to operate a fluid-bed gasifier to separate the products of combustion from the products of steam-coal gasification, and also to achieve good heat transfer of the solids. The product gas contained a minimum of 14 pct nitrogen, and temperature profiles showed good heat transfer. This gas is not satisfactory for a 900-Btu gas which would need to contain less nitrogen. However, it could be used for synthesis of liquid fuels, ammonia, or as a rich producer gas, and improved design and operation may lower the nitrogen content of the product gas so that a high-Btu gas may be possible.

References

1. Bowling, K. CSIRO, Australia. Personal communication.

2. Curran, G.P., C.H. Rice, and E. Gorin. Carbon Dioxide Acceptor Gasification Process. Division of Fuel Chemistry, Am. Chem. Soc., Philadelphia, Pa., April 5-10, 1964.

3. Forney, A.J., R.F. Kenny, and J.H. Field. Gasification of Caking Coal in a Free-Fall, Fluid-Bed Reactor. Division of Fuel Chemistry, Am. Chem. Soc., Chicago, Ill., Sept. 10-15, 1967.

4. Munday, J.C. Conversion Processes in the Presence of a Dense Turbulent Body of Finely Divided Solid Material. U.S. Patent 2,468,508, April 26, 1949.

5. Othmer, Donald F. Fluidization. Reinhold Publishing Co., New York, N.Y., 1956, 231 pp.

6. Pieroni, L.J., G.T. Skaperdas, and W.H. Heffner. Development of the Kellogg Coal Gasification Process. A.I.Ch.E. Symposium on Processing of Coal and Its Byproducts. Philadelphia, Dec. 5-9, 1965.

7. Raynor, J.W.R. Gasification by the Moving Burden Technique. Gasification and Liquefaction of Coal Symposium. A.I.M.E., New York, N.Y., Feb. 20-21, 1952.

8. Rummel, R. Coke and Gas, v. 21, 1959, pp. 493-501; 520.

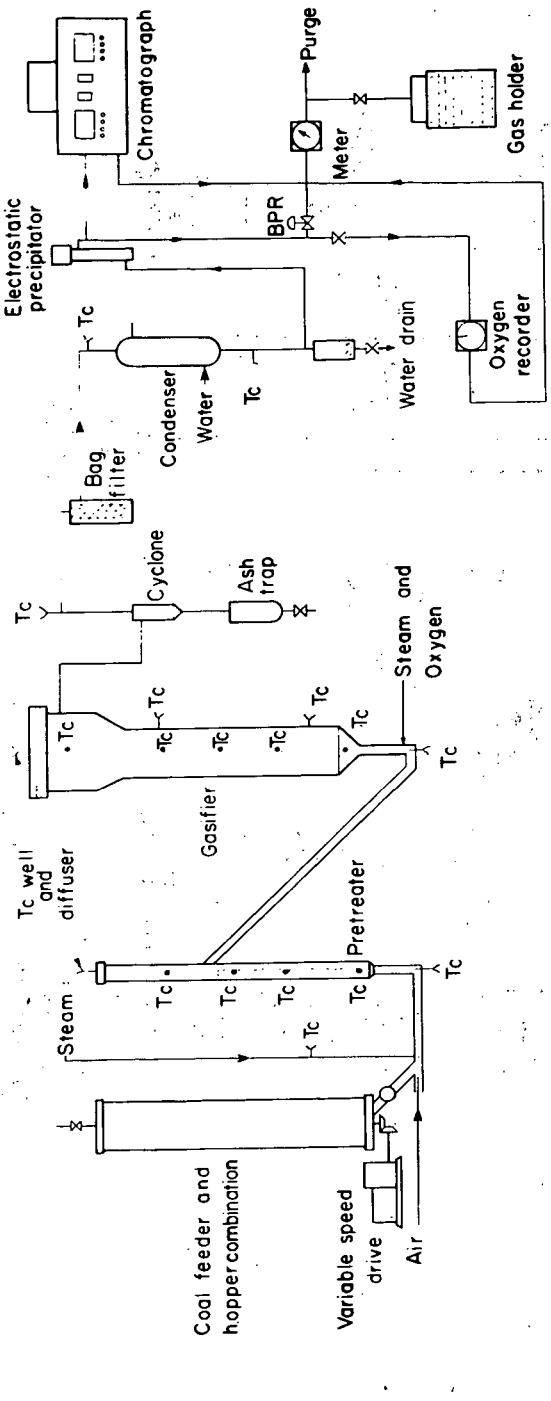

Figure 1. Gasification of caking coal with two fluid beds in series.

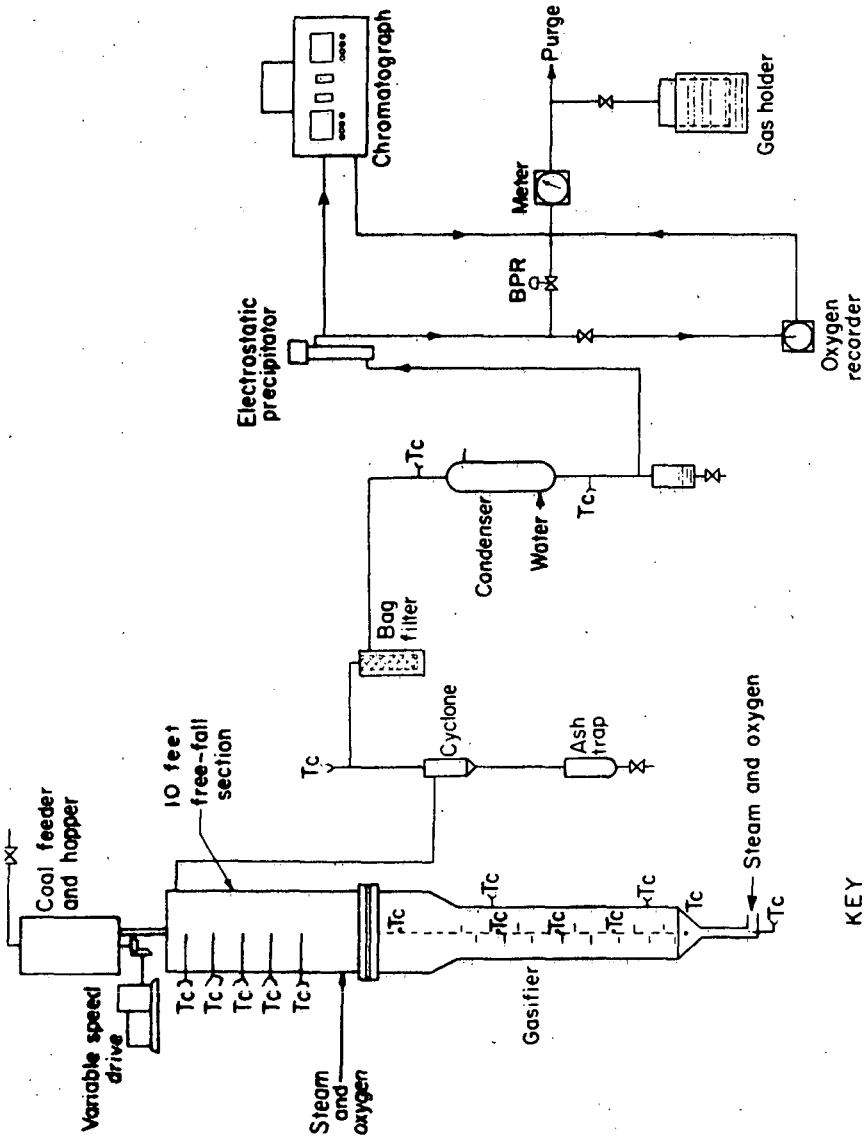

Figure 2. Free-fall reactor and fluid-bed gasification system.

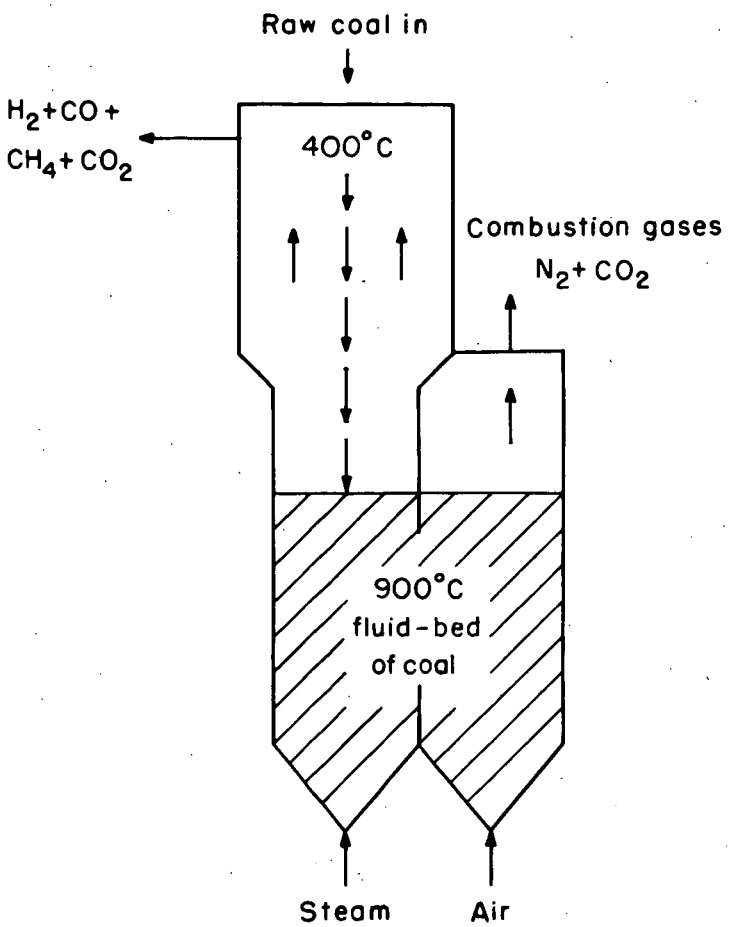

L-9749

Figure 3. Baffled reactor for gasification of coal with steam and air.

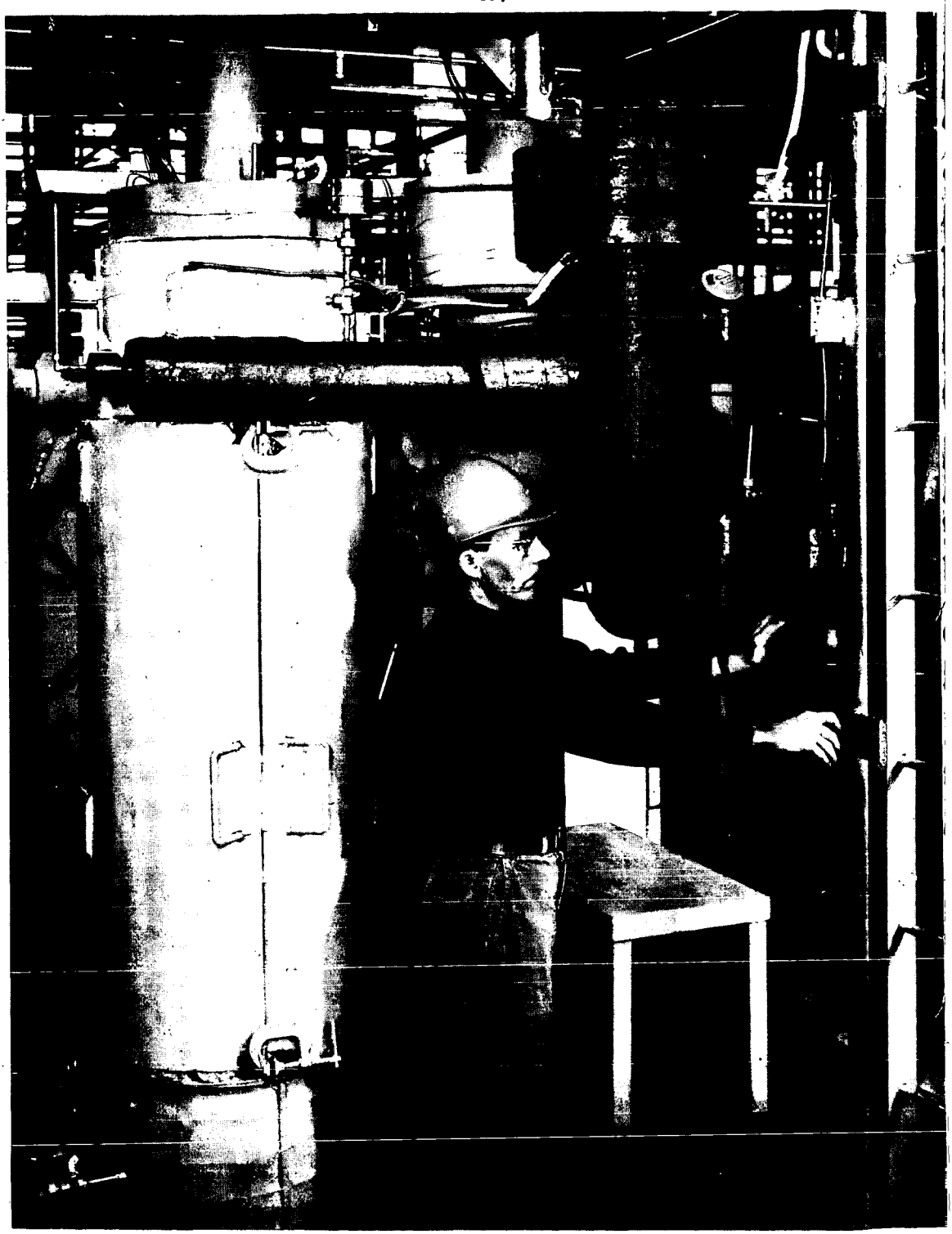

Figure 4. Gasification system for gasification of coal with steam and air.

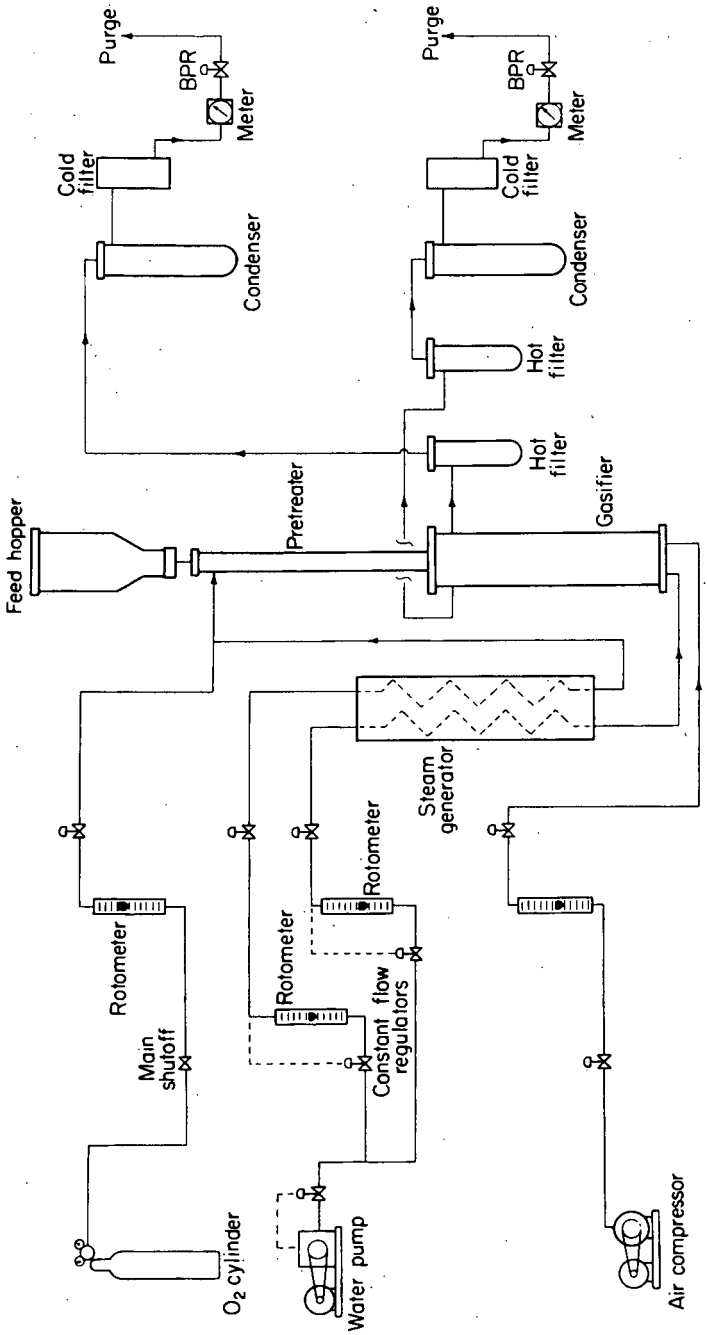

Figure 5. Flowsheet of gasification system.

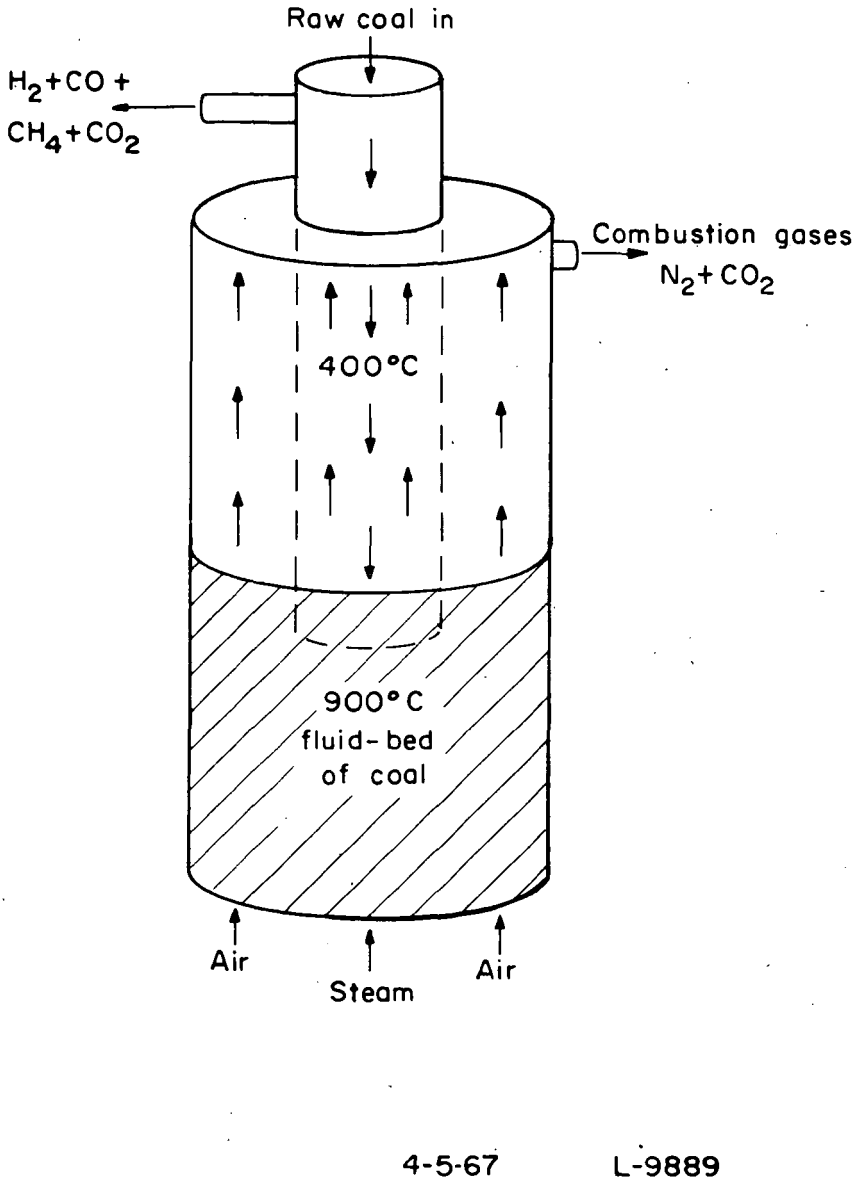

Figure 6. Two-tube reactor for gasification of coal with steam and air.

Coal Hydrogasification Catalyzed by Aluminum Chloride

Walter Kawa, Sam Friedman, L. V. Frank, and R. W. Hiteshue

U.S. Bureau of Mines, 4800 Forbes Avenue
Pittsburgh, Pennsylvania 15213

INTRODUCTION

The Bureau of Mines has been investigating the use of high concentrations of catalysts in the hydrogenation of coal to oil. A large number of materials including aluminum chloride have been screened as possible catalysts. Equal weights of catalyst and coal were used in these experiments, whereas catalyst concentrations of one weight-percent or less have been used in most previous studies. Aluminum chloride is well known as a catalyst for many organic reactions including hydrocracking. However, it is not known to be an effective coal hydrogenation catalyst. In the screening experiment with aluminum chloride at 450° C, very little oil was produced, but an exceptionally high yield of hydrocarbon gases was obtained.

Hydrogenation of coal to hydrocarbon gases (hydrogasification) is one method whereby high-Btu gas will probably be produced in the future. Coal hydrogasification processes now under development are noncatalytic and are operated at temperatures of about 700° C and higher.[1] High temperatures are used mainly to obtain high gas production rates. At lower temperatures, a much longer reaction time is needed to eliminate tarry products and caking problems are more severe. The results obtained with aluminum chloride demonstrated that catalytic hydrogasification at a practical rate was feasible at temperatures considerably lower than 700° C.

The present study was made to further explore the use of aluminum chloride in a batch reactor. It is a brief investigation of the effects of temperature, catalyst concentration, and type of feed material on hydrogasification yields.

EXPERIMENTAL

Equipment and Materials

The reactor was a 1.2-liter autoclave that was placed in a horizontal position and rotated during an experiment. A complete description of the vessel and accessory equipment has been published.[2] Charges were contained in a glass liner that fitted closely to the autoclave wall. The free volume of a charged and assembled autoclave was about 1.0 liter. Pressure was measured with a bourdon-tube type gage that was connected to and rotated with the autoclave. Temperature was measured with a chromel-alumel thermocouple in a thermowell positioned axially within the autoclave.

Experiments were made with high-volatile A bituminous coal from the Pittsburgh seam, high-volatile C bituminous coal from Rock Springs, Wyoming, a Pennsylvania anthracite, a Texas lignite, untopped high-temperature tar produced in a commercial slot-type oven, tar from low-temperature fluidized carbonization of a Texas lignite, and distillation residue from a Venezuelan crude oil. Analyses of feed materials are shown in table 1. Coal samples were pulverized to minus 60 mesh (U.S. Sieve) and dried in air at 70° C for about 20 hours.

Powdered anhydrous aluminum chloride of 99 percent purity was used. Charges of coal and aluminum chloride were premixed in the glass liner by rotating the liner and charge end-over-end for 2 hours. Hydrogen was obtained from commercial cylinders.

TABLE 1.- Analyses of feeds

Material	Anthracite	Hvab coal	Hvcb coal	Texas lignite	High-temp. tar	Low-temp. tar	Petroleum residue
Analyses, percent by weight							
Moisture	0.3	0.1	0.9	1.9	trace	trace	0.0
Ash	36.7	7.5	1.7	18.7	trace	0.1	0.1
Ultimate, maf							
C	91.1	83.8	76.4	68.3	92.2	83.3	85.7
H	2.5	5.4	5.3	5.3	5.3	9.6	10.5
N	1.1	1.6	1.6	1.3	1.2	0.7	0.6
S	1.0	1.2	0.9	2.3	1.0	1.0	3.1
O 1/	4.3	8.0	15.8	22.8	0.3	5.4	0.1

1/ By difference.

Operating and Analytical Procedures

All experiments were made with 50-gram charges of coal or other feed material. After purging air out of a charged and assembled autoclave, hydrogen was added to a specified initial pressure selected so that a pressure of 4,000 psi would be attained at reaction temperature. Rotation was started and the autoclave was heated to reaction temperature at a rate of about 7° C per minute. After a specified time at reaction temperature, the autoclave was cooled to room temperature at a somewhat slower rate.

Gases were depressurized through scrubbers that removed water vapor and acid gases (CO_2, H_2S, and HCl formed by reactions of $AlCl_3$). The remaining gases were metered, collected in a holder, sampled, and analyzed by mass spectrometry. In some experiments, aluminum chloride condensed in the autoclave outlet and obstructed the flow of gases during the depressurizing step. Some gas loss was incurred, and, as a result, reported gas yields are low for those experiments. Light oil and water were removed by vacuum distillation to about 110° C and 2 to 3 mm of Hg. Solid and heavy liquid products remaining in the autoclave were washed with water to remove aluminum chloride. Material insoluble in water was separated into benzene-insoluble and benzene-soluble fractions, and the ash content of the benzene insolubles was determined. When about 2 grams or more of benzene-soluble product was formed, it was separated into n-pentane-insoluble (asphaltene) and n-pentane-soluble (heavy oil) fractions.

Yields are expressed as percentages by weight of moisture- and ash-free (maf) charge. Organic benzene insolubles are defined as total benzene insolubles minus ash. Benzene-soluble oil is the sum of the asphaltene, heavy oil, and light oil. Coal conversion is given on a percentage basis and is defined as 100 minus the percent of organic benzene insolubles.

RESULTS AND DISCUSSION

The effect of temperature on the distribution of products from hvab coal is shown in table 2. Experiments were made with equal weights of coal and aluminum chloride at temperatures of 250° to 450° C for one hour. At temperatures of 300° C and lower, little or no hydrogenation of coal would occur in one hour at 4,000 psi when using low concentrations of conventional catalysts. In the presence of aluminum chloride, appreciable amounts of benzene-soluble oil and hydrocarbon gases were produced at 250° C. Oil yields decreased and hydrocarbon gas yields increased as temperature was increased. Conversion of coal increased between 250° and 300° C, but

TABLE 2.- Effect of temperature on the distribution of products from hvab coal at 4,000 psi (50 grams of coal, 50 grams of $AlCl_3$)

Temp., ° C	Time at temp., hr.	Conversion, weight-percent	Yields, weight-percent of maf coal: Organic benzene insols.	Benzene-soluble oil	Hydrocarbon gases	Net water	Acid gases
250	1	60	40	19	27	1	8
300	1	76	24	15	42	0	16
300	2	70	30	19	41	<1	20
350	1	81	19	3	59	0	-
450	1	74	26	<1	68	0	16

there was no significant trend in conversion between 300° and 450° C. At 300° C, increasing the reaction time to 2 hours resulted in no significant change in product distribution.

Very little light oil was produced at any temperature. Benzene-soluble oils produced at 250° and 300° C consisted of about two-thirds asphaltene and one-third heavy oil. Hydrocarbon gases produced at 250° C contained 35 percent methane, 17 percent ethane, 33 percent propane, 11 percent propylene, 3 percent butane, and 1 percent butylene on a volumetric basis. As temperature was increased, the proportions of lower hydrocarbons increased. Methane and ethane constituted 96 percent of the gas produced at 450° C.

Results obtained at 250° and 300° C may have practical significance as these temperatures are below the softening point of caking coals. In continuous hydrogasification systems, coal agglomeration and stoppage of flows is a problem with both caking and noncaking coals. Agglomeration is avoided in noncatalytic systems by pretreatment of a coal to destroy its caking properties or by rapid heating and rapid devolatilization to a dry residue. It may also be possible to avoid agglomeration in a continuous system by using aluminum chloride as a catalyst at about 300° C. The hydrocarbon gas yield of about 40 percent obtained at 300° C would be sufficiently high in such a process as the unconverted coal could be used for hydrogen production and power generation. Production of small amounts of heavy liquids would probably cause no difficulties in a continuous system, but large amounts would be undesirable; heavy liquids would tend to bind solid particles and render such systems inoperable.

The effect of aluminum chloride concentration on the distribution of products from hvab coal was determined at 300° C. Time at temperature was one hour. The amount of aluminum chloride charged was varied between 12.5 and 100 grams. As can be seen in table 3, very little reaction occurred with 12.5 grams of aluminum chloride in the charge. Hydrocarbon gas yields increased sharply as the amount of aluminum chloride was increased to 50 grams but remained essentially unchanged with a further increase to 100 grams.

Aluminum chloride sublimes at 180.2° C. It boils at 182.7° C under a pressure of 755 mm of Hg. The form of the vapor is the dimer, Al_2Cl_6, up to 440° C. Calculations based on available vapor pressure data indicate that 100 grams of aluminum chloride would be completely vaporized at 240° C in a 1-liter system. As complete vaporization could occur at the conditions used in all experiments listed in table 3, it would appear that results in table 3 show a dependence of hydrocarbon gas yield on the amount of aluminum chloride in the gas phase. However, it is also possible that a coal-aluminum chloride complex forms before catalysis occurs, and that the amount

TABLE 3.- Effect of $AlCl_3$ concentration on the distribution of products from hvab coal at 300° C
(50 grams of coal, 4,000 psi, 1 hour at temperature)

$AlCl_3$ charged, grams	Conversion, weight-percent	Yields, weight-percent of maf coal				
		Organic benzene insols.	Benzene-soluble oil	Hydrocarbon gases	Net water	Acid gases
12.5	4	96	4	1	<1	5
25.0	11	89	6	5	<1	9
37.5	25	75	11	11	1	11
50.0	76	24	15	42	0	16
100.0	73	27	16	40	0	-

of complex formed depends upon the amount of aluminum chloride charged (up to 50 grams). The literature indicates that the formation of an organo-aluminum chloride complex is a prerequisite for catalysis of many organic reactions by aluminum chloride. The complex is apparently formed by reaction of aluminum chloride with unsaturated organic structures. No effort was made in this investigation to determine whether or not complexes of coal and aluminum chloride were formed.

The effectiveness of aluminum chloride as a catalyst for the hydrogasification of coals of various ranks, tars, and a petroleum residue was investigated at 300° and 450° C with a reaction time of one hour. Experiments were made using equal weights of feed material and catalyst. Results are shown in table 4. In the experiments with coals, the highest yields of hydrocarbon gases were obtained from hvab coal at both temperatures. Conversion of anthracite was only about 3 percent at 300° C, but an appreciable yield of hydrocarbon gases (24 percent) was obtained from anthracite at 450° C. At 450° C, yields from hvcb coal and anthracite were nearly equal while a considerably lower yield was obtained from the lignite. High yields of hydrocarbon gases were obtained from both high- and low-temperature tars at 450° C and from low-temperature tar at 300° C. High-temperature tar was much less reactive at 315° C. Yields of organic benzene insolubles obtained in the experiments with high-temperature tar were 25 and 26 percent, whereas the tar initially contained 9 percent. The increase of insolubles indicates that appreciable polymerization or condensation of the tar occurred at both temperatures. The highest yield of hydrocarbon gases (91 percent) was obtained from petroleum residue at 450° C.

The results shown in table 4 indicate that the amenability of a carbonaceous material to hydrogasification catalyzed by aluminum chloride increases with increasing hydrogen content and with decreasing oxygen content of the material. The least suitable material for hydrocarbon gas production was the lignite which contained the most oxygen. Much of the oxygen in coals is normally removed as water during hydrogenation. Reaction of water with aluminum chloride would produce hydrochloric acid and decrease the aluminum chloride concentration. The yields of acid gases shown in table 4 provide evidence that reaction with water did occur. Acid gas yields increased nearly linearly with increasing oxygen content of the feed. Yields of hydrogen sulfide and carbon dioxide obtained from coals would amount to only a few percent. In the experiments in which yields of acid gases were high, most of the gas would therefore be hydrochloric acid.

Equilibrium data indicate that negligible amounts of aluminum chloride would react with either hydrogen or hydrogen sulfide at the conditions used in this study. However, a nearly quantitative reaction with water to form alumina and hydrochloric acid would occur at equilibrium. Aluminum oxychloride and aluminum hydroxychlorides

TABLE 4.- Distribution of hydrogenation products from various feed materials
(50 grams of feed, 50 grams of $AlCl_3$, 4,000 psi, 1 hour at temperature)

Feed material	Temp., ° C	Yields, weight-percent of maf charge: Organic benzene insols.	Benzene-soluble oil	Hydrocarbon gases	Acid gases
Anthracite	450	80	<1	24	6
Hvab coal	300	24	15	42	16
Hvab coal	450	26	<1	68	16
Hvcb coal	300	74	5	10	26
Hvcb coal	450	55	3	21	34
Lignite	300	78	<1	8	35
Lignite	450	33	15	13	44
High-temp. tar	315	25	47	21	1
High-temp. tar	450	26	4	81	1
Low-temp. tar	300	3	8	74	9
Low-temp. tar	450	4	<1	71	10
Petroleum residue	450	3	1	91	-

are other possible products of the reaction with water. In this study, reaction with water probably approached equilibrium as very little water was recovered in any of the experiments.

Further evaluation of aluminum chloride as a coal hydrogasification catalyst will require additional information concerning the chemical and physical changes the aluminum chloride undergoes during hydrogasification. With this information, an estimate of catalyst consumption can be made, catalyst recovery procedures can be devised, and the feasibility of operating a continuous system can be assessed.

SUMMARY

This investigation has shown that aluminum chloride in high concentrations is an effective catalyst for hydrogasification of various carbonaceous materials. With equal weights of hvab coal and aluminum chloride at 4,000 psi and 450° C for one hour, a hydrocarbon gas yield of 68 percent and a benzene-soluble oil yield of less than 1 percent are obtained. The oil yield increases and the gas yield decreases as the temperature is decreased. However, the gas yield of 27 percent at 250° C is still appreciable. At 300° C, hydrocarbon gas yields obtained from hvab coal increase sharply with increasing concentrations of aluminum chloride up to a 1:1 ratio with coal. In general, the amenability of a carbonaceous material to hydrogasification catalyzed by aluminum chloride increases with increasing hydrogen content and with decreasing oxygen content of the material.

REFERENCES

1. Lewis, P. S., Sam Friedman, and R. W. Hiteshue. High B.t.u. Gas by the Direct Conversion of Coal. Advances in Chemistry Series, No. 69, Fuel Gasification, 1967, pp. 50-63.

2. Hawk, C. O. and R. W. Hiteshue. Hydrogenating Coal in the Batch Autoclave. BuMines Bull. 622, 1965, 42 pp.

Coal Char Gasification in an Electrofluid Reactor

T. M. Knowlton, A. H. Pulsifer, and T. D. Wheelock

Department of Chemical Engineering and Engineering Research Institute
Iowa State University
Ames, Iowa

Introduction

The use of an electrofluid reactor for the production of synthesis gas from coal char and steam is being investigated. In this type of reactor heat is supplied electrically by passing current between electrodes which are placed in a gas-fluidized bed of conducting particles. Thus, in effect, the fluidized bed is a resistance heater. Preliminary experiments have been carried out in a 4-in.-diam, bench-scale reactor. Some typical results of the batch gasification runs are presented, together with information about the electrical characteristics of the system and a discussion of problem areas.

The previously reported work on the gasification of carbonaceous materials with steam is extensive and several reviews of this work are available (22, 23). At one atmosphere, the primary reactions are

(1) $C + H_2O = CO + H_2$

(2) $CO + H_2O = CO_2 + H_2$.

The rate of reaction 2, the water-gas shift reaction, is rapid above 1600°F and approaches equilibrium. The carbon-steam reaction, reaction 1, goes essentially to completion if allowed to reach equilibrium. The steam decomposition via this reaction, then, depends on the residence time and reaction rate. Methane-forming reactions can be ignored at atmospheric pressure since the equilibrium constants are extremely small.

The carbon-steam reaction is heterogeneous and occurs by a series of diffusional and chemical steps. The rate of the chemical steps follow a Langmuir-type rate equation of the form

$$\text{Rate} = \frac{k_1 P_{H_2O}}{1 + k_2 P_{H_2} + k_3 P_{H_2O}}$$

where k_1, k_2, k_3 = kinetic rate constants

P_{H_2O} = partial pressure of steam

P_{H_2} = partial pressure of hydrogen.

Since k_1 increases with increasing temperature, while k_2 and k_3 decrease, the apparent order of the reaction with respect to steam varies from 0 to 1 depending upon the temperature. Hydrogen has a strong inhibiting effect on the reaction and k_2 is large.

As noted, the electrofluid reactor is an electrically heated, fluidized bed of conducting solids. It offers several important advantages over other systems for carrying out reactions which are favored by high temperatures, require substantial energy inputs and, in addition, may involve reactants that are corrosive and difficult to contain. These advantages are due to the direct conversion of electrical energy to heat within the reacting system.

Johnson (8) was among the first to describe the characteristics and potential applications of the electrofluid reactor. He noted that Ohm's Law was obeyed except at high voltages where arcing occurred in the bed. Johnson and his coworkers have obtained patents on a number of processes which utilize the electrofluid reactor (9-15). These include processes for the manufacture of hydrocyanic acid, carbon disulfide, carbon monoxide and titanium tetrachloride.

The only report of a commerical application of an electrofluid reactor is in a process to produce hydrocyanic acid. In this process a bed of coke is fluidized with a mixture of ammonia and a hydrocarbon gas.

Goldberger, Hanway, and Langston (2) have reported development work on the electrofluid reactor. They suggested that its major potential uses lie in 1) the metallurgical field, 2) the chemical industry, particularly in organic chemical processing, and 3) as a high temperature gas heater. They found that the system could be rapidly heated and had excellent control properties.

A number of investigators have measured fluidized bed resistivities (3, 5, 6, 17, 20). They have concluded that the current flows along continuous chains of conducting particles. The bed resistivity increases with increasing gas velocity for settled beds. It passes through a maximum just after the incipient fluidization velocity is reached, and then decreases somewhat to a fairly constant value with further increase in gas flow rate.

Reed and Goldberger (20) studied the resistance of a fluidized bed of graphite. They found that the fluidized-bed behaved as a resistor element and that its resistance could be written as

$$R = \rho \cdot \frac{l}{A}$$

where ρ = resistivity

l = length of current path

A = cross-sectional area of current path.

Factors that caused break-up of particle chain linkages, such as vibration of the bed, were found to increase bed resistance. Arcing was observed at high current densities, greater than 2 amps per square inch, but did not affect the bed resistance in the range of variables investigated. These investigators observed a deviation in the voltage profile near the electrode and attributed this to the contact resistance. This resistance was strongly influenced by the condition of the electrode surface.

Apparatus

The apparatus consisted essentially of a batch-type, fluidized-bed reactor and a gas feeding and recycle system. The gas system could supply either steam or nitrogen or a mixture of these gases to the reactor at a measured but manually controlled rate. Nitrogen was used for fluidization during start-up and warm-up periods and in experiments where the basic characteristics of the system were being investigated. Steam, of course, was fed during the coal char gasification experiments. Since nitrogen is relatively expensive, a system was constructed to allow recycling of the nitrogen.

Figure 1 shows the equipment associated with the gasification experiments. Distilled water was fed at a constant rate through a calibrated, constant volume Zenith gear pump. It was vaporized in a double pipe heat exchanger and the resulting steam was conducted into the reactor.

The reactor was made of 4-in.-diam, 446 stainless steel pipe and is shown in more detail in Fig. 2. It was operated at atmospheric pressure. The steam entered the bottom of the reactor through a distributor. Both a porous Alundum plate and a capped, stainless steel pipe with four 1/8-in. holes drilled in it were used as gas distributors. Each of these was covered with a layer of ceramic pellets. The steam reacted with the carbon in the bed and the off-gases left at the top of the column. A sightport was situated at the top of the reactor, and a thermocouple well of Kanthal alloy projected into the bed from the bottom.

The reactor wall served as one electrode for internally heated runs and was grounded. The other electrode entered the bed through the top cover plate of the reactor and extended 12 in. into the unfluidized bed. It was centered in the reactor by a tube whose inside diameter was only slightly greater than the outside diameter of the electrode. This outside tube extended about 2 ft into the reactor.

An external furnace was provided to keep the outside wall of the reactor at the temperature of the bed so as to minimize heat losses. Kanthal tubular furnace elements and associated insulating materials were used to construct the external furnace.

The off-gases from the reactor first passed through a Pall Corporation high temperature, sintered, stainless steel filter where any entrained particles were removed. They were then cooled to about 50°F in a double pipe heat exchanger and any entrained moisture was removed in a knockout drum. The gases were then metered in a dry gas meter and vented to the atmosphere through a compressed air ejector.

Samples of the off-gases were withdrawn after the knockout drum and analyzed in a gas chromatograph. Provision was also made to take the dew point of the gases at this point.

A variable voltage transformer was used to manually control the voltage, and hence the temperature, in the reactor. An isolation transformer was installed in the line between the incoming power and the Variac. This allowed the reactor wall to be grounded.

Materials

Two different coal chars were used during this study. Five runs were conducted using a Rock Springs coal char supplied by the FMC Corporation from its COED process (18). The original coal came from the Rainbow No. 7 Mine of the Gunn-Quealy Coal Company, and was processed in a multistage fluidized-bed pyrolysis system using four levels of temperature, 600, 860, 990 and 1600°F. Three runs were made with a char produced from a Pittsburgh seam, high volatile bituminous coal. This material was supplied by the Institute of Gas Technology and was a hydrogasifier residue.

An analysis of the chars is shown in Table I and Table II shows the weight-size distribution of the two chars. The minimum fluidizing velocity of the FMC char between 1500 and 2000°F was about 0.0015 lb/min (0.024 ft/sec) of steam, while for the IGT char at 1600°F it was 0.0026 lb/min (0.0415 ft/sec).

Procedure

The reactor was first charged with coal char. A settled bed height of about 20 in. was used. The reactor was heated to the desired temperature using the external Kanthal heaters. During this time, nitrogen was circulated through the system. When the bed temperature reached the desired level, current was allowed

Table I. Analysis of coal chars.

Proximate analysis, wt %	FMC char	IGT char
Moisture	–	1.6
Volatile matter	4.0	2.9
Fixed carbon	89.8	79.1
Ash	6.2	16.4
Ultimate analysis, wt %		
Carbon	88.0	79.6
Hydrogen	1.0	1.21
Nitrogen	1.6	0.46
Sulfur	0.8	1.42
Oxygen	2.4	0.66
Ash	6.2	16.65
Ash to carbon ratio	0.071	0.209
Surface area		
Sq meters/g	40.0	500.0

(a) Proximate analysis on dry basis.

Table II. Differential screen analysis of chars.

Tyler mesh size	Wt % FMC char	Wt % IGT char
Greater than 20	5.3	15.8
20/28	12.6	22.4
28/35	12.2	21.0
35/48	16.4	15.3
48/65	16.6	12.4
65/100	15.4	7.9
100/150	11.3	2.4
150/200	6.1	2.4
Less than 200	3.6	0.5

to flow through the reactor. The power to the external heaters was then reduced to a low level. After the temperature of the bed had stabilized, the vent line was opened and the pressure at the outlet of the reactor was adjusted so that it was slightly less than atmospheric. The steam flow was then started. During the course of the run, the external heaters were adjusted to hold the wall of the reactor at a temperature near that of the bed. It was hoped that this would prevent any significant heat losses from the reactor.

During a run, the bed temperature, the off-gas flow rate, and the steam flow rate were recorded. The bed temperature was measured by the thermocouple in the bed, while the steam flow rate was calculated from the speed of the gear pump. The average off-gas flow rate was calculated from the amount of gas passing through a dry test meter in a known period of time. This rate did not include any unreacted steam as this was removed from the system before the meter. The off-gas was analyzed with the on-line chromatograph.

The current, voltage, and power supplied to the reactor were also noted. The voltage and power were measured directly on the appropriate type of electrical meter. The current varied in a rapid and erratic manner due to variations in the bed density. Therefore, the current was calculated using the measured voltage and power.

Results

Some results of a typical run which utilized fluidized bed resistance heating are shown in Figs. 3 and 4. This run was made at 1700°F with FMC char. The off-gas flow rate and composition remained essentially constant during most of the run. This was the case in all runs, even those in which all of the steam was not reacting. After 85 to 90 percent of the original carbon had reacted, the off-gas rate began to decrease. The amount of carbon dioxide and hydrogen in the gas began to increase at this point, while the percentage of carbon monoxide decreased. The percent of carbon gasified, then, increased at a constant rate during most of the run.

The resistance, current and voltage remained constant for a time after the start of the run, as shown in Fig. 4. Eventually the resistance of the bed began to increase, necessitating an increase in the voltage applied to the bed and causing a decrease in the current flow. The power input was fairly constant throughout the run. The trends exhibited in Fig. 4 are typical of the data collected in all of the runs. However, the resistance of the bed began to increase earlier in the runs made with IGT char than in those made with FMC char.

Table III summarizes the internally heated runs. Column 1 lists the eight runs and column 2 shows the type of char used. The operation of the electrofluid reactor was investigated at various temperatures and several steam flow rates and these are shown in columns 3 and 4. As noted previously, the reactor was operated in a batch-wise manner and the number of hours of operation are shown in the next column. Five electrode materials were tested, and these appear in column 6.

Column 7 shows the amount of char charged to the reactor. An initial bed height of 20 in. was used in each run and this was obtained by using either 2000 g of FMC char or 1000 g of IGT char. The next four columns give the amount of char left in the reactor and filter after the run, and its carbon composition. The char in the filter is material that was entrained in the off-gas during the course of the run. It contains a fairly high percentage of carbon and apparently is mostly fines from the original charge. In the next column is reported the percent of the original carbon that was gasified. This was calculated from the results in the previous five columns.

Column 13 shows the total amount of water removed from the off-gas in the knock-out drum during the course of the run. This was essentially all of the unreacted water since the gases contained very little water vapor beyond this point. The average fraction of the entering water being converted in the reactor is reported in column 14. The value listed was measured during the portion of the run when the off-gas rate was relatively constant (see Fig. 3).

Table III. Summary of internally heated runs.

Run number	Source of char	Bed temp (°F)	Steam flow rate (lb/min)	Hours ran	Electrode material	Char charged (g)	Char residue: Reactor wt (g)	Reactor wt % (C)	Filter wt (g)	Filter wt % (C)
10	FMC	1500	0.0085	10.5	Carbon	2044	1433	88.7	27	79.8
11	FMC	1600	0.0085	7.5	Copper	1917	1232	89.8	20	89.4
9	FMC	1700	0.0085	9.8	Carbon	1967	191	58.5	114	88.1
13	FMC	1900	0.0085	8.0	Tungsten	2000	234	59.9	123	71.8
7	FMC	1960	0.0085	9.8	Carbon	2136	205	52.0	158	90.0
24	IGT	1600	0.0245	6.3	Carbon	1000	456	59.0	42	61.7
25	IGT	1600	0.0245	8.0	Tantalum	1000	320	44.0	76	69.2
28	IGT	1600	0.0245	6.0	Molybdenum	1000	459	62.6	50	78.2

Carbon gasified (%)	H_2O condensed (g)	Avg fraction of H_2O converted	Off-gas produced (SCF)	Avg off-gas rate (SCF/min)	Avg off-gas composition (vol %): H_2	CO	CO_2
27	1514	0.34	90.2	0.12	57	15	23
33	676	0.60	85.7	0.19	59	20	19
88	156	1.00	222.0	0.41	53	46	1
87	0	1.00	220.5	0.39	54	41	1
87	0	1.00	240.5	0.43	54	45	1
62	2763	0.25	74.1	0.19	57	17	26
75	3562	0.27	85.2	0.11	57	30	11
58	1467	0.65	39.2	0.11	58	23	16

The total off-gas produced during the run, excluding any unreacted water, and the average rate of production of off-gas are shown in the next two columns. The average off-gas rate is the rate during the period when it was relatively constant. The average composition of the off-gas is shown in the last three columns. Again, this is the composition during the time when the off-gas rate was constant. As can be seen, the off-gas was generally 50 to 60 percent hydrogen. At 1500°F there were equal amounts of carbon monoxide and carbon dioxide present. As the temperature was increased, the concentration of carbon dioxide in the off-gas decreased, and above 1700°F the off-gas contained less than one percent CO_2. The gas also contained very small amounts of methane and nitrogen which are not shown in the Table.

The energy losses from the reactor were large despite the fact that the external heaters were used. The energy supplied to the reactor via internal heating was 4 to 8 times the amount required by the reaction and that needed to heat the steam to the reactor temperature.

Discussion of Results

Rate of Reaction

Both the FMC and IGT chars gave about the same off-gas rate at 1600°F. This indicates that they are about equally reactive since the off-gas rate is an indication

of the reaction rate in runs in which all of the steam is not consumed. Also, since the off-gas rate was fairly constant throughout all the runs, the reaction rate apparently increased with carbon burn-off for both chars. The data shown below from run 24 bear this out.

Carbon burn-off (%)	Specific gasification rate ($\frac{\text{lb C gasified/hr}}{\text{lb C in bed}}$)
7.6	0.12
19.2	0.12
29.7	0.14
39.2	0.15
48.1	0.17
57.1	0.21

Other investigators have reported a similar increase in specific gasification rate with carbon burn-off (4, 16).

The gasification rates for the FMC and IGT chars are similar to those found in other studies where a low temperature char was gasified in a fluidized bed. May, et al. (19), obtained gasification rates at 1600°F between 0.05 and 0.12 lbs of carbon per hour per lb of carbon in the bed, while Goring, et al. (4), reported values between 0.07 and 0.10.

To determine if the passage of electric current through the bed affected the reaction rate, and hence off-gas rate, a few runs were made with external heating alone. These runs are summarized in Table IV along with the appropriate internally heated runs. The data indicate that any effect of internal heating was small as the variations between runs at the same conditions, except for method of heating, were of the order of 20 to 30 percent. These variations are similar to those found between runs using the same heating method and are within experimental error.

Table IV. Comparison of externally and internally heated runs.

Run no.	Type of heating	Bed temp (°F)	Steam flow rate (lb/min)	Hours ran	Char to bed (g)	Carbon gasified (%)	Off-gas produced (SCF)	Average off-gas rate (SCF/min)
10	INT	1500	0.0085	10.5	2044	27	90.2	0.12
15	EXT	1500	0.0085	51.5	2009	74	255.5	0.10
11	INT	1600	0.0085	7.5	1917	33	85.7	0.19
17	EXT	1600	0.0085	22.0	2005	91	289.5	0.23
24	INT	1600	0.0245	6.3	1000	62	74.1	0.19
25	INT	1600	0.0245	8.0	1000	75	85.2	0.11
28	INT	1600	0.0245	6.0	1000	58	39.2	0.11
26	EXT	1600	0.0245	8.3	1000	51	40.6	0.09

Electrical Properties

As noted, the resistance, current and voltage remained constant for a time after the start of each run. During this time, the resistance between the center electrode and the wall was about 3 ohms. It then began to increase slowly and reached a value between 8 and 10 ohms near the end of the run. This increase in bed resistance was probably caused both by an increase in the resistivity of the bed material as the carbon content of the particles was depleted, and by a decrease in bed height. (This decrease in height decreased the contact area between the electrode and bed.) As the resistance of the bed increased, the current flowing through the bed decreased. Therefore, to maintain a constant power input to the reactor, the voltage had to be increased. The data do show that the power input to the reactor was fairly constant. In some of the runs, the power required decreased late in the run as the reaction rate decreased. The resistance also increased at this point to a value near 30 ohms.

The behavior of the bed resistance during the runs resembled the variation of bed resistance measured as a nonconductor is added to a bed of conducting material (1, 21). In this latter case, fluidized beds containing 50 percent or more of nonconducting material had to be prepared before the resistance of the original graphite bed was greatly increased. Concentrations of nonconducting material greater than 50 percent caused the bed resistance to increase rapidly and nonlinearly.

The increasing concentration of the nonconducting ash, then, is one of the causes of the rise in the fluidized bed resistance. However, there is a large variation between runs in the ash to carbon ratio in the bed at the point that the bed resistance began to increase (see Table V). (The increase referred to here occurred at about 410 minutes for run 9.)

Table V. Ash to carbon ratios at time that bed resistance began to increase.

Run	Carbon burn-off (%)	Ash to carbon ratio in bed
7	54	0.16
9	66	0.23
11	23	0.09
13	46	0.13
24	29	0.29
25	31	0.30
28	17	0.25

Examination of the current and voltage plots indicate that the power factor for the system was near one. It should also be noted that although the current tended to fluctuate rapidly, no difficulties were experienced in controlling the power supplied to the reactor. This meant that the temperature of the reactor was held quite constant.

Electrode Materials

Six different electrode materials (0.5 in. diam) were tried during the course of the study. Figure 5 shows some of the electrodes used with the FMC char. Those shown are:

Electrode A: 446 stainless steel pipe, used at 1900°F for 1.5 hrs. The end melted off.

Electrode B: Copper pipe, used at 1600°F for 2.7 hrs. The pipe corroded badly and finally melted.

Electrode C: Carbon rod, used at 1960°F for 10 hrs (run 7). The attack on the rod was slight. However, all the steam was being reacted in this run.

Electrode D: Tungsten rod, used at 1900°F for 8 hrs (run 13). This electrode was not attacked. However, 100 percent of the steam was being converted.

Figure 6 shows three electrodes used in internally heated beds of IGT char. The electrodes, from top to bottom, are tantalum, carbon and molybdenum rods. Each of these rods were used in runs at 1600°F for between 6 and 8 hrs (runs 24, 25 and 28). Both the tantalum and carbon rods were severely attacked and each suffered about a 25 percent weight loss. The molybdenum rod did not lose any weight.

A rough coating was formed on the electrodes used with the IGT char. This can be seen on the carbon and molybdenum rods in Fig. 6. This coating appears to be at least partly ashy material and did not form when FMC char was used. Presumably the higher ash content of the IGT char accounts for the formation of the coating. A second run was made with the molybdenum rod at the same conditions. The overall resistance between the electrodes did not change and, despite the coating, no difficulties were encountered in using the rod.

The copper and stainless steel pipes (electrodes A and B in Fig. 5) both melted at bed temperatures well below their melting points. Evidently, the electrodes were at least several hundred degrees hotter than the bed. The temperature difference between the electrode and bed was measured as a function of the power input to the reactor and gas flow rate and the results are shown in Fig. 7. The electrode temperature was measured with a shielded thermocouple which was inserted into the ½-in. stainless steel pipe that served as the electrode during this run. Ceramic insulators were placed between the thermocouple and the electrode. The bed temperature was held constant at 1500°F during the run and was fluidized with nitrogen.

The temperature difference increased with power input almost linearly between 0 and 4 kilowatts. The gas velocity did not seem to have a significant effect on the temperature difference. The exact reason for the temperature difference is as yet unknown.

Conclusions and Future Work

The investigation to date has shown that it is technically feasible to gasify coal char with steam in an electrofluid bed reactor. The production rate of synthesis gas was high and operating temperatures in the range of 1600 to 1800°F seem feasible. The resistance of the fluidized bed of coal char allowed use of reasonable applied voltages and temperature control of the reactor was not a problem.

The investigation is being continued and a 12-in.-diam, continuous reactor is being constructed to further study and develop the process. This reactor will be 32 in. high and will operate at temperatures approaching 2000°F. Coal char will be fed to the reactor with a Vibrascrew feeder and solids will be removed from the bottom of the bed and/or through an overflow tube. The electrode arrangement in this reactor will be similar to the one previously used, although another arrangement may be used at a later date. During operation of the continuous reactor, attention

will also be given to methods of power control and to the development of suitable electrodes.

Acknowledgment

This work was supported by the Engineering Research Institute, Iowa State University, through funds made available by the Office of Coal Research, U.S. Department of Interior under contract No. 14-01-0001-479.

Literature Cited

1. Damm, F., "Electrical Resistivity of Fluidized Beds of Conducting and Non-Conducting Particles." Chemical Engineering Department, Iowa State University, Ames, Iowa (May 24, 1965).

2. Goldberger, W. M., Hanway, J. E., Jr., and Langston, B. G., CEP 61, 63 (Feb 1965).

3. Goldschmidt, D. and LeGoff, P., Chem. Eng. Sci. 18, 805 (1963).

4. Goring, G. E., Curran, G. P., Tarbox, R. P. and Gorin, E., Ind. Eng. Chem. 44, 1051 (1952).

5. Graham, W. and Harvey, E. A., Can. J. Chem. Eng. 13, 146 (June 1965).

6. Ibid., 14, 17 (1966).

7. Huebler, J. and Schora, F., CEP 62, 87 (Feb 1966).

8. Johnson, H. S., Can. J. Chem. Eng. 39, 145 (1961).

9. Johnson, H. S. Electrothermic Fluidized Bed Apparatus. U.S. Patent 3,006,838 (Oct 31, 1961).

10. Johnson, H. S. and Andersen, A. H., Process for Preparation of Hydrocyanic Acid. Canadian Patent 573,348 (March 31, 1959).

11. Ibid. Process for Preparation of Carbon Monoxide. U.S. Patent 2,921,840 (Jan 19, 1960).

12. Ibid. Process for the Preparation of Titanium Tetrachloride. U.S. Patent 2,948,587 (August 9, 1960).

13. Ibid. Process for Preparation of Hydrocyanic Acid. U.S. Patent 2,958,584 (Nov 1, 1960).

14. Ibid. Process for Preparation of Carbon Disulfide and for the Desulfurization of Coke. U.S. Patent 3,009,781 (Nov 21, 1961).

15. Johnson, H. S. and Reid, J. Process for Preparation of Carbon Disulfide. U.S. Patent 3,034,863 (May 15, 1962).

16. Jolley, L. J. and Pohl, A., J. Inst. Fuel 26, 33 (1953).

17. Jones, A. L., "Electrical Resistivity of Carbon Granules in a Fluidized Bed." Unpublished Ph.D. Thesis. Library, Iowa State University, Ames (1966).

18. Jones, J., Eddinger, R. T. and Seglin, L., CEP 62, 73 (Feb 1966).

19. May, W. G., Mueller, R. H., Sweetser, S. B., Ind. Eng. Chem. 50, 1239 (1958).

20. Reed, A. K. and Goldberger, W. M., Chem. Eng. Progr. Symposium Ser. No. 67, 62, 71 (1966).

21. Schakel, L., "Electrical Resistivity of Fluidized Beds of Conducting and Non-Conducting Particles." Chemical Engineering Department, Iowa State University, Ames (August 14, 1964).

22. Von Fredersdorff, C. G. and Elliott, M. A., Chemistry of Coal Utilization, H. H. Lowry, Ed., John Wiley and Sons, New York, 1963, Supplementary Volume, pp. 892-1022.

23. Walker, P. L., Jr., Rusinko, F., Jr., and Austin, L. G., Advances in Catalysis, O. D. Eley, P. W. Selwood, and P. B. Weisy, Ed., Academic Press, Inc., New York, 1959, Vol. XI, pp. 133-221.

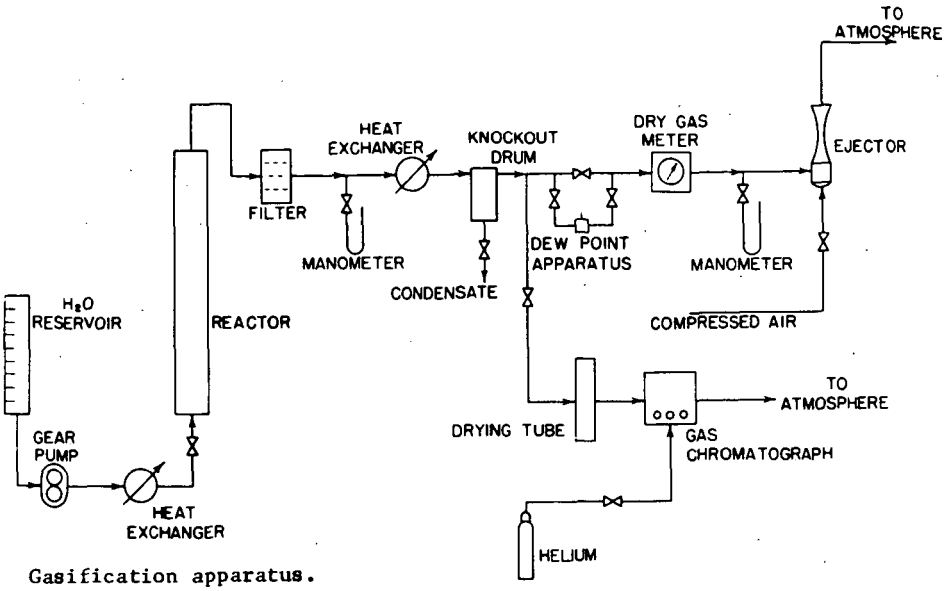

Fig. 1. Gasification apparatus.

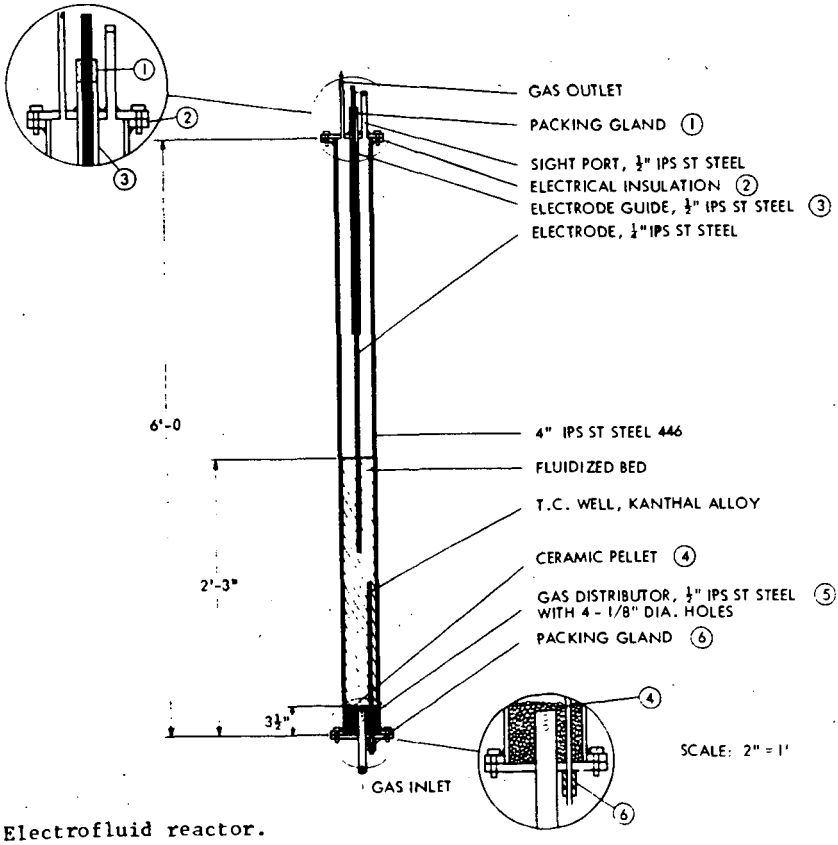

Fig. 2. Electrofluid reactor.

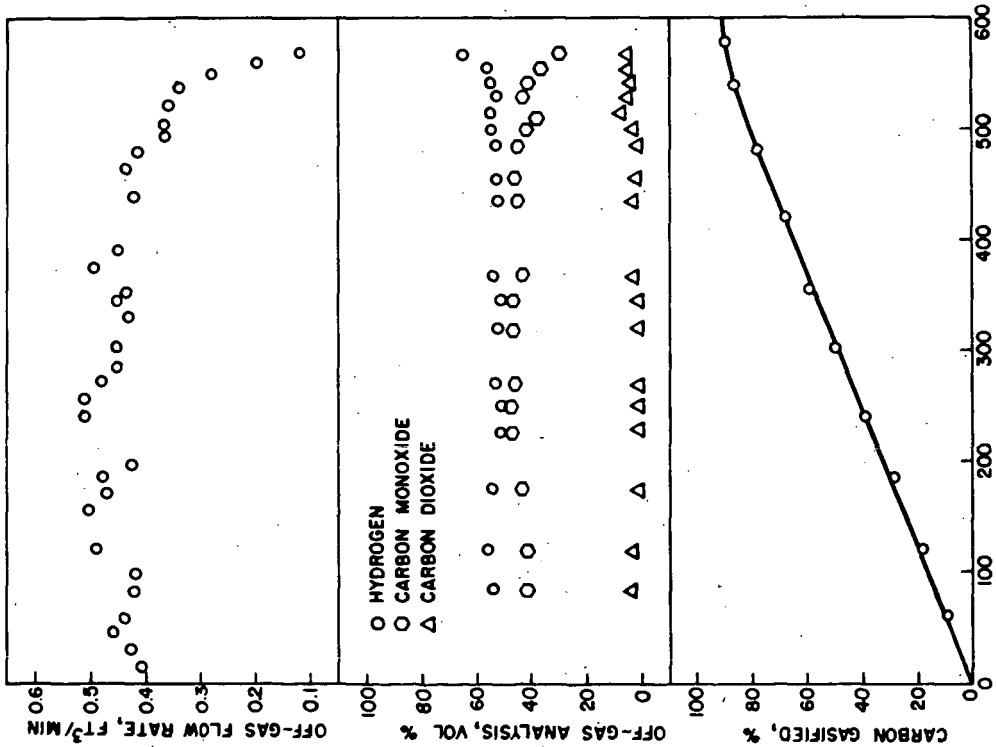

Fig. 3. Off-gas flow rate and composition and percent carbon gasified during Run 9.

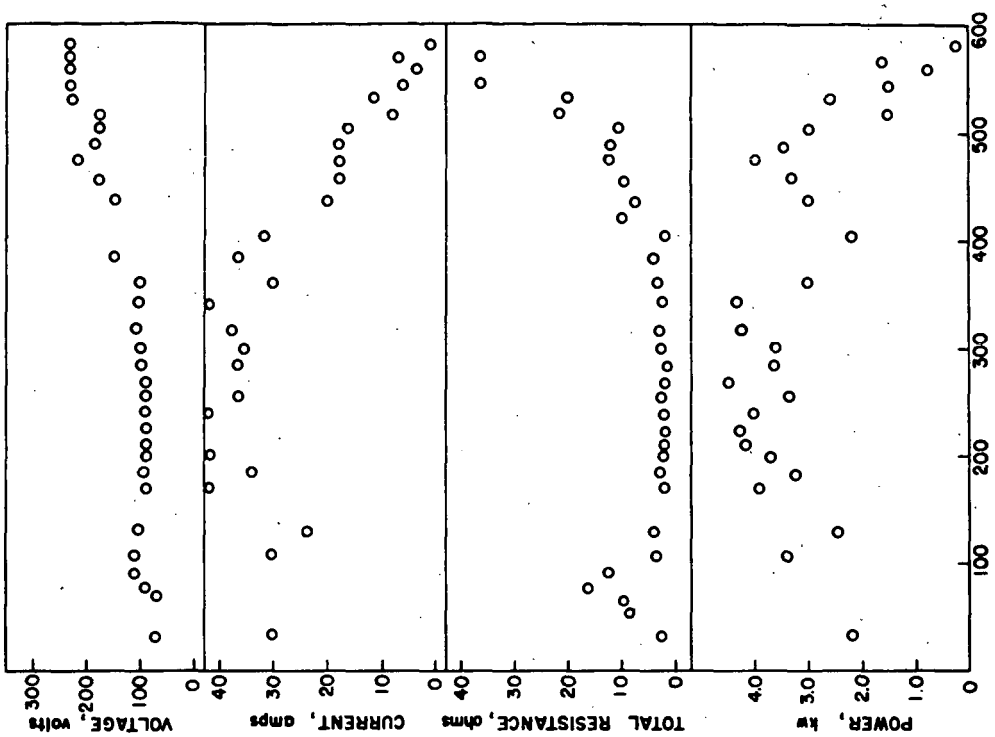

Fig. 4. Electrical properties of system during Run 9.

Fig. 5. Electrodes used with FMC char.

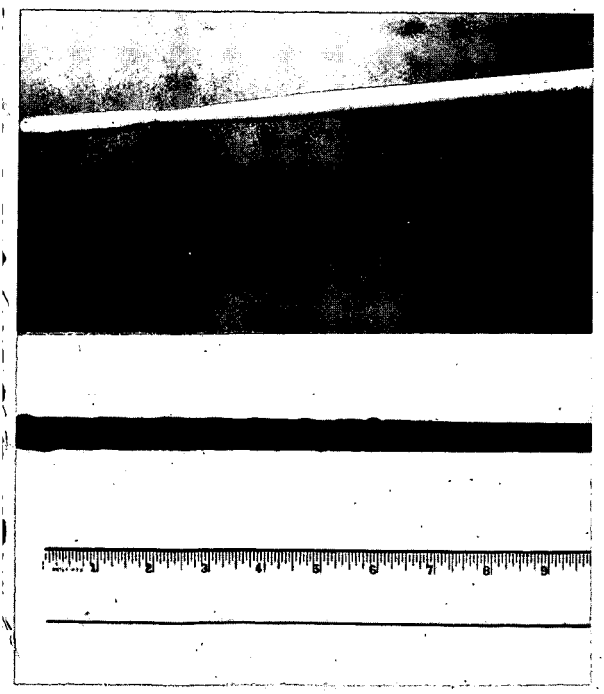

Fig. 6. Electrodes used with IGT char.

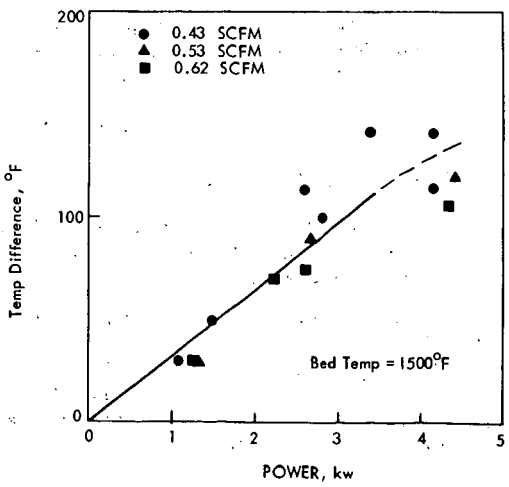

Fig. 7. Temperature difference between bed and electrode.

KINETICS OF LIGNITE CHAR GASIFICATION - ITS RELATION TO THE CO_2 ACCEPTOR PROCESS

G. P. Curran, C. E. Fink, and Everett Gorin

Research Division
Consolidation Coal Company
Library, Pennsylvania 15129

INTRODUCTION

The basic features of the CO_2 acceptor gasification process have been described in a series of recent publications. The general nature of the process was described, heat and material balances presented,[1,2,3] and the operating limitations of the process as determined by the thermodynamic properties of individual reactions of importance were discussed.[1] A more detailed discussion of the properties of dolomite and limestone based acceptors as dictated by the needs of the process was presented in a more recent publication.[4]

Due to thermodynamic limitations of the acceptor reactions, the maximum permissible temperatures and pressures for operation of the gasifier are approximately 1670°F and 380 psia, respectively. In general, it is desirable to operate the process below these extreme limits.

The kinetics of the gasification of chars from Pittsburgh Seam bituminous coals had been studied in some detail previously.[5] The gasification rates obtained are likely adequate for operation of the CO_2 acceptor process with bituminous coal chars provided partial gasification is practiced with low sulfur boiler fuel[6] as a byproduct. The gasification rates are, however, inadequate for total gasification of bituminous coal chars.

The emphasis on the development of the CO_2 acceptor process has, therefore, been on the use of lower rank Western coals, and in particular lignite chars, because their known higher reactivity makes them more suitable for the process.

The experimental techniques and methods of processing the data will be only briefly described here. Full details will be available in a report to be submitted to the Office of Coal Research in the near future.

Experimental and Calculational Procedures

Integral Batch Kinetics

The data were obtained in a fluidized bed unit which was operated batchwise with respect to solids and continuously with respect to the gas feed. The unit is illustrated schematically in Figure 1.

Char feedstocks were prepared by carbonizing the raw, dried lignites in N_2 at 1050°F at atmospheric pressure. The chars were devolatilized further by heating in a fluidized bed in H_2 at 1400°F for one hour at atmospheric pressure. The latter treatment also calcined the $CaCO_3$ and reduced the iron compounds which were present in the ash. The 35 x 65 mesh size fraction was used. Analyses of the prepared lignite chars are given in Table Ia.

Most of the runs were made with one of two initial char bed weights of either 5 or 10 grams. The char was mixed with 200 x 325 mesh fused periclase in order to hold a nearly constant fluidized bed height of 2-1/2 inches, regardless of the initial char weight or burnoff level.

The reactor consisted of a 7" x 1" I.D. Type 310 stainless steel thin-walled tube having a conical sealed end. The reactor with its heating elements and insulation was contained within a pressurized one-liter autoclave. Nitrogen was used as pressure balancing gas.

The temperature control point was a calibrated thermocouple contained in a well immersed in the fluidized bed. Axial traverses showed that the temperature throughout the bed was 1500° ± 2°F.

The inlet dry gases were preblended mixtures of H_2, CO, CO_2 and CH_4 in the desired proportions. The metered dry gas was passed through a steam generator in which the water temperature was controlled (± 0.2°F) to give the desired steam partial pressure. CO_2 was added to the dry gas mixtures in order to bring the composition of the total inlet gas to water-gas shift equilibrium. Otherwise, the partial pressures of the inlet H_2O, H_2 and CO would have been altered appreciably by shifting, catalyzed by the reactor surfaces and the char bed.

The total inlet gas entered the reactor through an axial diptube which extended to the bottom of the cone. The gas passed downward, reversed direction, and fluidized the bed. The superficial fluidizing velocity was held in the range, 0.14-0.18 ft/sec depending on the pressure level and gas composition in order to give a bed expansion of about 30% over the incipient fluidized bed height.

The exit gas was cooled to condense the unreacted steam, which was then throttled to atmospheric pressure and collected in the condensate receiver. The dry exit gas, after being throttled to atmospheric pressure, passed through the condensate receiver to pick up the dissolved gases which had flashed from the condensate. Most of the H_2S was removed by an acidified $Cd(NO_3)_2$ solution which had been charged initially to the condensate receiver. One side stream of the dried gas was diverted through a sample loop where, typically, a sample was taken every 12 minutes for analysis by gas chromatography. Another was diverted through a thermal conductivity cell which continuously monitored the exit gas composition in reference to the inlet dry gas. The diverted streams were recombined, saturated with water, and passed through a calibrated wet test meter.

In the runs where the inlet dry gas contained carbon oxides and/or CH_4, the dual-column gas chromatograph was operated differentially. Samples of the inlet dry gas and exit gas were simultaneously injected into their respective columns and the outputs of the thermal conductivity detector cells were arranged to give signals which were proportional to the differences in concentrations of CO, CO_2, and CH_4 in the two gas streams.

In all the runs the char was pretreated by fluidizing in pure H_2 for one hour at 1400°F and at 6 atm system pressure. During this period, 8.0% of the carbon in the feed char was reproducibly gasified.

The kinetics portion of the run was then started by raising the system pressure to the desired level, increasing the bed temperature to 1500°F, and replacing the hydrogen flow with the desired flows of steam and inlet dry gas. These operations, performed in the order given, were completed in about one minute.

At the end of a run the bed was rapidly cooled and removed from the reactor. The entire bed, i.e., char plus diluent was assayed for its carbon content.

It was found necessary to presulfide the reactor and char bed to eliminate spurious effects due to catalytic formation of methane or its hydrolysis, depending upon which side of equilibrium the gas composition in the reactor corresponded to in the reaction

$$CO + 3\,H_2 = CH_4 + H_2O \qquad (1)$$

With a presulfided system, all methane produced was derived from gasification of the char. Presulfiding was accomplished by passing a 1% H_2S-99% H_2 mixture through the system for one hour at 1200°F and at atmospheric pressure before the pretreatment period was started.

The integral gasification rates at time θ reported here are defined below:

$$R_T = \frac{\text{total mols of carbon gasified/min} \times 10^4}{\text{atom of carbon in bed}} = \frac{N \times 10^4}{w_o - \int_o^\theta N d\theta}$$

$$R_{CH_4} = \frac{\text{total mols } CH_4 \text{ formed/min} \times 10^4}{\text{atom of carbon in bed}} = \frac{N_{CH_4} \times 10^4}{w_o - \int_o^\theta N d\theta}$$

$$R_C = R_T - 2 R_{CH_4}$$

The carbon oxides rate, R_C, is defined as above because, as will be shown later, the reaction model for methane formation requires that a mol of CO be produced for each mol of methane formed.

N and N_{CH_4} in the above equations are the respective mols of total carbon gases and methane formed per minute from char gasification. They are calculated from the inlet and exit dry gas rates and their compositions at time θ. W_o is the atoms of carbon in the bed at time $\theta = 0$, i.e., just after the pretreatment period is completed. The carbon burnoff is calculated from the equation,

$$\% \text{ Burnoff} = \frac{100 \int_o^\theta N d\theta}{W_o}$$

Typical run data and calculations are illustrated in Table II.

Differential rate data are obtained from the two integral rates corresponding to initial char bed weights of 5 and 10 grams by linear extrapolation to zero bed weight.

Integral Rate Data from Continuous Unit

The continuous unit for obtaining integral rate data was described earlier.[4] Two methods of operation were employed. In one, the CO_2 acceptor was circulated through the gasifier. In the other, no acceptor was used. The latter involved operation only of the gasifier, but with continuous feed of hydrodevolatilized char and continuous withdrawal of partially gasified char.

The former operation involved operation of both the regenerator and gasifier vessels. The acceptor was continuously showered through the gasifier bed. The acceptor, segregated in the bottom of the gasifier as a separate phase, was withdrawn continuously and recirculated through the regenerator.

The gasifier was a 4" I.D. vessel and the char bed height was controlled by means of an overflow weir. The bed height in most kinetic runs was 40 inches.

The feedstocks were crushed to -35 mesh and dried with inert gas in a fluid bed at 500°F. The drying was conducted in such a way that almost all the -150 mesh particles were removed by elutriation.

The dried and elutriated feed was then hydrodevolatilized at 1500°F and about one hour residence time in a separate run in the continuous unit. The inlet gas composition was adjusted to simulate that in the corresponding step in the commercial version of the CO_2 acceptor process[3] wherein the partial pressure of hydrogen is about 6 atm. This was done by adding steam and hydrogen and recycling the make gas in the proper proportions.

Analyses of the hydrodevolatilized feedstocks are given in Table Ib.

The composition of the inlet gas during the kinetic runs was controlled by recycle of the product gas. The inlet dry gas was passed through a steam generator in which the water temperature was controlled to give the desired inlet steam partial pressure.

The inventory of carbon in the bed was determined from the bed weight and analysis of the product char. The composition of the product gas was semi-continuously monitored by sampling the dry product gas. Analyses were made with the same gas chromatograph equipment used for the batch kinetics program. The product char was sampled for analysis only when the unit had reached steady state, as evidenced by constant exit gas composition.

The bed weight was determined by ΔP measurement across the fluid bed. The gasification rate was determined from dry exit gas analysis and the metered exit gas rate. The integral gasification rates are then determined as follows when no acceptor is present:

$$R_T = \frac{\text{mols exit gas/min x mol fraction of total carbon x } 10^4}{\text{atom carbon in bed}}$$

$$R_{CH_4} = \frac{\text{mols exit gas/min x mol fraction of } CH_4 \text{ x } 10^4}{\text{atom carbon in bed}}$$

When acceptor was used, correction had to be made in R_T for CO_2 picked up by acceptor. Also, in these instances, CO_2 usually was added to the inlet gas and thus had to be deducted from the total carbon in the outlet gas in calculating R_T.

Results and Discussion

Batch Integral Data

Preliminary experiments showed that the subsequent gasification rates were relatively insensitive to the gas atmosphere or time of pretreatment. The particular procedure used was accepted as a standard because of its simulation of the hydrodevolatilization step in the projected commercial version of the process.

Integral rate data for R_C and R_{CH_4} are shown for several lignite chars in Figures 2 and 3, respectively. All data were obtained at 1500°F and 16 atmospheres total pressure using two different hydrogen steam mixtures in the feed, i.e., 62% H_2-38% H_2O and 32% H_2-68% H_2O. These two values correspond roughly to the H_2/H_2O ratios existing at the top and bottom, respectively, of the projected commercial version of the process. No CO was added and, as we will show later, this strongly inhibits the gasification rates. The rates shown therefore are higher than would be anticipated in practice.

The Renner Cove char is unusual for its high reactivity relative to the other lignite chars. Analyses in Table I show that this lignite is particularly high in sodium. After extraction of 90% of the sodium from this char with hot water, the reaction rates were reduced to a level comparable with those of the other lignite chars. The high reactivity of the Renner Cove char thus may be attributed to a high level of catalysis by sodium.

The high inhibiting effect of H_2 for the carbon oxides rates, R_C, is also noted and is in accord with prior observations on bituminous coal chars.[5] The total gasification rate actually is higher at 1500°F than the rates of gasification of bituminous coal chars previously observed under comparable conditions at 1700°F. Thus, it is clear that lignites are eminently suitable for use in the CO_2 acceptor process from the point of view of reactivity.

The methane rate, R_{CH_4}, in all cases decreases monotonically with increasing carbon burnoff. The behavior of the carbon oxides rate, R_C, is more complex. It increases with burnoff in most cases at low levels of H_2 inhibition. It tends to show the reverse behavior at high levels of hydrogen inhibition. Although in some cases, a maximum rate is observed at low burnoffs, i.e., up to 35% burnoff.

Differential Rate Data

All the differential rates were obtained with Renner Cove char at 1500°F. The tabulated data for both R_C and R_{CH_4} are given in Table III. These data span the gas compositions to be expected at the top and bottom of the gasifier in the commercial process and for total pressures of 11 and 20 atm. There is one exception, however, in that no CH_4 was added to the inlet gas. Separate runs were, therefore, made to determine the effect of CH_4 inhibition on the rates. These data are given in Table IV.

Correlation of Data

Inspection of the data in Table III clearly shows the strong inhibition by CO on both R_C and R_{CH_4}. To account for the inhibition of the methane formation rate by both CO and CH_4, the following reaction was used as a model to arrive at a suitable correlation.

$$2\,C + H_2 + H_2O = CH_4 + CO \qquad (2)$$

The rate controlling step in the above overall reaction was assumed to be the reaction of absorbed H_2 and H_2O on adjacent carbon sites to produce absorbed oxygen and CH_4.

For the carbon oxides rate, the model reaction was,

$$C + H_2O = CO + H_2, \qquad (3)$$

with the rate controlling step assumed to be the reaction of absorbed H_2O with an adjacent empty carbon site to produce absorbed oxygen and H_2.

Rate equations are readily developed for each case using the standard Langmuir isotherms to represent the fraction of the surface covered with each absorbed gas. The corresponding rate equations are given below:

$$R_C = \frac{k\left[P_{H_2O} - \frac{P_{CO}\,P_{H_2}}{K}\right]}{\left[1 + K_1P_{H_2O} + K_2P_{H_2} + K_3P_{CO}\right]^2} \qquad (4)$$

$$R_{CH_4} = \frac{k'\left[P_{H_2O}P_{H_2} - \frac{P_{CH_4}\,P_{CO}}{K}\right]}{\left[1 + K'_1P_{H_2O} + K'_2P_{H_2} + K'_3P_{CO} + K'_4P_{CH_4}\right]^2} \qquad (5)$$

The negative terms in the numerators correspond to the retardation by the reverse reactions.

It is clear from Reaction (2) why R_C is defined as equal to $R_T - 2\,R_{CH_4}$. This is because, by the proposed mechanism, one mol of CO accompanies the formation of every mol of methane.

The constants in the above rate equations were determined from the experimental data using a non-linear least squares technique. The necessary iterative calculations were made with the aid of a digital computer.

The values of the constants thus determined are listed as a function of carbon burnoff in Table V. The agreement between the calculated and observed rates for both R_C and R_{CH_4} is shown in Tables III and IV.

The effect of the reaction, $C + CO_2 = 2\ CO$, on R_C has been neglected in the runs in which CO_2 was a component of the inlet gas. This reaction is slow relative to the steam-carbon reaction and it is strongly inhibited by CO. The data of Blackwood and Ingeme[7] taken on the reaction of CO_2 with a reactive coconut shell charcoal show that, at the conditions used in the present work, much less than 1% of the observed values of R_C could have been contributed by gasification with CO_2.

The correlating equations must be regarded as semi-empirical. The constant, K, in Equation (4) for R_C has values considerably smaller than the equilibrium value of 9.2 at 1500°F for the reaction,

$$\text{graphite} + H_2O = CO + H_2.$$

This is unexpected and no explanation is advanced here.

In the methane addition runs, the product, $P_{CO}\ P_{CH_4}$, was too small to allow evaluation of the constant, K', in Equation (5). Therefore, the equilibrium value of 0.388 for the reaction,

$$2\ \text{graphite} + H_2 + H_2O = CH_4 + CO,$$

has been assigned tentatively.

If the same active sites are involved in both reactions, then methane should be an inhibitor for the carbon oxides reaction as well as for the methane formation reaction. The data in Table IV show that this is not the case.

Finally, the values of K_1, K_2 and K_3 should be the same as those for K'_1, K'_2 and K'_3. As Table V shows, the values are similar, but not identical.

The effects of the principal variables on the carbon oxides rate, R_C, are illustrated by the curves of Figure 4, derived from Equation (4). The strong inhibiting effects of both H_2 and CO are shown for the 20% burnoff level. Similar effects exist at other burnoff levels. Figure 4 also shows that Equation (4) predicts that the rates go through a maximum with increasing total pressure at constant gas composition. The experimental data of this study do not fall in the region of the maxima. The validity of Equations (4) and (5) has, however, been confirmed by their use to correlate the rate data of the earlier study[5] for bituminous coal char at 1600° and 1700°F with an average deviation of ± 20%. The range of total pressure in the earlier work was 1-30 atm, but the effect of CO on the differential rates was not studied.

The strong inhibition by CO and CH_4 on the rate, R_{CH_4}, is shown in Figure 5 for the 20% burnoff level. As with R_C, similar effects exist at other burnoff levels.

The effects of H_2 and total pressure on R_{CH_4} are illustrated in Figure 6. There is an optimum value of the ratio H_2/H_2+H_2O in the range of 0.4-0.5, depending on the particular values of the other variables. In contrast with R_C, Equation (5) shows that R_{CH_4} continues to increase with increasing total pressure at constant gas composition, but approaches a limiting value beyond the range of the experimental data.

Equation (5) also predicts that R_{CH_4} will decrease to zero with a gas composition of 100% H_2. Actually, considerable gasification does occur at this condition through another reaction, $C + 2\ H_2 = CH_4$. However, a run not otherwise reported here showed that Equation (5) remains valid at values of the ratio H_2/H_2+H_2O up to 0.9.

Integral Rate Data from Continuous Unit

The bulk of the operations in the continuous unit were aimed at a study of operability problems and problems related to handling of the acceptor rather than kinetics. In most cases the feedstocks used were different from the particular lignite (Renner Cove) for which differential rate data were available. Limited operations were, however, carried out with a high sodium lignite (Glenharold) from the same geographical area and from the same Fort Union deposit. Thus, in this case direct comparison with the differential data is possible.

Predictions of integral rate data from differential data is difficult in fluidized systems, since the gas flow pattern is unknown. Complications exist due to gas back mixing and bypassing of the bed by the bubbles which form. It is to be expected, however, that in a smoothly operating fluid bed such as one obtains in pressure operation that the integral rate will lie somewhere between the differential rate predicted for the bottom and top of bed conditions. A summary of the conditions and feedstocks used in the operations and integral rates obtained are given in Table VI.

Unfortunately, a direct comparison between predicted rates from the correlation of differential data is only possible in the case of two of the runs with Glenharold char, i.e., K-1-1 and K-1-2 as shown in Table VII. It is seen that the values of R_C tend to be close to but somewhat higher than the predicted values at the outlet conditions.

A comparison of Run K-1-1 with Run K-1-3 shows the powerful effect of a small increase in temperature of 30°F on rate.

The second group of runs in Table VII shows the effect of using less reactive lignite feedstocks on rate. These runs were made with the acceptor circulating through the bed, which reduces the CO_2 pressure and consequently also the CO pressure by virtue of water-gas-shift reaction. The reduction in inhibiting effect of CO thus compensated for the use of less reactive chars as seen by comparison of Run A-28 (Glenharold char with most of the sodium removed by water washing) with Run K-1-1. The lower reactivity is evidenced, however, by the comparison of the observed rates with those calculated for the more reactive chars. The rates in this case tend to be somewhat lower as expected with one exception (Run A-21) than those calculated even at the outlet conditions.

The results in Tables VI and VII again illustrate the increase in rate effected by reduction in pressure from 20 to 11 atm. They also show the large increase in rate effected by increase in temperature to 1600°F. It should be remarked here, that at 1600°F the operating pressure must be maintained at 20 atm to achieve adequate CO_2 partial pressure for the CO_2 acceptor reaction, even though the rate increases on lowering the pressure.

Data for a few runs with subbituminous chars are given in Table VI. It is seen by a comparison of Runs D-2A and D-2B with Run A24-1 that the reactivity of the subbituminous chars is similar to that of the low-sodium lignite char (Husky II).

A minimum rate for commercial operation is of the order of

$$\frac{50 \times 10^{-4} \text{ lb C gasified/min}}{\text{lb C inventory}}$$

at a steam conversion of about 70%. The results in Table VI indicate, therefore, that for low sodium lignite chars operating temperatures slightly above 1500°F should give adequate rates provided lower pressures of the order of 11 atm are used.

The sponsorship of this work by the Office of Coal Research, U. S. Department of the Interior, is gratefully acknowledged.

Literature Cited

(1) Curran, G. P., Rice, C. H., Gorin Everett, ACS Div. Fuel Chem., Preprints (8) 128 (1964).

(2) Curran, G. P., Clancey, J. T., Scarpiello, D. A., Fink, C. E., Gorin, Everett, Chem. Eng. Progress 62, 80 (1960).

(3) "Pipeline Gas from Lignite Gasification - A Feasibility Study." J. T. Clancey - Consolidation Coal Co., Report to U. S. Department of Interior, Office of Coal Research (Jan. 13, 1965).

(4) Curran, G. P., Fink, C. E. and Gorin, Everett, Fuel Gasification. Advances in Chemistry Series, 69, 141 (1967).

(5) Goring, G. E., Curran, G. P., Tarbox, R. P. and Gorin, Everett. Ind. Eng. Chem., 44, 1057 (1952).
Goring, G. E., Curran, G. P., Zielke, C. W. and Gorin, Everett. Ibid 45, 2586 (1953).
Zielke, C. W. and Gorin, Everett. Ibid 49, 396 (1957).

(6) "Low Sulfur Boiler Fuel Via the Consol CO_2 Acceptor Process." F. W. Theodore - Consolidation Coal Co., Report to U. S. Department of Interior, Office of Coal Research (June 6, 1967).

(7) Blackwood, J. D. and Ingeme, A. J., Australian J. Chem., 13, 194 (1960).

TABLE Ia

Analyses of Lignite Chars Used in Batch Kinetic Studies

Wt. % Dry Basis	Renner Cove	Dakota Star	South Dakota	Renner Cove Water Extracted	Husky
Hydrogen	1.01	1.10	1.21	--	1.55
Carbon	82.41	83.29	84.00	--	75.18
Nitrogen	.88	.86	.85	--	.82
Oxygen (diff.)	2.03	-.14	.91	--	1.49
Sulfur	.83	1.42	.48	--	2.64
Ash	12.84	13.47	12.52	--	18.96
		Ash Composition, Sulfur-Free Basis			
Al_2O_3, Wt. %	14.9	10.7	9.3	12.8	10.9
SiO_2	17.6	14.4	33.3	14.1	21.0
Fe_2O_3	8.7	18.1	8.8	10.2	28.1
CaO	26.0	37.5	35.2	35.9	25.7
MgO	9.7	10.6	2.7	14.5	8.9
Na_2O	14.7	3.9	4.3	2.0	.7
K_2O	.5	.2	.5	.04	.2
TiO_2	.5	.3	.7	.7	.5
P_2O_5	.6	.5	.1	.8	.4

TABLE Ib

Analyses of Chars Used in Continuous Gasifier

Wt. % Dry Basis	Glenharold	Glenharold Water Extracted	Husky I	Husky II	Rosebud, Subbituminou
Hydrogen	.73	.75	.94	.86	.87
Carbon	83.16	84.71	82.78	80.68	89.71
Nitrogen	.50	.52	.35	.45	.25
Oxygen (diff.)	1.53	1.49	1.42	1.79	2.04
Sulfur	1.21	.95	1.32	1.47	.18
Ash	12.87	11.58	13.19	14.75	6.95
		Ash Composition, Sulfur-Free Basis			
Al_2O_3, Wt. %	10.6	11.5	15.6	15.5	26.4
SiO_2	24.4	19.4	24.7	26.0	21.9
Fe_2O_3	8.6	11.8	5.3	5.7	5.8
CaO	33.3	40.1	33.0	35.0	30.8
MgO	7.4	8.7	15.4	11.2	10.2
Na_2O	11.7	5.3	4.3	4.6	2.0
K_2O	.7	.3	.4	.4	.3
TiO_2	.6	.7	1.2	.7	1.0
P_2O_5	.3	.4	.1	.4	.4

TABLE II

Calculations for Typical Run

Run 53: 10 gram Charge, Renner Cove Char, 1500°F, 16.97 atm System Pressure

Inlet Conditions

Dry Gas Rate, SCFH*	7.66
Steam Rate, SCFH	8.19

	H_2O	H_2	CO	CH_4	CO_2
Dry Gas Composition, mol %	0	88.93	5.30	0	5.77
Partial Pressures, atm	8.76	7.29	.435	0	.473

Exit Conditions

Elapsed Oxidizing Time, min	0	6	18	30	42	54
Dry Exit Gas Composition						
CO, mol %	-	6.96	6.61	6.20	5.96	5.75
CH_4	-	1.16	.708	.479	.333	.255
CO_2	-	8.20	7.72	7.47	7.15	6.92
H_2 (by diff.)	-	83.69	84.96	85.85	86.56	87.08
Dry Exit Gas Rate, SCFH	-	8.93	8.79	8.38	8.18	8.01
Calculated Quantities						
Rate of Oxygen Appearance in Dry Exit Gas, gm O/min	-	.244	.194	.152	.118	.093
Steam Conversion, %	-	9.50	7.55	5.93	4.61	3.62
Wet Exit Gas Composition						
CO, mol %	-	3.80	3.55	3.23	3.05	2.90
CH_4	-	.632	.380	.250	.170	.128
CO_2	-	4.48	4.15	3.89	3.66	3.48
H_2	-	45.73	45.64	44.73	44.28	43.87
H_2O	-	45.35	46.27	47.90	48.84	49.62
Gasification Rate, N, gm C gasified/min	.1510	.1384	.1059	.0812	.0624	.0481
Cumulative Carbon Gasified, gm	0	.561	2.019	3.135	3.992	4.652
Instantaneous Wt of C in Bed, W, gm	7.500	6.939	5.481	4.365	3.508	2.848
Integral Total Gasification Rate, N/W, gm C gasified/gm C in Bed/min x 10^4	201	200	193	186	178	169
Integral Methane Formation Rate, gm C gasified/gm C in Bed/min x 10^4	38.5	34.9	26.6	21.6	18.2	16.8
Burnoff, % C Gasified	0	7.5	26.9	41.2	53.2	62.0

* Standard conditions are 70°F, 29.92 inches Hg.

TABLE III

Differential Rates for 1500°F Isotherm

Renner Cove Lignite Char

R = lb C Gasif./min/lb C in Bed x 10^4

Run No.	Inlet Gas Composition, atm H_2O	H_2	CO	0% Burnoff R_{obs}	0% Burnoff R_{calc}	0% Burnoff % Diff	20% R_{obs}	20% R_{calc}	20% % Diff	40% R_{obs}	40% R_{calc}	40% % Diff	60% R_{obs}	60% R_{calc}	60% % Diff
								$R_T - 2\,R_{CH_4} = R_C$							
42-45	5.58	10.51	1.33	18	16.6	-7.8	34	32.0	-5.9	28	27.2	-2.8	9	8.6	-4.4
46-47	5.42	10.22	1.08	27	29.8	+10.4	41	43.3	+5.6	38	38.2	+0.5	20	20.5	+2.5
50-51	5.47	10.48	.198	95	102	+7.3	106	103	-2.8	94	97.4	+3.6	85	88.4	+4.0
52-53	8.76	7.29	.435	217	222	+2.3	226	231	+2.2	227	225	-0.9	214	209	-2.3
48-49	10.80	5.17	.478	398	388	-0.2	411	410	-0.2	415	412	-0.7	401	402	+0.2
43-44	10.49	5.48	.267	435	425	-0.2	460	446	-3.0	479	451	-5.8	479	446	-6.9
54-57	4.52	6.60	.760	89	83.9	-5.7	93	95.4	+2.6	86	89.0	+3.5	71	71.4	+0.6
55-56	7.36	3.64	0	649	642	-1.1	667	680	+1.9	691	713	+3.2	709	744	+4.9
					mean	4.4		mean	3.0		mean	2.6		mean	3.2
								R_{CH_4}							
42-45	5.58	10.51	1.33	33	31.4	-4.8	18	19.2	+6.7	11	12.0	+9.1	7	7.8	+11.4
46-47	5.42	10.22	1.08	36	34.4	-4.4	22	21.3	-3.2	13	13.6	+4.6	8	8.9	+11.2
50-51	5.47	10.48	.198	56	57.1	+2.0	38	37.2	-2.1	27	26.1	-3.3	19	18.5	-2.6
52-53	8.76	7.29	.435	50	52.2	+4.4	41	39.3	-4.2	31	29.7	-4.2	24	22.3	-7.1
48-49	10.80	5.17	.478	42	43.6	+3.8	37	36.3	-1.9	31	29.3	-5.5	26	23.5	-9.6
43-44	10.49	5.48	.267	50	50.9	-1.8	40	43.1	+7.8	33	36.1	+9.4	28	29.9	+6.8
54-57	4.52	6.60	.760	29	31.2	-7.6	21	20.3	-3.3	15	13.3	-11.3	11	8.9	-19.1
55-56	7.36	3.64	0	52	47.2	+9.2	44	41.5	-5.7	37	36.6	-1.1	29	32.2	+11.0
					mean	4.8		mean	4.4		mean	6.1		mean	9.8

$$\% \text{ Diff} = 100\,\frac{(\text{Calc}-\text{obs})}{\text{obs}}$$

TABLE IV

CH_4 Addition Runs

Run Nos.	H_2O	H_2	CO	CH_4	0% Burnoff			20%			40%			60%		
					R_{obs}	R_{calc}	% Diff	R_{obs}	R_{calc}	% Diff	R_{obs}	R_{calc}	% Diff	R_{obs}	R_{calc}	% Diff
					$R_T - 2\,R_{CH_4} = R_C$											
59-60	5.36	10.55	0	1.32	120	124	+3.2	119	121	+1.6	111	115	+3.4	101	110	+8.2
61-62	5.82	10.13	0.72	1.33	66	62	-6.1	70	71	+1.4	69	65	-5.8	57	50	-12.3
					R_{CH_4}											
59-60	5.36	10.55	0	1.32	32	(1)	-	25.3	(1)	-	18.8	(1)	-	11.6	(1)	-
61-62	5.82	10.13	0.72	1.33	23	23	0	16	17.2	+7.5	11	12	+9.1	8	7.2	-10.0

(1) These data used to calculate K_4 in rate equation.

TABLE V

Tabulated Constants in Rate Equations

R_C

% Burnoff	0	20	40	60
k	576	647	759	934
K	3.26	4.67	4.33	2.92
K_1	.035	.026	.017	.010
K_2	.360	.400	.460	.540
K_3	1.30	1.42	1.63	1.90

R_{CH_4}

k'	15.64	11.51	8.05	5.84
K'	←	.388	→	
K_1'	.19	.13	.08	.04
K_2'	.16	.21	.23	.25
K_3'	1.25	1.51	1.80	2.10
K_4	1.18	.88	.81	1.12

TABLE VI

Continuous Unit Gasification Rate Data

Run No.	Temp. °F	Press. atm	Feed-Stock	R_C	R_{CH_4}	% Burn-off	Partial Pressures, atm: Inlet H_2O	Inlet H_2	Inlet CO	Inlet CH_4	Outlet H_2O	Outlet H_2	Outlet CO	Outlet CH_4	lb/hr C Fed	lb C in Bed	Acceptor Present
K1-1	1500	20	(1)	13.2	3.3	17	7.00	5.57	2.22	.83	5.02	6.73	2.69	1.01	4.16	6.03	No
K1-2	1500	20		31.9	5.8	30	8.51	5.62	2.00	.61	5.64	7.28	2.59	.79	4.16	4.78	No
K1-3	1530	20		43.3	7.4	40	8.51	5.60	2.33	.62	4.84	7.65	3.19	.84	4.16	4.70	No
A-28	1500	20	(2)	13.5	6.5	32	5.37	7.43	2.85	.69	4.39	8.71	1.26	.84	1.35	2.74	Yes
A-13	1500	20	(3)	8.2	4.0	39	5.26	7.81	1.36	1.01	3.94	8.48	1.66	1.24	1.31	5.30	Yes
A-21	1500	11	(4)	28.4	4.2	46	4.95	3.34	.88	.20	2.72	4.90	1.48	.33	2.01	4.20	Yes
A-24-1	1600	20		47.9	12.6	42	4.98	6.44	2.37	.83	2.20	7.99	3.32	1.17	4.03	3.83	Yes
A-23-2	1600	11		82.9	7.6	48	5.21	2.53	1.55	.15	1.87	4.25	3.11	.29	4.03	3.28	No
D-2A	1600	20	(5)	29.9	7.4	24	5.43	7.43	2.85	.69	3.08	8.70	3.68	.89	3.40	3.01	No
D-2B	1600	20		47.3	12.1	36	5.35	7.48	2.60	.76	2.82	9.04	3.60	1.05	2.70	2.29	Yes

(1) Glenharold.
(2) Glenharold water extracted.
(3) Husky I.
(4) Husky II.
(5) Rosebud.

TABLE VII

Comparison of Observed and Predicted Rates

Run No.	Temp °F	Press. Atm	Feedstock	Observed Rates		Predicted Rates at 1500°F for Glenharold			
						Outlet	Inlet	Outlet	Inlet
				R_C	R_{CH_4}	R_C		R_{CH_4}	
K1-1	1500	20	Glenharold	13.2	3.3	11	64	5.1	8.1
K1-2	1500	↓	Glenharold	31.9	5.8	18	96	5.2	9.0
K1-3	1530	↓	Glenharold	43.5	7.4	(1)	74	2.6	6.0
		↓	Water Extracted						
A-28	1500	↓	Glenharold	13.5	6.5	29	66	8.7	12.3
A-13	1500	↓	Husky I	8.2	4.0	9	45	4.3	7.3
A-21	1500	11	Husky II	28.4	4.2	20	192	2.9	7.4

(1) Totally inhibited.

SCHEMATIC DIAGRAM
STEAM-CARBON REACTION KINETICS APPARATUS

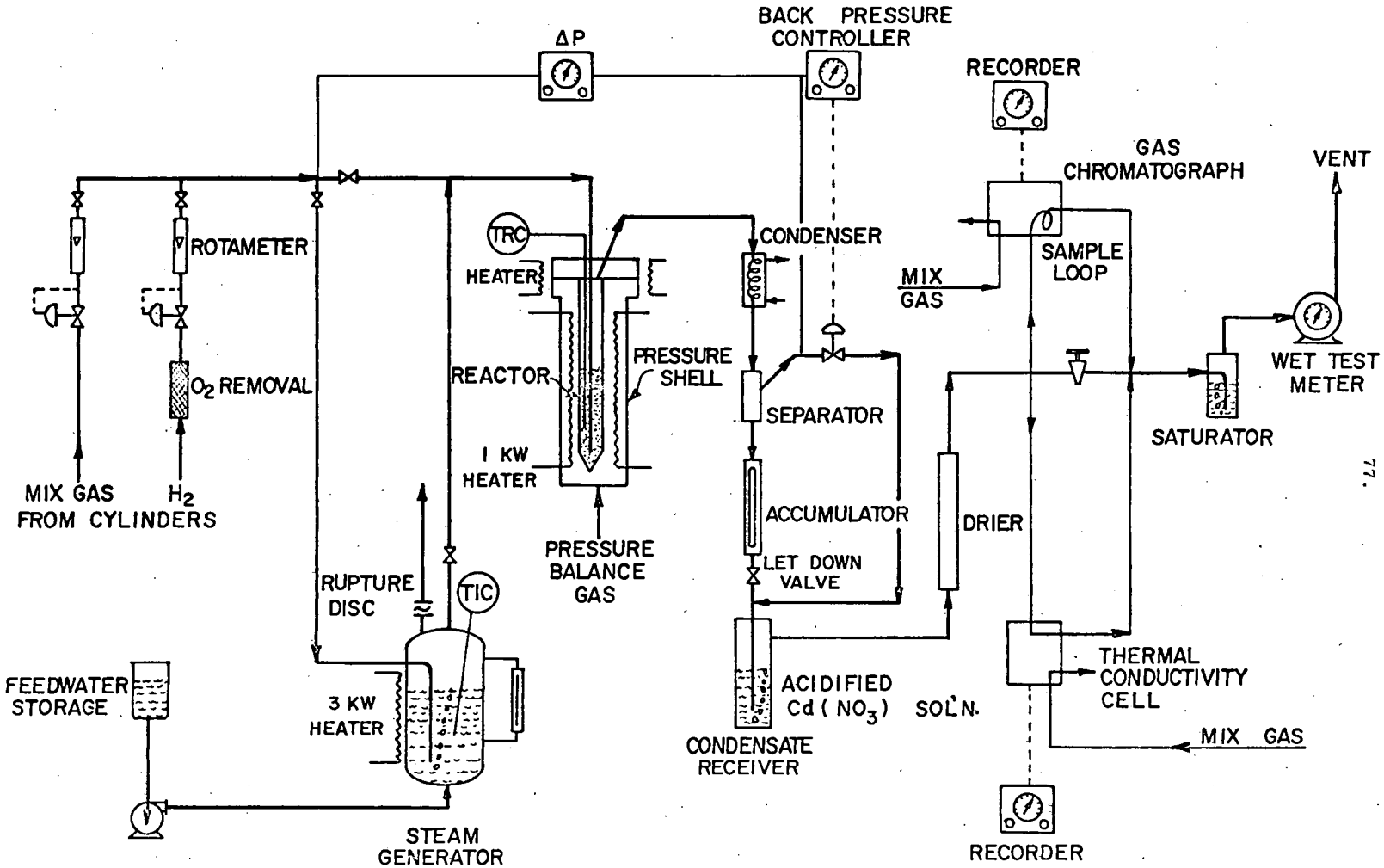

Figure 2

INTEGRAL CARBON OXIDE RATES FOR 10 GRAM CHARGE AT 1500° F

TOTAL PRESSURE, 16 ATM.

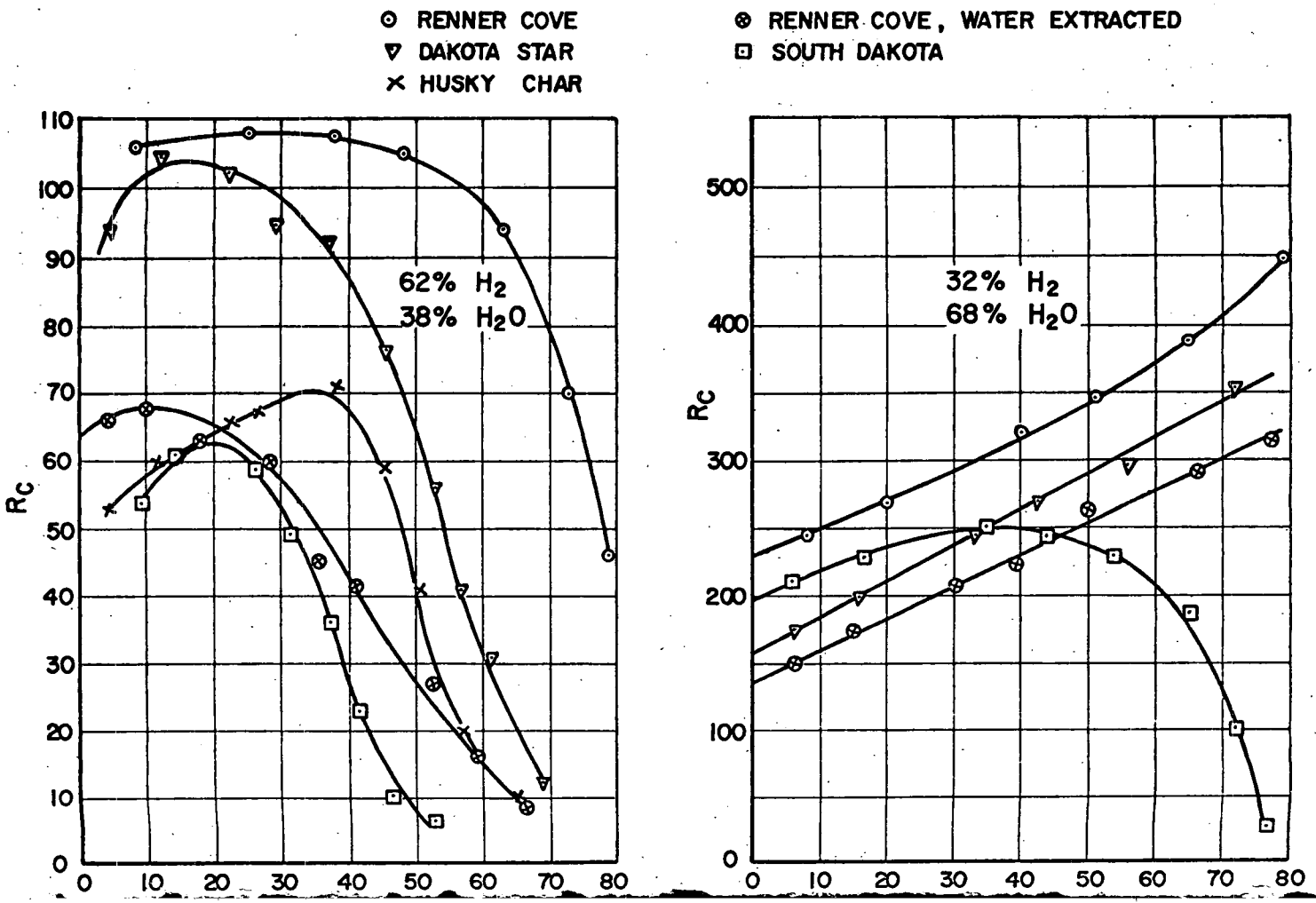

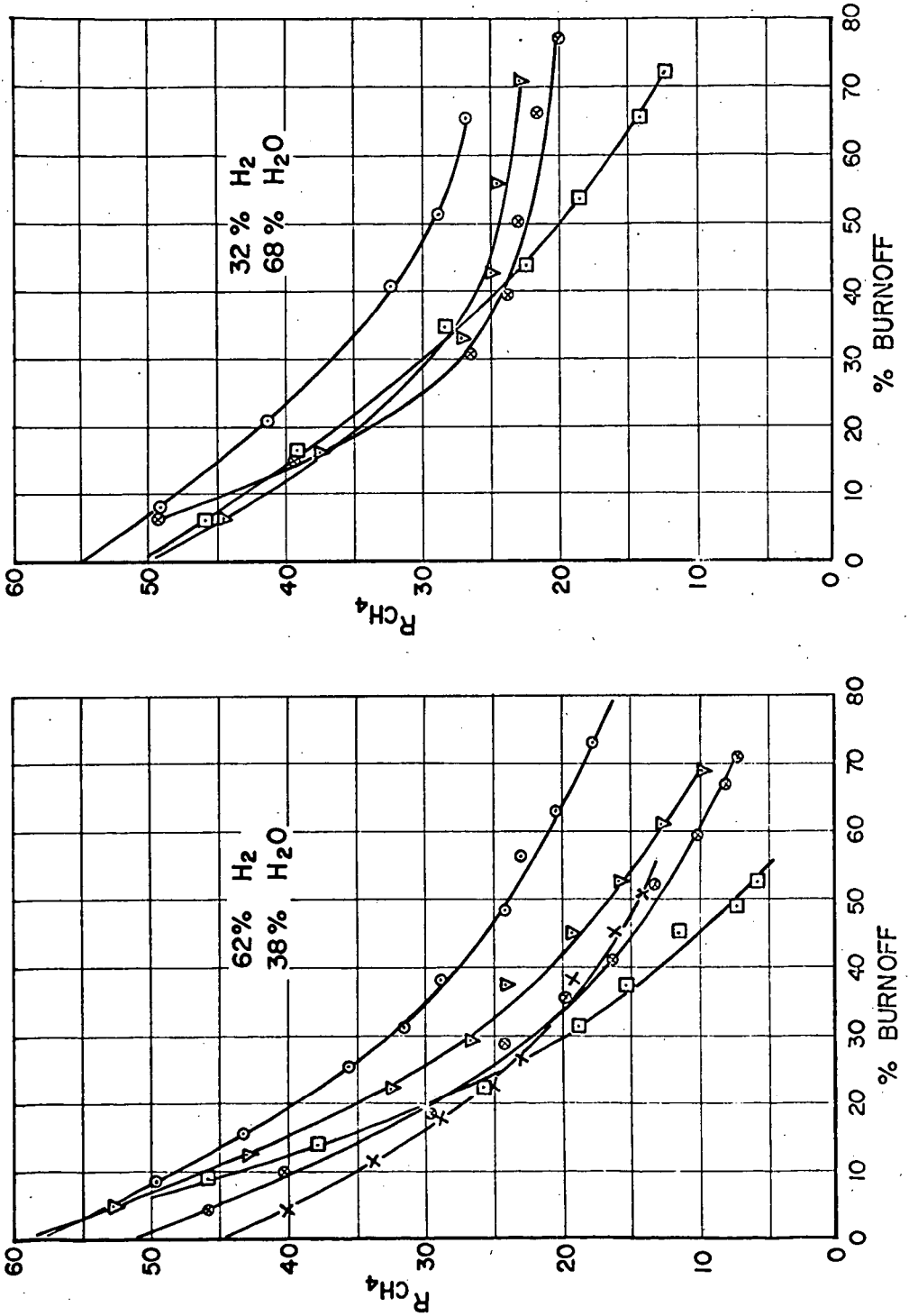
TOTAL PRESSURE, 16 ATM.
⊙ RENNER COVE
▽ DAKOTA STAR
× HUSKY CHAR
⊗ RENNER COVE, WATER EXTRACTED
⊡ SOUTH DAKOTA
62% H2
38% H2O
32% H2
68% H2O
R CH4
% BURNOFF
0
10
20
30
40
50
60
70
80

Figure 4

DIFFERENTIAL CARBON OXIDES GASIFICATION RATES
EFFECTS OF INHIBITION BY H_2 AND CO AT 20% BURNO

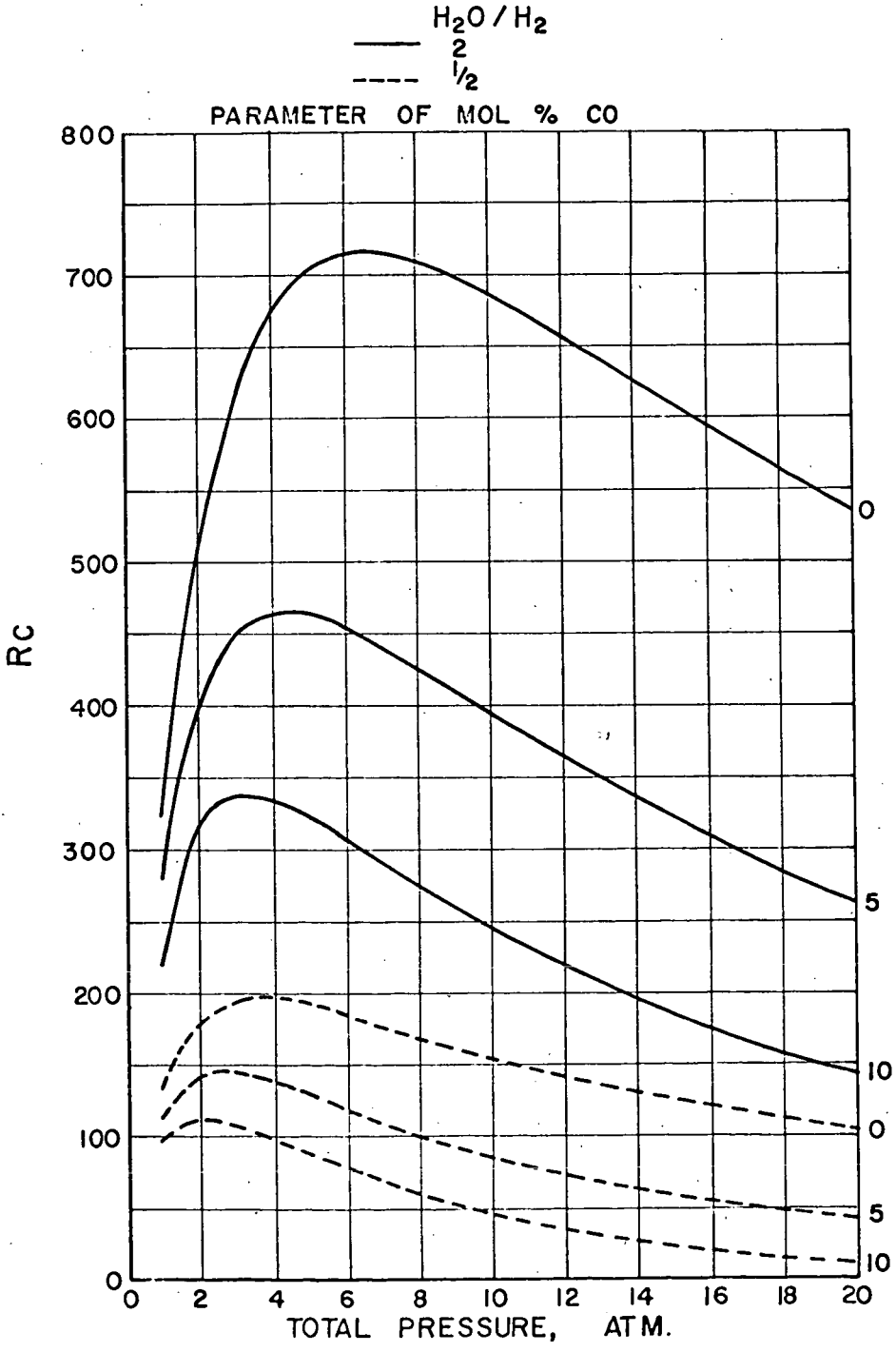

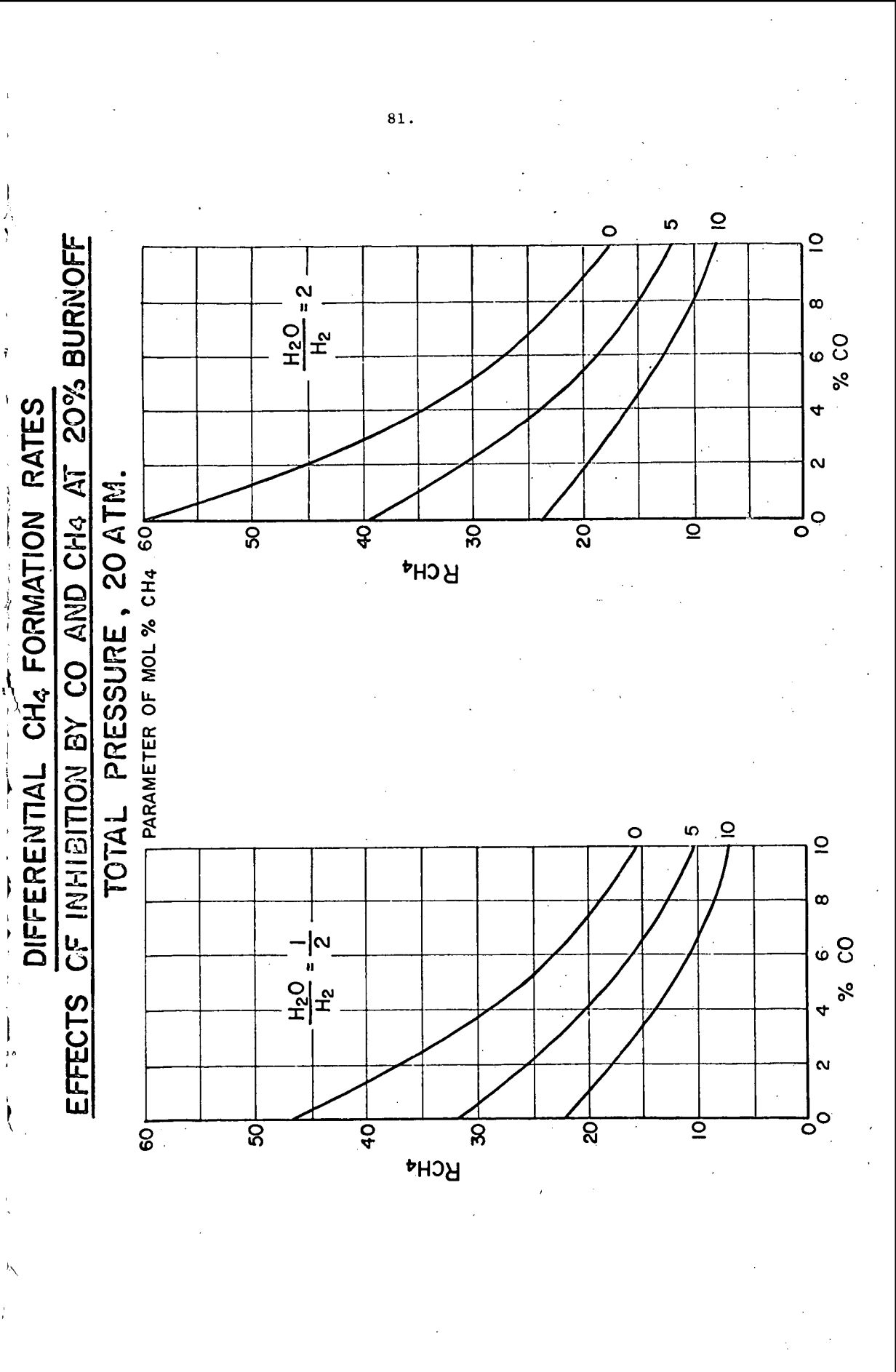
DIFFERENTIAL CH_4 FORMATION RATES
EFFECTS OF INHIBITION BY CO AND CH_4 AT 20% BURNOFF
TOTAL PRESSURE, 20 ATM.
PARAMETER OF MOL % CH_4
$\frac{H_2O}{H_2} = \frac{1}{2}$
$\frac{H_2O}{H_2} = 2$
R_{CH_4}
% CO
0
5
10
0
10
20
30
40
50
60
0
2
4
6
8
10

Figure 6

DIFFERENTIAL CH_4 FORMATION RATES

EFFECTS OF INHIBITION BY CO AND CH_4 AT 20% BURNOFF

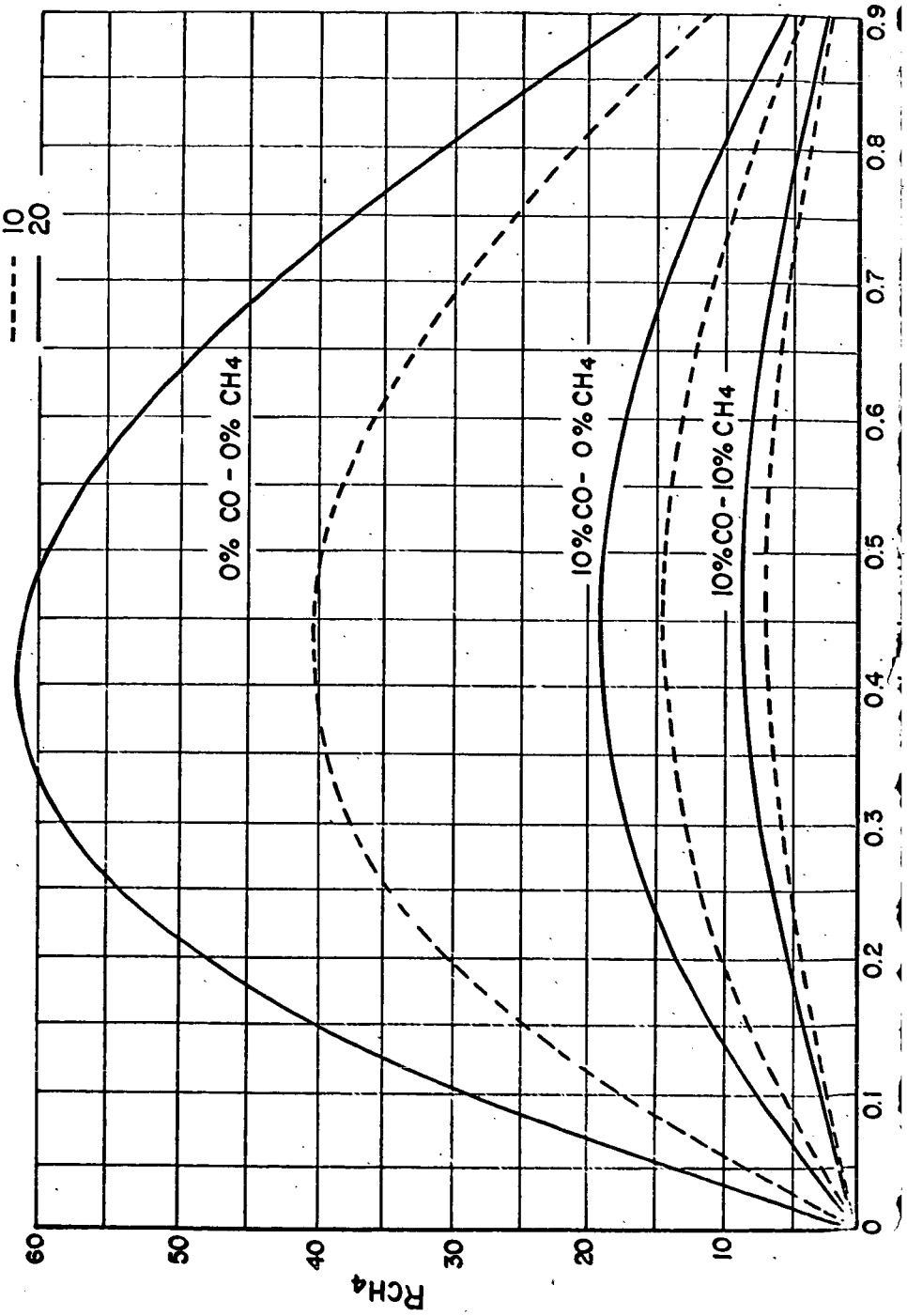

COAL AND CHAR TRANSFORMATION IN HYDROGASIFICATION – LIGNITE TO LOW-VOLATILE BITUMINOUS COAL

David M. Mason

Institute of Gas Technology
3424 S. State Street
Chicago, Illinois 60616

In a previous paper we discussed the behavior of a high-volatile A bituminous coal from the Pittsburgh No. 8 seam in the hydrogasification process (5). This study of the petrographic and physical properties of the coal and chars at different stages of the process had two objectives:

1. To find out as much as possible about what happens to the coal and how it behaves in the process.

2. To develop a correlation between the petrographic properties of the coals and their suitability for hydrogasification.

In the present paper the investigation has been extended to coal ranks ranging from lignite to low-volatile bituminous.

As noted previously, bituminous coal is treated in three successive stages:

1. Pretreatment with air at about 800°F to destroy the agglomerating power of the coal.

2. First-stage hydrogasification at 1200°-1300°F with pretreated coal as the feed.

3. Second-stage hydrogasification at 1700°-2000°F with first-stage residue as the feed.

However, in the present work the hydrogasification processing method was different from that previously reported. In that study, the first and second stages were conducted separately in different moving-bed runs. This time the two stages were combined in a single operation. The first stage was limited to a period of a few seconds while the pretreated coal dropped in free fall through the rising gas in the upper 9 ft of the reactor tube. The second-stage hydrogasification occurred in a fluid bed in the lower 3-4 ft of the reactor tube. With this processing regime it was not possible to obtain samples of char between the two stages. Most of the char residues investigated here were from runs in which the hydrogen fed was 25-30% of the stoichiometric amount required for complete gasification, and the steam comprised 50% of the steam-hydrogen mixture.

The sources and ranks of the coals processed are shown in Table 1. Work is continuing on two or three other coals.

Our petrographic methods have been described previously (5). The only change is that a 40X Achromat objective was used for both maceral analysis and reflectance determination. Surface areas were determined by Numec Instruments and Controls Corporation with carbon dioxide adsorption at 198°K.

Table 1. COAL SOURCES AND RANKS

Seam	Mine	County and State	Rank
Pocahontas No. 4	Stotesbury No. 10	McDowell County, West Virginia	Low-volatile bituminous
Sewell Seam (Lower Kittanning)	Lochgelly	Fayette County, West Virginia	Medium-volatile bituminous
Pittsburgh No. 8	Ireland	Marshall County, West Virginia	High-volatile A bituminous
W. Va. No. 5 Block	Kanawha	Randolph County, West Virginia	High-volatile A bituminous
Ohio No. 6	Broken Arrow	Coshocton County, Ohio	High-volatile B bituminous
Indiana No. 6	Minnehaha	Sullivan County, Indiana	High-volatile C bituminous
Illinois No. 6	Crown	Montgomery County, Illinois	High-volatile C bituminous
Colorado Subbituminous	Eagle	Weld County, Colorado	B subbituminous
N. Dakota Lignite	Glenharold	Mercer County, North Dakota	A lignite

HIGH-VOLATILE BITUMINOUS COALS

The high-volatile bituminous coals ranged in rank from an Illinois No. 6 high-volatile C coal with a mean maximum vitrinite reflectance of 0.45% to a West Virginia No. 5 Block high-volatile A coal with a mean maximum vitrinite reflectance of 0.81%. All of these coals required pretreatment of about the same severity. The effect of pretreatment on any of these coals is not noticeably different from that described previously for the Pittsburgh No. 8 coal – mainly inflation to cenospheres, disappearance of most of the exinite, development of a high-reflectance skin differing in thickness from particle to particle (Figure 1), and a varying lesser increase in reflectance (over that of the coal) in the interior of the particles. Particle structure appears quite similar, although perhaps quantitative determinations of cell wall thickness and vesicle size would show differences.

Several different types of particle structures are found in the char residues after hydrogasification (Figure 2). A fine-textured foam structure is prevalent in the residue from the highest rank coal (West Virginia No. 5 Block) but becomes less frequent with decreasing rank until it is virtually absent in the residue from the Illinois No. 6 coal (Figure 3). Otherwise, the residue particles from the different high-volatile bituminous coals appear quite similar in form. Also, there is little difference in reflectance; the mean reflectance of the residue from the lowest rank coal (Illinois No. 6) does not differ significantly from that of the Pittsburgh No. 8 (Table 2).

Table 2. REFLECTANCE OF HYDROGASIFICATION RESIDUES

Coal	Pittsburgh No. 8	Illinois No. 6	Colorado Subbituminous	N. Dakota Lignite
Run No.	HT-126	HT-155	HT-184	HT-139
Reflectance in Oil, %	Distribution of Reflectance Readings, %			
0-0.9	--	--	--	6.3
1.0-1.9	--	0.4	2.6	19.8
2.0-2.9	2.2	1.3	22.6	47.8
3.0-3.9	22.7	17.1	59.1	20.7
4.0-4.9	48.4	62.8	12.2	4.5
5.0-5.9	22.9	16.2	3.5	0.9
6.0-6.9	3.0	1.3	--	--
7.0-7.9	0.8	0.8	--	--
8.0-8.9	--	0.4	--	--
No. of Readings	362	234	115	111
Avg Reflectance in Oil, %	4.49	4.45	3.36	2.44
Standard Deviation, %	0.80	0.71	0.70	0.90

There is some difference in the anisotropy of the particles. The residue from the Illinois No. 6 coal exhibits very little anisotropy when observed with crossed polars. Less than half of the particles show any anisotropy, and these only in small areas (Figure 4a). Anistropy of the residue increases with coal rank. Thus in the residue from the West Virginia No. 5 Block coal most of the particles show at least a little anisotropy, while some, especially those with the foam structure, are predominantly anisotropic except for the pretreatment skin (Figure 4b). The greater degree of anisotropy and the greater prevalence of foam structure in the residue from the higher rank coals indicates that a greater degree of fluidity is attained in the interior of these particles when the coal is rapidly heated in the hydrogasification reactor.

Surface areas of 503 and 463 sq m/g were obtained on the residues from Pittsburgh No. 8 and Illinois No. 6 coals, respectively. The surface area of the original Pittsburgh No. 8 coal was 131 sq m/g; that of the Illinois No. 6 coal may have been somewhat higher, but was not measured. After pretreatment the Pittsburgh No. 8 coal had a surface area of 148 sq m/g. Thus most of the increase in the surface area occurred during hydrogasification.

Very few differences were evident in processing characteristics among the high-volatile bituminous coals, in either pretreatment or hydrogasification. However, our data indicate that the pretreatment yield increases with the rank of the vitrinite. This is shown in Table 3, where the coals are listed in order of increasing vitrinite reflectance. Yields were calculated by two methods for runs from which the char was either free-flowing or only very lightly caked in a laboratory agglomeration test (2). In one method the yield of moisture- and ash-free coal was calculated from the measured total char yield and the feed and product analyses. (Runs in which the material balance recovery was less than 85 or greater than 100% were excluded.) In the other method, the yield was calculated from the proximate analyses of feed and product, with the assumption that the amount of fixed carbon did not change. A similar calculation based on ash content is sometimes used, but is distrusted here because of the tendency for dense, high-ash particles to accumulate in the pretreatment fluid bed.

The yields from the second method are consistently less than those from the pilot plant data, but both show a trend of increasing yield with rank. The yield, no doubt, also depends on maceral composition because the yield from inertinite is expected to be greater than that from vitrinite, while that from exinite is expected to be much less. The two higher rank coals have, on the average, more of both exinite and inertinite than the two low rank coals. Because the higher exinite content counterbalances the higher inertinite content, it appears that the higher average yield of the two higher rank coals can be attributed entirely to the higher ranks of their vitrinites.

HIGH-RANK BITUMINOUS COALS

The pretreated Pocahontas No. 4 coal showed the usual development of oxidized pretreatment skin, but very little or no vesicle formation (Figure 5) and no significant loss of volatile matter. The pretreatment skin extends into many cracks. Many additional fine cracks were present in many particles. A high rate of attrition was observed in the pretreatment processing, which we attributed to the development of these cracks.

Table 3. YIELDS FROM PRETREATMENT OF HIGH-VOLATILE BITUMINOUS COALS

Coal	Reflectance,[a] %	Maceral Content, Vol %		No. of Pretreatment Runs	Yield of Pretreated Coal, % MAF	
		Exinite	Inertinite[b]		From Pilot Plant Data[c]	From Proximate Analysis[d]
Illinois No. 6	0.45	3	11	7	78.8	82.65
Indiana No. 6	0.48	4	6	6	80.8	80.0
Ohio No. 6	0.53	6	14	2	78.8	83.4
Pittsburgh No. 8	0.68	3	13	6	82.9	89.4
W. Va. No. 5 Block	0.81	10	21	3	82.1	84.7

a. Mean maximum reflectance of vitrinite in oil.

b. Including semifusinite.

c. Two runs on Illinois coal and two runs on Pittsburgh seam coal were excluded because of poor material balances.

d. Fixed carbon assumed to remain unchanged.

Pretreatment of the Sewell seam coal, which is on the borderline between medium- and low-volatile rank, did result in vesicle formation (Figure 6), although not to as great an extent as in the high-volatile coals. Fine cracks were also observed in the pretreated particles of this coal, and a high rate of attrition occurred in the pretreatment processing.

Hydrogasification of these two coals was difficult because the reactor plugged with agglomerating coal particles. To investigate this, agglomerated particles of residue from the Pocahontas coal were examined petrographically. With crossed polars, the pretreatment skin was readily identified. Particles without skins and the interiors of particles with skin were anisotropic and had a foam structure. Agglutination or cementing of particles was done by this foam material only. It was obvious (Figure 7) that the foam material was supplied not only by the particles that had undergone little or no pretreatment, but also by particles with holes or breaks in the skin. It appears that the pretreatment skin can be broken and the contents discharged to the outside of the particle as a result of the simultaneous development of pressure and fluidity in the interior of the particles.

Only a small fraction of the residue from the Pocahontas coal – , probably that derived from inertinite – does not have a foam structure. The residue from the Sewell coal also has a large amount of foam structure, but has an appreciable, perhaps predominant, amount of material with vesicular structure similar to that of the residue from high-volatile bituminous coals. This can be attributed to the greater amount of devolatilization that occurred in the pretreatment of the Sewell coal. Some particles of the residue from the latter coal display the discharge of foam material from the inside of the particle that was observed in the residue from Pocahontas coal. However, the smaller proportion of foam structure in the Sewell residue indicates that its agglomerating tendency should be appreciably less than that of the Pocahontas residue.

SUBBITUMINOUS COAL AND LIGNITE

The residues from lignite and subbituminous coal hydrogasified without pretreatment have a different type of pore structure (Figures 8 and 9). The pores are typically lenticular in cross section rather than rounded, but rounding and expansion of the pores in some areas indicate the development of a greater degree of plasticity in some entire particles and parts of others. More of this pore expansion seems to have occurred in the lignite than in the subbituminous coal. This pore expansion is probably caused by the greater fluidity conferred by the presence of exinite or resinite or both (1,4); these are somewhat more plentiful in the lignite than in the subbituminous sample.

Average reflectance of these residues is substantially less than that of residues from the bituminous coals (Table 2), with that from lignite being least. The surface area of the residue from the lignite, 4 [illegible] so m/g, is in the range of the values obtained in the residues from the high-volatile bituminous coals.

CONCLUSIONS

Petrographic study of the feed coals and chars at different stages of processing has been fruitful in several ways. The detection of contamination of a nonagglomerating coal by a coking coal explained some anomalous processing results, although the examination was not

early enough to avoid their occurrence. Agglomeration of pretreated high rank bituminous coals was shown to result from the discharge of fluid material from the interior of pretreated particles as well as from the fluidity of the few particles that escaped pretreatment. Lack of anisotropy in the residue chars from lignite, subbituminous coal, and pretreated high-volatile C coal indicated that little or no fluidity developed in these coals, and accounts for the successful processing of lignite and subbituminous coal without pretreatment. Increasing amounts of anisotropy, indicating development of fluidity, were observed in chars from the higher rank bituminous coals. Increased anisotropy and a very different char particle structure were found when a high-volatile A bituminous coal was fed without pretreatment (5). These differences in structure may become important if process development makes it possible to feed the coal without pretreatment. Because graphitization at higher temperature occurs only when the char has passed through a fluid stage with resulting anisotropy (3), the degree of anisotropy or lack of it may indicate differences in the electrical characteristics of the char; this may affect its behavior in the electrothermal gasification process for production of hydrogen.

With respect to the second objective of our work – the development of a correlation between the petrographic properties of a coal and its suitability for hydrogasification – we find:

1. Exinite is largely lost in pretreatment and, therefore, is of value only if the coal can be processed without pretreatment.

2. High-reflectance inertinite is believed to behave as an unreactive diluent in at least the first stage of the hydrogasification process. We have no information on the degree of activity of semifusinite.

3. Very little difference was evident in the processing characteristics of the high-volatile bituminous coals in either pretreatment or in hydrogasification. The yield of coal from pretreatment increased with rank of the vitrinite; 3 - 6% increase in yield was noted when the reflectance-in-oil of the vitrinite increased from an average of 0.46% for two high-volatile C coals to an average of 0.74% for two high-volatile A coals.

ACKNOWLEGMENT

The writer wishes to thank the American Gas Association and the U. S. Department of the Interior, Office of Coal Research, joint sponsors of the project, for permission to publish these results. William Moffett and Ellen Maeda did some of the work.

LITERATURE CITED

1. Brown, H. R., Taylor, G. H. and Cook, A. C., "Prediction of Coke Strength From the Rank and Petrographic Composition of Australian Coals", Fuel 43, 43-54 (1964).

2. Havlick, V. J. and Lee, B. S., "Coal Pretreatment in a Fluidized Bed" in Fuel Gasification; A Symposium, Advan. Chem. Ser. No. 69. Washington, D.C.: ACS, 1967.

3. Kipling, J. J. and Shooter, P. V., "Factors Affecting the Graphitization of Carbon: Evidence From Polarized Light Microscopy," Carbon, 4, 1-4 (1966) May.

4. Mackowsky, M. T., "Progress in the Field of Coal Petrography". Paper 1 presented at the Petrography of Coal and Coke Session of the Symposium on the Application of Science and Technology to Coal, Ottawa, March 29-31, 1967.

5. Mason, D. M. and Schora, F. C., Jr., "Coal and Char Transformation in Hydrogasification," in Fuel Gasification; A Symposium, Advan. Chem. Ser. No. 69. Washington, D. C.: ACS, 1967.

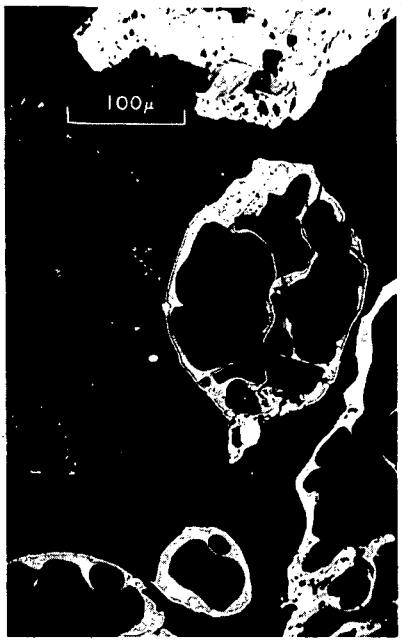

Figure 1. PRETREATED ILLINOIS No. 6 COAL

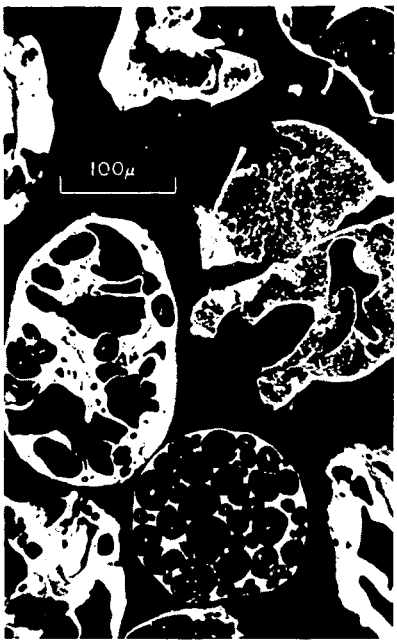

Figure 2. TYPES OF CHAR STRUCTURE IN RESIDUE FROM W.VA. NO. 5 BLOCK COAL

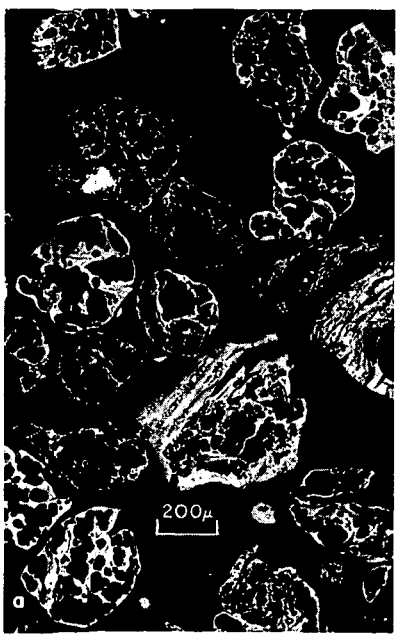

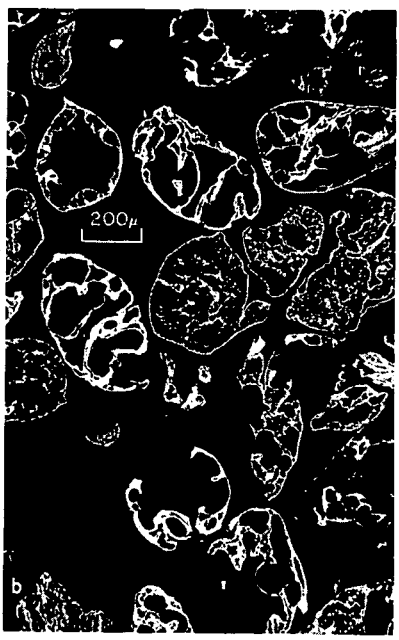

Figure 3. RESIDUE CHARS FROM a) ILLINOIS NO. 6 COAL AND b) W. VA. NO. 5 BLOCK COAL

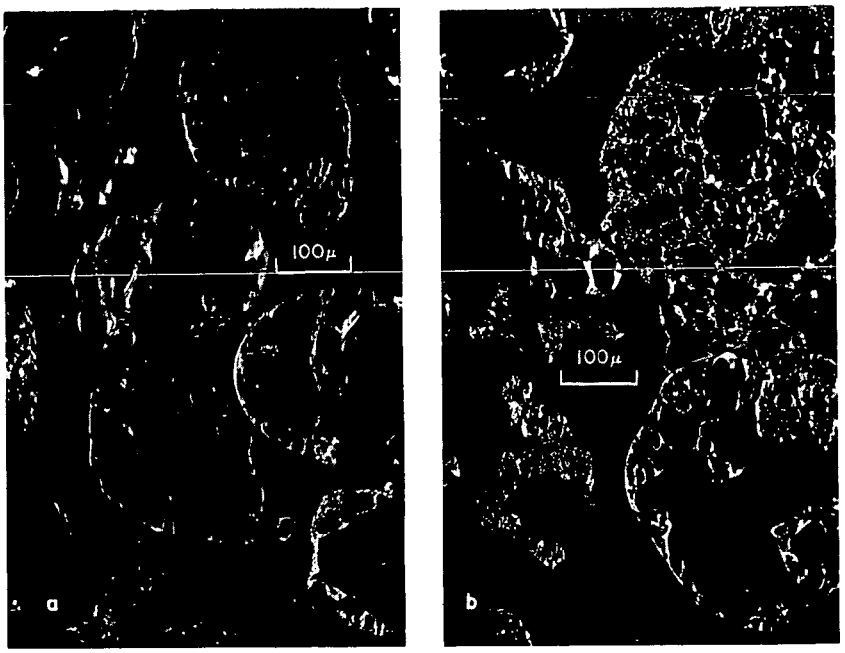

Figure 4. ANISOTROPY OF RESIDUE CHARS OBSERVED WITH CROSSED POLARS. a) FROM ILLINOIS NO. 6 AND b) FROM W. VA. NO. 5 BLOCK COAL

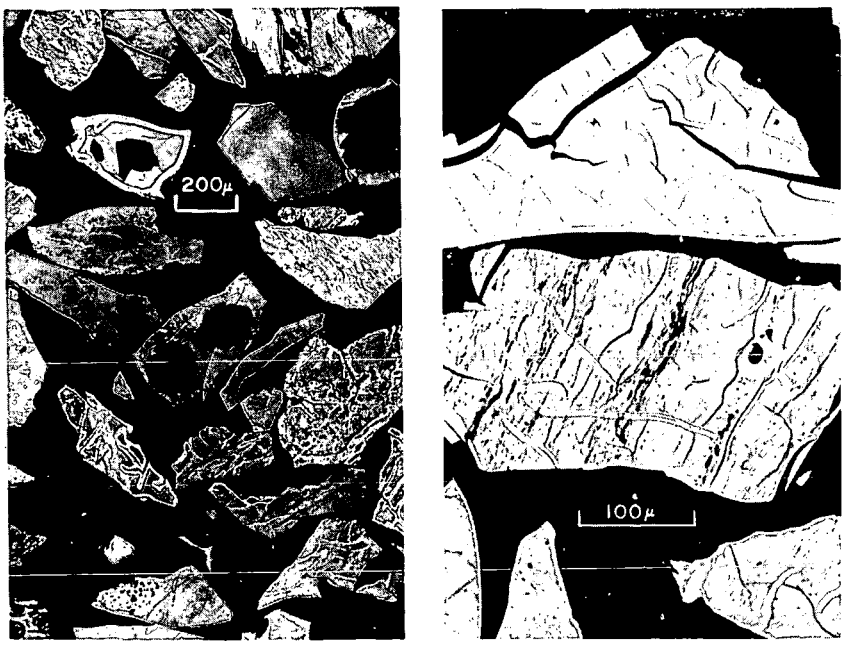

Figure 5. PRETREATED POCAHONTAS NO. 4 COAL

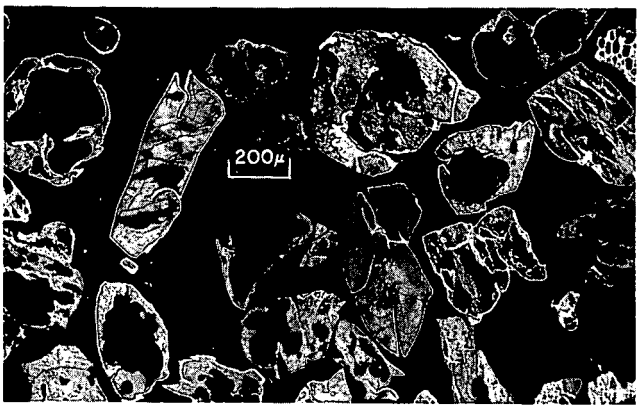

Figure 6. PRETREATED SEWELL SEAM COAL

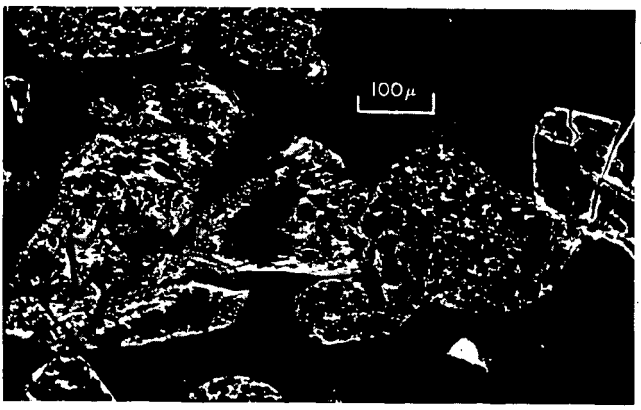

Figure 7. RESIDUE CHAR FROM POCAHONTAS No. 4 COAL OBSERVED WITH CROSSED POLARS

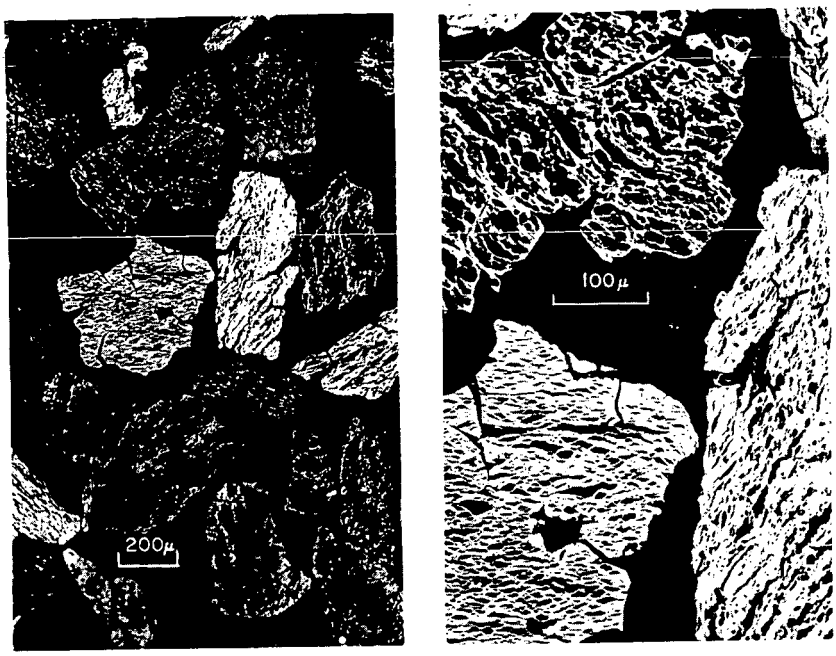

Figure 8. RESIDUE CHAR FROM NORTH DAKOTA LIGNITE

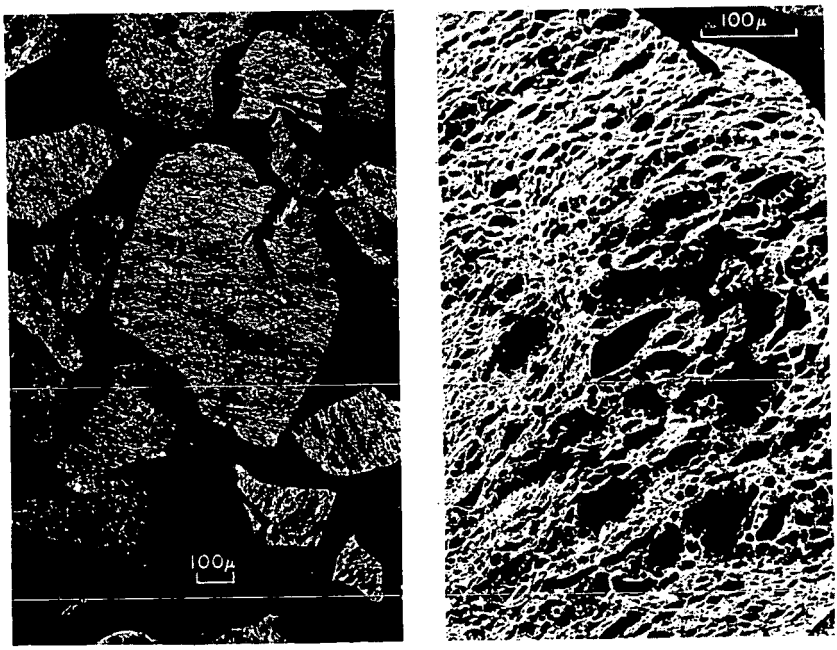

Figure 9. RESIDUE CHAR FROM COLORADO SUBBITUMINOUS

INTEGRATION OF COAL-BASED PIPELINE GAS AND POWER PRODUCTION

C. L. Tsaros

Institute of Gas Technology
3424 S. State Street
Chicago, Illinois 60616

The upgrading of the energy in coal and other fossil fuels to electric energy is a well-established technology. A future technology, now being developed, will be the conversion of solid fossil fuels, such as coal and oil shale, to fluid fuels. Both private and public funds have been and are being spent to develop processes to make such conversion practical. This paper will explore the possibility of integrating a projected pipeline gas process with a conventional power plant.

PIPELINE GAS FROM COAL

The Institute of Gas Technology has studied the conversion of coal to pipeline gas for many years. Our process is the direct hydrogenation of pretreated coal to produce a gaseous effluent, which is then upgraded to pipeline gas quality. In our process about half of the coal is gasified, using most of the volatile matter and leaving a spent char as the basis for hydrogen production. The hydrogen-making step, based on the spent char, is the subject of a number of variations in making pipeline gas by coal hydrogasification.

A current process concept, which will be studied in a large pilot plant project sponsored jointly by the Office of Coal Research and the American Gas Association, bases hydrogen production on the electrothermal steam gasification of char in a fluidized bed. Figure 1 shows a simplified flow diagram of the major process features of a commercial plant based on this process (1). A hydrogen stream as such is not used. Instead, raw, hot synthesis gas containing 48% hydrogen and 37% carbon monoxide is fed to the hydrogasifier. The use of synthesis gas directly is technically feasible and saves money by eliminating the carbon monoxide conversion and carbon dioxide removal steps necessary to make a high-purity hydrogen stream. About 44% of the hydrogasifier spent char is fed to the electrothermal gasifier where it is gasified with steam, heat being provided by electricity. About 52% of the spent char is sold as by-product fuel. The fluidized electrothermal gasifier has been studied in a pilot plant at Iowa State University and will be developed on a larger scale at IGT.

Table 1 presents an economic summary of a mine mouth pipeline-gas-from-coal plant. Economic studies, carried out as part of the OCR-A.G.A. development of the IGT hydrogasification process, are based on the manufacture of 250 billion Btu/day of pipeline gas heating value. In this design a total of 17,790 tons/day of coal is required, and the total investment is $93,245,000. With coal at 16.1¢/million Btu ($4.00/ton), the 20-year average gas price is estimated at 51.1¢/million Btu of product gas heating value. Approximately 20% of the gas price is represented by purchased power at 3 mills/kWhr. This cost is based on a nearby modern power plant of the 800-MW level, a 90% load factor for the gas plants, and a 16.1¢/million Btu fuel. A charge of 1 mill is worth 3.4¢/million Btu pipeline gas.

Table 2 gives figures for the pipeline gas plant on the overall conversion of input thermal energy to product heating values.

Table 1. ECONOMIC SUMMARY FOR PIPELINE GAS PLANT THAT PERFORMS HYDROGASIFICATION OF COAL USING SYNTHESIS GAS

Product Gas	258 X 10^9 Btu/day, 937 Btu/SCF	
Total Investment	$93,245,000	
Coal Required	17,790 tons/day	
By-product Char	4160 tons/day	
Operating Costs, $/Year		
Coal, at 16.1¢/10^6 Btu		23,377,000
Electric Power at 3 mills/kWhr at Process Voltage		8,410,000
Other Operating Expenses		13,636,000
Total Operating Expense		45,423,000
By-product Credit		(7,030,000)
Char and Pretreatment Fines	5,398,000	
Sulfur	1,632,000	
	7,030,000	
Net Operating Expense		38,393,000
Return Plus Federal Income Tax, 20-yr Average		4,867,000
		43,260,000

20-yr Average Price of Gas – 51.1¢/10^6 Btu

Table 2. PIPELINE GAS PLANT CONVERSION EFFICIENCY

	In, 10^6 Btu/hr			Out, 10^6 Btu/hr
Coal	18,369		Product Gas	10,776
Electricity	1,162		By-Product Char	4,006
Total	19,531			14,782
Overall Eff, ¢		75.6		
Coal	18,369			
Fuel for Electric Power at 40% Eff	2,910			
Total	21,279			14,782
Overall Eff, ¢		69.5		

If the input electric energy to the gasifier is included, the overall efficiency for the gas plant is 75.6%. However, if the fuel energy required to produce the electricity at 40% efficiency is counted as an input, the overall fuel conversion efficiency drops to 69.5%. Power requirements for the pipeline gas plant are summarized in Table 3.

Table 3. PIPELINE GAS PLANT POWER SUMMARY

	kW
Electrothermal Gasifiers, Purchased Power	340,120
Electric Motors, Purchased Power	15,340
Steam Turbine Drives Powered by Heat Recovery Steam	47,330
Total Power	402,790

The electrothermal gasifier consumes 84% of the total plant power, of which 88% is purchased. Of the total motive power, 76% is supplied by steam turbines driven by steam generated from waste heat that otherwise would be rejected to cooling water.

Table 4 summarizes the heat recovery plus process cooling for a pipeline gas plant. The table shows the amounts and temperature levels of heat requirements and where there might be possibilities of energy interchange with an adjacent power plant. Heat going to cooling water could be used to preheat the feedwater for the power plant turbine in the low-temperature part of the cycle. Instead of using it to generate low-temperature steam, the 870 million Btu/hr of hydrogasifier effluent, in cooling from 750° to 280°F, could be used to heat the turbine feedwater at the higher temperature. The required regeneration steam, 796,000 lb/hr, could then be extracted from the power plant turbine at 100 psia, thus saving the heat going to cooling water.

ELECTRIC POWER GENERATION

Integrated power production and industrial operation has been previously suggested. A recent paper presents a general discussion of the various aspects of this question (3). The present paper discusses the potential for integration of pipeline gas plants and power plants. This presentation is an initial look at a specific case and is designed to show the advantages of joint operation. We have not estimated all the economic effects nor optimized the conditions for joint pipeline gas and power production versus separate operation. However, we made calculations of the effect of energy interchange on the power plant cycle.

Figure 2 shows a simplified drawing of a typical modern power plant cycle. The efficiency of such a cycle for a given boiler efficiency is raised by decreasing the heat going to cooling water per kWhr of energy generated. This is accomplished by the expansion of most of the steam to a very low pressure, 1-2 in. Hg, followed by condensation. Intermediate extraction of steam from the turbine raises the temperature of the feedwater to the 500°-550°F level. Eight feedwater heaters may be used in a typical system, with progressively higher extraction steam and feedwater temperatures. This system produces a higher efficiency than a nonextraction system because, although the extracted steam does not expand to the lowest pressure, the heat that would otherwise go to cooling water is recovered to heat the boiler feedwater.

Table 4. SUMMARY OF PIPELINE GAS PLANT HEAT RECOVERY AND COOLING

Heat Source	Temperature Range	Service	10^6 Btu/hr
Pretreatment Reactor	750°F fluidized bed	Generate process steam, 1200 psig, 510°F	624
		Generate turbine steam, 1200 psig, 570°F	254
		Preheat boiler feedwater, 525°-570°F	84
Hydrogasifier Effluent	1200°-750°F	Superheat reaction steam, 570°-700°F	133
		Superheat turbine steam, 570°-900°F	109
		Preheat high-pressure boiler feedwater, 320°-525°F	334
Hydrogasifier Effluent	750°-280°F	Preheat feedwater and generate low-pressure regeneration steam, 100°-238°F	870
Hydrogasifier Effluent	280°-260°F	Preheat high-pressure boiler feedwater, 60°-100°F	60
Methanation Effluent	900°-300°F	Preheat high-pressure boiler feedwater, 100°-325°F	325
Methanation Effluent	300°-100°F	Heat to cooling water	247
Hot Carbonate Regeneration Steam Condenser-Cooler	230°-100°F	Heat to cooling water	870
Fired Superheater	--	Superheat reaction steam, 700°-1200°F	315

Methods to rapidly determine the improvement in heat rate resulting from feedwater heating have been published (2). Thus, for initial steam conditions of 3000 psig at 1000°F, with expansion to 2 in. Hg, the nonextraction input to steam heat at 100% turbine efficiency is 7730 Btu/kWhr. With an average turbine efficiency of 87% and a boiler efficiency of 90%, the overall heat rate will be 9870 Btu/kWhr and overall efficiency will be 34.6%. However, with extraction feedwater heating to 500°F (Figure 2), the heat rate is reduced to about 8500 Btu/kWhr, corresponding to the 40% overall efficiency typical of modern power plants.

JOINT PIPELINE GAS AND ELECTRIC POWER GENERATION

If all or most of the turbine feedwater preheat can be obtained from waste heat in an adjacent pipeline gas plant, then the steam that would otherwise be extracted can be expanded to the lowest pressure, 1-2 in. Hg, with an increase in power output per Btu of boiler input to the steam cycle.

Calculations have been made for two such cases, with the resultant heat rates based on the above boiler and turbine efficiencies. In the first case, Figure 3, the turbine feedwater absorbs low-temperature heat from methanation reactors, the regeneration tower steam condenser, and waste heat that otherwise would be used to generate low-pressure regeneration steam for hot carbonate scrubbing units. The required low-pressure steam is then obtained by extraction from the power plant turbine at 100 psia. Waste heat recovered in the gas plant to generate steam for individual turbine drives is not used to preheat the feedwater for the large power plant in this case. To complete the preheating of this feedwater to 500°F, some extraction is necessary.

The power cycle assumed for these calculations is the expansion of 3000 psig, 1000°F steam to 700 psia followed by reheating to 1000°F. Part of the 700-psia steam is used for the heating prior to reheat. Except for the extraction of 796,000 lb/hr steam, as noted above, at 100 psia for use in the gas plant, most of the steam then expands to 2 in. Hg. The overall efficiency for the power plant with this system is 43.0%; the heat rate is 7940 Btu/kWhr.

If no turbine steam is generated in the pilot plant, this heat can then be used to raise the power plant turbine feedwater to approximately 500°F. In the scheme shown in Figure 4, there is no extraction for feedwater preheat, but 100-psia steam is again extracted for use in the gas plant. At these conditions, the overall efficiency is 46.7% and the heat rate is 7310 Btu/kWhr. However, in the second case, 402,800 kW must be sent to the gas plant compared to 355,460 kW when part of the motive power is provided by individual steam turbines in the gas plant. In an integrated operation there may be capital cost advantages in having all the power generated in a very large unit because of economies of scale. However, there would be a charge for the added 47,330 kW sent to the gas plant, which reduces the effect of savings in the capital and fuel components of power cost. The exact cost would have to be derived from the total operation as influenced by the improvements resulting from the integration of gas-electric operation.

ADVANTAGES OF INTEGRATED OPERATION

The effect of integrated operation is to increase the overall efficiency of coal conversion to pipeline gas plus electricity for sale from 64.8% for separate operation to 66.5% for joint operation.

A single cooling-water facility could be used for both gas and electric plants. Superheating of the process steam for the gas plant (315 million Btu/hr) can be carried out more economically in the power plant boiler (6 billion Btu/hr level) as an incremental increase in the superheater section than as a separately fired superheater. Cooling-water requirements for the gas plant are greatly reduced.

This, plus the economies of scale, can save several million dollars in offsite costs.

Since the gas plant operates on a 90% annual stream factor, the load factor for the power plant will be improved over the more typical 60% industry average. This improvement, plus the improved fuel economy, could reduce power costs on the order of 1 mill/kWhr. Part of the basis for the 3-mill power cost used in Table 1 is the high load factor resulting from joint operation.

Spent char from the gas plant can be used as fuel for the power plant. A high-sulfur coal, a liability in power generation, can be an asset in hydrogasification. During hydrogasification, most of the sulfur is converted to H_2S, from which the sulfur can be recovered and sold as a by-product. In the pipeline gas plant design used as a basis for this study, a 4.4% sulfur coal yields a char containing 1.7% sulfur. To increase the production of char, the percentage conversion during hydrogasification can be decreased, raising the coal throughput for constant gas production. More hydrogen can then be obtained from the coal, which reduces that obtained from the synthesis gas, which, in turn, gives a lowered gas price. The degree of coal conversion to gas would have to be optimized in relation to the gas-electric operations.

Not only the degree of conversion, but the sizes of the gas and the power plants would need to be optimized. A combination gas-electric utility interested in a pipeline-gas-from-coal plant would also find the study of integrated operation of interest.

Integrated gas-electric operations would involve regulated industries, with similar rates of return. This is not true, however, for joint power plant-industrial operation, where the differing rates of return and depreciation cause more complicated cost allocation.

As a result of potential savings in gas plant investment and power charges, it appears that the price of gas can be reduced by several cents per million Btu compared to completely separate operation.

In summary, the following advantages are possible for an integrated operation:

1. Increased power plant efficiency and load factor.
2. Reduction of investment for the pipeline gas plant through economies of scale by combining facilities for power generation, steam superheat, and cooling-water facilities with those of the power plant.
3. Lowered pipeline gas price.
4. Production of low-sulfur power plant fuel as a by-product of the pipeline gas plant, thus reducing air pollution problems when high-sulfur coal is used.

ACKNOWLEDGMENT

The work reported herein is under the cosponsorship of the American Gas Association and the U.S. Department of the Interior, Office of Coal Research. Permission of the sponsors to present this paper is greatly appreciated.

LITERATURE CITED

1. Knabel, S. J. and Tsaros, C. L., "Process Design and Cost Estimate for a 258 Billion Btu/Day Pipeline Gas Plant – Hydrogasification Using Synthesis Gas Generated by Electrothermal Gasification of Spent Char," Office of Coal Research Report. Chicago: Institute of Gas Technology, 1967.

2. Salisbury, J. K., "A Short Cut to Turbine Cycle Heat Rates–Part 1," Power 87, 664-67, 709b, 709c (1943) October; Part II, ibid. 87, 734-37 (1943) November.

3. Trommershausen, W. E. and Rossie, J. P., "Integration of Power Production and Industrial Operation." Paper presented at the Symposium on Fossil Hydrocarbon and Mineral Processing, 62nd Annual Meeting, American Institute of Chemical Engineers, Salt Lake City, Utah, May 21-24, 1967.

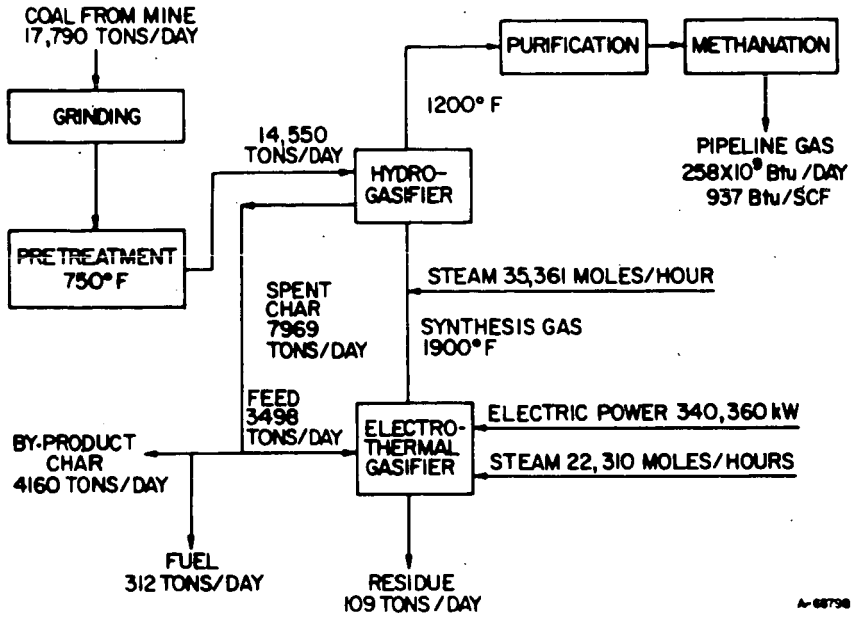

Figure 1. 258 Btu/DAY PIPELINE GAS BY HYDROGASIFICATION OF COAL USING SYNTHESIS GAS GENERATED BY ELECTROTHERMAL GASIFICATION OF SPENT CHAR

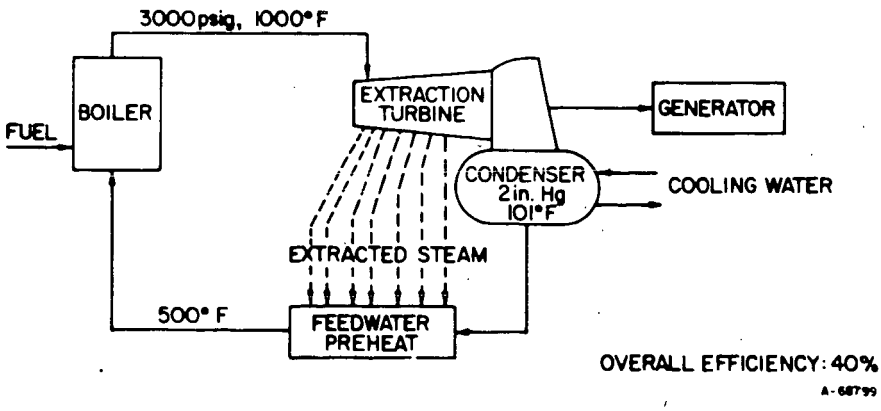

Figure 2. SIMPLIFIED FLOW DIAGRAM OF CONVENTIONAL POWER PLANT

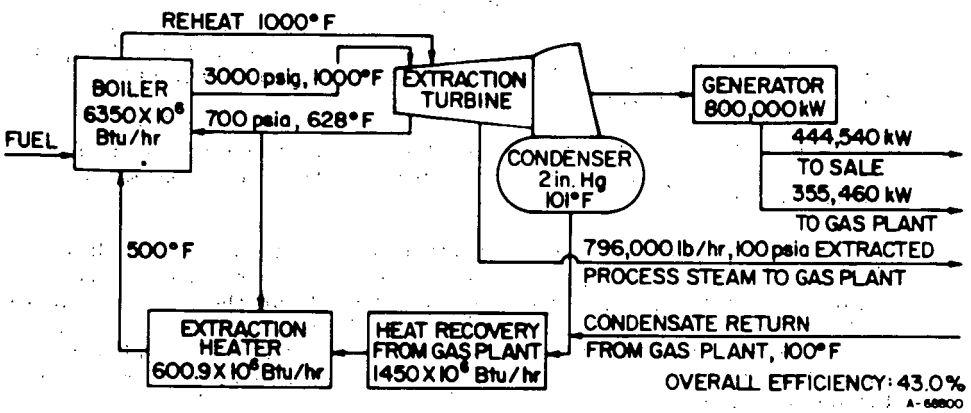

Figure 3. POWER PLANT CYCLE FOR JOINT OPERATION WITH PIPELINE GAS PLANT WASTE HEAT STEAM USED FOR TURBINE DRIVE IN GAS PLANT

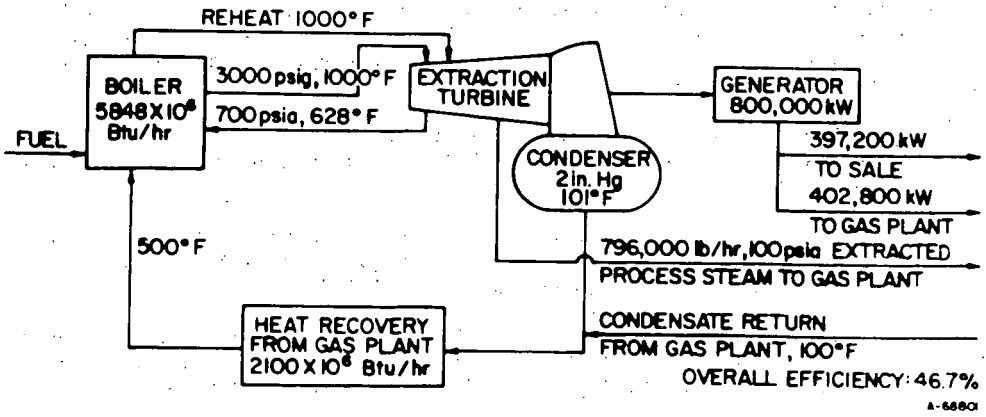

Figure 4. POWER PLANT CYCLE FOR JOINT OPERATION WITH PIPELINE GAS PLANT
(No Turbine Drives in Gas Plant)

OPTIMIZATION OF FIXED BED METHANATION PROCESSES

C. Y. Wen, P. W. Chen
K. Kato and A. F. Galli

Department of Chemical Engineering
West Virginia University
Morgantown, West Virginia

ABSTRACT

As a part of the study on optimization of coal gasification processes for the production of pipeline gas, optimization of methanation processes is performed.

Since the heat of reaction for the methanation reaction is so large that heat removal from the reactor is the major problem in the process design.

Various systems of catalytic fixed bed reactors are considered. They are the adiabatic system, the heat extraction system, the cold quench system and the recycle system. The size of the plant considered is for the production of 250 x 10^9 B.t.u./day of pipeline gas. Three different feed gas compositions likely to result from the primary gasification phases are treated. Only the total equipment cost of the methanation processes is considered.

Prior to the optimization of the methanation processes, the heat exchanger optimization is performed. A computer simulation of the methanation process is then programmed based on the kinetic information, the cost information and heat and material balance. Suitable techniques of optimization for the methanation processes are selected and the optimum conditions and designs of the various systems are found.

The result indicates that for the low CO case, an adiabatic reactor without internal or intermediate cooling is the most economical system. For the intermediate CO and high CO cases, the cold quench system offers the minimum total equipment cost. Cost of equipments associated with heat removal is found to occupy the major portion of the total equipment cost.

From the operational and maintenance point of view, the recycle system seems to be the easiest while the heat extraction system seems to be most difficult to control.

The effects of temperature and pressure on the optimum design of the process are discussed. The system parameters which affect the optimum design of the processes are identified.

Information on the methanation catalyst is not complete particularly the reaction rate at high CO concentration and the temperature effect on activity and durability should be further investigated.

1. INTRODUCTION

The gasification of coal to produce methane as a substitute for a supplement to pipeline natural gas is currently being extensively studied under the sponsorship of the Office of Coal Research, Department of the Interior.

Although a variety of routes and several raw materials are being investigated, it appears that any system for gasification of coal will require additional units for conversion of excess carbon monoxide and hydrogen to methane to achieve heating value equivalent to natural gas.

The magnitude of methanation will vary considerably, depending on the undecided choice of the process in the primary gasification phases. The degree of methanation may vary from a major operation involving conversion of the feed gas containing a minor amount of methane to simple gas composition clean-up.

Since it is presently impossible to predict the exact composition of the gaseous effluent from the various primary coal gasification processes, the compositions of the three different feeds as listed in Table 1-1 will be considered as approximate gas mixtures.

Although CO concentration as high as 25% can be considered, lacking actual experimental reaction rate data at such a high CO concentration level, it is not possible to make a reasonable assessment of the process for this case. Besides, for such a high CO concentration feed, recycle system is more than likely to be used for excess heat removal, some methane will be present at the reactor entrance. The gas compositions listed in Table 1-1 may result from the primary gasification phases now under investigation after the adjustment of the composition by the water-gas shift reaction and purification is made.

Since the methanation reaction is a highly exothermic reaction, the heat removal from the reacting gas becomes the major problem in economic optimization. Several types of methanation reactors, such as fixed beds and fluidized beds, have been tested on pilot plant scale.

Fluidized bed operation is found to be difficult because of technical problems involved. Particle elutriation caused by the breaking of catalyst pellets may become severe. Lack of ruggedness of the catalyst and the unavailability of small particle sizes prevents good fluidization of catalysts. Therefore, three types of fixed bed downflow catalytic reactors are considered. They are:

1. The heat extraction system.
2. The cold quench system.
3. The recycle system.

TABLE 1-1 FLOW RATE AND CONCENTRATION OF FEED AND PRODUCT GASES

A. 950 B.t.u./SCF Gas

Low CO Case

	Feed Gas [lb.mole/hr.]	[mole%]	Product Gas [lb.mole/hr.]	[mole%](dry base)
CH_4	23,962.8	75.500	25,355.1	92.100
CO	1,419.9	4.474	27.5	0.100
H_2	5,594.4	17.626	1,417.4	5.148
CO_2	63.5	0.200	63.5	0.231
H_2O	31.7	0.100	1,424.1	0.000
N_2	666.5	2.100	666.5	2.421
Total	31,738.8	100.0	28,954.1	100.0

Intermediate CO Case

	Feed Gas [lb.mole/hr.]	[mole%]	Product Gas [lb.mole/hr.]	[mole%](dry base)
CH_4	21,378.8	62.100	24,115.0	92.100
CO	2,762.4	8.024	26.1	0.100
H_2	9,562.3	27.776	1,353.8	5.170
CO_2	68.9	0.200	68.9	0.263
H_2O	34.4	0.100	2,770.6	0.000
N_2	619.7	1.800	619.7	2.367
Total	34,426.5	100.0	28,954.1	100.0

High CO Case

	Feed Gas [lb.mole/hr.]	[mole%]	Product Gas [lb.mole/hr.]	[mole%](dry base)
CH_4	16,397.5	41.400	21,724.3	92.100
CO	5,350.3	13.508	23.6	0.100
H_2	17,107.2	43.192	1,126.9	4.777
CO_2	118.8	0.300	118.8	0.504
H_2O	39.6	0.100	5,366.4	0.000
N_2	594.1	1.500	594.1	2.519
Total	39,607.5	100.0	28,954.1	100.0

B. 900 B.t.u./SCF Gas

Low CO Case

	Feed Gas [lb.mole/hr.]	[mole%]	Product Gas [lb.mole/hr.]	[mole%](dry base)
CH_4	24,632.3	75.500	25,663.8	87.000
CO	1,061.0	3.252	29.5	0.100
H_2	6,149.3	18.848	3,054.9	10.356
CO_2	65.3	0.200	65.3	0.221
H_2O	32.6	0.100	1,064.1	0.000
N_2	685.1	2.100	685.1	2.323
Total	32,625.6	100.0	30,562.7	100.0

Intermediate CO Case

	Feed Gas [lb.mole/hr.]	[mole%]	Product Gas [lb.mole/hr.]	[mole%](dry base)
CH_4	22,004.3	62.100	24,439.8	87.000
CO	2,463.6	6.953	28.1	0.100
H_2	10,221.7	28.847	2,915.2	10.377
CO_2	70.9	0.200	70.9	0.252
H_2O	35.4	0.100	2,470.9	0.000
N_2	637.8	1.800	637.8	2.271
Total	35,433.7	100.0	30,562.7	100.0

High CO Case

	Feed Gas [lb.mole/hr.]	[mole%]	Product Gas [lb.mole/hr.]	[mole%](dry base)
CH_4	16,919.1	41.400	22,071.4	87.000
CO	5,177.7	12.670	25.4	0.100
H_2	17,994.1	44.030	2,537.1	10.000
CO_2	122.6	0.300	122.6	0.483
H_2O	40.9	0.100	5,193.2	0.000
N_2	613.0	1.500	613.0	2.417
Total	40,867.4	100.0	30,562.7	100.0

The distinguishing features among the three systems are the manners by which heat is removed and the temperature is controlled in the reactors.

The goal of this study is to economically evaluate their relative technical merits for prospective application in coal gasification processes. To achieve this, it will require all three reactor systems being analyzed from both the technical and economic points of view. Each component information must be integrated by programming it into the computer for simulation. Finally, optimum conditions must be searched by an appropriate technique to arrive at the best economic process and design.

The following specifications and bases are chosen in this study.

1. Production rate is 250×10^9 B.t.u./day of pipeline gas.

2. The product gas should have a heating value of approximately 950 B.t.u./S.C.F. or the product gas should contain approximately 92.1% methane on a dry base. In addition, the concentration of CO must be less than 0.1%. Product gas with heating value of 900 B.t.u./S.C.F. is also considered.

3. Three different feeds; low CO case, intermediate CO case and high CO case, are considered. The temperature of the feed gas is fixed at 100°F for comparison. However, the effect of feed gas temperature will be discussed. The pressure of the feed gas is varied up to 1065 psia.

4. The compositions of feed gases and corresponding product gases are listed in Table 1-1. In addition, the feed gas containing 20% CO is also discussed.

Since it is presently impossible to estimate the costs of the various feed gases which depend largely on the primary gasification phases, only the equipment costs are considered. However, in the optimization study of heat exchangers, in addition to equipment cost, coolant water cost and steam benefit are also considered.

After optimization of the sub-system which involves the primary gasification phases, purification phases and other necessary phases including methanation phases has been completed, the overall plant optimization will be performed. Costs not included in the methanation study will then be taken into consideration in the overall plant optimization study. However, the optimization based on the equipment costs alone at this stage should be sufficient to provide necessary information for the selection of the best system among those considered for methanation.

2. REACTION KINETICS

(1) Reaction Rate Expressions for Methanation Reaction

The reactions taking place in the methanation process are:

1. Methanation Reactions:

$$CO + 3H_2 = CH_4 + H_2O \quad (2\text{-}1)$$

$$CO_2 + 4H_2 = CH_4 + 2H_2O \quad (2\text{-}2)$$

$$2CO + 2H_2 = CH_4 + CO_2 \quad (2\text{-}3)$$

2. Water-Gas Shift Reaction:

$$CO + H_2O = CO_2 + H_2 \quad (2\text{-}4)$$

3. Carbon Deposition Reactions:

$$2CO = C + CO_2 \quad (2\text{-}5)$$

$$CO + H_2 = C + H_2O \quad (2\text{-}6)$$

$$CH_4 = C + 2H_2 \quad (2\text{-}7)$$

Although reactions (2-1), (2-2), (2-3) and (2-4) must take place to a larger or smaller extent regardless of the feed compositions employed, for a high hydrogen concentration feed, only a small amount of CO_2 has been detected experimentally [1]. Therefore, reactions (2-2), (2-3) and (2-4) may be regarded as secondary reactions.

Because carbon deposition reduces the catalyst activity drastically, it is imperative that a range of temperature, pressure and feed compositions within which no carbon deposition takes place must be found. These conditions will become the constraints in the optimization of the processes.

A number of catalysts have been investigated for methanation reactions. The best catalyst for which kinetic data are available seems to be Harshaw Ni-0104 T and Harshaw Ni-0116 T having an average particle diameter of 1/4 inch and 1/8 inch, respectively. This catalyst contains 59% Ni, it has been shown that the catalyst behaves satisfactorily in the temperature range from 550°F to 850°F and the pressure range from 14.7 to 1000 psia without any carbon deposition [15].

A quantitative kinetic rate expression of the methanation reaction on the Harshaw catalyst is very difficult to obtain because extensive accurate kinetic data are not available. Therefore, it is necessary

to simplify the reaction mechanism to consider only reaction (2-1). The experimental data obtained from I.G.T. [15] using Harshaw catalysts can be correlated by two empirical equations, one for the temperature range at 550 to 600°F where reaction rate is controlling and another equation for temperature range of 600 to 850°F where diffusion is the rate controlling factor.

The empirical rate equations obtained are:

1. For temperature between 550°F and 600°F:

$$r_{CH_4} = 120 \exp\left[-\frac{15,660}{R(T+460)}\right] P_{CO}^{0.7} P_{H_2}^{0.3} \qquad (2\text{-}8)$$

2. For temperatures between 600°F and 850°F:

$$r_{CH_4} = 0.0696 P_{CO}^{0.7} P_{H_2}^{0.3} \qquad (2\text{-}9)$$

These equations are adequate for the present optimization purpose in getting a reasonably accurate assessment of the various processes and subsequent study shows that the overall optimum cost of the reactor system is not very strongly affected by the kinetic expresssions.

(2) Approach to Equilibrium

Although the above kinetic expressions were obtained from the experimental rate data of the methane forming reactions on the Harshaw catalyst including the runs under equilibrium hindrance, the equations do not provide the reverse reaction term. It would then be necessary to assure that the rate equations are not applied to conditions too close to the equilibrium.

The equilibrium constant based on mole fraction for the methanation reaction expressed as

$$K_{x_1^*} = \frac{(x^*_{CH_4})(x^*_{H_2O})}{(x^*_{CO})(x^*_{H_2})^3} \qquad (2\text{-}10)$$

and computed from the values given by the Bureau of Standards [14], is plotted in Figure 2-1 with the operating pressure as the parameter. Here, x_2^* refers to the equilibrium mole fraction of each component. As shown in the figure the equilibrium constant, $K_{x_1^*}$, is affected by the pressure and very strongly by the temperature. The equilibrium constant for the water gas shift reaction expressed as

$$K_{x_2^*} = \frac{(x^*_{CO_2})(x^*_{H_2})}{(x^*_{CO})(x^*_{H_2O})} \tag{2-11}$$

is also calculated from the Bureau of Standards [14] and is plotted in Figure 2-1. The extent of approach to the equilibrium for the methane reaction can be evaluated by computing the mass action law ratio of the product gases, K_{x_1}, defined as

$$K_{x_1} = \frac{(x_{CH_4})(x_{H_2O})}{(x_{CO})\ (x_{H_2})^3} \tag{2-12}$$

x's are the mole fraction of each component present in the reactor. It is decided arbitrarily to maintain $K_{x_1} < K_{x_1^*}/10$ at all time to assure the negligible reverse reaction. Whenever the above criterion is exceeded in the reactor, the temperature of the reactor is lowered to the point where the above condition is again satisfied. Such provision is necessary for the high CO case particularly near the exit of the reactor.

(3) Mass and Heat Transfer Within Catalyst Bed

Since the methanation reaction is highly exothermic and quite rapid, it will be necessary to examine the possible temperature and concentration difference between the bulk phase of reacting gas and the surface of the catalyst. Temperature difference between the bulk phase and the catalyst surface can be approximated by

$$T_s - T_b = \frac{r_s\ \Delta H}{h_p \pi d_p^2} \tag{2-13}$$

When particle-fluid radiation may be neglected, h_p can be calculated by [17]

$$J_H = \frac{h_p}{C_p G} N_{Pr}^{2/3} = 1.95 \left(\frac{d_p G}{\mu}\right)^{-0.51} \tag{2-14}$$

A maximum temperature difference $(T_s - T_b)_{max}$ can be calculated when the maximum reaction rate is used. When the temperature difference is too great, many undesirable phenomena may take place. A minimum mass flow rate corresponding to an allowable temperature difference exists for a given reaction rate. This becomes one of the constraints in the reactor optimization. Experimental measurement of temperature difference on the Harshaw catalyst carried out by I.G.T. [15] indicates a maximum temperature difference of approximately 11°F for the intermediate CO case under complete mixing of gas stream.

As the reaction is quite exothermic, it is also necessary to check the temperature gradient in the catalyst particles. If the reaction takes place uniformly in the catalyst particle, the heat balance equation in the catalyst can be written as

$$\frac{d^2T}{dr^2} + \frac{2}{r}\frac{dT}{dr} = \frac{r_s}{ke}\Delta H \quad , \tag{2-15}$$

where ke, the effective thermal conductivity of the catalyst particles, is expressed as

$$\frac{1}{ke} = \frac{1}{(1-\theta)k_s + \theta k_g} \tag{2-16}$$

Using the proper boundary conditions, Equation (2-15) can be solved for the temperature within the catalyst pellet as,

$$T = T_s + \frac{1}{6}\left(-\frac{r_s}{ke}\Delta H\right)\left[\left(\frac{d_p}{2}\right)^2 - r^2\right] \tag{2-17}$$

Numerical calculation shows the largest temperature difference in the catalysts particle to be about 30°F.

The concentration difference between the bulk phase and at the surface of catalyst pellets can be estimated by

$$C_s - C_b = \frac{r_s}{k_f \pi d_p^2} \tag{2-18}$$

where k_f is the fluid-particle mass transfer coefficient in a packed bed and is computed by [8]

$$\frac{J_M}{(1-\epsilon)^{0.2}} = 1.40\left[\frac{d_p G}{\mu(1-\epsilon)}\right]^{-0.41} \tag{2-19}$$

Numerical calculations show no appreciable difference between the catalyst surface concentrations and the bulk gas concentration of each component.

3. REACTOR PERFORMANCE EQUATIONS

Flow behavior in a fixed bed usually can be represented either by the dispersion model or by the cells-in-series model.

The following material balance equations are obtained around the n-th cell based on the cells-in-series model:

$$F_1^n = F_1^{n-1} + \rho_c V_c^n r_{CH_4} \tag{3-1}$$

$$F_2^n = F_2^{n-1} - \rho_c V_c^n r_{CH_4} \tag{3-2}$$

$$F_3^n = F_3^{n-1} - 3\rho_c V_c^n r_{CH_4} \tag{3-3}$$

$$F_4^n = F_4^{n-1} \tag{3-4}$$

$$F_5^n = F_5^{n-1} + \rho_c V_c^n r_{CH_4} \tag{3-5}$$

$$F_6^n = F_6^{n-1}$$

The heat balance equations around the n-th cell can be obtained similarly as

$$T^n \sum_{i=1}^{6} C_{P_i}^n F_i^n - T^{n-1} \sum_{i=1}^{6} C_{P_i}^{n-1} F_i^{n-1} = (\Delta H) \rho_c V_c^n r_{CH_4} - Q^n \tag{3-7}$$

The heat of reaction, ΔH, is in B.t.u. per pound mole of CH_4 formed and is given as

$$\Delta H = 87787.8 + 11.87\, T^n - 0.00668\, (T^n)^2 \tag{3-8}$$

The pressure drop across the n-th cell can be computed based on Ergun's equation [6]:

$$\Delta P = \frac{150(1-\varepsilon)\left(\frac{\mu}{d_p G}\right) + 1.75}{[\varepsilon^3/(1-\varepsilon)](d_p/C_L)(g\rho/G^2)} \tag{3-9}$$

4. COST INFORMATION

The costs of equipment required in the methanation processes are estimated based on the following equations:

(1) In methanation processes, heat exchangers are required to preheat the feed gas, to cool the product gas and to cool the intermediate product in the case of the cold quench system.

The following equation is used to estimate the heat exchanger cost based on the required heat transfer area, A_o (sq.ft.) [12]:

$$E_H = C_y I_f \left[850 \left(\frac{A_o}{50}\right)^{0.56}\right], \qquad A_o > 1{,}000 \text{ ft}^2 \tag{4-1}$$

(2) In the heat extraction system, heat generated in the reactor must be removed internally. The fin tubes may be used effectively for this purpose by embedding them into the catalyst. The cost of fin-tubes based on the bare tube heat transfer area, A_b(sq.ft.), used in the computation is given as [12],

$$E_F = C_y I_f \left[350 \left(\frac{A_b}{60}\right)^{0.88}\right], \qquad A_b > 1{,}000 \text{ ft}^2 \tag{4-2}$$

(3) The cost of the Harshaw catalysts used may be expressed as [5]

$$E_C = 2.5\ W_C \tag{4-3}$$

(4) The estimated cost of high pressure reactor shell is based on the weight of an empty reactor. The thickness of the reactor wall, T_h (inches), is calculated based on ASME boiler and pressure vessel code section 8 [2] given as,

$$T_h = PR/(SE - 0.6\ P) \tag{4-4}$$

The top and the bottom of the reactor are calculated based on an equivalent flat blank diameter necessary to form the required dome.

The weight of the reactor, W_R, is then computed by

$$W_R = \rho_m \left\{ \left[\frac{\pi}{4}\left(D + \frac{T_h}{6}\right)^2 - \frac{\pi}{4} D^2\right] L + 2\left(\frac{\pi F_d^2}{4}\right)\left(\frac{T_h}{12}\right) \right\} \tag{4-5}$$

The cost of the reactor becomes

$$E_R = C_R I_f W_R \tag{4-6}$$

(5) Cost of mild steel catalyst support trays:

$$E_S = 0.195\ I_f (D + 5)^{3.13} \tag{4-7}$$

For a chrome-type tray:

$$E_S = 0.216\ I_f\ (D + 5)^{3.13} \tag{4-8}$$

The total tray cost is

$$E_{ST} = N \cdot E_S \tag{4-9}$$

(6) The cost of a control valve can vary widely depending on the sizes and is rather difficult to estimate. An average of $4,000 per valve is used in this estimation.

(7) Since the heat insulation cost of the reactor is rather small, an approximate cost of 1.5% of the total fixed cost is added as the insulation cost [3].

(8) Compressors are needed for compressing the feed gas or product gas if necessary, and for recycling the product gas. The following equations are used to estimate the brake horse power [11]

$$B = \frac{Ta}{520} \frac{0.0643\ q_p}{E\eta} \left[\left(\frac{P_b}{P_a}\right)^{\eta} - 1\right] \tag{4-10}$$

The feed compressor cost can be computed by [4]

$$E_{cp} = 696\ (B)^{0.81} \tag{4-11}$$

The cost of recycle compressor may be determined using the following equations:

$$Br = \frac{(T^N)(0.0643)\ q_r}{520\ E\eta} \left[\left(\frac{P^0}{P^N}\right)^{\eta} - 1\right] \tag{4-12}$$

and

$$E_{CR} = 698\ (Br)^{0.81} \tag{4-13}$$

(9) Pumps are required to deliver the water coolant. The following equations are used to estimate pump costs [4, 11]

For steel-made water pump,

$$B_p = \frac{q'_w \rho \Delta h}{246,800} \tag{4-14}$$

and

$$E_P = 684\ (B_p)^{0.467} \tag{4-15}$$

In the process optimization of the heat exchangers, water is used for cooling. The costs of treated and spent water are $0.12 per thousand

gallon and $0.05 per thousand gallon, respectively. The prices for 400 psia steam and 35 psia steam produced in the heat exchangers are $0.30 per thousand pound and $0.15 per thousand pound, respectively. The annual capitalization charge for the equipments are calculated at 13% of the initial cost per year, as recommended by the Office of Coal Research, Department of the Interior.

5. PROCESS OPTIMIZATION OF HEAT EXCHANGERS

Since a large amount of heat is released in the methanation reaction, heat removal from reactors and product gases become the major problem in the optimization study. Three different types of heat exchangers are required in the methanation process, namely the preheater, the product gas cooler and the intermediate cooler. In this section, a process optimization of these heat exchangers is discussed.

(1) Preheater

The feed gas must be preheated to a temperature above the reaction initiation temperature. The feed gas preheating is accomplished by exchanging heat between the product gas and the feed gas.

The total annual cost for the preheater can be represented by the following equation [13]

$$C_T = A_o K_F C_{Ao} + A_o E_i H_y C_i + A_o E_o H_y C_o \qquad (5\text{-}1)$$

The area for heat transfer, A_o, is a function of h_i, h_o and Δt_m as given by the following equation

$$\frac{F_T \Delta t_m}{q} = \frac{1}{U_P A_o} = \frac{1}{A_o}\left(\frac{D_o}{D_i h_i} + \frac{1}{h_o} + R_{dw}\right) \qquad (5\text{-}2)$$

Thus Equation (5-2) may be written in terms of h_i, h_o and A_o as,

$$G = A_o K_F C_{Ao} + A_o \alpha_i h_i^{3.5} H_y C_i + A_o \alpha_o h_o^{4.75} H_y C_o \qquad (5\text{-}3)$$

where α_i and α_o are the proportionality constants which depend on designing condition and fluid properties.

Applying the "Lagrange multiplier method," Equation (5-3) becomes

$$G = A_o K_F C_{Ao} + A_o \alpha_i h_i^{3.5} H_y C_i + A_o \alpha_o h_o^{4.75} H_y C_o + \lambda'\left[\frac{F_T \Delta t_m}{q} - \frac{1}{A_o}\left(\frac{D_e}{D_i h_i} + \frac{1}{h_o} + R_{dw}\right)\right] \qquad (5\text{-}4)$$

where λ' is the Lagrange multiplier. A computer program of Equation (5-4) is already available [9]. From this computation the optimum overall heat transfer coefficient is found to be about 70 B.t.u./ft.^{2}hr.°F. This value is used in the subsequent design calculation of the preheaters associated with the various methanation processes.

(2) Product Gas Cooler

After flowing through the preheater, the product gas is cooled to 100°F by three heat exchangers. The exit product gas from the preheater has the temperature ranging between 400°F and 750°F.

400 psia steam is produced in the first heat exchanger while steam of about 35 psia is produced in the second heat exchanger. The product gas cooler is finally cooled down to 100°F by the counter-current product gas cooler. The coolant water enters at a temperature of 85°F and leaves at 150°F. If the inlet gas temperature to the first heat exchanger is below 500°F, only two heat exchangers are required.

In the first heat exchanger, treated water enters the tube side. Approximately 50% of the water entered is vaporized producing high pressure steam. The product gas flows in the shell side providing the main heat transfer resistance of this exchanger. The shell side film coefficient can be calculated by

$$\left(\frac{h_o D_e}{k}\right) = 0.36 \left(\frac{D_e G_s}{\mu}\right)^{0.55} \left(\frac{C_p \mu}{k}\right)^{1/3} \qquad (5\text{-}5)$$

Pressure drop for shell side fluid is calculated by the following equation [10]

$$\Delta P_S = \frac{f G_S^2 D_S L_H}{5.22 \times 10^{10} D_e s B'} \qquad (5\text{-}6)$$

and

$$f = 1.2 \times 10^{-2} \left(\frac{D_e G_S}{\mu}\right)^{-0.189} \qquad (5\text{-}7)$$

If the combined pressure drop of the three product gas coolers is limited to 10 psia, the corresponding maximum mass velocity is about 100,000 lb./ft.^{2}hr. The shell side film heat transfer coefficient corresponding to this mass velocity is about 110 B.t.u./ft.^{2}hr.°F.

Since two phases exist in tube side, the inside tube film heat transfer coefficient may vary from 200 to 1000 B.t.u./ft.^{2}°Fhr. The overall heat transfer coefficient of the first heat exchanger then becomes approximately 85 B.t.u./ft.^{2}hr.°F.

Similar to the previous case treated, water is introduced into the second heat exchanger with 50% of water being vaporized in the tube side. The product gas is passed through the shell side which again provides the main heat transfer resistance of this exchanger. However, when the temperature of the product gas is reduced below 370°F, partial condensation of the water takes place in the shell side. The quantity of condensation depends upon the partial pressure of water in the product gas.

Heat flux accompanied by steam condensation is expressed as

$$q_c = K_G M_v \lambda_c (P_v - P_c) \qquad (5\text{-}8)$$

Since steam condensing on the tube may be regarded as simultaneous heat and mass transfer phenomena, K_G may be expressed as

$$K_G = \frac{h_o (C_p \mu / k)^{2/3}}{C_{p,p_{gf}} M_m (\mu / \rho k_d)^{2/3}}, \qquad (5\text{-}9)$$

The total heat flux is a sum of the heat flux due to non-condensing vapor and the heat flux accompanied by the condensation. Hence,

$$q_T = h_o(T_g - T_c) + K_G M_v \lambda_c (P_v - P_c) = h_c(T_g - T_c) \qquad (5\text{-}10)$$

Calculations using Equations (5-5) and (5-10) give the range of the shell side film heat transfer coefficient to be between 110 and 210 B.t.u./hr.ft.^{2}°F under an allowable combined pressure drop of 10 psi.

The tube side film heat transfer coefficient is practically the same as that for the first heat exchanger. The overall heat transfer coefficient of the second heat exchanger then becomes approximately 90 B.t.u./ft.^{2}hr.°F.

In the third heat exchanger, process water is used in the tube side and product gas is passed through the shell side. Using Equations (5-5) and (5-10), the film coefficient of shell side fluid, which is also affected by the partial condensation of water, is calculated to be between 110 to 150 B.t.u./hr.ft.^{2}°F under the allowable pressure drop. The tube side heat transfer coefficient is about 250 ~ 300 B.t.u./hr.ft.^{2}°F for this operating condition. Thus, the overall heat transfer coefficient of the third heat exchanger is calculated to be approximately 80 B.t.u./ft.^{2}hr.°F.

In the process optimization of product gas coolers, the optimum temperatures of gas entering the second and the third heat exchanger are to be found so as to minimize the total equipment and operation costs of the three heat exchangers under the specified temperature constraints. The total cost consisting of the equipment cost of the three heat exchangers, the water cost and the steam benefit, is expressed as

$$C_T = \emptyset' E_H + (C_1 W_1 + C_2 W_2) - (C_3 W_{S1} + C_4 W_{S2}) \qquad (5\text{-}11)$$

The heat duties of the first, the second and the third heat exchanger are expressed as:

$$q^I = \bar{M} W^N (\bar{C}_p^P T^P - \bar{C}_p^I T^I) \qquad (5\text{-}12)$$

$$q^{II} = \bar{M} W^N (\bar{C}_p^I T^I - \bar{C}_p^{II} T^{II}) + 18 \left(\frac{P_w}{P_t} - \frac{P^{II}}{P_t}\right) \lambda_c W^N \qquad (5\text{-}13)$$

$$q^{III} = \bar{M} W^N (\bar{C}_p^{II} T^{II} - \bar{C}_p^F T^F) + 18 (P_v/P_t) \lambda_c W^N \qquad (5\text{-}14)$$

The heat transfer area of the first exchanger is calculated as follows:

First, the water flow rate through the first exchanger is calculated from

$$WC^I = \frac{q^I}{C_{pw}(t_{C1} - t_C') + 0.5\lambda_c} \qquad (5\text{-}15)$$

After entering the first heat exchanger, the water is preheated to the vaporization temperature. This assures a near constant water temperature in the tube as long as the constant steam pressure is maintained. The product gas temperature corresponding to the point at which steam starts to vaporize can be found from,

$$T_m^I = T^I + \frac{WC^I \cdot C_{pw}}{\bar{M}\, W^N\, \bar{C}_P^I} \quad (t_{c1} - t_c') \tag{5-16}$$

The heat transfer area of the first heat exchanger is

$$A^I = \frac{WC^I}{U^I} \quad \frac{C_{pw}(t_{c1} - t_c')}{\Delta t_1} + \frac{0.5\lambda_c}{\Delta t_1'} \tag{5-17}$$

where Δt_1 and $\Delta t_1'$ are the log-mean temperature differences corresponding to the liquid phase and the subsequent vaporization phase, respectively. Next the heat transfer area of the second heat exchanger is calculated by the same procedure as the first exchanger.

The heat transfer area of the third heat exchanger is calculated as follows:

$$A^{III} = \frac{q^{III}}{U^{III}\Delta t_3} \tag{5-18}$$

where Δt_3 is the log-mean temperature difference in the third heat exchanger. The water flow rate in the third heat exchanger is calculated from

$$W_2 = \frac{q^{III}}{\bar{C}_{pw}(t_{c3} - t_c)} \tag{5-19}$$

Therefore, all terms in Equation (5-11) are expressed as the function of the inlet gas temperatures of the second and third heat exchangers. According to the numerical calculation, the optimum inlet gas temperatures of the second and third heat exchangers are 460°F and 270°F, respectively.

It is not possible however, at this stage to estimate how much process steam will be required for each of the various routes to be considered. Therefore, low costs of steam, $0.35/1,000 lb. for 400 psi steam and $0.15/1,000 lb. for 35 psi steam are used.

(3) Intermediate Cooler

In the cold quench system with a high CO content feed gas, the heat generated in the reactor is so large that it is necessary to cool the reactnat to a suitable temperature to recycle them. In this intermediate cooler, high pressure steam (400 psia) is recovered. The gas enters the heat exchanger at 850°F and must leave at a temperature higher than the reaction initiation temperature of 550°F. Since steam benefit is the over riding factor, it is clear that the optimum outlet temperature of the intermediate cooler must be the lowest possible temperature of 550°F. Since the fluid properties in the intermediate cooler are almost the same as that in the first heat exchanger of the product gas cooler, the overall heat transfer coefficient of this heat exchanger may be taken to be 85 B.t.u./ft.^{2}hr.°F. Water flow rate, W_{im}, and steam rate obtained in the intermediate cooler are,

$$W_{im} = \frac{w^o(\bar{C}_p^N T^N - \bar{C}_p^A T^A)}{C_{pw}(t_{c1}-t_c'')+0.5\lambda_c} \tag{5-20}$$

The heat transfer area of the intermediate cooler is obtained from

$$A_{im} = \frac{W_{im}}{U^I}\left[\frac{C_{pw}(t_{c1} - t_c'')}{\Delta t_A} + \frac{0.5\lambda_c}{\Delta t_B}\right] \tag{5-21}$$

where Δt_A and Δt_B are log-mean temperature differences in the intermediate cooler corresponding to the liquid phase and the subsequent vaporization phase, respectively.

6. THE HEAT EXTRACTION SYSTEM

(1) Process Analysis

The gaseous effluent from the primary gasification system, is fed into the methanation system at 100°F and 1065 psia. The gas has been preheated to 550°F, a temperature high enough to initiate the reaction before it is introduced to the top of the reactor.

In the upper portion of the reactor, reaction is carried out adiabatically until the maximum allowable temperature of 850°F (1) is reached. The reaction thereafter is carried out isothermally by removal of the excess heat of reaction from the reactor through the embedded fin tubes. In the high CO case, the temperature near the exit of the reactor is reduced to 810°F in order to avoid equilibrium hindrance. Heat is removed from the reactor by generating 400 psia steam in the fin tubes.

The exit gas pressure of the methanation process is fixed at 1015 psia. Therefore the total pressure drop, both in the reactor and in the heat exchangers must be kept less than 50 psia. These are the constraints in the design of the optimum reactor diameter.

(2) Calculation Procedure

As previously stated, in the heat extraction system the reactor is operated adiabatically until the temperature of 850°F is reached, after which the reactor is operated isothermally. Thus, the heat balance around the n-th cell can be written as,

For $T_1 < T < 850°F$

$$\sum_{i=1}^{6} C_{P_i}^{n} F_i^{n} T^{n} - \sum_{i=1}^{6} C_{P_i}^{n-1} F_i^{n-1} T^{n-1} = (\Delta H)\, \rho_c V_c^{n} r_{CH_4} \qquad (6\text{-}1)$$

and $T = 850°F$,

$$Q^{n} = (\Delta H)\, \rho_c V_c^{n} r_{CH_4} = U_o A_t^{n} (T^{n} - T_w) \qquad (6\text{-}2)$$

Since the main resistance to heat flow is across the gas film outside of the fin tubes, the resistance across the tube wall and that due to inside film of the coolant can be neglected. The overall heat transfer coefficient based on the outside surface of the fin tube is approximated to be 11 B.t.u./hr.ft.^{2}°F.

From the equations developed, the concentration of each component, the temperature and the pressure at each cell can be calculated under the adiabatic condition from the previous cell. The calculation is continued until the reactor temperature reaches 850°F. The calculation thereafter is repeated but under the isothermal condition until the

concentration of methane reaches 92.1% on a dry base. Since heat transfer area in a single cell does not have a practical meaning, an average heat transfer area of 40 cells-in-series which make up one tray length is calculated.

Since the heat generated in the low CO case is not very great, no heat removal from the reactor is necessary for this case. For the high CO case, the heat generation rate near the entrance of the reactor is so large that the catalyst are packed only partially in order to keep the gas temperature at 850°F. Also the temperature near the exit of the reactor is reduced to 810°F to avoid equilibrium hindrance of the methanation reaction.

The heat transfer areas of the preheater and the product gas cooler are calculated by the method mentioned in Section 5.

The total cost of the system can be computed from the summation of the individual costs; preheater, product gas cooler, catalyst, insulation, reactor, supporting tray, control valves and fin tubes. Here, the number of the control valves and their cost is estimated from the number of trays.

From the optimization point of view, the decision variables are the reactor diameter, D, the inlet pressure, P^o, and the inlet gas temperature to the reactor, $T^{(1)}$. A search technique as described in the next section is developed to determine these three variables by minimizing the total equipment cost. Since the gas temperature at the reactor inlet should be kept as low as possible to minimize the heat removal cost, the problem is reduced to that involving two decision variables; the reactor diameter and the inlet pressure.

(3) Optimum Search Techniques

In this study, the method of the steepest descent is used for the optimization study. This method starts with locating the direction of the steepest descent from an initial point, then search along this line until no further improvement can be made along this line. A new direction of the steepest descent is located at this point and searching is continued along the new line until no further improvement is possible. At this point, another new direction is found and the search continues.

For the search involving two independent variables, once the starting point is selected the search direction can be located by varying one variable at a time. When there are more than two variables involved, Powell's method which does not require the computation of derivatives is more conveniently employed. However, this procedure has no way of recognizing constraints on the variables and consequently this method is not effective for the problems with inequality constraints [7]. Computer programs were written to carry out the optimization calculations.

(4) Results and Discussion

The optimum process conditions and the optimum equipment costs for the three feeds are listed in Tables 6-1 and 6-2.

Since the heat generated in the low CO case is not very large, no heat removal from the reactor is necessary. The reactor is essentially operated adiabatically without internal heat removal or quenching.

Although the decision variables selected for optimization are the reactor diameter, the inlet pressure and the feed gas temperature, the feed gas temperature has been fixed at 550°F in actual calculation. This is because the reaction is not affected by temperature significantly after 600°F is reached probably due to the slow catalyst pore diffusion. Hence, there is no reason to increase the inlet temperature above 600°F.

As is evident from Tables 6-1 and 6-2, the heat exchanger costs, particularly the preheater cost and the product gas cooler cost, are the major items of the total equipment cost. Any effective scheme to reduce the size of heat exchanger will reduce the total cost most significantly. Had the reactor been permitted to oeprate at a feed gas temperature of 500°F, the total cost would have been reduced further.

Each section of the reactor between the two adjacent trays is made up by forty cells equivalent to 40 inches of fixed bed packed with catalyst and fin tubes. The fin tubes have equal heat transfer area in each section. Therefore, the temperature in the isothermal portion of the reactor is not necessarily maintained at the specified 850°F. The temperature deviation is not serious, however, with the largest deviation of only 16°F occurring at the final tray in the high CO case.

TABLE 6-1 OPTIMUM PROCESS CONDITIONS
IN TWO DIFFERENT FEEDS
FOR HEAT EXTRACTION SYSTEM

	Intermediate CO	High CO
Inlet temperature, °F	100	100
Outlet temperature, °F	100	100
Inlet pressure, psig	1,050	1,050
Outlet pressure, psig	1,000	1,000
Reactor diameter, ft.	7.0	8.0
Reactor height, ft.	15.2	23.5
Space velocity,* $hr.^{-1}$	1,420	1,270
Catalyst weight, lbs.	17,390	22,340
Total heat transfer surface area of fin tube, $ft.^2$	31,400	94,500
Heat transfer surface area of preheater, $ft.^2$	10,320	13,520
Heat transfer surface area of product gas cooler II, $ft.^2$	10,900	18,360
Heat transfer surface area of product gas cooler III, $ft.^2$	20,000	21,140
Flow rate of 35 psia steam in heat exchangers, lb./hr.	55,530	76,670
Flow rate of treated water in heat exchangers, lb./hr.	111,000	153,400
Flow rate of process water in heat exchangers, lb./hr.	149,200	157,600
Flow rate of 400 psia steam in fin tubes, lb./hr.	105,790	356,600
Flow rate of treated water in fin tubes, lb./hr.	105,790	356,500

*Based on inlet condition. (550°F, 1065 Psia)

TABLE 6-2 OPTIMUM EQUIPMENT COSTS
IN TWO DIFFERENT FEEDS
FOR HEAT EXTRACTION SYSTEM

	Intermediate CO	High CO
Catalyst, $	43,500	55,900
Reactor and tray, $	124,800	223,000
Control valve, $	20,000	28,000
Fin tube, $	49,600	131,140
Preheater, $	81,600	81,400
Product gas cooler I, $	0	0
Product gas cooler II, $	84,130	112,800
Product gas cooler III, $	118,300	122,000
Separator drum and recycling pump (in fin tube system), $	20,250	36,850
Total equipment, $	542,180	754,240

7. THE COLD QUENCH SYSTEM

(1) Process Analysis and Calculation Procedure

In the cold quench system, only a small portion of the fresh feed is preheated and enters the top of the reactor. The remainder of the fresh feed at relatively low temperature enters at prescribed intervals into the reactor in such a way that the effluent from the preceding bed is cooled substantially to maintain the reactor temperature below the maximum allowable temperature. In effect, the excess heat generated by the reaction is absorbed into the sensible heat of the feed gas. If the excess heat generated by the reaction is more than that can be absorbed by the sensible heat of the feed gas, it is necessary to use more than one reactor with provisions for intermediate cooling. The maximum allowable temperature is again taken to be 850°F for all cases except for the high CO case in which the exit temperature from the last reactor is reduced to 810°F for reasons previously discussed. The pressure drop in both the reactor and the product gas coolers is limited to less than 50 psia.

Since the amount of heat generated by the reaction, Q_c, is strongly affected by the feed gas composition as can be seen from

$$Q_c = (\Delta H)\, F^0 \cdot y^N \qquad (7\text{-}1)$$

As mentioned previously, the heat generated for the low CO case is less than the sensible heat of the reactant gas so it is not necessary to perform cold quenching. From the heat generation as well as from the economics points of view, only one reactor without the intermediate cooling will be necessary for the intermediate CO case. However, for the high CO case, three reactors with two intermediate coolers will be needed.

1. Intermediate CO Case

A portion of the feed gas is preheated to $T^{(1)}$ by the preheater prior to entering the top of the reactor. The first cold shot of feed is introduced to cool the reacting gas at a point where the gas temperature has reached the maximum allowable value of 850°F. Since the reaction rate is not significantly affected by the temperature above 600°F, an exact amount of cold quench that will bring down the gas temperature to 600°F should be introduced.

The heat balance across the reactor can be written as

$$T^N \sum_{i=1}^{6} C_{P_i}^N F_i^N = (1 - \lambda_1')T^F \sum_{i=1}^{6} C_{P_i}^F F_i^0 + \lambda_1' T^{(1)} \sum_{i=1}^{6} C_{P_i}^{(1)} F_i^0 + Q_c \qquad (7\text{-}2)$$

If $T^{(1)}$ is known, λ_1' is calculated from Equation (7-2). The concentration of each gaseous component and temperature profiles can then be calculated by the same method described in the heat extraction system. The calculation is continued until the temperature in the reactor reaches 850°F.

In the cold quench system, the reactor is subdivided into a number of sections which are separated by the cold quench point. At each quenching point, both the flow rate of the cold quenching gas required and the gas composition after the quenching, can be calculated from the flow rate and the temperature of the gas before quenching. Therefore knowing the inlet temperature, $T^{(1)}$, the concentrations of each component and the temperature distribution in the reactor can be calculated.

The total equipment cost for the intermediate CO case is obtained by the summation of the individual equipment cost; preheater, product gas cooler, catalyst, reactor and tray, control valves and thermal insulation. These costs are calculated from the design condition of the reactor and the heat exchangers together with the cost equations described in Section 4.

In obtaining the reactor and tray cost, the distance between the two adjacent sections of catalyst allowed for the quenching gas to mix with the hot gas, is taken to be 0.5 feet.

The decision variables studied in the optimization of this system for the intermediate CO case are the gas temperature at the reactor inlet, $T^{(1)}$, and the reactor diamter, D. Optimization technique used is the same as that for the high CO case in the cold quench system.

2. High CO Case

Since a large amount of heat is released in this case, a single reactor cannot accommodate the necessary conversion. Two process arrangements are considered. In System I, a portion of the fresh feed gas is preheated and enters the top of the first reactor. The remainders of the feed are introduced at intervals along the reactor in order to cool the reactant gas.

When the gas temperature in the first reactor reaches 850°F after the final quenching, the reactant gas leaves the first reactor and is cooled by the preheater and the intermediate cooler I.

A portion of the reactant gas then enters the top of the second reactor. The remainder of the reactant gas is cooled by the intermediate cooler II and is fed at intervals along the second reactor to cool the reactant gas. After leaving the second reactor, the product gas is cooled in the product gas coolers I, II and III to 100°F. 400 psia steam is recovered from the intermediate cooler I and the product gas cooler I and 35 psia steam is recovered by the intermediate cooler II and the product gas cooler.

In System II, the arrangement for the first reactor is the same as in System I. When the gas temperature in the first reactor reaches 850°F after the last quenching, the reactant gas is introduced to the intermediate cooler I and is cooled to $T^{(2)}$ and fed to the second reactor. When the temperature in the second reactor reaches 850°F, the reactant gas leaves the second reactor and is cooled by the intermediate cooler II to $T^{(3)}$ and thereafter enters the third reactor.

As the product gas leaves the third reactor, it is cooled by the feed gas preheater and subsequently by the product gas coolers I, II and III to 100°F. Again 400 psia steam is recovered from the intermediate coolers I and II and the product gas cooler I, while 35 psia steam is recovered from the product gas cooler II.

A rough calculation shows that the total heat exchanger cost for System II is smaller than that for System I and the steam benefit for System II is larger than that for System I. It also shows that the catalyst weight for System II is smaller than that for System I because no quenching for the second and the third reactor is required. Therefore, System II is selected for the optimization study. The calculation procedure for the optimization of System II is as follows:

The heat balance across the third reactor can be written as

$$T^E \sum_{i=1}^{6} C_{P_i}^E F_i^E - T^{(3)} \sum_{i=1}^{6} C_{P_i}^{(3)} F_j^{(3)} = \Delta H\, F^0\, (y^N - y^{(3)}) \qquad (7\text{-}3)$$

If the temperature, $T^{(3)}$, is known, the conversion, $y^{(3)}$, is calculated from Equation (7-3).

The heat balance across the second reactor is

$$T^N \sum_{i=1}^{6} C_{P_i}^N F_i^{(3)} - T^{(2)} \sum_{i=1}^{6} C_{P_i}^{(2)} F_i^{(2)} = \Delta H\, F^0 (y^{(3)} - y^{(2)}) \qquad (7\text{-}4)$$

If the inlet temperature $T^{(2)}$ is known, the conversion $y^{(2)}$ is calculated from Equation (7-4).

The heat balance across the first reactor can be written as,

$$T^N \sum_{i=1}^{6} C_{P_i}^N F_i^{(2)} = (1 - \lambda_1')T^F \sum_{i=1}^{6} C_{P_i}^F F_i^0 + \lambda_1' T^{(1)} \sum_{i=1}^{6} C_{P_i}^{(1)} F_1^0 + \Delta H \cdot F^0 \cdot y^{(2)} \qquad (7\text{-}5)$$

If the inlet temperature of the first reactor $T^{(1)}$ is given, the fraction of feed gas required for the first quenching, λ_1', is calculated by Equation (7-5). The catalyst weight and reactor sizes of three reactors are calculated from λ_1', $y^{(2)}$ and $y^{(3)}$.

The total equipment cost for the high CO case is obtained by the summation of the individual equipment costs; preheater, product gas coolers I, II and III, intermediate coolers I and II, catalyst, reactors and trays, control valves, and heat insulation.

In optimization of System II, the decision variables are the diameters and inlet temperatures for the three reactors. The inlet temperatures for the first reactor should be as low as possible, because under this condition the preheater cost is the lowest and steam benefit for the product gas cooler I is the highest. The inlet temperature of the second and the third reactors also should be as low as possible

because the steam benefits for the intermediate coolers I and II are the highest under this condition. Thus, the optimum inlet temperature for the three reactors must be selected at 550°F. Hence the optimization problem for this case is reduced to that of searching the optimum reactor diameters.

(2) Results and Discussion

Table 7-1 and 7-2 show the operating conditions and the optimum equipment costs for the cold quench system under the two different feeds.

The quantity of the quenching gas and the locations of the quenching points are determined by assuming the reactant temperature before and after quenching to be at 850°F and 600°F, respectively. The reactor and catalyst costs calculated based on such temperature constraints are not necessarily the true optimum values, however. According to Tables 6-3 and 7-2, the catalyst cost for the cold quench system is no more than 1.3 times that for the heat extraction system. Therefore the cost of reactor and catalyst estimated can be considered to be very close to the true optimum value.

TABLE 7-1 OPTIMUM PROCESS CONDITIONS IN THREE DIFFERENT FEEDS FOR COLD QUENCH SYSTEM

	Low CO	Intermediate CO	High CO
Inlet temperature, °F	100	100	100
Outlet temperature, °F	100	100	100
Inlet pressure, psig	1,050	1,050	1,050
Outlet pressure, psig	1,000	1,000	1,000
First reactor diameter, ft.	5.9	6.2	6.2
First reactor height, ft.	10.1	18.75	3.4
Second reactor diameter, ft.	--	--	6.6
Second reactor height, ft.	--	--	3
Third reactor diameter, ft.	--	--	7.2
Third reactor height, ft.	--	--	8.5
Space velocity,* $hr.^{-1}$	1,890	1,080	1,200
Catalyst weight, lbs.	12,030	22,930	23,740
Heat transfer surface area of preheater, $ft.^2$	9,015	2,175	6,090
Heat transfer surface area of intermediate cooler I, $ft.^2$	--	--	7,680
Heat transfer surface area of intermediate cooler II, $ft.^2$	--	--	7,530
Heat transfer surface area of product gas cooler I, $ft.^2$	--	8,480	6,075
Heat transfer surface area of product gas cooler II, $ft.^2$	5,920	11,930	15,670
Heat transfer surface area of product gas cooler III, $ft.^2$	18,600	26,630	21,240
Flow rate of 400 psia steam in intermediate cooler I and II, lb./hr.	--	--	336,670
Flow rate of treated water in intermediate cooler I and II, lb./hr.	--	--	336,670
Flow rate of 400 psia steam in heat exchangers, lb./hr.	--	108,100	22,000
Flow rate of 35 psia steam in heat exchangers, lb./hr.	38,450	101,000	138,130
Flow rate of treated water in heat exchangers, lb./hr.	76,900	202,000	276,280
Flow rate of process water in heat exchangers, lb./hr.	138,000	1,249,500	1,319,470

*Based on inlet condition. (55°F, 1065 Psia)

TABLE 7-2 OPTIMUM EQUIPMENT COSTS
IN THREE DIFFERENT FEEDS
FOR COLD QUENCH SYSTEM

	Low CO	Intermediate CO	High CO
Catalyst, $	30,000	57,300	59,350
Reactor and tray, $	66,100	88,270	167,400
Control valve, $	12,000	18,000	14,000
Preheater, $	75,510	34,000	53,490
Intermediate cooler I, $	--	--	62, 270
Intermediate cooler II, $	--	--	61,560
Product gas cooler I, $	--	73,030	56,360
Product gas cooler II, $	55,730	88,470	92,720
Product gas cooler III, $	109,260	118,600	110,160
Total Equipment, $	348,600	477,670	677,320

8. THE RECYCLE SYSTEM

(1) Process Analysis and Calculation Procedure

In the recycle system, total heat generated in the reactor is absorbed by the portion of the product gas being recycled to absorb the heat.

From the heat balance across the reactor, the following equations are obtained.

$$T^N \sum_{i=1}^{6} C_{P_i}^N F_i^N - T^{(1)} \sum_{i=1}^{6} C_{P_i}^{(1)} F_i^{(1)} = Q_c \tag{8-1}$$

and

$$F_i^{(1)} = F_i^0 + F_i^r \tag{8-2}$$

If the total amount of heat generated in the reactor, Q_c, is known, the recycle flow rate $\sum_{i=1}^{6} F_j^r$ is calculated from Equations (8-1) and (8-2). The inlet flow rate and the compositions are then calculated. The reactor size and the catalyst weight for this system are determined from the performance equations.

When the enthalpy of the inlet gas $T^{(1)} \sum_{i=1}^{6} C_{P_i}^{(1)} F^{(1)}$ is larger than both the enthalpy of the feed gas, $T^F \sum_{i=1}^{6} C_{P_i}^F F_i^0$ and that of the recycle gas, $T^N \sum_{i=1}^{6} C_{P_i}^N F_i^r$, it is necessary to preheat the feed gas to $T^{(PF)}$. The temperature $T^{(PF)}$ to which the gas must be preheated is calculated from the heat balance around the point where the feed mixes with the recycle gas, according to the following equation:

$$T^{(PF)} \sum_{i=1}^{6} C_{P_i}^{(PF)} F_i^0 + T^N \sum_{i=1}^{6} C_{P_i}^N F_i^r = T^{(1)} \sum_{i=1}^{6} C_{P_i}^{(1)} F_i^{(1)} \tag{8-3}$$

The size of the preheater required is calculated from $T^{(PF)}$ by the same procedure described in Section 5.

When the enthalpy of the inlet gas is smaller than that of the feed gas and the recycle gas, it is necessary to cool the recycle gas to $T^{(Nr)}$. The temperature $T^{(Nr)}$ of the gas leaving the recycle gas cooler is calculated from the heat balance around the mixing point as

$$T^F \sum_{i=1}^{6} C_{P_i}^F F_i^0 + T^{(Nr)} \sum_{i=1}^{6} C_{P_i}^{(Nr)} F_i^r = T^{(1)} \sum_{i=1}^{6} C_{P_i}^{(1)} F_i^{(1)} \tag{8-4}$$

The size of the recycle gas cooler producing 400 psia steam is calculated from $T^{(Nr)}$ by the same procedure used in the intermediate cooler. The size of the recycle gas is calculated based on the pressure drop in the reactor and the flow rate of the recycle gas.

TABLE 8-1 OPTIMUM PROCESS CONDITION IN TWO DIFFERENT FEEDS FOR RECYCLE SYSTEM

	Intermediate CO	High CO
Inlet temperature, °F	100	100
Outlet temperature, °F	100	100
Inlet pressure, psig	1,050	1,050
Outlet pressure, psig	1,000	1,000
Number of reactors	4	8
Reactor diameter	5.8	6.0
Reactor height, ft.	6.02	5.95
Catalyst weight, lbs.	28,030	58,730
Space velocity*, $hr.^{-1}$	882	484
Heat transfer surface area of preheater, $ft.^2$	1,593	--
Heat transfer surface area of recycle gas cooler I, $ft.^2$	--	6,140
Heat transfer surface area of product gas cooler I, $ft.^2$	8,500	10,150
Heat transfer surface area of product gas cooler II, $ft.^2$	11,775	15,630
Heat transfer surface area of product gas cooler III, $ft.^2$	19,900	21,195
Flow rate of treated water in heat exchangers, lb./hr.	320,000	317,930
Flow rate of spent water in heat exchangers, lb./hr.	1,236,170	1,316,140
Flow rate of 400 psia steam in heat exchangers, lb./hr.	108,330	178,330
Flow rate of 35 psia steam in heat exchangers, lb./hr.	95,330	139,670
Recycle ratio	0.7796	2.911
Flow rate of treated water in recycle gas cooler, lb./hr.	--	147,860
Flow rate of 400 psia steam from recycle gas cooler, lb./hr.	--	147,860

*Based on inlet condition. (550°F, 1065 Psia)

TABLE 8-2 OPTIMUM EQUIPMENT COSTS IN TWO DIFFERENT FEEDS FOR RECYCLE SYSTEM

	Intermediate CO	High CO
Catalyst, $	70,080	146,830
Reactor and tray, $	169,970	363,560
Valve and flow meter, $	48,000	80,000
Preheater, $	28,540	0
Recycle gas cooler, $	0	60,930
Product gas cooler I, $	73,170	80,880
Product gas cooler II, $	87,840	103,030
Product gas cooler III, $	117,990	122,230
Recycling compressor, $	81,000	244,000
Total equipment, $	676,590	1,201,460

9. DISCUSSION

(1) Comparison of the Equipment Costs for the Three Different Feeds

1. Heat Exchanger Costs

For heating and cooling of the process fluids, preheaters, product gas coolers, intermediate coolers, recycle coolers and embedded fin tubes are used. The preheater cost for the heat extraction system is most expensive among the three systems considered. This is because the entire feed gas must be heated to the required inlet reactor temperature. In the cold quench system, only a fraction of the feed gas is preheated while in the recycle system, the preheater is not needed except for the intermediate CO case.

It appears evident that the cost of the product gas cooler is highest for the recycle system and is lowest for the heat extraction system. For the cold quench system, the cost of the product gas cooler depends largely on the fraction of the feed gas introduced to the top of the reactor, λ_1', and is in general between that of the recycle system and the heat extraction system. As to the costs of fin tubes, intermediate coolers and recycle gas coolers, they are related to the amount of heat removed during the reaction and therefore are higher as the CO content of the feed gas is increased.

2. Catalyst and Reactor Costs

It is readily seen that the catalyst cost for the heat extraction system is the cheapest and that for the recycle system is the most expensive among the three systems. The catalyst cost for the cold quench system ranks in the middle of the two, leaning closely to that of the heat extraction system. In contrast to the lowest catalyst cost for the heat extraction system, the reactor cost is larger than the cold quench system because a large reactor volume is occupied by the embedded fin tubes. However, for the high CO case when three reactors are needed to accomplish the cold quenching, the reactor costs of the two systems becomes approximately the same.

The reactor cost for the recycle system is the highest since the catalyst volume required is the largest among the three systems.

In view of the high reactor and the catalyst costs as well as the high recycle gas compressor cost in the recycle system, this system is the least economical system.

Figure 9-1 shows the relation between the total equipment cost and the concentration of CO in the feed gas. From this figure, it may be concluded that the cold quench system is the most economical system among the three systems for the intermediate CO case and the high CO case.

(2) Effect of Temperature of the Feed Gas on Total Equipment Cost

In the optimization of this process, the decision variables considered are the reactor diameter, the inlet and outlet temperature of the gas $T^{(1)}$ and T^{N}, and the number of reactors in parallel. In the recycle system, volumetric flow rate in the reactor and consequently the reactor diameter is so large, especially for the high CO case, it is necessary to find the optimum number of reactors for this case. In the cost estimation of this process, as the number of reactors is increased, $8,000 per each reactor is added as the costs of control valves and other instrumentation.

However, as the temperature difference between $T^{(1)}$ and T^{N} increases, the recycle gas rate is decreased, reducing the reactor cost, catalyst cost and recycle pump cost. Therefore, the optimum gas temperature at the reactor inlet is 550°F for each CO case and the optimum gas temperatures at the outlet of the reactor are 850°F for the intermediate CO case and 810°F for the high CO case, respectively.

Consequently, the remaining decision variable, the numbers of reactors in parallel, and the reactor diameters are searched in the optimization study of this system.

(2) Results

Figure 8-1 and 8-2 show the effect of the reactor diameter on the total equipment cost with the number of reactors as parameter for the intermediate CO case and the high CO case, respectively. From Figure 8-1, the optimum number of reactors in parallel is seen to be 4, and the optimum reactor diameter to be 5.8 ft. for the intermediate CO case. From Figure 8-2, the optimum number of reactor and the reactor diameter for the high CO case are 8 and 6.0 ft., respectively. Comparing Figure 8-1 with 8-2, a considerable effect of the number of reactors in parallel on the total equipment cost is noted for the cases where large-diameter reactors are used. The differences between the optimum equipment cost for one reactor and that with optimum number of reactors in parallel are $190,000 for the high CO case, but only $13,000 for the intermediate CO case. Table 8-1 and 8-2 list the optimum operating conditions and the optimum equipment costs for the recycle systems.

From Table 8-2, the reactor and catalyst costs for this system are seen to be most expensive among the three systems. In addition, recycle pumps are also considerably expensive resulting in the highest total equipment cost among the three systems investigated.

Although in this study the feed gas is assumed to be available at a temperature of 100°F and a pressure of 1065 psia, the optimum temperature and pressure are largely affected by the undecided choice of the primary gasification phases and to a lesser extent by the gas purification phase and the water-gas shift reaction phase which proceeds the methanation phase. It is therefore necessary to study how the feed gas temperature and pressure will affect the equipment cost and what the optimum temperature and pressure should be as far as the methanation process is concerned.

Figure 9-2 shows the relation between the total equipment costs and the feed gas temperature for the low CO case in the adiabatic reactor and for the intermediate CO case and the high CO case in the cold quench systems.

(3) Effect of Pressure of the Feed Gas on Total Equipment Cost for Two Different Product Gas Heating Values

Figure 9-3 shows the relation between total equipment cost and the feed CO composition with pressures of the feed gas as parameter. Since it is necessary to maintain the outlet product gas pressure above 1000 psig in order to meet pipeline transportation, the product gas must be compressed to this pressure when the gas effluent from the methanation reactor does not have enough pressure to meet this requirement. The operating pressure of the primary gasification system has the predominating effect on the compressor requirements, compressor placement and the methanation reactor pressure so that the methanation processes cannot be optimized without the selection and co-optimization of primary gasification. However, the compressor cost is by far the largest portion of the total equipment cost. If we neglect the cost of compression, Figure 9-3 shows that the equipment cost decreases with pressure of the feed gas.

The product gas having the heating value of 900 B.t.u./SCF is believed to be enough to meet pipeline gas qualities. Its total equipment cost versus feed CO composition with pressure of the feed gas as parameter is also shown in Figure 9-3.

(4) Parameter Sensitivity Analysis

In this study, the optimum conditions (decisions) are obtained based on the specific values of system parameters which characterize the performance (kinetic constants, heat transfer coefficient, etc.) to minimize the total equipment cost (the objective function). The values of these parameters are usually obtained from the experimental studies or from careful evaluations based on established correlations. Often these values are somewhat inaccurate due to lack of time and funds required for an accurate evaluation. If the performance of the system under the optimal conditions is significantly dependent on these parameters, and if these values are uncertain, the actual system performance may deviate considerably from the specification. Therefore, to ensure a better system performance, it is necessary to analyze how sensitive the system parameters are to the objective function (total equipment cost).

The sensitivity of a given parameter, σ, is defined [16] as

$$\sigma = [(\alpha - \bar{\alpha})/\bar{\alpha}] \;/\; [(\beta - \bar{\beta})/\bar{\beta}] \qquad (9\text{-}1)$$

The result of parameter sensitivity study on the total equipment cost based on the low and the high CO cases for optimum methanation processes is shown in Table 9-1. Among the parameters studied, the maximum allowable temperature, T^{*}, is a moderately sensitive factor, particularly for the high CO case. This means if the maximum allowable temperature could be higher than 850°F, the total equipment cost may be decreased, provided of course that the equilibrium hindrance is avoided by cooling the gas near the exit of the reactor. From the heat removal point of view the maximum temperature at which the catalyst can be operated without deactivation due to local sintering or carbon deposition, should be as high as possible. However, high temperatures also limit the material for construction of the reactor and equilibrium concentration for methane. Therefore, further study of catalyst reactivity, durability and regenerability are required.

Since the heat transfer coefficient is directly related to the cost of heat exchangers, an increase in the heat transfer coefficient will directly decrease the total equipment cost, particularly for the low CO case. Among the heat transfer coefficients studied as shown in Table 9-1, the coefficient of the product gas cooler III seems the most sensitive one, this is due to its large heat transfer area required. Comparatively speaking, the heat transfer coefficients are less sensitive among the parameters studied.

The kinetic expression seems to be the most sensitive factor among the parameters considered for both the low and the high CO cases.

Other factors studied gave negligible sensitivities on the total equipment cost.

(5) Uncertainty Analysis of Kinetic Expression

Lacking the reliable experimental data, it is difficult to obtain an accurate kinetic rate expression. However, in the previous section, the frequency factor, k, and the orders of the reaction, m and n are found to be very sensitive, therefore it becomes necessary to study how the optimum policy changes over a range of uncertainty in k, m and n.

In this analysis, a range of uncertainty in the kinetic rate expression is obtained based on the positive and the negative maximum deviations in the Arrhenius plot. The orders of reaction m and n are varied from 0.2 to 0.4 and from 0.6 to 0.9, respectively. The optimum reactor design as well as the total equipment cost for various sets of m, n and the corresponding maxima and minima values of k for the low CO case are shown in Table 9-2.

The result indicates that the range of uncertainty in the rate expression can cause the total optimum equipment cost to vary from $490,200 when the minimum rate expression is used to $267,900 when the maximum rate expression is used. For other rate expressions inside the range of uncertainty, the cost falls between them. Since the optimum

TABLE 9-1 PARAMETER SENSITIVITY ON TOTAL EQUIPMENT COST OF OPTIMUM METHANATION PROCESSES

Parameters	Sensitivity	
	Low CO	High CO
U_{II}^{I}	--	-0.051
U^{III}	-0.103	-0.087
U_p	-0.196	-0.104
μ	-0.131	-0.051
ρ	-0.263×10^{-4}	-0.13×10^{-6}
T^N	0.398×10^{-2}	0.486×10^{-3}
T^E	-0.175	-0.331
T^O	--	0.161
k*	--	0.077
m*	-0.155	-0.126
n*	-0.435	-0.357
	-0.764	-0.627

*Based on the rate equation:

$$r_{CH_4} = k\, e^{-E/RT}\, p_{H_2}^{m}\, p_{CO}^{n}$$

TABLE 9-2 UNCERTAINTY STUDY OF KINETIC RATE EXPRESSION FOR OPTIMUM METHANATION PROCESSES IN LOW CO CASE

k	m	n	Reactor Diameter ft	Reactor Height ft	Total Equipment cost, dollar
100	0.3	0.7	6.1	11.3	366,000
110	0.3	0.7	6.0	10.7	355,800
120	0.3	0.7	5.9	10.1	348,600
130	0.3	0.7	5.8	9.7	343,160
140	0.3	0.7	5.7	9.3	338,230
			* * *		
200	0.2	0.6	6.8	18.15	441,200
148	0.2	0.6	7.1	22.4	490,200
			* * *		
142	0.2	0.9	5.4	7.17	317,940
104	0.2	0.9	5.7	8.75	334,570
			* * *		
157	0.4	0.6	5.4	7.58	320,360
115	0.4	0.6	5.7	9.25	337,720
			* * *		
85	0.4	0.9	4.8	3.5	287,900
62	0.4	0.9	5.0	4.2	295,100

design is considerably affected by the kinetic rate expression, a more extensive investigation of the reaction kinetics and further development of improved catalyst are necessary for methanation reaction. The dependency of the rate equation on concentration and temperature should be more firmly established.

(6) Use of Harshaw Ni-0116T - 1/8" Catalyst

Instead of Harshaw Ni-0104T - 1/4", Harshaw Ni-0116T - 1/8" catalyst pellet may be used. The pressure drop across the reactor bed and the kinetic rate expression are affected and therefore must be adjusted. Again it is rather difficult at present to obtain an accurate rate equation, a rough correlation is obtained. The orders of the reaction are considered to be the same and a value of 240 for the frequency factor, k, is used. The optimum reactor design as well as the total equipment costs for the low CO case for the adiabatic reactor system and for the high CO case for the cold quench system are shown in Table 9-3. Apparently, the reactor diameters are about the same and the reactor heights are about halves as those when 1/4" pellets are used. This is due to the pressure drop across the reactor bed being twice as big as previous case. The total equipment cost is also slightly decreased in both cases.

(7) Feed with CO Composition Higher Than 15%

Since the experimental kinetic data are available only up to 15% of feed CO concentration, the present optimization study is restricted within this range. However, when the feed CO composition is higher than 15%, reactors with better heat removal systems must be considered. One of the ways to reach better heat removal is to utilize the sprayed catalyst on heat transfer surface to facilitate quick removal of heat. Also, there is the hot-gas-recycle system in which two methanators are used. The bulk of the methanation, 80 to 90 percent conversion of the feed gas, occurs in the main reactor over steel catalysts; the remainder of the methanation occurs in the second reactor over a Raney nickel catalyst.

In order to obtain a rough estimate of the total equipment cost for the feed CO concentration higher than 15%, a feed containing approximately 20% of CO is studied. Since a large amount of heat is generated in the reactor, the heat extraction system is poor for the heat removal under this condition and the cold quench system is difficult due to the fact that the reactor temperature quickly reaches the maximum allowable reactor temperature causing the cold shot difficulty. Besides, the temperature difference between the catalyst surface and the bulk gas phase could become excessive due to the large reaction heat generated. The "temperature run-away" may cause the catalyst sintering and the carbon deposition. A recycle system is therefore considered. The flow rate and composition in both feed and product gases are listed in Table 9-4. Assuming that all the properties including kinetic rate expression used in the previous optimization study can be applicable and the exit reactor temperature is changed to 790°F due to the equilibrium hindrance, the system is optimized by the similar way as used in the high CO case for the recycle system. Figure 9-4 shows the effect of the reactor diameter on the total equipment cost with the number of reactors in parallel as parameter. In the cost estimation, as the number of reactors is increased, $3,000 per each reactor is added as the costs for control valves and other instrumentation.. The

TABLE 9-3 OPTIMUM REACTOR DESIGN AND TOTAL EQUIPMENT COST IN TWO DIFFERENT FEEDS FOR TWO DIFFERENT CATALYSTS

	LOW CO		HIGH CO	
	Ni-0104T 1/4"	Ni-0116T 1/8"	Ni-0104T 1/4"	Ni-0116T 1/8"
First Reactor Diameter, ft	5.9	5.9	6.2	6.2
First Reactor Height, ft	10.1	5.2	3.4	2.1
Second Reactor Diameter, ft	--	--	6.6	6.8
Second Reactor Height, ft	--	--	3.0	1.5
Third Reactor Diameter, ft	--	--	7.2	7.2
Third Reactor Height, ft	--	--	8.5	4.42
Total Equipment Cost, $	348,600	315,650	677,320	627,840

TABLE 9-4 FLOW RATES AND CONCENTRATION OF FEED AND PRODUCT GASES FOR THE FEED CONTAINING APPROXIMATELY 20% OF CO

	Feed Gas		Product Gas	
	[lb.mole/hr.]	[mole %]	[lb.mole/hr.]	[mole %](dry base)
CH_4	8,267.1	17,200	17,822.2	92.100
CO	9,574.5	19.920	19.3	0,100
H_2	29,357.6	61.080	692.3	3.577
CO_2	96.1	0.200	96.1	0.497
H_2O	48.1	0.100	9,603.2	0.000
N_2	721.0	1.500	721.0	3.726
Total	48,064.4	100.0	28,954.1	100.0

optimum number of reactors in parallel is seen to be 16, the optimum reactor diameter to be 5.8 feet, and the optimum reactor height is 4.75 feet. The optimum total equipment cost is $1,799,780 and is much larger than the previous cases studied.

(8) Miscellaneous

In this study, only the equipment costs are considered in the objective function due to the difficulty in estimating the costs of various feed gases which depend greatly upon the primary gasification phases. After the optimization of the other sub-system, such as the primary gasification phases, purification phases and other necessary phases has been completed, the overall plant optimization must then be performed.

10. CONCLUSION

An optimization study of methanation processes in the coal gasification plant has been performed. Three different feed compositions, namely the low CO case, the intermediate CO case and the high CO case have been considered. Four different systems employing fixed bed downflow, catalytic reactors have been examined. They are the adiabatic reactor system, the heat extraction system, the cold quench system and the recycle system. The heat exchanger optimization has also been simulated due to the fact that it occupies a major portion of the total equipment cost. The following conclusions are drawn from the results of the study.

1. Owing to the extremely large heat of reaction, removal of heat from the reacting gas is the major problem associated with methanation process. The cost of equipment involved in heat removal such as heat exchangers, etc., occupies a major portion of the total equipment cost. The problem of heat removal becomes more complicated when the feed gas contains a large amount of CO.

2. In the low CO case, since CO concentration in the feed gas is less than 4.6%, an adiabatic reactor system is sufficient to achieve a product gas equivalent to the pipeline gas quality. The consideration of other systems is unnecessary. The adiabatic reactor system then becomes the optimum system for the low CO case.

In the intermediate and high CO cases, since CO concentration in the feed gas is over 4.6%, some devices for removal of the heat are needed. Among three systems considered, the cold quench system offers the least total equipment cost followed by the heat extraction system. The recycle system is by far the most expensive system.

The above analysis is based on the feed gas temperature of 100°F, the inlet reactor temperature of 550°F and the maximum reactor temperature of 850°F.

3. Among three systems considered in the intermediate and high CO cases, from the total equipment cost point of view, the heat extraction system is not too far away from the cold quench system, but from the maintenance and operational points of view, the heat extraction system is not easy to control during the operation and may become unstable when small disturbances in the operating conditions are present.

The recycle system on the other hand may be most costly, but is easiest to control, particularly when the CO concentration in the feed gas is high and when the gas distribution through the catalyst bed is not uniform.

4. The total equipment cost is also affected by the feed gas temperature and pressure. There is an optimum feed temperature for a given concentration. The optimum feed gas temperature for the low CO case is 200°F, for the intermediate CO case is 250°F and for the high CO case is 300°F. Since the smaller volumetric flow rate would significantly reduce the cost of the compressor, the gas should be compressed to meet the pipeline gas specifications after the methanation process and the feed pressure to the methanation process should be as low as possible.

5. The minimum total equipment costs for the methanation processes are 348.6×10^3 for the low CO case employing the adiabatic reactor system, 477.67×10^3 for the intermediate CO case and 677.32×10^3 for the high CO case both employing the cold quench system.

6. Sensitivity analysis of the system parameters shows that the accuracy of the kinetic rate constants and the orders of reaction would have some effects on the total equipment cost. Also the maximum allowable temperature does have moderate effect on total equipment cost. The heat transfer coefficients are comparatively less sensitive.

7. Uncertainty study of the kinetic rate expression demonstrates how the optimum reactor design and the total equipment cost change over the ranges of uncertainty in the frequency factor, k and the orders of the reaction, m and n. The result indicates that the kinetic rate expression greatly affects the optimum design of the processes and a more extensive study of the methanation reaction kinetics is needed.

8. Instead of Harshaw Ni-0104T - 1/4" catalyst, Harshaw Ni-0116T - 1/8" catalyst pellets are used to optimize the processes by adjusting the kinetic rate expression and using the same operation conditions. The result shows that the pressure drop across the reactor bed causes the reactor height to reduce to one half of the previous cases. The optimum reactor diameter is about the same.

9. Since the experimental kinetic data are available only up to 15% of feed CO concentration, the present optimization study is restricted within this range. If the feed CO composition is higher than 15%, reactors with better heat removal systems, such as utilizing the sprayed catalyst on the heat transfer surface to facilitate the quick removal of heat and the hot-gas-recycle system should be considered.

Assuming that the kinetic rate expression used in this study is applicable, the recycle system is optimized employing a feed containing approximately 20% of CO. The optimum number of reactors in parallel is found to be 16, the optimum reactor diameter of 5.8 feet, and the optimum reactor height of 4.75 feet and the optimum total equipment cost of $1,799,780 are obtained from the results.

NOMENCLATURE

A_o	heat transfer area	($ft.^2$)
A_t^n	total heat transfer area of fin tube in n-th cell	($ft.^2$)
A^I, A^{II}, A^{III}	heat transfer area of first, second and third product gas cooler, respectively	($ft.^2$)
A_h	bare tube heat transfer area of fin tube	($ft.^2$)
B_p	brake horse power	(HP)
B_r	brake horse power of recycle compressor	(HP)
B'	baffle spacing	(ft.)
C_{AO}	installed cost of heat exchanger per unit heat transfer area based on outside	($/ft.^{2})
C_b	concentration of product gas in bulk of gas phase	(lb.mole/$ft.^3$)
C_i	cost for supplying one ft.-lb.force to pump fluid flowing through inside of tubes	($/ft.-lb.force)
C_L	height of a unit cell	(ft.)
C_o	cost for supplying 1 ft.-lb.force to pump fluid flowing through shell side	($/ft.lb.force)
C_P	heat capacity of gases	(B.t.u./lb.°F)
$C_{P_i}^{(I)}$	molar heat capacity of i-th component at temperature $T^{(I)}$	(B.t.u./ lb.mole°F)
$\bar{C}_P^{(I)}$	heat capacity of product gas at temperature $T^{(I)}$	(B.t.u./lb.°F)
C_{pw}	heat capacity of water	(B.t.u./lb.°F)
C_R	cost per pound of material used for construction of reactor-shell	($/lb.)
C_S	concentration of product gas at surface of catalyst	(lb.mole/$ft.^3$)
C_T	total annual variable cost	($/years)
C_Y	cost year index	(--)
D	inside diameter of reactor	(ft.)
De	equivalent diameter for heat transfer tube	(ft.)
D_i	inside diameter of tube	(ft.)

D_S	inside shell diameter of heat exchanger	(ft.)
d_p	diameter of catalyst particle	(ft.)
E	efficiency of longitudinal joints or mechanical efficiency	(---)
E_C	catalyst cost	($)
E_{CP}	compressor cost	($)
E_{CR}	recycle compressor cost	($)
E_F	embedded fin tube cost	($)
E_H	heat exchanger cost	($)
E_i	power loss inside tube per unit of outside tube area	(ft.-lb.force/ hr.ft.^{2})
E_o	power loss outside tube per unit of outside tube area	(ft.-lb.force/ hr.ft.^{2})
E_R	reactor cost	($)
E_S	cost of unit tray	($/unit tray)
E_T	total equipment cost	($)
F_1^n	molar flow rate of CH_4 at n-th cell	(lb.mole/hr.)
F_2^n	molar flow rate of CO at n-th cell	(lb.mole/hr.)
F_3^n	molar flow rate of H_2 at n-th cell	(lb.mole/hr.)
F_4^n	molar flow rate of CO_2 at n-th cell	(lb.mole/hr.)
F_5^n	molar flow rate of H_2O at n-th cell	(lb.mole/hr.)
F_6^n	molar flow rate of N_2 at n-th cell	(lb.mole/hr.)
F^0	total molar flow rate of feed gas	(lb.mole/hr.)
F_i^0, F_i^n, F_i^r	molar flow rate of i-th component in feed, product and recycle gas, respectively	(lb.mole/hr.)
$F_i^{(2)}, F_i^{(3)}$	molar flow rate of i-th component at inlet of second and third reactor, respectively	(lb.mole/hr.)
F_d	flat blank diameter of top and bottom of domes of reactor	(ft.)

F_T	correction factor on Δt_m	(--)
G	superficial mass velocity	(lb./ft.^{2}hr.)
G_S	shellside mass velocity	(lb./ft.^{2}hr.)
ΔH	heat of reaction	(B.t.u./lb.mole CH_4)
H_y	hours of operation per year	(hr./year)
Δh	hydraulic head	(ft.H_2O)
h_i	inside film heat transfer coefficient of tube	(B.t.u./ft.^{2}hr.°F)
h_o	outside film heat transfer coefficient of tube	(B.t.u./ft.^{2}hr.°F)
h_p	fluid-particles heat transfer coefficient	(B.t.u./ft.^{2}hr.°F)
I_f	cost factor	(--)
J_H	heat transfer factor	(--)
J_M	mass-transfer factor	(--)
K	ratio of specific heats	(--)
k	thermal conductivity of fluid	(B.t.u./ft.hr.°F)
k_d	diffusion coefficient	(ft.^{2}/hr.)
K_F	annual fixed charges	(--)
K_G	mass transfer coefficient	(lb.mole/hr.ft.^{2}atm.)
$K^*_{X_1}$	equilibrium constant of methanation reaction	(--)
$K^*_{X_2}$	equilibrium constant of shift reaction	(--)
K_{X_1}	mass action law ratio of product gas in methanation reaction	(--)
ke	effective thermal conductivity of catalyst particles	(B.t.u./ft.hr.°F)
k_f	fluid-particle mass transfer coefficient	(ft./hr.)
kg	thermal conductivity of gas	(B.t.u./ft.hr.°F)
k_s	thermal conductivity of catalyst	(B.t.u./ft.hr.°F)
L	length of reactor	(ft.)
L_H	length of heat exchanger	(ft.)

$\bar{M}$	average molecular weight of product gas	(lb./lb.mole)
M_m	mean molecular weight of fluid	(lb./lb.mole)
M_v	molecular weight of steam	(lb./lb.mole)
N	number of trays	(--)
N_{Pr}	Prandtl number	(--)
P	design pressure	(psig)
ΔP	pressure drop per unit cell	(lb./ft.^{2})
P_a	pressure at suction to compressor	(atm.)
P_b	pressure at discharge from compressor	(atm.)
P_c	partial pressure of steam at surface of tube	(atm.)
P_{gf}	logarithmic-mean pressure difference of non-condensing gas	(atm.)
P^N	outlet pressure of reactor	(atm.)
P^O	inlet pressure of reactor	(atm.)
ΔP_S	shell side pressure drop in heat exchanger	(psi)
P_v	partial pressure of steam at bulk fluid	(atm.)
P_v^{II}	vapor pressure of water at temperature T^{II}	(atm.)
P_w	partial pressure of steam in product gas	(atm.)
P_{CO}	partial pressure of CO	(atm.)
P_{H_2}	partial pressure of H_2	(atm.)
Q_c	total amount of heat generated in reactor	(B.t.u./hr.)
Q^n	amount of heat removed from n-th cell	(B.t.u./hr.)
q	total heat transfer rate in heat exchangers	(B.t.u./hr.)
q^I, q^{II}, q^{III}	heat duties of first, second and third product gas coolers, respectively	(B.t.u./hr.)
q'	volumetric flow rate	(gal./min.)
q_c	heat flux accompanied with condensation	(B.t.u./hr.ft.^{2})

q_p	volume of gas compressed	(S.C.F./min.)
q_r	recycle gas flow rate	(S.C.F./min.)
R_{dw}	resistance to heat flow due to scaling	($ft.^2$hr.°F/B.t.u.)
r	distance from center of catalyst particle	(ft.)
r_s	reaction rate per unit catalyst particle	(lb.mole CH_4/ hr.unit catalyst)
r_{CH_4}	reaction rate	(lb.mole CH_4/ hr.lb.catalyst)
S	maximum allowable stress	(psig)
s	specific gravity	(--)
T	temperature	(°F)
$T^{(1)},T^{(2)},T^{(3)}$	inlet temperatures of first, second and third reactor, respectively	(°F)
T^I,T^{II}	outlet gas temperature from first and second product gas cooler, respectively	(°F)
T^A	outlet gas temperature from intermediate cooler	(°F)
T^E	exit temperature of final reactor for high CO case	(°F)
T^F	feed gas temperature	(°F)
T^N	exit gas temperature of reactor	(°F)
T^{NP}	gas temperature leaving recycle gas cooler	(°F)
T^n	temperature at n-th cell	(°F)
T^P	outlet product gas temperature from preheater	(°F)
$T^{(PF)}$	outlet feed gas temperature from preheater for recycle system	(°F)
T_a	temperature at suction to compressor	(°F)
T_b	bulk gas temperature in reactor	(°F)
T_h	thickness of reactor	(in.)

T_s	surface temperature of catalyst particles	(°F)
t_{C1}, t_{C3}	outlet coolant temperature of first, and third product gas coolers, respectively	(°F)
t'_c	inlet water temperature of first product gas cooler	(°F)
t_c	temperature of treated or spent water	(°F)
Δt_m	logarithmic-mean temperature difference	(°F)
U^I, U^{II}, U^{III}	overall heat transfer coefficients of first, second and third product gas coolers, respectively	(°F)
U_o	overall heat transfer coefficient of fin tubes	(B.t.u./ft.^{2}hr.°F)
U_P	overall heat transfer coefficient of preheater	(B.t.u./ft.^{2}hr.°F)
V_c^n	catalyst volume per unit cell	(ft.^{3})
W^N	molar flow rate of product gas	(lb.mole/hr.)
W_1, W_2	flow rate of treated and process water in product gas coolers, respectively	(lb./hr.)
WC^I	the water flow rate through the first exchanger	(lb./hr.)
W_C	catalyst weight	(lb.)
W^O	mass flow rate of feed gas	(lb./hr.)
W_R	weight of reactor tube	(lb.)
W_{S1}, W_{S2}	flow rate of 400 psia steam and 35 psia steam in product gas cooler, respectively	(lb./hr.)
$X^*_{CH_4}$	equilibrium mole fraction of CH_4	(--)
$X^*_{H_2O}$	equilibrium mole fraction of H_2O	(--)
X^*_{CO}	equilibrium mole fraction of CO	(--)
$X^*_{H_2}$	equilibrium mole fraction of H_2	(--)
$X^*_{CO_2}$	equilibrium mole fraction of CO_2	(--)
X_{CH_4}	mole fraction of CH_4 in product gas	(--)
X_{H_2}	mole fraction of H_2O in product gas	(--)
X_{CO}	mole fraction of CO in product gas	(--)
X_{H_2}	mole fraction of H_2 in product gas	(--)

$Y^{(2)}, Y^{(3)}$	conversion of CO to CH_4 at inlet of second and third reactor	(--)
Y^N	total conversion of CO to CH_4	(--)

Greek Letters

α, $\bar{\alpha}$	objective function and that at optimum, respectively	
β, $\bar{\beta}$	system parameter subject to variation and a specific value of system parameters, respectively	
ϵ	void fraction of reactor	(--)
θ	internal porosity of catalyst	(--)
λ'	Lagrange multiplier	(--)
λ'_1	fraction of feed gas passing through preheater	(--)
λ_c	heat of condensation for steam	(B.t.u./lb.)
μ	gas viscosity	(lb./ft.hr)
ρ	gas density	($lb./ft.^3$)
ρ_c	catalyst density	($lb./ft.^3$)
ρ_m	density of reactor shell	($lb./ft.^3$)
ρ_w	density of cooling water	($lb./ft.^3$)
σ	sensitivity defined as $[\alpha - \bar{\alpha}/\bar{\alpha}] / [\beta - \bar{\beta}/\bar{\beta}]$	(--)
ϕ	cost factor	(--)
η	$(K-1)/K$	(--)

LITERATURE

1. Akers, W. W. and White, R. R., Chem. Engr. Progr. 44, 553-566 (1948).

2. ASME Boiler and Pressure Vessel Code, Section VIII, Unfired Pressure Vessels, The American Society of Mechanical Engineers, New York, 1956.

3. Bauman, H. C., "Fundamentals of Cost Engineering in the Chemical Industry," Reinhold, New York, 1964.

4. Chilton, C., "Cost Engineering in the Process Industries," McGraw Hill, New York, p. 50, 1960.

5. Communication, Harshaw Chemical Co., Cleveland, Ohio, July, 1967.

6. Ergun, S., Chem. Eng. Progr., 48, 89 (1952).

7. Fan, L. T., Lee, E. S. and Erickson, L. E., "Proceedings of the MASUA Conference on Modern Optimization Techniques and their Application in Engineering Design," Part II, The Mid-America State Universities Association, 1966.

8. Gamson, B. W., Chem. Eng. Progr., 47, 19 (1951).

9. Jones, P. R. and Katell, S., "Computer Usage for Evaluation of Design Parameters and Cost of Heat Exchangers with No Change in Phase and Pumping Costs of Both Fluids as Prime Parameters," IC Bureau of Mines Information Circular 8334, 1967.

10. Kern, D. Q., "Process Heat Transfer," McGraw Hill, New York, 1950.

11. McCabe, W. L. and Smith, J. C., "Unit Operations of Chemical Engineering," McGraw Hill, New York, 1956.

12. Page, J. S., "Estimator's Manual of Equipment and Installation Costs," Gulf, Houston, 1963.

13. Peters, M. W., "Plant Design and Economics for Chemical Engineers," McGraw Hill, New York, 1958.

14. Rossini, F. D., et al., "Selected Values of Properties of Hydrocarbons," U.S. Department of Commerce, National Bureau of Standards, Washington, D. C., 1947.

15. Tajbl, D. G., Feldkirchner, H. L. and Lee, A. L., "Fuel Gasification," Ed. R. F. Gould, ACS, Washington, D. C., p. 166, 1967.

16. Wen, C. Y. and Chang, T. M., Ind. Eng. Chem. Process Design Develop. 7, 49 (1968).

17. Wilke, C. R. and Hougen, O. D., Trans, A. I. Ch. E. 41, 445 (1949).

ACKNOWLEDGMENT

The financial support of the Office of Coal Research, Department of the Interior, Washington, D. C. is acknowledged.

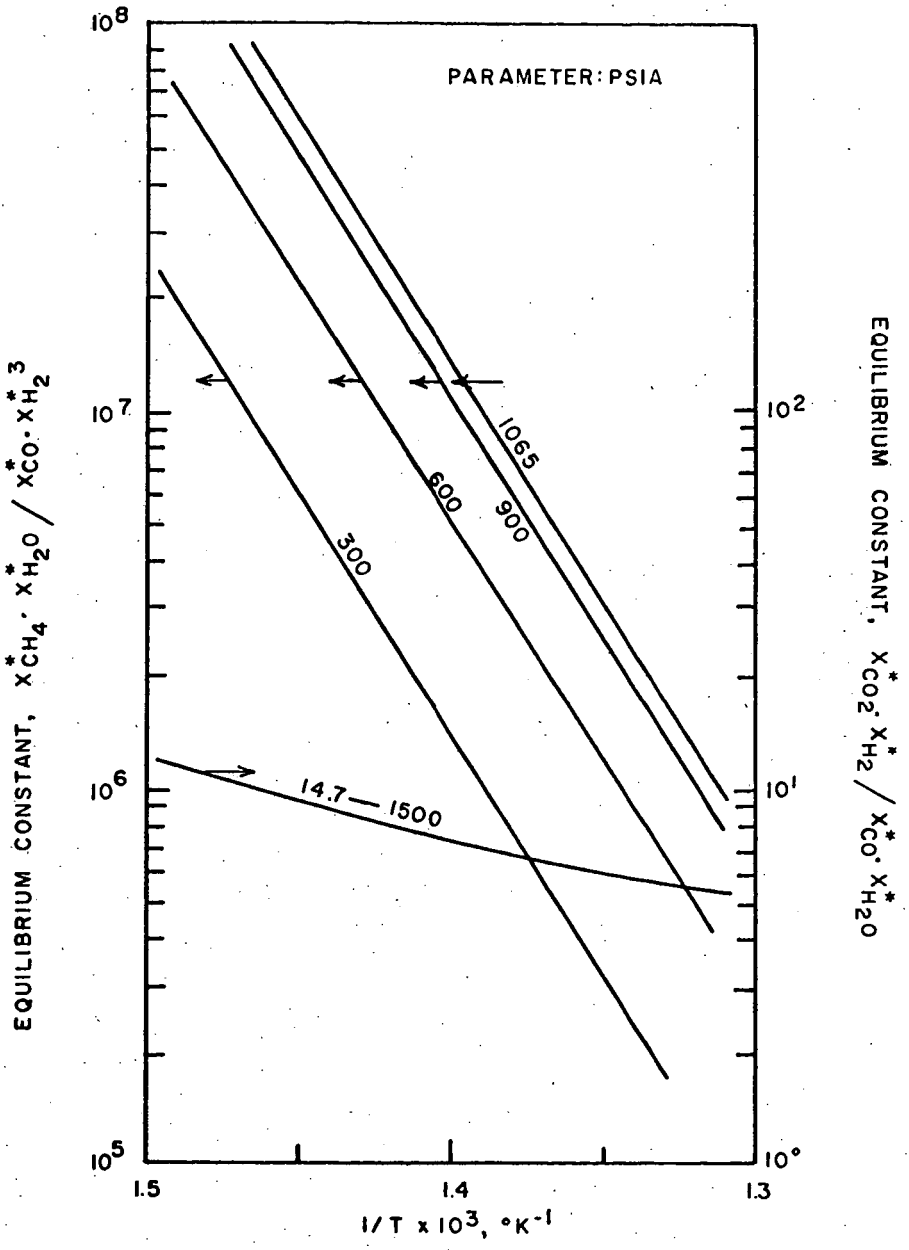

FIGURE 2-1 EFFECT OF TEMPERATURE ON EQUILIBRIUM CONSTANTS FOR REACTIONS $CO+3H_2 \rightarrow CH_4+H_2O$ AND $CO+H_2O \rightarrow CO_2+H_2$

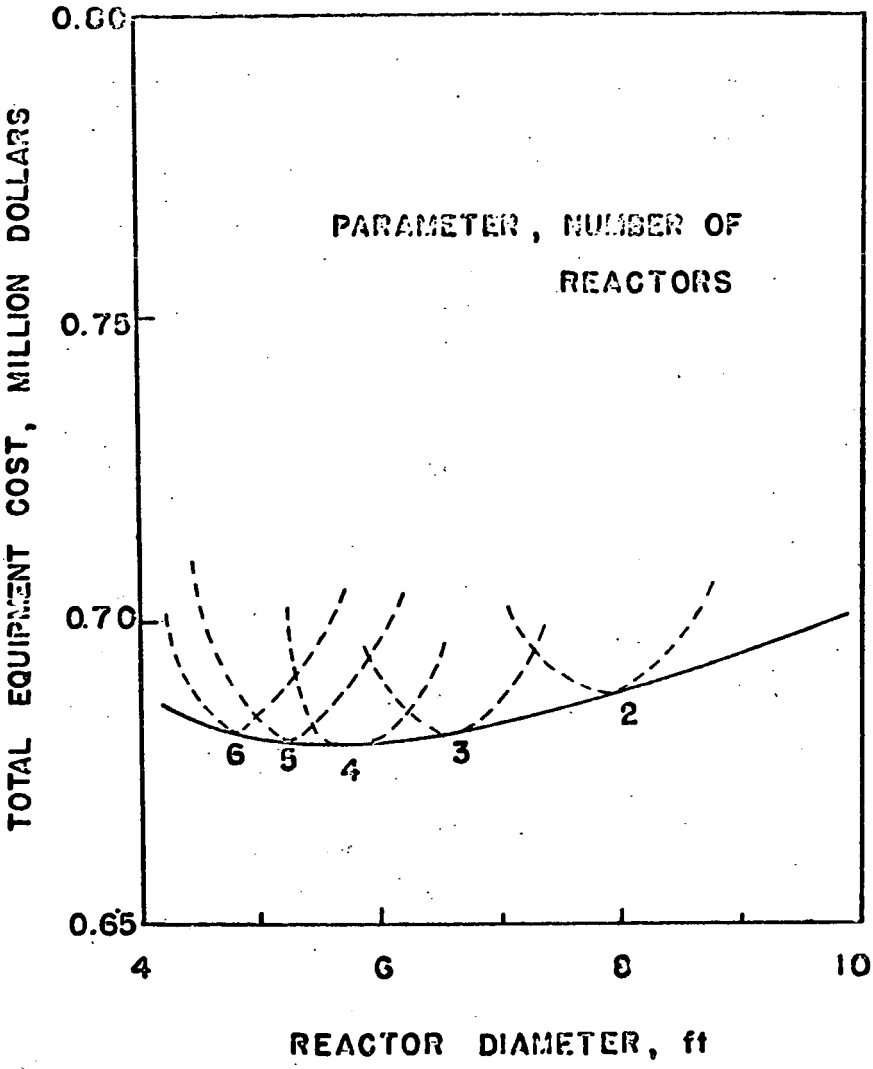

FIGURE 8-1 TOTAL EQUIPMENT COST VERSUS REACTOR DIAMETER IN INTERMEDIATE CO CASE FOR RECYCLE SYSTEM

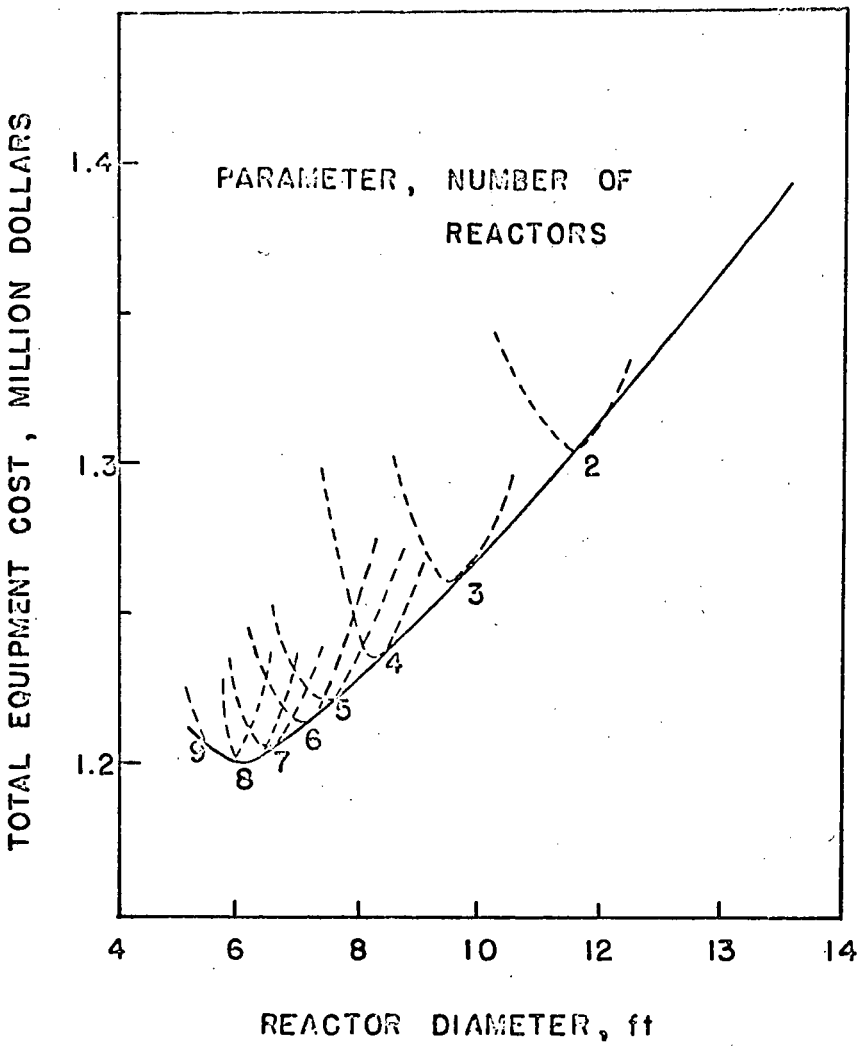

FIGURE 8-2 TOTAL EQUIPMENT COST VERSUS REACTOR DIAMETER IN HIGH CO CASE FOR RECYCLE SYSTEM

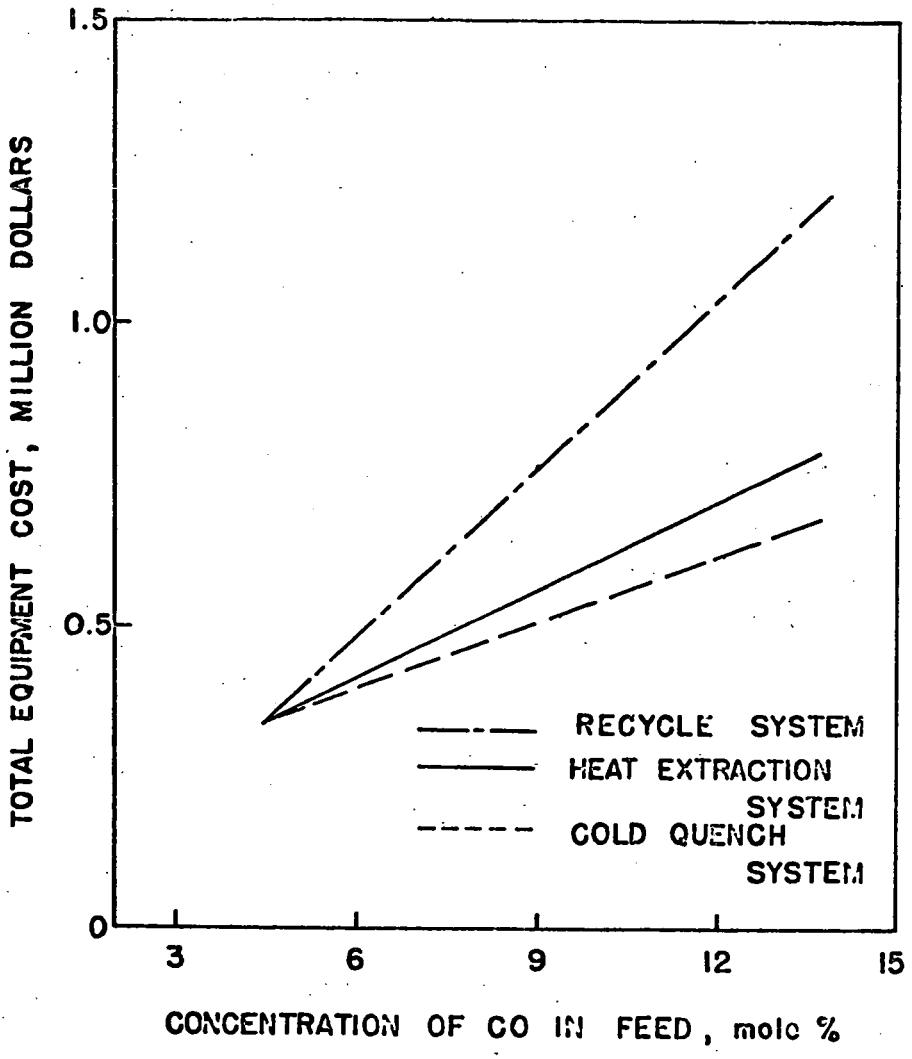

FIGURE 9-1 RELATION BETWEEN TOTAL EQUIPMENT COST AND CONCENTRATION OF CO IN THE FEED GAS FOR THREE DIFFERENT SYSTEMS.

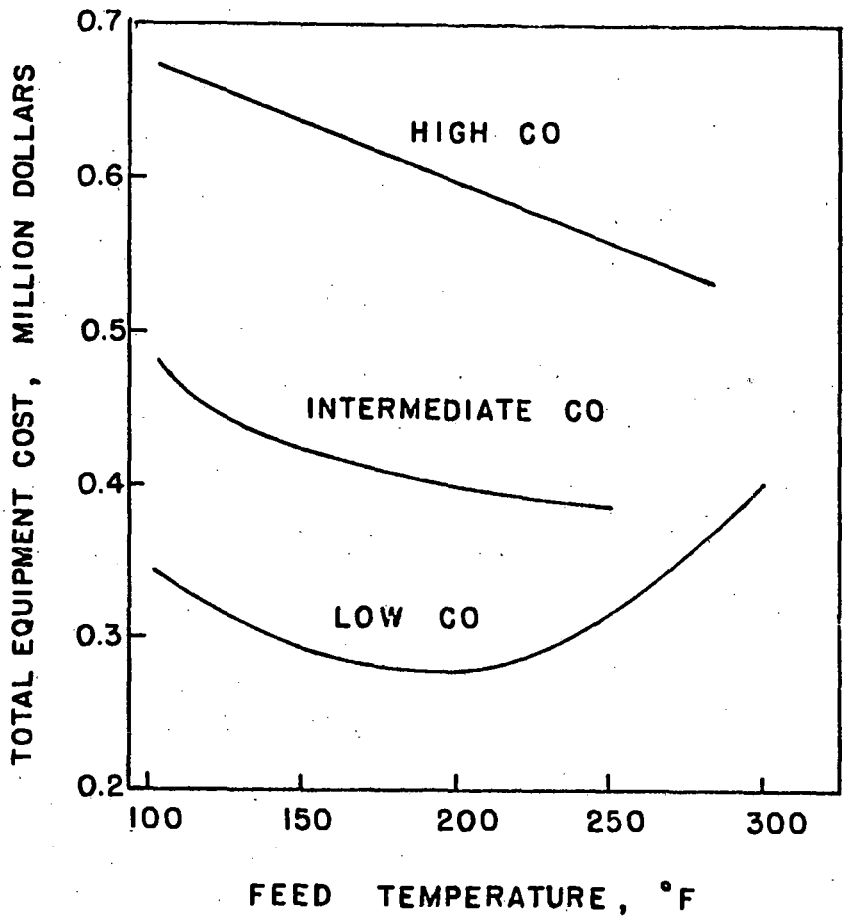

FIGURE 9-2 TOTAL EQUIPMENT COST VERSUS FEED TEMPERATURE IN LOW CO CASE AND IN TWO CASES FOR COLD QUENCH SYSTEM

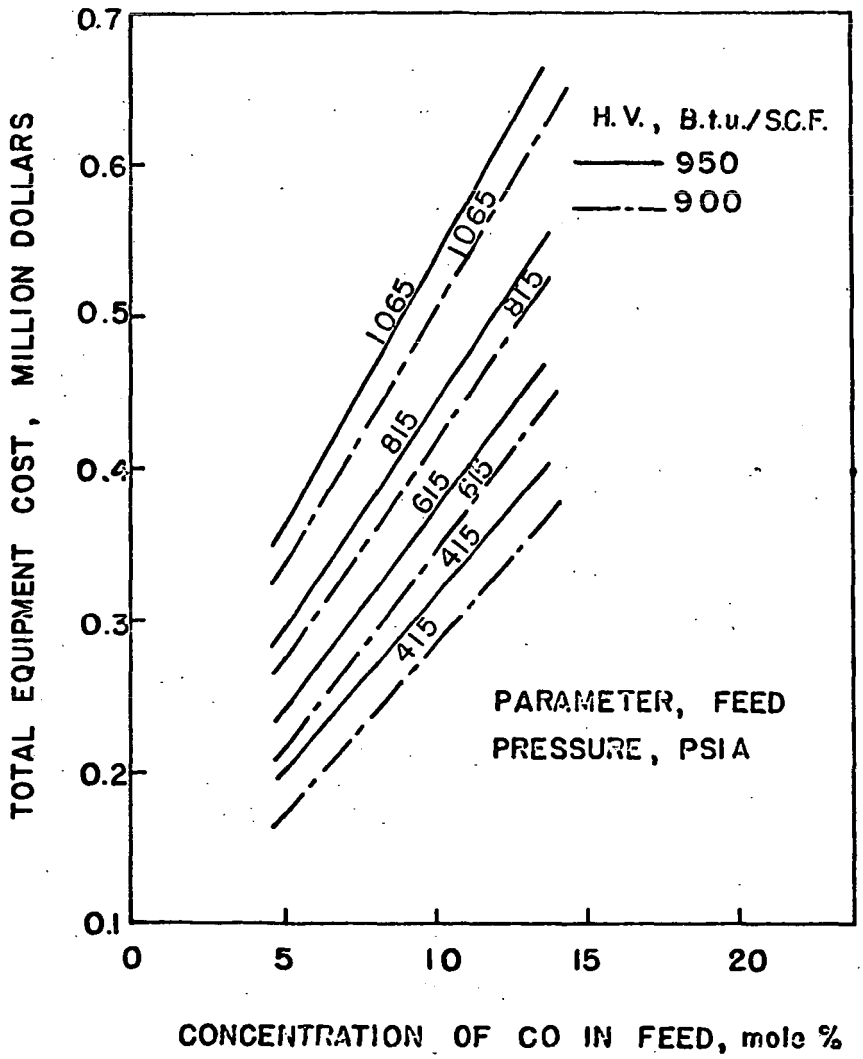

FIGURE 9-3 TOTAL EQUIPMENT COST ESTIMATING COST [illegible] SYSTEM VERSUS FEED CO CONCENTRATION FOR TWO DIFFERENT HEATING VALUES WITH FEED PRESSURE AS PARAMETER

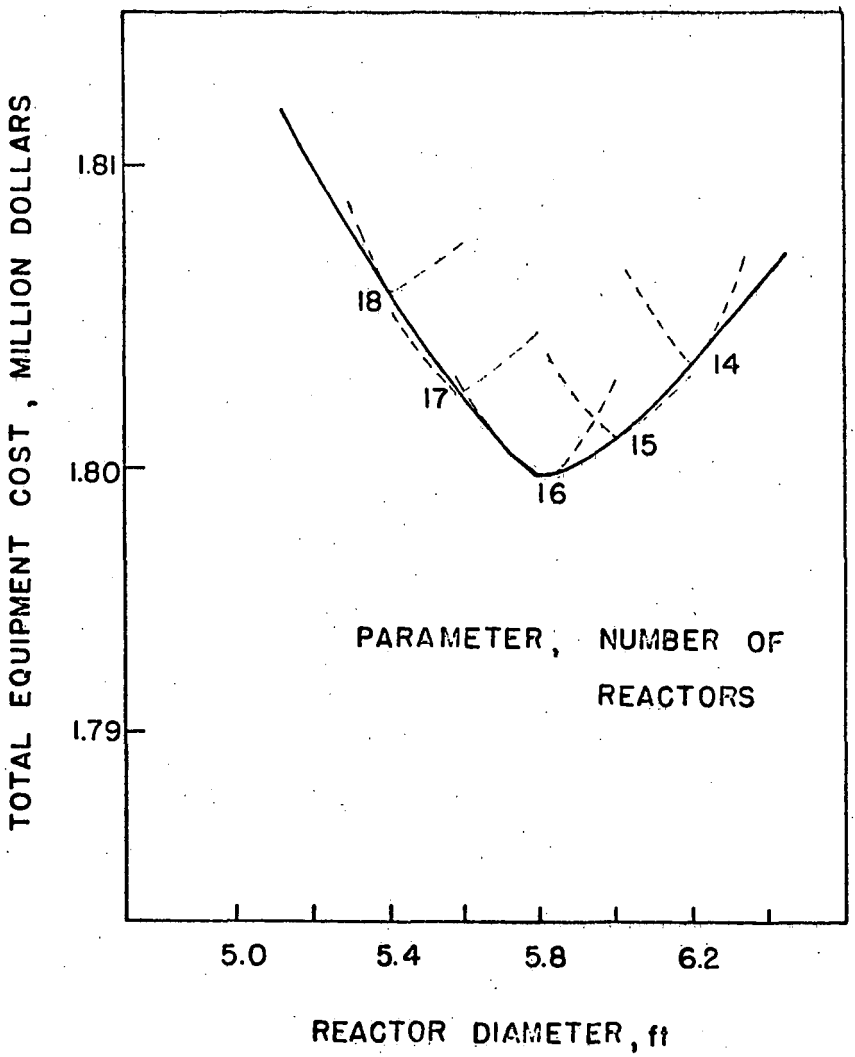

FIGURE 9-4 TOTAL EQUIPMENT COST VERSUS REACTOR DIAMETER FOR FEED CONTAINING 20 PERCENT CO EMPLOYING RECYCLE SYSTEM

PRODUCTION OF SYNTHETIC FUELS FROM COAL BY HYDROGENATION UNDER MEDIUM PRESSURES

S. A. Qader, R. A. Haddadin,
L. L. Anderson, and G. R. Hill

Fuels Engineering Department

University of Utah, Salt Lake City, Utah 84112

Abstract

The results of a two stage process for the conversion of a high volatile bituminous coal from Utah to gasoline, diesel oil, gas, and char are described. In the first stage, coal was hydrogenated in a bench scale reactor at high temperatures and medium pressures to get a heavy oil as the main product which was hydrocracked in a subsequent bench scale operation to produce gasoline and diesel oil. The overall material balance indicated that coal can be converted to 30% high octane gasoline, 5% high speed diesel oil, 35% high B.T.U. gas, and 30% char. A conceptual scheme for the processing of 100 tons of coal is proposed.

Introduction

High pressure hydrogenation of coal for the production of synthetic liquid fuels was practised in Germany during World War II. Hydrogenation was carried out at pressures from 5000 to 10,000 psi and the processes were found economically uncompetitive (Gordon, 1947). A demonstration plant for coal hydrogenation at 7500 to 10,000 psi pressure was operated by the U. S. Bureau of Mines during 1949 to 1953 for an economic evaluation of the process (U. S. Bureau of Mines, 1962). The process was found to be economically unfavorable. The technology developed during the last decade indicated the economic feasibility of hydrogenation of coal under medium pressure conditions. The H-coal process was developed for coal hydrogenation under medium pressures of 1500 to 3000 psi and it was operated in an ebullated bed reactor. The pilot plant data demonstrated the economic feasibility of the H-coal process (Alpert, et al., 1964). In the present communication, the results of a two stage hydrogenation process for the conversion of coal to gasoline, diesel oil, gas, and char under medium pressure conditions, are reported.

Experimental

Materials.

A high volatile bituminous A-seam, King Mine, Spring Canyon coal from Utah and high temperature coke (Table 1) were used for

hydrogenation. Analar grade stannous chloride was used as the catalyst. The catalyst was completely soluble in water and insoluble in benzene.

Equipment.

The flow sheet of the bench scale unit for coal hydrogenation is shown in Figure 1. Hydrogen was drawn from the cylinder 1, compressed by the compressor 4, and stored in the storage tank 5. Hydrogen from the storage tank was preheated to about 300°C before it entered the reactor 9. The coal was fed continuously to the reactor from the hopper 7, by a horizontal screw feeder 9, operated by a motor 8. The coal feed rate was controlled by a calibrated device attached to the motor. The reactor was made of 316 stainless steel and was 4 feet high and 2 inches inside diameter. It was provided with a thermowell extending to the center for temperature measurements and lines for the injection of cold hydrogen. Coal gets hydrogenated while it falls down the reactor. The solid and liquid products were collected in the liner of the quench tank 11. The gases passed through the condenser 12 and the condensed liquid was collected in the trap 13. The uncondensed gas was metered by the wet gas meter 14 and let out into the atmosphere. No recycling of the exit gas was practised. The hydrogen flow rate was controlled manually by the high pressure regulating valves 2A-2F. The whole system was designed for a maximum working pressure of 5000 psi at room temperature and the reactor and preheater for 5000 psi at 700°C.

The heavy oil obtained by coal hydrogenation was refined in a continuous bench scale unit with a static bed reactor shown in Figure 2. It consisted of a vertical tubular stainless steel reactor of 0.75-inch inside diameter and 40-inch length with extensive means for controlling temperature, pressure, and gas and liquid flow rates. The first 20 inches of the reactor length from the top was packed with ceramic beads of 0.17-inch diameter, the next 6.5 inches with the catalyst (60 c·c), and the following 12 inches again with ceramic beads. The top bed of ceramic beads acts as the preheating zone. The temperature at the center of the catalyst bed was measured with a thermocouple placed between the reactor and furnace walls. The hydrogen supply was taken from a hydrogen cylinder with a maximum pressure of 2300 psi.

Procedure for coal hydrogenation.

Coal was ground in a hammer mill, screened, and dried at 110°C. The dry coal was impregnated with the catalyst by spraying a water solution of the latter in a mixer. The impregnated coal was again dried to remove all the water. The dry impregnated coal was mixed with an equal quantity of high temperature coke of the same size. About 10 pounds of the coal-coke mixture was charged into the hopper and pressurized with hydrogen. The whole system was first flushed with preheated hydrogen from the storage tank and the

system was pressurized to the desired pressure. The rate of hydrogen flow was maintained at about 15 liters per minute. When the temperature in the reactor was stabilized, coal-coke mixture was fed to the reactor at the rate of about 5 grams per minute. The pressure and temperature inside the reactor were maintained constant throughout. The outlet gas was sampled every half hour for analysis. Each run was carried out for about 15 to 16 hours. After all the coal-coke mixture was fed to the reactor, heating and hydrogen flow were stopped and the system was allowed to cool down to atmospheric temperature. After the system attained atmospheric temperature and pressure, the liner from the quench tank was taken out. The contents of the liner and the light oil trap were weighed. The percentage conversion of coal to gas was calculated from the total quantity of gas passed through the system during each experiment and its analysis. The weight of all the products exceeded the weight of feed and the difference in weight was taken as percent hydrogen consumed in the process. The amount of water formed was found almost equal to the hydrogen consumed and the yield of gaseous, liquid, and solid products was 100% on the basis of coal feed. The oil from the contents of the liner were extracted with benzene and the char separated. The benzene was distilled off to get the oil product. The light oil collected in the trap was added to the oil obtained by benzene extraction to get the total oil product. The char was washed with water to dissolve the catalyst. The resultant char was dried at 110°C and analyzed. The amount of stannous chloride dissolved in the water extract was determined.

Procedure for hydrotreating of oil.

The total oil product obtained from coal was hydrorefined at 420°C, 1500 psi pressure, and a space-velocity of 1.0 over a cobalt-molybdate on alumina industrial catalyst. It was also hydrocracked at 490°C, 2000 psi pressure, and 1.0-space-velocity. The hydrogen consumption in these operations was obtained from the difference in the weight of total products and feed. The liquid product was distilled into different fractions. The light oil fraction boiling up to 200°C was designated as gasoline, the fraction from 200° to 360°C as diesel oil, and the remaining as residue. The diesel oil fraction was refined by extraction with a mixture of dimethyl formamide and n-heptane to improve the diesel index (Qader and Vaidyeswaran, 1966). In the hydrotreating work, the coke deposit inside the reactor was burnt off after each experiment by flushing the reactor at 500°C with air for 10 hours.

Product analysis.

The proximate and ultimate analysis of coal, coke, and char were done by conventional methods. Sulfur was determined by the bomb method and nitrogen by the C-H-N chromatographic analyzer, F. M. Model 185. Hydrocarbon type analysis of the gasoline was done by the Fluorescent-Indicator-Adsorption method (ASTM D-1319-65T). The hydrocarbon types in the heavy oil feed and diesel oil were

determined by chemical methods (ASTM D-1019-62). The naphthenes in the gasoline were estimated by the refractivity intercept method (ASTM D-1840-64). The n-paraffin content was determined by adsorption on 5-A molecular sieves in a glass column of 0.5-inch diameter and 1.5-foot height. The isoparaffins were obtained by the difference. The tar acids and bases were estimated by extraction with 10% sodium hydroxide and 20% sulfuric acid, respectively. The diesel index was calculated from API gravity and aniline point. The octane number was determined by the Research Method. The gas analysis was done by gas chromatography in the F. M. Model 720 dual column programmed temperature gas chromatograph.

Results and Discussion

The admixture of coke with coal in 1:1 ratio eliminated almost all the caking and agglomeration problems in the reactor. No significant conversion of coke was found when it was hydrogenated alone. The presence of coke in the feed did not affect the product distribution to any appreciable extent. The feed particles attained the reaction temperature while they were halfway down the reactor. The coking of the liquid product was minimized due to the short residence time. The hydrogen consumption in the process varied between 4 and 7% of the feed coal and the conversion to water was found to be about 5 to 8%. About 50% of the sulfur and nitrogen in the coal was retained in the char while the remaining was evenly distributed in the liquid and gaseous products. About 70 to 80% of oxygen in the coal was converted to water. About 80% of the catalyst used was recovered by washing the char with water.

The residence time of the feed particles in the reactor was expected to be about 5 seconds and hence the particle size of the feed was of great significance in this work. Coal and coke are bad conductors of heat and need long residence times to get heated to the reaction temperature. Because of the short residence times involved in this process, the size of the coal feed was kept as fine as possible. The influence of the size of feed particles on product distribution is shown in Figure 3. The conversion of coal to liquid and gaseous products decreased with an increase in the particle size while the yield of char increased. A particle size of about 50 microns was found to affect maximum conversion of coal. However, for practical reasons, a particle size of about 250 microns was used in this investigation. A longer reactor might be necessary for feeding larger particles effectively.

A large excess of the catalyst was used in these experiments to bring about adequate contact between the coal particles, catalyst, and hydrogen. Several catalysts were used for coal hydrogenation (Table II) and stannous chloride affected maximum coal conversion of 75% at an optimum concentration of 15% by weight of coal (Figure 4). A part of the stannous chloride might vaporize and decompose during the process and may not take part in the hydrogenation of coal. Only the undecomposed stannous chloride might be catalyzing

the reactions, as also pointed out by Zielke, et al. (1966), necessitating the usage of a large excess of the catalyst. The higher conversions obtained with stannous chloride might probably be due to its known better thermodynamic stability toward decomposition when compared to the other metal halides used.

Temperature and pressure had marked influence on product distribution. The yield of liquid product increased up to 515°C but decreased at higher temperatures while the yield of gas increased linearly with temperature. The yield of char decreased up to 515°C but remained almost the same at higher temperatures (Figure 5). A temperature of 515°C was found to be optimum for maximum liquid product yield. Above 515°C, cracking of the liquid product took place with the production of gas. The liquid product increased with pressure with a corresponding decrease in the yield of char. Pressure had little effect on gas yield (Figure 6). A pressure of 2000 psi was found to be optimum for maximum conversion.

The analysis of the products obtained at 515°C and 2000 psi pressure is given in Table III. The liquid product was somewhat similar to low temperature tar. It was light and contained 20% light oil boiling up to 200°C and 20% tar acids. The composition of the liquid product indicated that considerable cracking of the primary product took place during the process. The gaseous product, exclusive of process hydrogen, contained about 85% methane with small quantities of ethane and propane. The gas composition indicated that it can be used as a substitute for natural gas. The char (Table III) was produced when coal was hydrogenated without mixing with high temperature coke and it was found to be as good as high temperature coke in reducing caking and agglomeration of coal during hydrogenation. It can be used for power generation or hydrogen production.

Hydrorefining of the liquid product at 420°C, 1500 psi pressure, and 1-space-velocity (Table IV) yielded 26% gasoline of 78 research octane and 56% of diesel oil with 43 diesel index. Solvent refining of diesel oil yielded 48% of high speed diesel oil. The hydrocracking of the liquid product over the dual-functional catalyst yielded 69% of gasoline of 93 research octane and 17% of low speed diesel oil. After solvent refining, high speed diesel oil was obtained in a yield of 12% (Table V). The tar acids, sulfur, and nitrogen were removed almost completely during hydrorefining and hydrocracking operations. Hydrogen consumption varied between 2 and 3% of the oil in these operations.

The overall material balance is schematically shown in Figure 7. Scheme I represents the yield of various products from a single charge of 10 pounds containing 5 pounds of coal. The amount of hydrogen consumed in the process was found to be approximately equal to the amount of water formed. Scheme II represents the nature and overall yield of the products from coal. The gas yield in this scheme comprised of the yield of gas in both the operations

in Scheme I. Similarly, the char comprised of the char and residue produced in Scheme I. The conceptual product yields (Table VI) were calculated from the data covering several batch runs. The char produced in the process was used in admixture with coal in 1:1 ratio and the hydrogen consumption in both the stages of the process was approximated to 6% of the coal feed. The material balance in Table VI was obtained by calculating the yields after normalization of the total product recovery to 106 wt. % of coal feed. A conceptual schematic diagram of a coal refinery utilizing the two stage process described in this paper is shown in Figure 8. The results obtained in this investigation demonstrated the technical feasibility of the two stage process for the conversion of coal to high octane gasoline, high speed diesel oil, and high B.T.U. gas.

Acknowledgement

The research work reported in this paper was sponsored by the U. S. Office of Coal Research and the University of Utah.

Literature Cited

1. Alpert, S. B., Johanson, E. S , Schuman, S. C., Chem. Eng. Progress, 60, No. 6, 35 (1964).

2. Gordon, K., et al., Report on the Petroleum and Synthetic Fuel Oil Industry of Germany, Ministry of Fuel and Power, H.M.S.O., London (1947).

3. Qader, S. A., Vaidyeswaran, R , Ind. J. Tech., 4, 128 (1966).

4. U. S. Bureau of Mines Information Circular, 8040 (1962).

5. Zielke, C. W., Struck, R. T., Evans, J. M., Costanza, C. P., Gorin, E., Ind. Eng. Chem., 5, No. 2, 151 (1966).

Table 1. Properties of coal and coke.

	Coal	Coke
Proximate analysis, wt. % (moisture free basis)		
Volatile matter	46.8	2.5
Ash	6.7	10.0
Fixed carbon	46.5	87.5
Ultimate analysis, wt. %		
Carbon	75.88	-
Hydrogen	5.58	-
Oxygen	9.50	-
Sulfur	0.94	-
Nitrogen	1.50	-
Calorific value, BTU/lb	13,250	-

Table II. Product distribution with different catalysts. Temperature, 515°C; pressure, 2000 psi

Catalyst	Product distribution, wt. %			
	Total conversion	Oil	Gas	Char
Stannous chloride	75.0	43.0	32.0	25.0
Ammonium molybdate	69.0	39.0	30.0	31.0
Nickel chloride	71.0	41.0	30.0	29.0
Ferrous chloride	65.0	38.0	27.0	35.0
Zinc chloride	55.0	29.0	26.0	45.0

Table III. Properties of products.
Temperature, 515°C
Pressure, 2000 psi

Liquid product	
Sp. gr, 20°C	0.9946
Sulfur, wt. %	0.3214
Nitrogen, wt. %	0.5820
Tar acids, vol. %	20.0
Tar bases, wt. %	1.50
Distillation data	
I.B.P., °C	75
Up to 200°C, vol. %	20.0
Up to 350°C, vol. %	72.0
Residue, vol. %	28.0
Hydrocarbon types in neutral oil up to 350°C, vol. %	
Saturates	46.0
Olefins	6.0
Aromatics	48.0
Gas composition, vol. %	
Hydrogen	94.0
Methane	5.0
Ethane	0.5
Propane	0.5
Char analysis, wt. %	
Volatile matter	7.0
Ash	12.0
Fixed carbon	81.0
Carbon	77.5
Hydrogen	5.4
Oxygen	2.6
Sulfur	0.38
Nitrogen	0.62
Calorific value, BTU/lb	14,000

Table IV. Yields and quality of hydrorefined products. Temperature, 420°C; pressure, 1500 psi; sp. vel., 1.0; catalyst, cobalt-molybdate on alumina

Yields, vol. %	
Total product	99.0
Gasoline	26.0
Diesel oil	56.0
Refined diesel oil	48.0
Gas	2.0
Residue	12.0
Composition of gasoline, vol. %	
Saturates	58.0
Olefins	3.0
Aromatics	39.0
Research octane number	78.0
Diesel index of diesel oil	43.0
Diesel index of refined diesel oil	50.0

Table V. Yields and quality of hydrocracked products. Temperature, 490°C; pressure, 2000 psi; sp. vel., 1.0; catalyst, nickel sulfide-tungsten sulfide on silica-alumina

Yields, vol. %	
Total product	100.0
Gasoline	69.0
Diesel oil	17.0
Refined diesel oil	12.0
Gas	8.0
Residue	6.0
Composition of gasoline, vol. %	
Aromatics	52.0
Isoparaffins	21.0
Olefins	2.0
Naphthenes	8.0
N-paraffins	17.0
Research octane number	93.0
Diesel index of diesel oil	31.0
Diesel index of refined diesel oil	50.0

Table VI. Conceptual product yields.
Coal, 100 tons (m.a.f.)
Hydrogen, 6 tons

Products	Quantities
C_1-C_3 gases, cu. ft.	1,384,930
Gasoline, Bbl.	232
Diesel oil, Bbl.	33
Char, tons	28
Water, gallons	1,670
Hydrogen sulfide, cu. ft.	20,833
Ammonia, tons	1

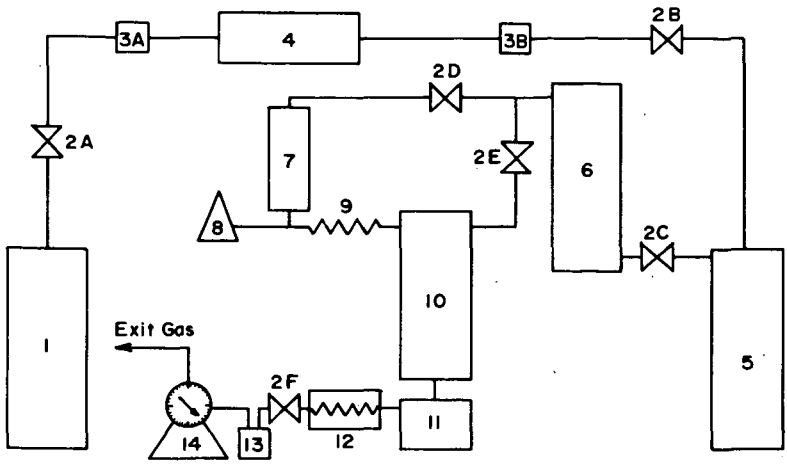

Figure 1. Flow sheet of coal hydrogenation unit.
1. Hydrogen cylinder, 2A-2F. High pressure regulating Valves, 3A & 3B. Filters, 4. Compressor, 5. Storage tank, 6. Preheater, 7. Hopper, 8. Motor, 9. Screw feeder, 10. Reactor, 11. Quench tank, 12. Condenser, 13. Liquid trap, 14. Wet gas meter.

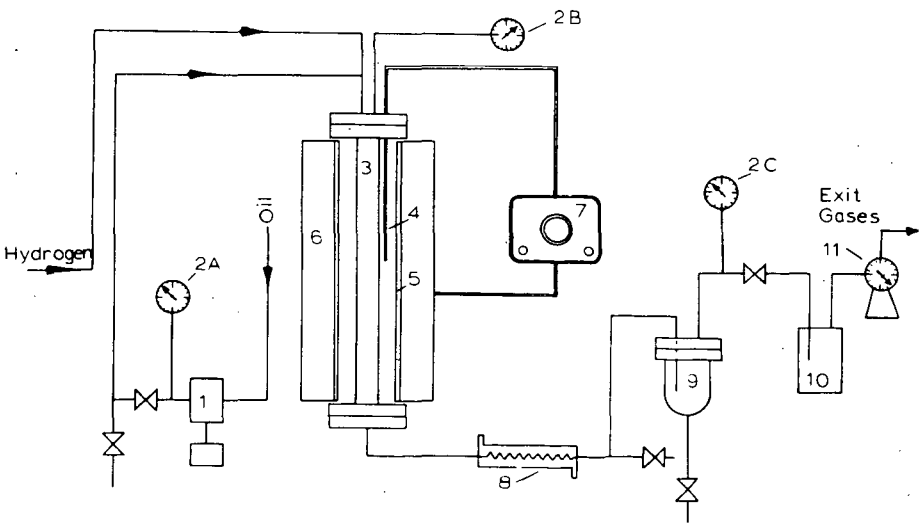

FIGURE 2. FLOW SHEET OF THE HYDROTREATING UNIT.
1. HIGH PRESSURE PUMP, 2A, 2B, 2C. PRESSURE GAUGE, 3. REACTOR, 4. THERMO-COUPLE, 5. CERAMIC FURNACE, 6. INSULATION, 7. TEMPERATURE CONTROLLER, 8. CONDENSER, 9. SEPARATOR, 10. ACTIVE CARBON TOWER, 11. GAS METER.

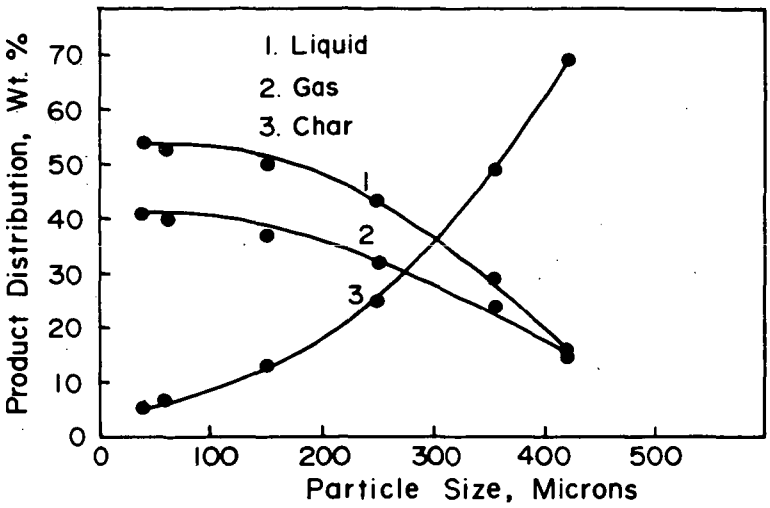

Figure 3. Effect of particle size on product distribution. Pressure, 2000 psi; Catalyst, 15% by weight; Temperature, 515° C.

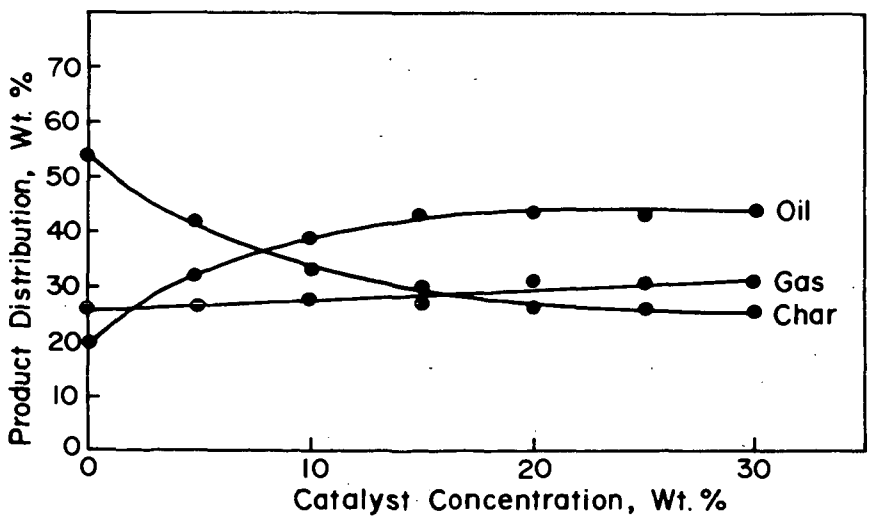

Figure 4. Effect of catalyst concentration on product distribution. Temperature, 515° C.; Pressure, 2000 psi.; Size, 250 microns.

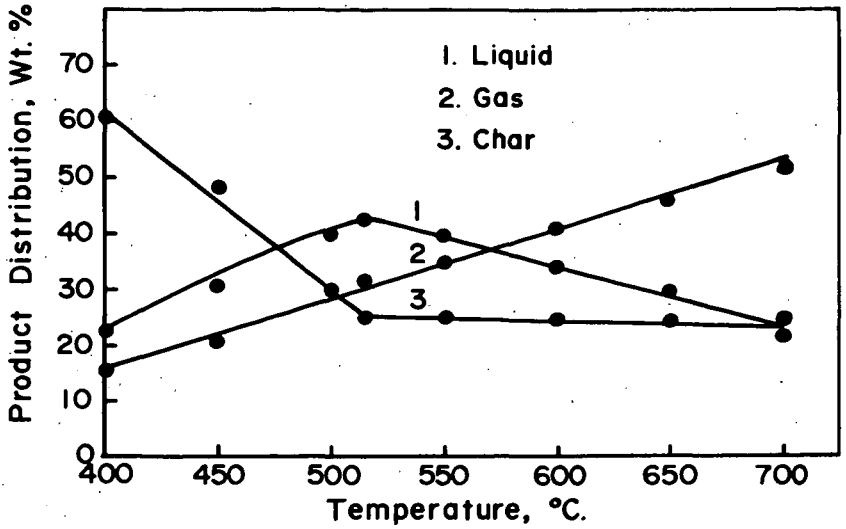

Figure 5. Effect of temperature on product distribution. Pressure, 2000 psi; Size, 250 microns; Catalyst, 15% by weight.

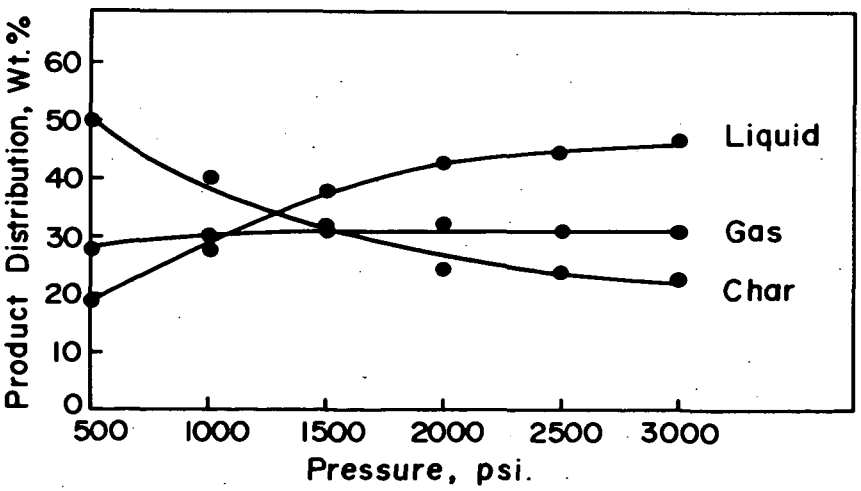

Figure 6. Effect of pressure on product distribution. Temperature, 515° C.; Size 250, microns; Catalyst, 15% by weight.

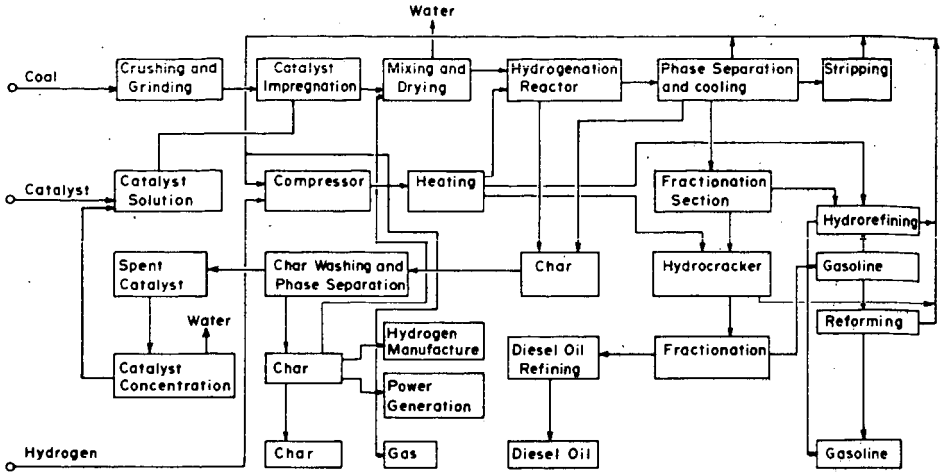

Figure 8. Flow sheet of the conceptual coal refinery.

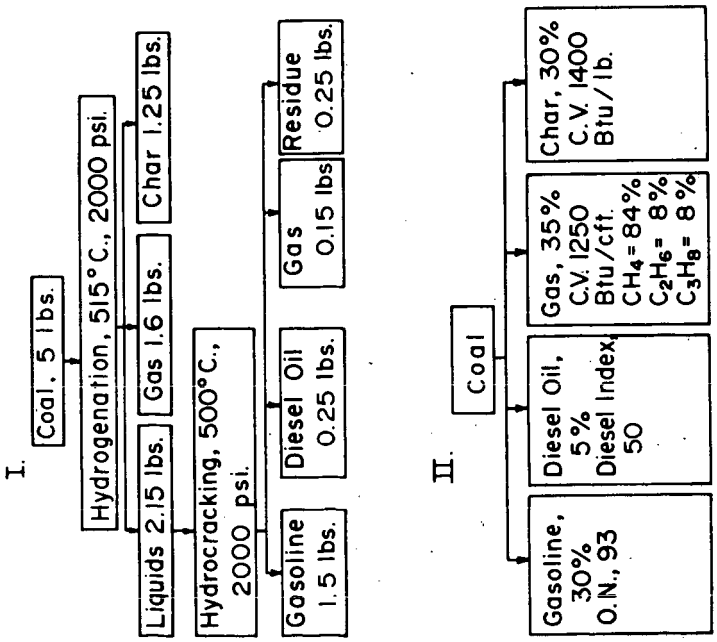

Figure 7. Schematic representation of material balance.

KINETICS OF HYDROGENOLYSIS OF LOW TEMPERATURE COAL TAR

L. L. Anderson, M. L. Badawy,
S. A. Qader, and G. R. Hill

Department of Fuels Engineering

University of Utah, Salt Lake City, Utah 84112

Abstract

The hydrogenolysis of a low temperature coal tar in a batch autoclave over a molybdenum trioxide catalyst yielded 77% gasoline at 475°C and 3000 psi pressure. The highest quality gasoline, containing 60% aromatics, was obtained in a yield of 47% at 450°C and a pressure of 2500 psi. Hydrogenolysis of tar proceeds through a mechanism involving a combination of simultaneous and consecutive cracking and hydrogenation reactions and the overall kinetics observed indicated that the formation of gasoline from tar is of first-order with an activation energy of 11.5 K cal./mole. Chemisorption of tar molecules on the catalyst surface appears to be the rate-determining step.

Introduction

Hydrogenolysis is a potential method for the treatment of low temperature tars, mainly to convert the whole tar or selected fractions to motor fuels. Most of the work reported was done in batch or continuous systems and the product distributions were investigated over different catalysts (Kalechits and Salimgareeva, 1956; Lang and Lacey, 1960; (Mrs.) Mirza, et al., 1965). Very few data are so far published on the kinetics of coal tar hydrogenolysis, though some work was reported on the kinetics of the hydrogenation of pure compounds present in tars (Wilson, et al., 1957; Owens and Amberg, 1962; Tarama, et al., 1963). In the present communication, the results of the hydrogenolysis of a low temperature tar in a batch autoclave over a molybdenum trioxide catalyst are reported. The influence of process variables on product distribution and an overall kinetic evaluation of the data are presented.

Experimental

Materials.

Low temperature tar (Table I) obtained from a high volatile bituminous coal by carbonization at 650°C was used as the feed material. Analar grade molybdenum trioxide with a surface area of 190 square meters per gram and -200 mesh size was used as the catalyst. Pure hydrogen was taken from a cylinder with a maximum pressure of 2300 psi.

Equipment.

A 1-litre high pressure autoclave (Figure 1), provided with a magnetic drive stirrer of 1800 r.p.m., pressure and temperature control devices, liquid and gas sampling lines, and water quenching system was used for the experimental work.

Experimental procedure.

In each experiment, 100 grams of tar and 5 grams of the catalyst were used. The equipment was evacuated to remove most of the air, filled with hydrogen, and heated to the desired temperature. The temperature rose to 300°C in 21 minutes and 500°C in 28 minutes. The reaction time was taken from the start of heating the equipment. When the reaction temperature was reached, the hot pressure was adjusted to the experimental value. Pressure was maintained constant except in experiments conducted at pressures higher than 2000 psi where there was a reduction of about 100 psi during the course of the experiment. Experiments were conducted at different reaction times depending upon the reaction temperature (Table II). At the end of the reaction time, heating was stopped and the product was quenched rapidly by circulating water in the cooling coil immersed in it. It took 1 to 2 minutes to cool the product down to 250°C and 15 minutes to atmospheric temperature. The pressure was then released and the autoclave opened. The product was transferred to a beaker, filtered to remove the catalyst, and the water was separated to get the total oil product. The mechanical losses were found to be less than 1%. The yield of the product was taken as 100% and 100 minus the volume of the total oil product was taken as percent conversion to gas. The total oil product was washed with 10% sodium hydroxide and 20% sulfuric acid to remove tar acids and bases, respectively. The neutral oil was then distilled to get a gasoline fraction boiling up to 230°C, a middle oil fraction from 230° to 360°C and residue.

Product analysis.

Tar acids and bases were estimated by extraction with 10% sodium hydroxide and 20% sulfuric acid, respectively. Hydrocarbon type analysis was done by the Fluorescent-Indicator-Adsorption method (ASTM, D-1319-65T). The hydrocarbon types in the neutral oil fraction from the feed were determined by washing with 20% sulfuric acid for olefins and a mixture of 70% concentrated sulfuric acid and 30% phosphorus pentoxide (ASTM, D-1019-62) for aromatics The gas analysis was done by gas chromatography in the F.M. Model 720 dual column programmed temperature gas chromatograph.

Results and Discussion

The liquid product from hydrogenolysis contained 1 to 3 c.c of water which might have been formed by the hydrogenation of tar acids. The gaseous product contained hydrogen sulfide and ammonia

which could not be quantitatively estimated. They might have been formed by the hydrogenation of heterocompounds containing sulfur and nitrogen.

Product distribution.

The yield of gasoline and gas increased linearly with temperature while the middle oil and residue decreased. Gasoline and gas were formed by the hydrogenolysis of middle oil and residue (Figure 2). The composition of gasoline (Figure 3) indicated that hydrogenation reactions took place under all temperature conditions at 3000 psi. The gasoline yield increased at different rates with pressure with a corresponding decrease in the yields of middle oil and residue (Figure 4). The rate of gasoline formation was high in the pressure range 500 to 1500 psi, slowing down in the range 1500 to 2500 psi and increasing again at higher pressures. The residue decreased rapidly but the gas yield remained almost constant in the range 500 to 1500 psi (Table III). Pressure does not seem to have a marked influence on cracking reactions in the range 500 to 1500 psi but the increase in gasoline yield may be due to the suppression of coke-forming reactions. In the range 2000 to 2500 psi, partial hydrogenation of aromatics to hydroaromatics takes place, followed by the cracking of the latter which increases the yield of gasoline and its aromatic content. At higher pressures, complete hydrogenation of aromatics to the corresponding naphthenes takes place, thus increasing the gasoline yield and its saturated hydrocarbon content (Figure 5). High aromatic gasolines were formed in the pressure range 2000 to 2500 psi. A maximum yield of 77% of gasoline was obtained at 475°C and 3000 psi pressure but the highest quality product containing 60% aromatics was formed at 450°C and 2500 psi pressure in a yield of 47%.

Kinetics.

Equilibrium was reached at different time periods at different temperatures with respect to gasoline formation (Figure 6). Plot of $\log \frac{a}{a-x}$ versus time (Figure 7), where "a" is the equilibrium conversion to gasoline, is linear and the hydrogenolysis reactions with respect to gasoline formation from tar are first-order. The first-order rate constant can thus be represented by equation 1.

$$\frac{d\ (\text{Gasoline})}{dt} = k_g\ (\text{Tar}) \qquad (1)$$

Where k_g is the rate constant for gasoline formation The gasoline formation reactions follow true Arrhenius temperature dependence (Figure 8) and the rate constant can be represented by equation 2.

$$k_g = 1.0 \times 10^7\ e^{11,500/RT}\ \text{mints.}^{-1} \qquad (2)$$

The enthalpy and entropy of activation calculated from Eyring's plot (Figure 9) are 10,500 cal./mole and -57.8 e.u., respectively.

The product distribution data indicated that the hydrogenolysis of low-temperature tar produces middle oil, gasoline, and gas by a mechanism involving a combination of simultaneous and consecutive cracking and hydrogenation reactions as can be represented by steps (i) to (xiii).

$$H_2 \rightleftharpoons H^{\bullet} + H^{\bullet} \qquad \text{(i)}$$

$$R_1 - R_2 \longrightarrow R_1^{\bullet} + R_2^{\bullet} \qquad \text{(ii)}$$

$$R_3H_2C - SR_4 \longrightarrow R_3H_2C^{\bullet} + R_4S^{\bullet} \qquad \text{(iii)}$$

$$R_5H_2C - NR_6 \longrightarrow R_5H_2C^{\bullet} + R_6N^{\bullet} \qquad \text{(iv)}$$

$$R_7H_2C - OR_8 \longrightarrow R_7H_2C^{\bullet} + R_8O^{\bullet} \qquad \text{(v)}$$

$$R_1^{\bullet} + H^{\bullet} \longrightarrow R_1H \qquad \text{(vi)}$$

$$R_2^{\bullet} + H^{\bullet} \longrightarrow R_2H \qquad \text{(vii)}$$

$$R_3H_2C^{\bullet} + H^{\bullet} \longrightarrow R_3CH_3 \qquad \text{(viii)}$$

$$R_5H_2C^{\bullet} + H^{\bullet} \longrightarrow R_5CH_3 \qquad \text{(ix)}$$

$$R_7H_2C^{\bullet} + H^{\bullet} \longrightarrow R_7CH_3 \qquad \text{(x)}$$

$$R_4S^{\bullet} + H^{\bullet} \longrightarrow R_4H + H_2S \qquad \text{(xi)}$$

$$R_6N^{\bullet} + H^{\bullet} \longrightarrow R_6H + NH_3 \qquad \text{(xii)}$$

$$R_8O^{\bullet} + H^{\bullet} \longrightarrow R_8H + H_2O \qquad \text{(xiii)}$$

Where "R" represents a hydrocarbon radical or hydrogen atom. Step (i) represents dissociation of hydrogen molecules and the concentration of hydrogen atoms depends upon the dissociation equilibrium. Steps (ii) to (v) represent breakage of C-C, C-S, C-N, and C-O bonds present in the hydrocarbon and heteromolecules of tar and steps (vi) to (xiii) indicate hydrogenation reactions. The steps listed above are the principal reactions that are likely to occur during the hydrogenolysis of tar and indicate that the overall kinetics observed resulted from a sequence of this type. In the presence of an initial excess of hydrogen, there will be a preponderance of hydrogen atoms and the reactions between radicals and hydrogen atoms occur freely and rapidly. Steps (vi) to (xiii) are thus expected to be fast and cannot be rate-controlling. Any step involving hydrogen may limit the rate only when hydrogen concentration is very low. The cracking reactions taking place must be purely of a thermal nature and need higher activation energies than those obtained in the present work. Hence, steps (ii) to (v) cannot be rate-determining. It is well established that all the heterogeneous catalytic processes involve (1) diffusion of the reactants from the bulk phase to the catalyst surface, (2) adsorption of the

reactants on the catalyst surface, (3) reaction of the adsorbed molecules to form products, (4) desorption of the products, and (5) diffusion of the desorbed products from the catalyst surface to the bulk phase. The magnitude of the activation energy obtained will exclude steps 1, 4, and 5 from being rate-limiting. It was shown by the foregoing discussion that step 3 did not control the rate. Therefore, step 2, involving the adsorption of the reactants on the catalyst surface, must be rate-determining. Physical adsorption cannot occur at high temperatures used in this investigation. Hence, chemisorption of the tar molecules on the surface of the catalyst must be the rate-controlling step in the hydrogenolysis of tar.

Adknowledgement

The research work reported in this paper is sponsored by the U. S. Office of Coal Research and the University of Utah.

Bibliography

1. Kalechits, I. V., Salimgareeva, F. G., Trudy Vostochnosibir, Filiala, Akad, Nauk, S.S.S.R., Ser. Khim., 4, 5 (1956).

2. Lang, E. W., Lacey, J. C., Jr , Ind. Eng. Chem., 52, 137 (1960).

3. (Mrs.) Mirza, A., Ramaswamy, A. V., Aziz Masood, M., Qader, S. A., Vaidyeswaran, R., Ind. J. Tech., 3, 57 (1965).

4. Owens, P. J., Amberg, C. H., Cana. J. Chem., 40, 951 (1960).

5. Tarama, K., Teranishi, S., Hattori, K., Higashi, M., J. Fuel Soc. Japan, 42, 42 (1963).

6 Wilson, W. A., Voreck, W. E., Malo, R. V., Ind. Eng. Chem., 49, 657 (1957).

Table 1. Properties of low temperature tar

Sp. gr., 25°C	1.0426
Sulfur, wt. %	0.9424
Nitrogen, wt. %	0.8213
Oxygen, wt. %	4.1
Carbon, wt. %	84.9
Hydrogen, wt. %	9.3
Distillation data	
I.B.P., °C	180
14 wt. %	230
50 wt. %	325
55 wt. %	345
Residue, wt. %	45.0
Hydrocarbon types in neutral fraction up to 345°C, vol. %	
Saturates	20.0
Olefins	15.0
Aromatics	65.0

Table II. Effect of temperature on product distribution. Pressure, 3000 psi

Temperature, °C	350	375	400	425	450	475
Reaction time, hrs.	26	20	18	14	12	10
Product distribution, wt. %						
Gasoline	23	33	46	56	65	77
Middle oil	50	46	34.5	26	17.5	4
Gas	nil	1	2.5	3	4.5	6
Residue	27	20	17	15	13	13
Tar acids, vol. %	15	2	nil	-	-	-
Tar bases, vol. %	2	1	nil	-	-	-
Composition of gasoline, vol. %						
Saturates	71	73	74	79	80	82
Olefins	2	2	2	1	1	1
Aromatics	27	25	24	20	19	17

Table III. Effect of pressure on product distribution.

Pressure, psi	500			1000			1500			2000			2500			3000		
Temperature, °C	350	400	450	350	400	450	350	400	450	350	400	450	350	400	450	350	400	450
Reaction time, hrs.	26	18	12	26	18	12	26	18	12	26	18	12	26	18	12	26	18	12
Product distribution, wt. %																		
Gasoline	7	16	25	14	23	34	23	29	42	23	32	44	23	36	47	23	46	65
Middle oil	53	46	40	51	43	37	47	43	31	49	40	29	50	40	29	50	34.5	17.5
Gas	nil	1	1	nil	1	1	nil	1	1	nil	2	4	nil	2	4	nil	2.5	4.5
Residue	40	37	34	35	33	28	30	27	26	28	26	23	27	22	20	27	17	13
Tar acids, vol. %	30	26	20	27	23	15	25	17	7	22	10	4	20	5.5	nil	15	nil	-
Tar bases, vol. %	4	3.5	2	3	2	1	2	1.5	0.5	1.5	1	nil	2	1	nil	2	nil	-
Composition of gasoline, vol. %																		
Saturates	55	52	52	55	53	53	56	54	56	58	43	36	59	43	37	71	74	80
Olefins	10	10	12	9	8	10	7	6	8	5	4	5	4	3	3	2	2	1
Aromatics	35	38	36	36	39	37	37	40	39	37	53	59	37	54	60	27	24	19

1 CERAMIC FURNACE
2 LIQUID SAMPLING TUBE
3 GAS SAMPLING TUBE
4 THERMOWELL
5 COOLING COIL
6 COOLING JACKET
7 MAGNETIC DRIVE ASSEMBLY
8 SHAFT
9 IMPELLER

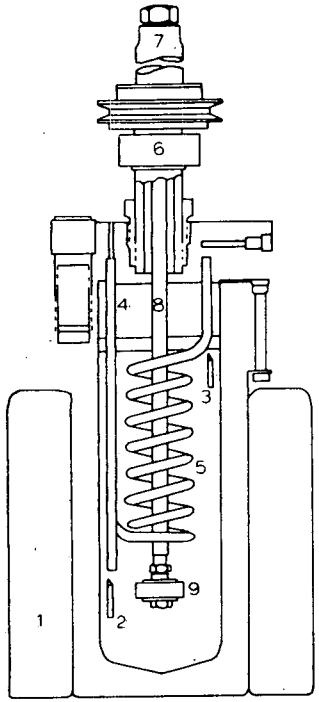

FIGURE 1. ASSEMBLY OF EQUIPMENT

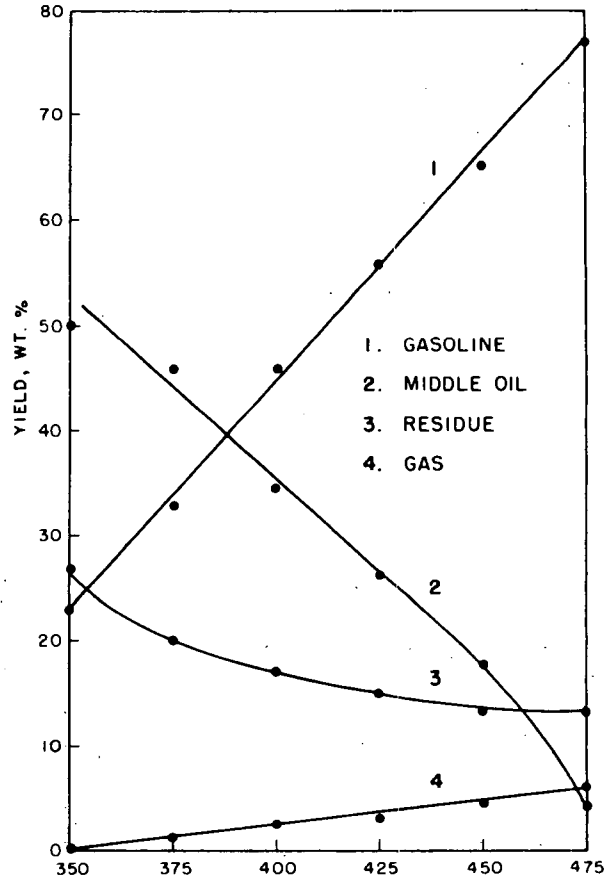

Figure 2. Effect of temperature on product distribution. pressure, 3000 psi.

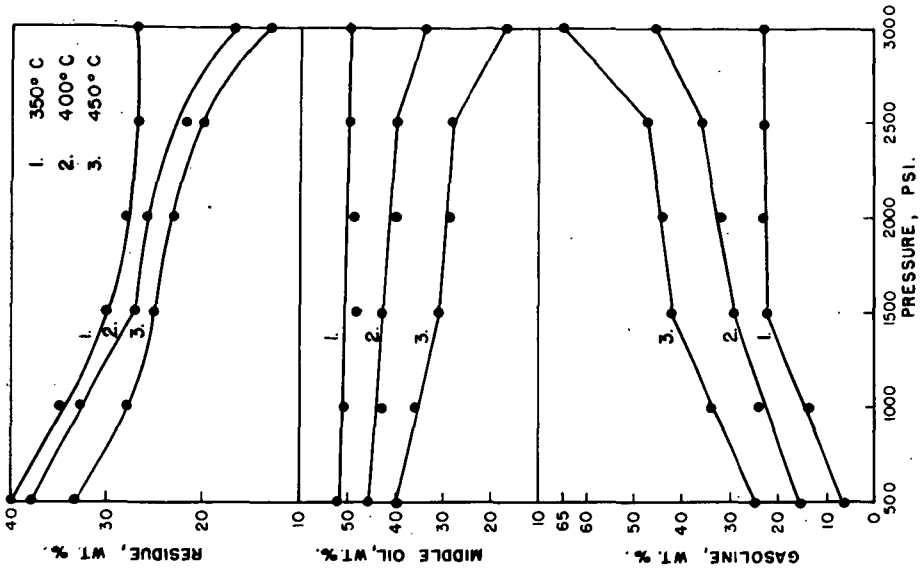

Figure 4. Effect of pressure on product distribution.

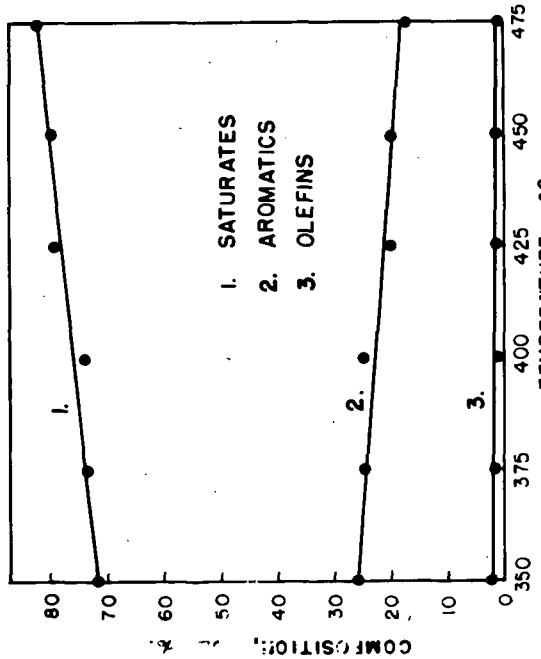

Figure 3. Effect of temperature on the composition of gasoline. pressure 3000 psi.

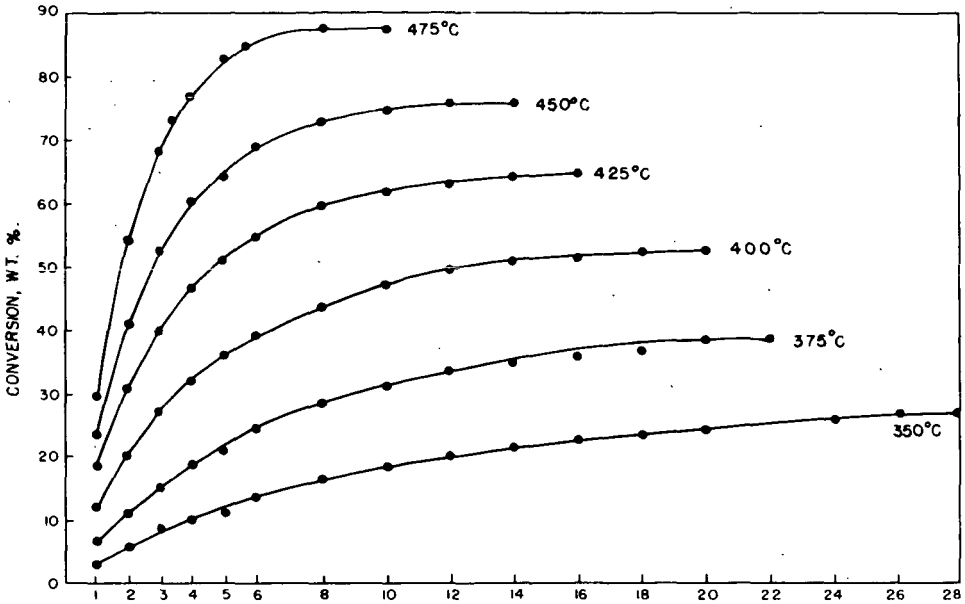

Figure 6. Effect of reaction time on conversion.

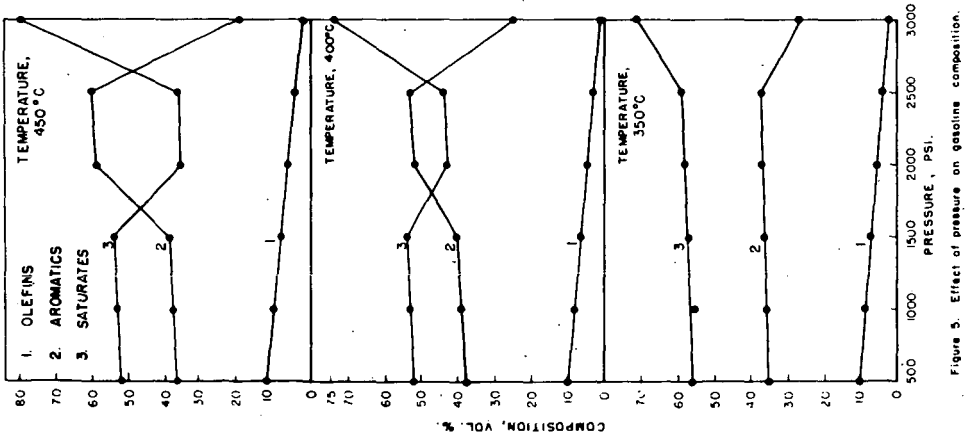

Figure 5. Effect of pressure on gasoline composition.

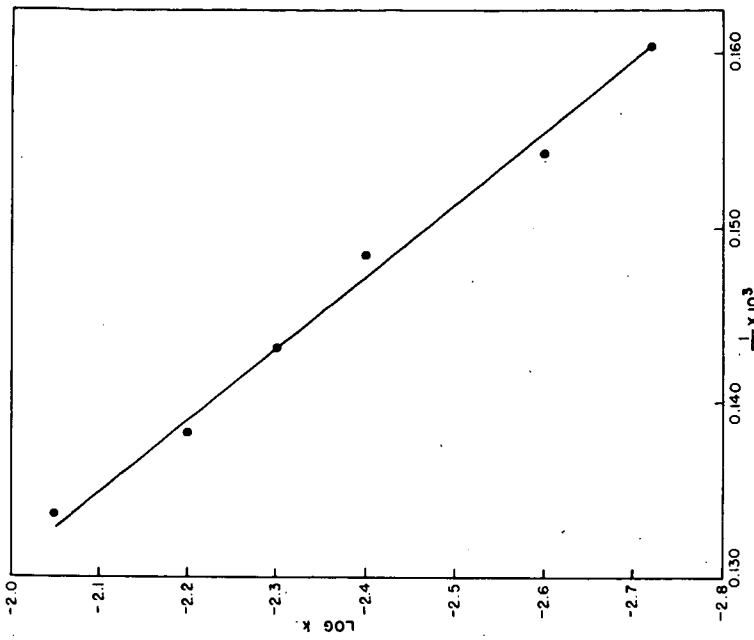

Figure 8. Arrhenius Plot.

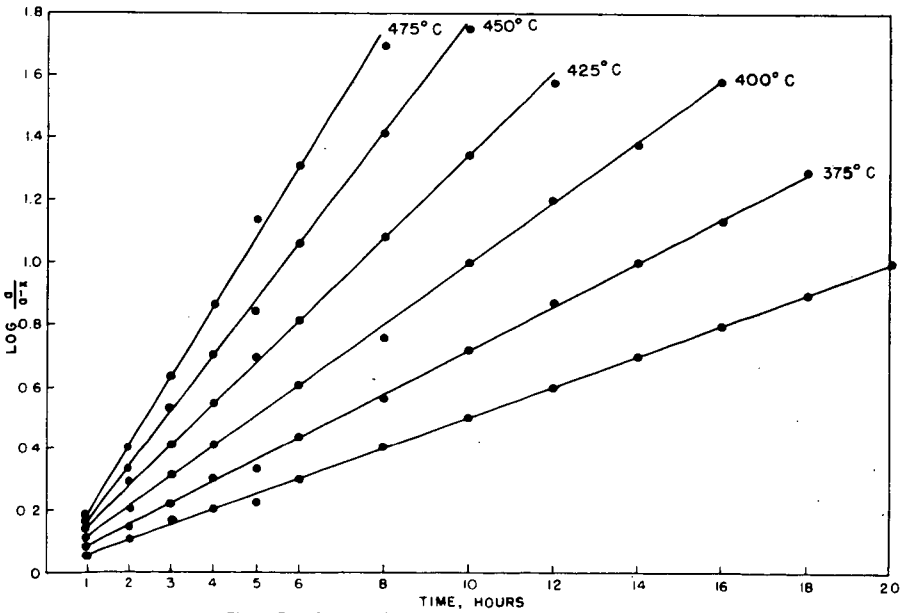

Figure 7. Plot of first-order equation.

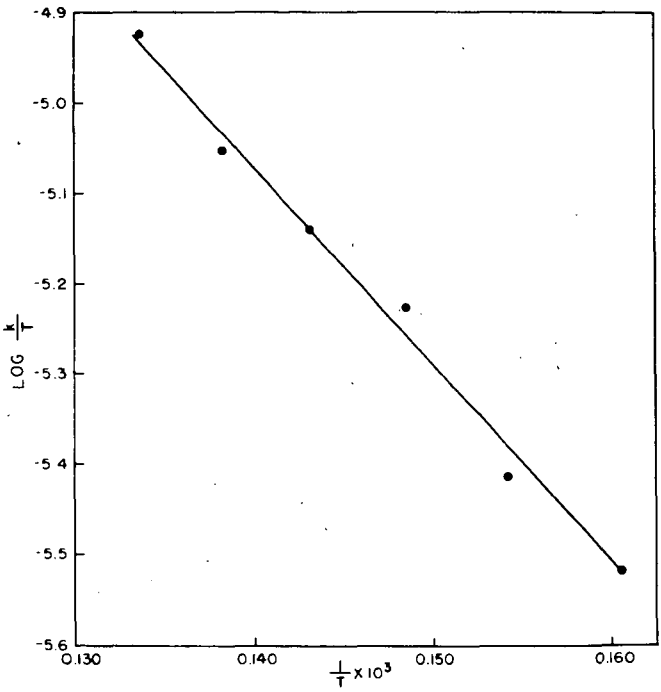

Figure 9. Absolute rate reaction plot.

KINETICS OF HYDROCRACKING OF COAL EXTRACT WITH MOLTEN ZINC CHLORIDE CATALYSTS IN BATCH AND CONTINUOUS SYSTEMS

R. T. Struck, W. E. Clark, P. J. Dudt, W. A. Rosenhoover, C. W. Zielke, and E. Gorin

Research Division
Consolidation Coal Company
Library, Pennsylvania 15129

INTRODUCTION

The use of molten zinc chloride as a catalyst for hydrocracking of polynuclear hydrocarbons has been previously described.[1,2] The superiority of zinc chloride over conventional hydrocracking catalysts was shown for pyrene, coal, and coal extract. Results in batch autoclaves showed that zinc chloride gave more rapid reaction, more complete conversion to gasoline-range naphtha, and a very high octane number without reforming. The high octane number is due primarily to the ability of the Lewis acid, zinc chloride, to maintain acid catalysis in the presence of considerable amounts of nitrogen in the feed, -- thus giving a high percentage of branched-chain hydrocarbons with high octane numbers.

Since the previous reports, a continuous zinc chloride hydrocracker has been built and operated, confirming the batch work, and also providing effluent catalyst for regeneration studies, as well as information on corrosion. A continuous catalyst regeneration unit was also operated, and will be described in the following paper. A complete report on all of the work is available from the U. S. Office of Coal Research.[3]

The purpose of this paper is to report rate data on the hydrocracking of extract with zinc chloride via a correlation which predicts conversion of extract in both batch and continuous units.

EXPERIMENTAL

Feedstock

The feedstock used for all of the work described here was a coal extract prepared by continuous extraction of Pittsburgh Seam coal, Ireland Mine, using tetralin solvent at 750°F with a residence time of 40 minutes. Unextracted coal and mineral matter were removed by filtration at 646°F. The final extract represents 81% of the moisture- and ash-free coal (MAF coal). Properties are given in Table I.

A measure of the asphaltic nature of extract is given by solvent fractionation. "Benzene-insolubles" is the fraction of extract insoluble in benzene at its atmospheric boiling point. "Asphaltenes" is the fraction soluble in benzene, but insoluble in cyclohexane, determined by mixing one part of benzene-soluble extract with nine parts of benzene and 100 parts of cyclohexane, by weight, and filtering at room temperature. The fraction soluble in this mixture is termed "oil."

Catalyst

The zinc chloride used was Fisher Scientific Co. certified reagent, 96 to 98% pure, dried before used in a vacuum at 110°C. After this treatment, it contained 1 to 1.5 wt % water and 1 to 1.8 wt % zinc oxide. Before feeding this to the continuous unit, the remaining water was removed by melting the salt under full pump vacuum.

For a number of tests, zinc oxide was added to the zinc chloride to bring the total zinc oxide up to that required for stoichiometric reaction with HCl liberated by sulfur in the extract reacting with zinc chloride (4.65 wt % of the catalyst). The zinc oxide used was Baker and Adamson certified reagent; the lots used were 99.0 to 99.5% pure.

Equipment

The basic unit for the batch hydrocracking tests was a 300-ml rocking autoclave (American Instrument Company, Catalog No. 40-2150). The normal rocking motion of 36 cycles/min about the axis was revised to give 86 cycles/min through an angle of 30° on the end of a 12-inch lever arm. The equipment and procedures have been described previously.[1]

The continuous hydrocracking unit flow sheet is given in Figure 1. The reactor is a "stirred-tank" reactor, to which extract, catalyst, and hydrogen are fed separately Constant inventory in the reactor is maintained by a pressure-drop controller operating on a valve in the "spent" catalyst withdrawal line. The reactor is 3 inches in diameter and contains a liquid inventory of 400 to 600 grams. All products were collected, analyzed, and the results consolidated. Elemental balances were then made and the zinc balance forced by adjusting the residue collected. This avoided errors due to differing bed levels at beginning and end of the balance period. The carbon balance was then forced by adjusting the amount of extract fed (uncertainty existed as to the density in the feed pump). The nitrogen, oxygen, and sulfur balances were forced by assuming the unaccounted-for products to be NH_3, H_2O, and H_2S, respectively, which have reacted with the catalyst. Chlorine was forced by assuming the unaccounted-for chlorine was present in the catalyst as the double salt $ZnCl_2 \cdot NH_4Cl$. The hydrogen consumption was then obtained by difference between the hydrogen in the products and that in the feedstock (exclusive of H_2 gas). After forcing all elemental balances, the overall material balance also closes, and the conversions reported in Table IV are reported on this basis.

Conversion, as used here, is the conversion of extract to products boiling below 400°C (752°F) at normal atmospheric pressure. It is calculated by subtracting the percentage of +400°C residue from 100%. Because of the heat-sensitivity of the materials involved, the 400°C cut point in a distillation is defined as 240°C in the pot of a simple flask when the pressure is 1 torr.

DISCUSSION OF RESULTS

Results in the continuous unit generally confirmed previous batch results, showing higher conversion at lower levels of zinc oxide. Temperature has the expected result - more rapid reaction at higher temperatures, but at temperatures above 750°F, the maximum liquid yield decreases. Straight run gasolines from zinc chloride hydrocracking show Research Octane Numbers (clear) of 87 to 91 and a high sensitivity to lead. With 3 ml of tetraethyllead per gallon, the RON values rise to 99 to 101. If reformed, the product would be 85 to 90% aromatics, suitable for a high-octane blending stock for gasolines or as a source of benzene via hydrodealkylation.

Kinetic Model

The basic model used to correlate hydrocracking results assumes that extract is composed of many different compounds, each hydrocracking independently at a different rate that can be expressed as a first-order reaction. The situation has been greatly simplified by assuming only three species present: an unconvertible fraction, a fraction which converts rapidly, and a fraction which converts relatively slowly. For simultaneous independent reactions in a batch unit,

$$C_e - C = N_1 C_e e^{-k_1 t} + (1-N_1) C_e e^{-k_2 t} \qquad (1)$$

where "C_e-C" is the convertible material remaining at time "t", and "N_1" is the fraction of the convertible material which reacts via the fast reaction. A table of nomenclature is given at the end of the text.

For a single perfectly-mixed, continuous reactor, the probability that a microscopic drop of liquid will have a residence time in the reactor between t and t + dt is $\frac{1}{\tau} e^{-t/\tau} dt$.

where τ = residence time in the continuous unit.

The average fraction of extract unconverted then would be

$$\frac{C_e - C}{C_e} = \frac{1}{\tau} \int_o^\infty \left(\frac{C_e - C}{C_e}\right)_B e^{-t/\tau} dt$$

where $\left(\frac{C_e - C}{C_e}\right)_B$ is the fraction unconverted at the time "t" as determined from batch data. Substituting from Equation 1 for $\left(\frac{C_e - C}{C_e}\right)_B$, gives the following:

$$\frac{C_e - C}{C_e} = \frac{1}{\tau}\left[N_1 \int_o^\infty e^{-(1+k_1\tau)t/\tau} dt + (1-N_1) \int_o^\infty e^{-(1+k_2\tau)t/\tau} dt\right]$$

$$\frac{C_e - C}{C_e} = \frac{N_1}{1 + k_1\tau} + \frac{1 - N_1}{1 + k_2\tau} \qquad (2)$$

Evaluation of Constants

The data available consist of 38 runs in the batch autoclave and 14 runs in the continuous unit, covering the following ranges:

	Batch Unit	Continuous Unit
Temperature, °F	700-775	700-800
Partial Pressure of H_2, psig	1500-3500	2730-3300
Residence Time, minutes	15-360	22.8-192.6
Catalyst/Extract Weight Ratio	1.0	0.9-1.3
$ZnO/ZnCl_2$ Mole Ratio	0.013-0.0765	0.01-0.08
Conversion, Wt % of Extract	41-92	62-89

The more extensive batch data have been used to determine constants in the kinetic equations wherever applicable. However, because of the uncertainty in low residence times inherent in batch runs (i.e., some conversion takes place as the reaction temperature is approached), the continuous unit data have been used to determine the rate constant for the fast reaction.

It is assumed that a certain fraction of the extract fed is not convertible under the conditions of temperature, pressure, and catalyst composition used, even at infinite residence time, although the amount may vary with operating conditions. The extent of possible conversion, C_e, has been determined by plotting conversion versus residence time for each set of conditions (batch data). Tangents drawn to each curve yield the slope, or rate of reaction, dC/dt. These instantaneous rates were then plotted versus conversion yielding results such as shown in Figure 2. The straight lines obtained confirm the fact that the data can be represented as first order reactions and when extrapolated to zero rate of conversion yield C_e. The values of C_e so obtained are listed in Table II as "Observed C_e". It can be seen that variables of temperature, hydrogen pressure and $ZnO/ZnCl_2$ ratio all affect the value of C_e obtained. The value of C_e is independent of whether batch or continuous data are involved, since they are equal at infinite residence time.

In order to estimate C_e for conditions other than those at which runs were made, empirical equations have been developed. The first equation applies over the hydrogen partial pressure range of 2500 to 3500 psig:

$$C_e = 90 + \frac{(p - 2500)}{600} + \frac{(750 - T)}{25} + 10\,(0.08 - x) \qquad (3)$$

where p = partial pressure of hydrogen, psig.
T = temperature, °F.
x = mole ratio of $ZnO/ZnCl_2$.

For the pressure range, p = 1500 to 2500:

$$C_e = 90 - \frac{(2500 - p)}{200} + \frac{(750 - T)}{25} + 10\,(0.08 - x) \qquad (4)$$

The calculated values of C_e for the batch runs are also listed in Table II, and compare well with the observed values. Equations 3 and 4 were used in calculating conversions for both batch and continuous runs. The equations illustrate the facts that C_e increases at low levels of ZnO, at higher pressures, and at lower temperatures (within the 700 to 800°F range).

At long residence times where the fast reaction is substantially complete, and wh N_1 is constant, Equation 1 shows that a plot of log (C_e-C) versus residence time should be a straight line:

$$\log (C_e - C) = \log (1-N_1)\, C_e - k_2 t.$$

The slope of such a line is k_2 and the intercept on the ordinate is log $[(1-N_1)C_e]$ This provides a technique for determining k_2 and N_1. Figure 3 is a representative plot of this type. Again, we see the confirmation of straight lines if we ignore runs at lc residence times where the fast reaction is incomplete.

The values of k_2 and N_1 from plots like Figure 3 are listed in Table II. It can be seen that 67 to 81% of the convertible extract reacts via the fast reaction (N_1). T simplify further calculations, a constant value of $N_1 = 0.75$ has been taken as representative of all conditions.

The reaction rate constants for the slow reaction, k_2, have been plotted for the hydrogen pressure level of 2500 psig as an Arrhenius plot in Figure 4. Because the rat of ZnO to $ZnCl_2$ is an important parameter, only two points are available at a single condition. A line was drawn through these points and lines at other $ZnO/ZnCl_2$ ratios drawn parallel to it. A line at $ZnO/ZnCl_2 = 0.02$ was interpolated for future use with continuous unit data. Based on the relatively mild effect of pressure on k_2 shown in Table II, the values in Figure 4 have been used for estimating conversions at all pressures.

The remaining constant in Equations 1 and 2 is k_1, the reaction rate constant for the fast reaction. This has been determined from the continuous unit data by using the data from one run at each condition and solving for k_1 in Equation 2. Values of C_e were calculated from Equations 3 or 4, those for k_2 were taken from Figure 4, and N_1 was taken as 0.75. Generally, the run with the lowest conversion in each set was used to calculate k_1, since it would be most representative of the fast reaction.

The values of k_1 obtained are listed in Table IV along with other information on the continuous runs. An Arrhenius plot of k_1 is given in Figure 5, showing the desired straight line and indicating an activation energy for the fast reaction of 35 kcal/g mole. It will be noted that the values of k_1 are independent of the $ZnO/ZnCl_2$ ratio, in contrast to those for k_2. Since the range of hydrogen pressures was quite narrow in the continuous data, the effect of hydrogen pressure, if any, on k_1 could not be determined.

The energy of activation of 35 kcal/g mole indicates that the rate-determining step involves a chemical reaction rather than being limited by accessibility of hydrogen in the bulk liquid or through a boundary film. It coincides with the value found by Weller[4] for hydrogenation of asphaltenes from coal with tin catalyst. This also was a first-order reaction.

Comparison of Calculated and Observed Conversions

The values of C_e, N_1, k_1 and k_2 as determined above were used in Equation 1 to predict the conversion for each run in the batch unit. Table III compares these calculated conversions with those actually observed. The "fit" is quite good, particularly at high conversion levels. The poorest fit occurs at low conversions and low hydrogen pressures. This suggests that the reaction rate constant for the fast reaction, k_1, actually is a function of pressure, although the data do not permit this relationship to be properly defined.

Similar calculations for data from the continuous unit via Equation 2 are shown in Table IV. Again, the observed and predicted conversions show good agreement. The experimental data and calculated curves for 3000 psia of hydrogen are shown in Figure 6. The "fit" is quite good except for a few of the 775°F points at 0.07 to 0.08 mole ratio $ZnO/ZnCl_2$, which show 2 to 6% higher conversions than predicted

CONCLUSIONS

The kinetic model which assumes that the hydrocracking of coal extract with zinc chloride catalyst can be represented by two or more simultaneous first-order reactions has been shown to represent both batch and continuous unit data. An average of 75% of the extract converts via a fast reaction with an activation energy of 35 kcal/g mole. The reaction rate constant for this reaction is affected somewhat by hydrogen pressure, but is independent of the ratio of ZnO to $ZnCl_2$. The rate constant for the slow reaction, which may be lower by a factor up to 40 times, is independent of hydrogen pressure (1500-3500 psig), but a strong function of how much ZnO is present.

ACKNOWLEDGEMENT

The assistance of the U. S. Office of Coal Research in sponsoring this work is gratefully acknowledged.

Many individuals of the Consolidation Coal Company, Research Division, in addition to the authors were involved in the experimental work for this paper. Especially noteworthy were the contributions of C. P. Costanza, J. M. Evans, and J. M. Pazzo.

NOMENCLATURE

- C = conversion of extract to -400°C products, wt % of MAF extract.
- C_e = conversion at which the rate of conversion becomes zero.
- k_1 = reaction rate constant for extract conversion via the fast reaction, $min.^{-1}$
- k_2 = reaction rate constant for extract conversion via the slow reaction, $min.^{-1}$
- N_1 = fraction of C_e which occurs via the fast reaction.
- p = partial pressure of hydrogen, psig.
- T = temperature.
- t = residence time in a batch or plug flow reactor, min.
- x = $ZnO/ZnCl_2$ mole ratio in the catalyst.
- τ = Average residence time in the continuous reactor, = weight of liquid phase in the reactor divided by the weight rate of liquid product/min. The liquid is the "natural" liquid existing at reactor conditions, i.e., catalyst plus unvaporized oil.

References

(1) Zielke, C. W., Struck, R. T., Evans, J. M., Costanza, C. P., and Gorin, Everett, I&EC Process Design & Dev., 5, April 1966, p 151-157.

(2) Zielke, C. W., Struck, R. T., Evans, J. M., Costanza, C. P., and Gorin, Everett, I&EC Process Design & Dev., 5, April 1966, p 158-164.

(3) Summary Report I - Consol Synthetic Fuel Development, U. S. Office of Coal Research, Contract 14-01-0001-310, 1968.

(4) Weller, Sol, Pelipetz, M. G., and Friedman, Sam, Ind. Eng. Chem., 43, p 1572 (1951).

TABLE I

Properties of Coal and Extract Used

	Ireland Mine Coal	Coal Extract
	MF Basis	
Volatile Matter	40.32	
Fixed Carbon	46.66	
FeS	0.08	
FeS_2	4.19	
Other Ash	10.15	
	MAF Basis	
Hydrogen	5.73	6.03
Carbon	81.90	84.65
Nitrogen	1.58	1.53
Oxygen (by diff.)	8.61	6.14
Sulfur	2.18	1.65
Solvent Fractions		
Benzene-insolubles		33
Asphaltenes		47
Oil		20

TABLE II

Values of C_e, N_1 and k_2 Determined from Batch Runs

Temp., °F	$ZnO/ZnCl_2$ Mole Ratio	H_2 Partial Pressure, psig	C_e, Wt % of Extract		N_1(3)	k_2,(4) $min.^{-1}$
			Observed(1)	Calculated(2)		
700	0.013	1500	87	87.7	0.670	0.0058
700	0.013	2500	92	92.7	0.712	0.0048
750	0.03	2500	91	90.5	0.736	0.020
750	0.03	3500	92	92.1	0.740	0.030
750	0.0765	1500	85	85.0	0.750	0.0062
750	0.0765	2500	90	90.0	0.773	0.0063
775	0.0765	2500	88	89.0	0.810	0.021
775	0.0765	3500	(90)	89.6	0.788	--

(1) Intercepts on Figure 2 and similar plots.
(2) Calculated from Equations 3 and 4.
(3) Determined from intercepts on Figure 3 and similar plots.
(4) From the slopes of Figure 3 and similar plots.

TABLE III

Calculated and Observed Conversions for Batch Runs

Temp., °F	$ZnO/ZnCl_2$ Mole Ratio	H_2 Partial Pressure, psig	k_1 (1) $min.^{-1}$	Residence Time, (2) min	Conversion Wt % of Extract Observed	Conversion Wt % of Extract Calculated (3)
700	0.013	1500	0.078	15	41.2	46.8
				60	61.2	71.0
				120	71.0	76.1
				180	76.6	79.3
				360	82.6	84.3
		2500		15	49.1	49.5
				60	70.6	73.6
				120	78.8	80.5
				180	83.4	83.9
				360	89.0	89.2
750	0.03	2500	0.24	15	73.0	72.3
				60	82.6	84.3
				120	88.7	88.9
				180	90.3	90.4
		3500		15	78.6	73.1
				60	87.1	85.1
				120	91.6	89.9
				180	92.1	91.4
750	0.0765	1500	0.24	15	52.0	64.0
				60	68.8	70.5
				120	74.9	74.9
				180	80.0	78.1
				360	83.4	82.8
		2500		15	58.1	67.8
				60	76.7	74.6
				120	80.5	79.3
				180	83.8	82.7
				360	88.3	87.7
775	0.0765	2500	0.43	15	71.3	71.9
				60	81.9	80.2
				120	86.4	86.2
				180	87.6	87.5
				360	87.7	88.0
		3500		15	71.7	73.5
				60	80.4	82.6
				120	83.5	87.2
				180	86.5	89.5
				360	89.9	90.0

(1) From Figure 5.
(2) Residence time at reaction temperature.
(3) Calculated from Equation 1.

TABLE IV

Calculation of Rate Constants and Comparison of Experimental and Calculated Conversions in Continuous Unit

Temp., °F	$ZnO/ZnCl_2$ Mole Ratio	H_2 Pressure psig	Residence Time, min	C_e (1)	k_2 (2) $min.^{-1}$	k_1 (3) $min.^{-1}$	Conversion Wt % of Extract Observed	Conversion Wt % of Extract Calculated
775	0.07	3040	46.7	89.5	0.021	0.43	75.0 (4)	75.0
↓	0.07	3000	95.0	↓	↓	↓	83.1	80.5
	0.09	2860	96.8				82.0	80.5
	0.08	2860	101.0				85.0	80.7
	0.08	3100	102.6	90.0			87.1	81.4
750	0.08	3300	22.8	91.0	0.0063	0.24	61.7	60.7
↓	↓	3090	51.2	↓	↓	↓	68.8 (4)	68.6
		3040	105.0				74.1	74.6
750	0.02	3190	24.3	92.0	0.051	0.24	71.7 (4)	71.7
↓	↓	3150	26.6	↓	↓	↓	72.2	72.0
		3040	102.0				84.0	87.9
800	0.08	2815	102.0	88.5	0.070	0.72	86.6	85.0
776	0.02	2730	111.7	90.0	0.16	0.43	88.5	87.5
700	0.02	3210	80.5	93.0	0.003	0.078	64.3 (4)	64.3

(1) Calculated via Equation 3.
(2) From Figure 4.
(3) Calculated via Equation 2 using $N_1 = 0.75$.
(4) Experimental point used to calculate k_1.

SIMPLIFIED FLOW DIAGRAM OF CONTINUOUS HYDROCRACKER USING ZINC CHLORIDE CATALYST

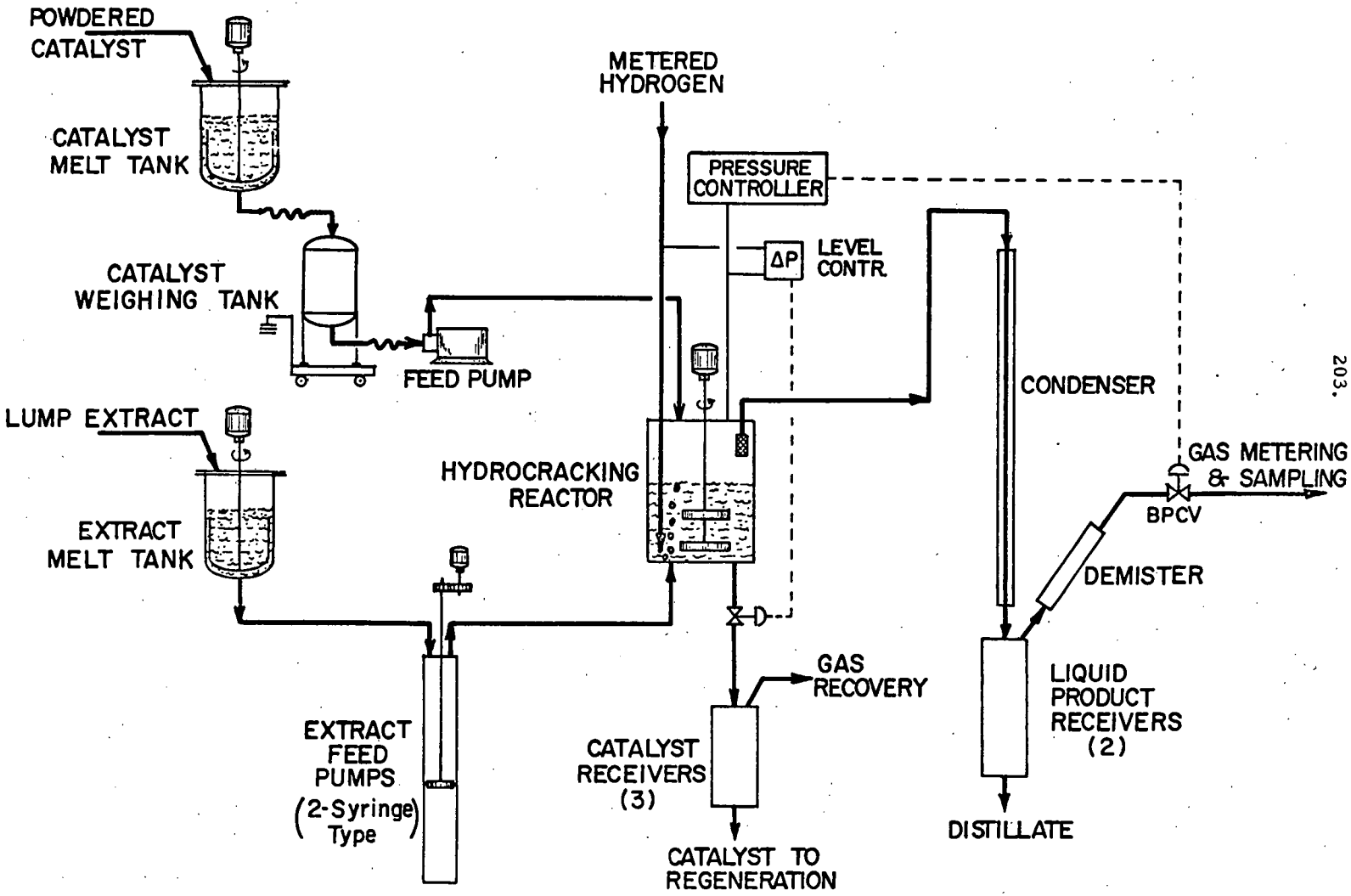

Figure 2

EXTRAPOLATION OF BATCH RATE DATA TO DETERMINE C_e

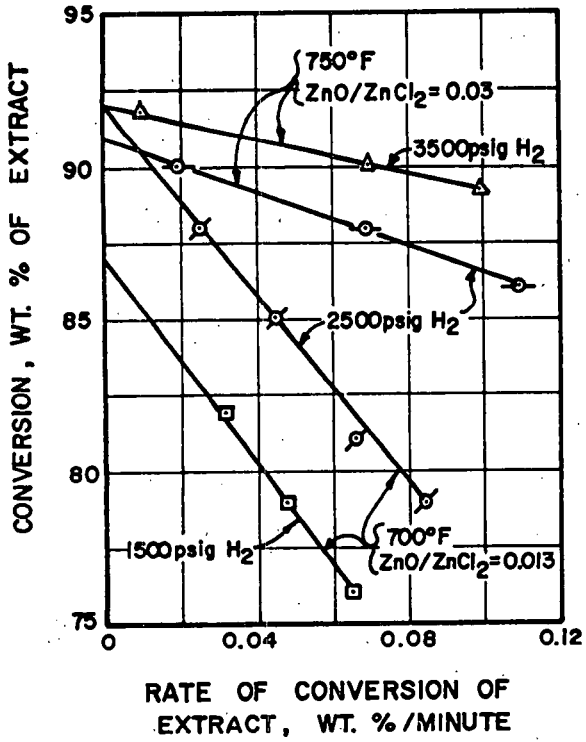

Figure 3

RESIDUE REMAINING vs RESIDENCE TIME

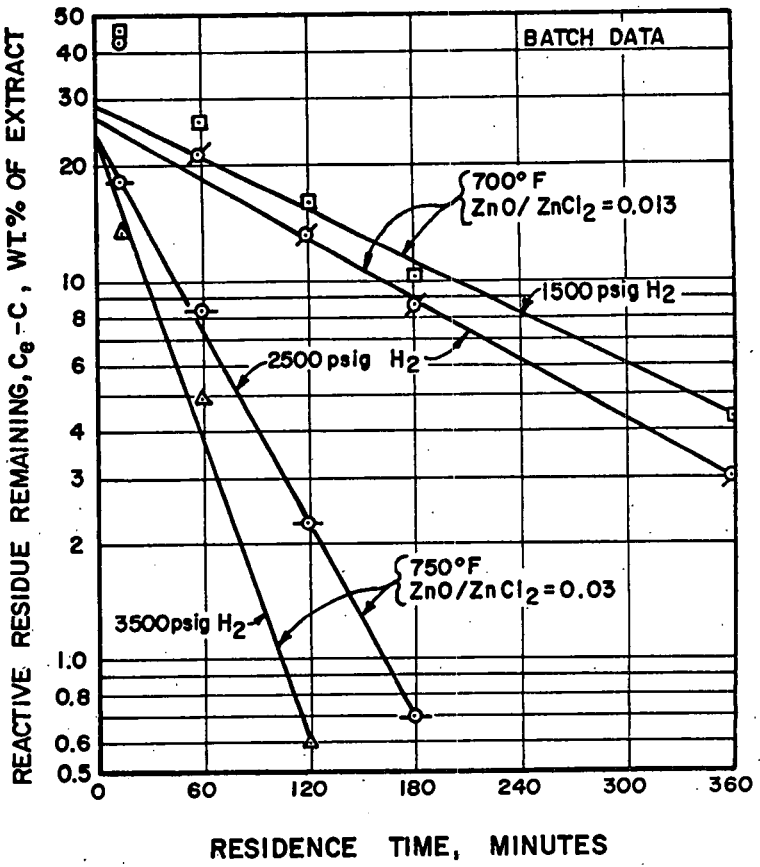

Figure 4

REACTION RATE CONSTANT FOR THE SLOW REACTION vs RECIPROCAL TEMPERATURE

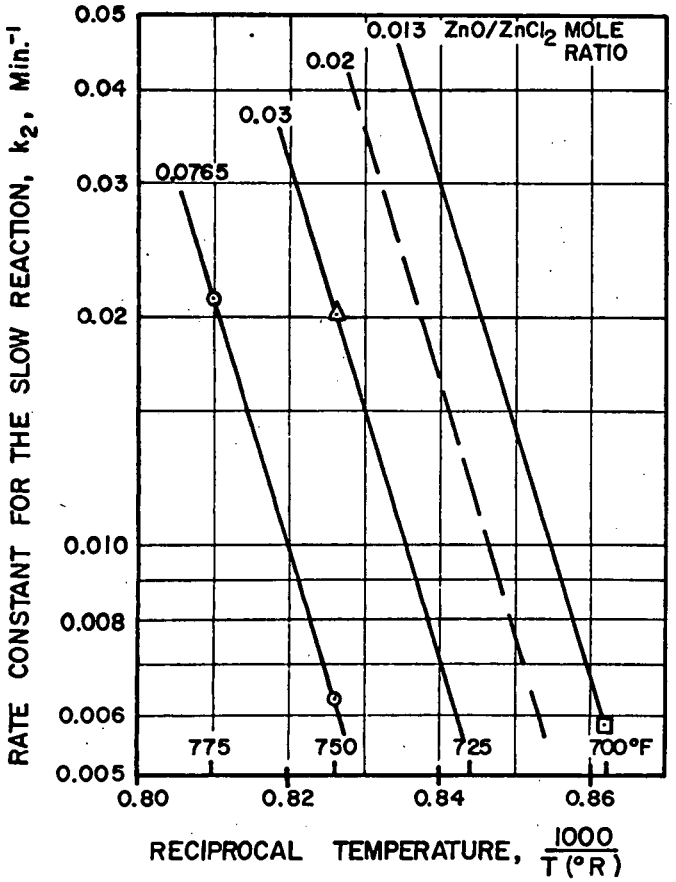

Figure 5

REACTION RATE CONSTANT FOR THE FAST REACTION vs RECIPROCAL TEMPERATURE

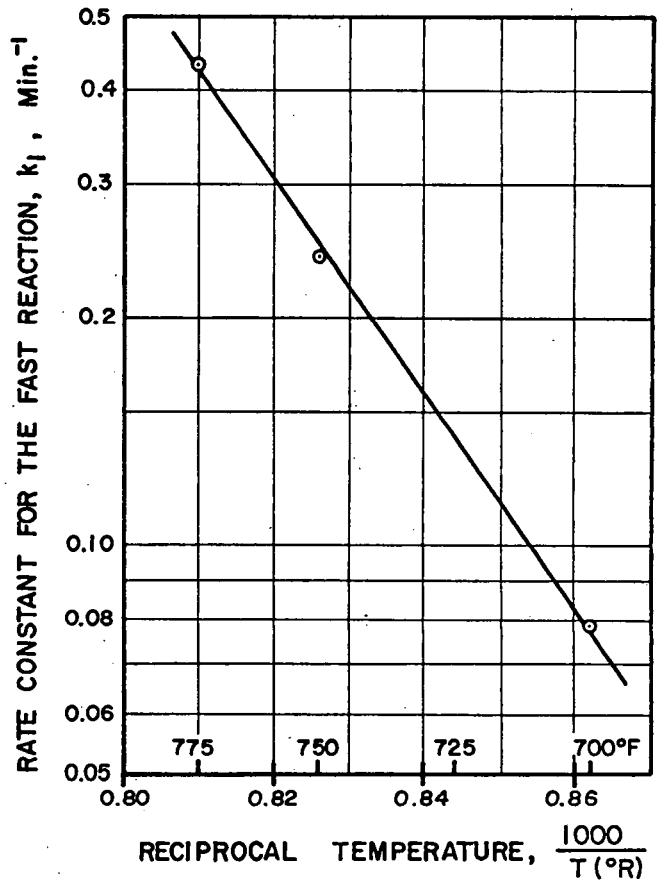

Figure 6

VARIATION OF CONVERSION WITH RESIDENCE TIME IN THE CONTINUOUS REACTOR

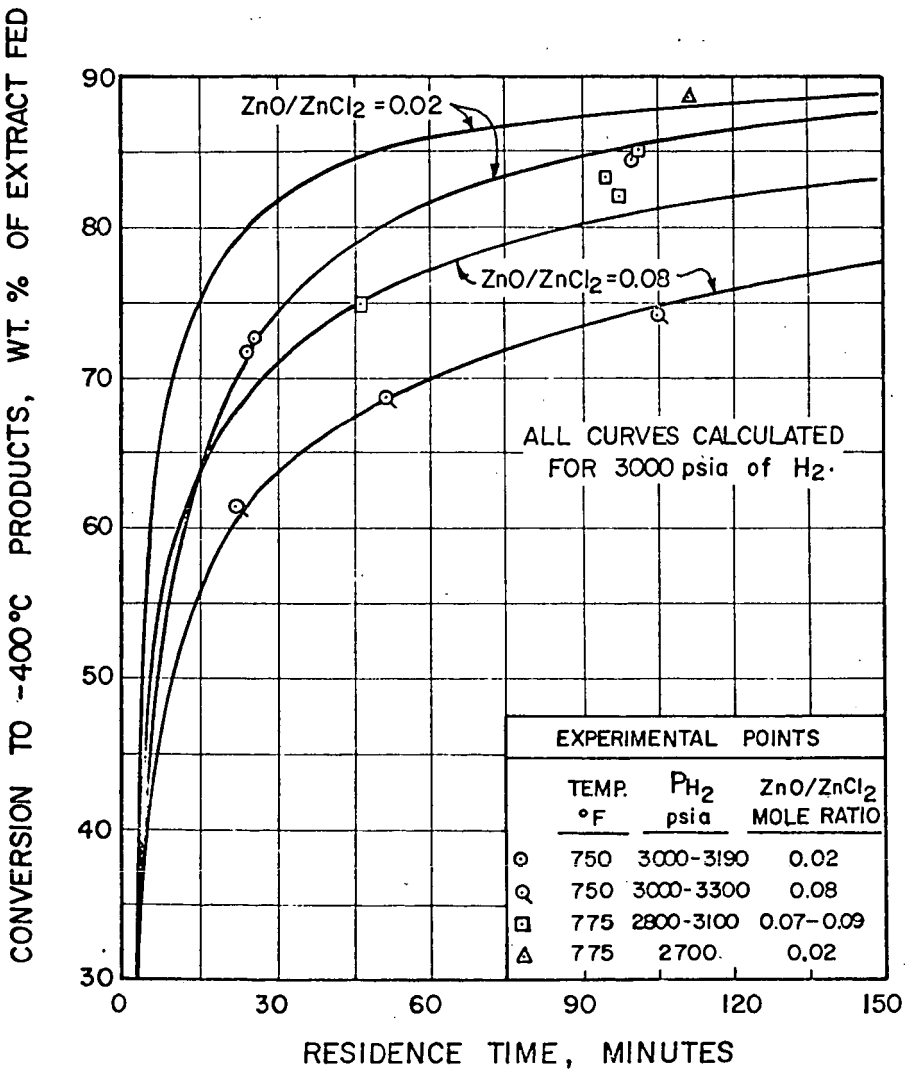

FLUO-SOLIDS COMBUSTION PROCESS FOR REGENERATION OF SPENT ZINC CHLORIDE CATALYSTS

C. W. Zielke, R. T. Struck, and Everett Gorin

Research Division
Consolidation Coal Company
Library, Pennsylvania 15129

INTRODUCTION

The application of molten zinc chloride catalysts to the hydrocracking of polynuclear hydrocarbons, coal, and coal extract has been discussed previously.[1,2,3] During the hydrocracking process, the catalyst partially reacts with nitrogen and sulfur in the feed according to the reactions,

$$ZnCl_2 + H_2S = ZnS + 2\ HCl \quad (1)$$

$$ZnCl_2 + xNH_3 = ZnCl_2 \cdot xNH_3 \quad (2)$$

$$ZnCl_2 \cdot yNH_3 + yHCl = ZnCl_2 \cdot yNH_4Cl \quad (3)$$

Addition of zinc oxide to the hydrocracking catalyst eliminates reaction (3) and introduces a new reaction

$$ZnO + 2\ HCl = ZnCl_2 + H_2O \quad (4)$$

The melt leaving the hydrocracker thus, in general, will contain in addition to $ZnCl_2$, the following compounds: ZnS, $ZnCl_2 \cdot xNH_3$, $ZnCl_2 \cdot yNH_4Cl$. The ratio of the NH_4Cl to NH_3 adducts is dependent on the ratio of nitrogen to sulfur in the feed and the amount of ZnO added to the feed melt. In addition to inorganic impurities, the melt contains organic residue that cannot be distilled out of the melt. These impurities are quite uniformly distributed in the melt and normally do not settle out of the bulk melt phase.

A commercial process using zinc chloride must provide a viable scheme for regeneration of the catalyst. Regeneration of the melt comprises removal of the bulk of the nitrogen, sulfur and carbon impurities and return of the melt as relatively pure zinc chloride.

The purpose of this paper is to present data on regeneration of the melt using a fluo-solids combustor. The combustion process removes carbon, nitrogen and sulfur from the melt, simultaneously vaporizing the zinc chloride which is subsequently condensed downstream from the combustor.

EXPERIMENTAL

Equipment

A diagram of the equipment is shown in Figure 1. The melt feed is dropped from a drip tip on the top flange of the combustor into the fluo-solids bed contained in the mullite reactor liner. The fluidizing air is supplied via a tube that enters the combustor at the upper flange and extends to within 3/4" of the tip of the liner cone where it discharges into the fluo-solids bed. The vapors from the combustor are cooled to 650-700°F in the condenser where the zinc chloride condenses and HCl and ZnO, formed by hydrolysis in the oxidation zone, interact to re-form $ZnCl_2$ and H_2O. Residual $ZnCl_2$ fog from the condenser is removed from the gas stream by electrostatic precipitators operated at 650°F, i.e., above the melting point of $ZnCl_2$.

The effluent gas from the precipitators (essentially $ZnCl_2$-free) is passed through a cooler where water and some HCl are removed. A small side-stream of the "dry" gas is passed through an Ascarite trap to remove acid gases and then to a Beckman Model E-2

oxygen analyzer. The main stream of dry gas is passed through tandem scrubbers containing aqueous hydrogen peroxide which removes SO_2 plus HCl and aqueous sodium hydroxide which removes CO_2 from the product gas. A fraction of the offgas is diverted to a gas holder and the remainder is metered and vented.

Procedure and Product Workup

To charge the fluo-solids bed and start a run, the thermowell of the combustor is replaced with a tube surmounted by a closed hopper containing fluosolids. The fluidizing air and argon purge flows are then established, and the fluosolids are charged to the reactor held at 1200-1400°F. After replacing the thermowell, the desired pressure is established, and the combustor is heated to about 50°F below the desired run temperature. The feed is then started with the vapors going to the line-out train. When all temperatures are lined out and the oxygen content of the effluent gas is constant, the vapors are diverted through the balance train to start the balance period. The weight of melt fed during the balance varied from 900 to 6700 grams, depending on the feed rate.

All products, including the fluo-solids, are collected and analyzed. Determinations are made of chlorine on the product water, chlorine and sulfur on the hydrogen peroxide scrubber effluent, and chlorine and CO_2 on the sodium hydroxide scrubber effluent to obtain the amounts of HCl, SO_2 and CO_2 collected in these materials. The scrubbed gas collected in the gas holder is analyzed for H, CO, CO_2, SO_2, N_2, A and O_2 by two-stage gas chromatography.[4] The results from the water, scrubbers, and gas holder are consolidated to obtain the effluent gas composition. Material balances and elemental balances are made. The amount of ammonia decomposition is determined by the difference between inorganic nitrogens in the feed and effluent melts. The methods for determining the amount of ZnS and NH_3 in the melts have been described previously.[2]

Range of Variables Explored

Temperature, °F	1800 and 1900
Pressure, psia	15-46
Superficial air velocity, fps	0.16-2.67
Melt feed rate, lb/(ft^2-hr)	7.1-347
Superficial vapor residence time, sec.	0.4-6.3
% of Stoichiometric air	44-115
Fluo-solids bed depth, inches	12-16
Types of fluo-solids	Silica sand, ZnO sinter, mullite

Superficial air velocity is defined as the velocity of the air feed at process conditions based on the empty reactor. Superficial residence time is based on the superficial velocity and the fluo-solids bed depth. Stoichiometric air is defined as the amount to completely burn the NH_3, ZnS and organic residue contents of the feed melt according to the following reactions,

$$NH_3 + 3/4\ O_2 = 1/2\ N_2 + 3/2\ H_2O \quad (5)$$

$$ZnS + 3/2\ O_2 = ZnO + SO_2 \quad (6)$$

$$CH_x + \left(1 + \frac{x}{4}\right) O_2 = CO_2 + \frac{x}{2} H_2O \quad (7)$$

The size consists of the fluo-solids were chosen to match the fluidizing velocities used. The criteria are that the bed be well fluidized (bed expansion over the fixed bed is typically 50-150%) and the terminal velocity of the smallest particle is such that it is not elutriated out of the bed. The size consists used varied from 100 x 150 mesh at a fluidizing velocity of 0.16 fps to 20 x 28 mesh at a fluidizing velocity of 2.67 fps.

Feedstocks Used

Analyses of the melt feedstocks are given in Table I. The natural melts were produced in a continuous $ZnCl_2$ hydrocracker with coal extract feed as described previously.

The low carbon and high carbon melts contained, respectively, 7.2 and 11.6% of the carbon in the feed extract. A synthetic melt was used before natural melt became available. It was prepared from lampblack (Columbian Eagle Brand), $ZnCl_2$ (Fisher Scientific Co., certified reagent, 98.3% pure), ZnS (Fisher Scientific Co., "purified" grade, 97% pure, 0.3 μ particle size) and anhydrous NH_3 (Matheson Co., 99.99% pure).

RESULTS

Results With Low-Carbon Feedstocks and Near-Stoichiometric Air

Some basic features of fluo-solids combustion with the amount of stoichiometric air varying between 77 and 116% are illustrated in Runs 1 through 4 of Table II. In these runs, the air input was maintained constant to give a linear velocity of 0.4 fps and the percent of stoichiometric air was varied by changing the melt feed rate. Nearly complete burn-out of the organic, sulfur, and nitrogen impurities is obtained at air inputs from 115 to 90% of stoichiometric. Sulfur is burned to SO_2, carbon to CO_2 plus CO, and ammonia to nitrogen plus water. With excess air, there is a substantial amount of oxygen in the off-gas since the impurities are insufficient to utilize all of the oxygen fed. However, with a slight deficiency of air a substantially oxygen-free offgas is generated which contains sufficient CO to provide for reduction of the SO_2 to elementary sulfur by the reaction

$$2\ CO + SO_2 = 1/2\ S_2 + 2\ CO_2 \qquad (8)$$

As the percent of stoichiometric air is lowered further from 90 to 77%, the CO content of the gas further increases and a substantial amount of hydrogen appears. There is also a very marked decrease in the burnout of inorganic sulfur, but only a moderate decrease in carbon burnout. Thus, in this case, sulfur rejection to gas is poor and the amount of CO in the gas is in large excess of that required for reduction of the SO_2 to elementary sulfur. The rejection of NH_3 by combustion is also poorer at low air rates.

The heating value of the gas increases with decreasing amounts of stoichiometric air due to the increasing amounts of CO and H_2 produced, but at 77% of stoichiometric the heating value is still too low for the gas to be of value.

The above data show that the impurities are selectively oxidized from the melt in preference to zinc chloride.

Zinc chloride is essentially inert to direct oxidation according to the reaction

$$ZnCl_2 + 1/2\ O_2 = ZnO + Cl_2 \qquad (9)$$

This is shown by the fact that no Cl_2 was found in the effluent gas at any condition tested. However, significant quantities of HCl appear in the effluent gas as the data of Table II show. It is produced by hydrolysis of $ZnCl_2$ vapor with the steam generated in the combustion process. This is discussed more fully below.

Operability of the fluo-solids combustor was demonstrated over a wide range of spent melt feed rates, i.e., 7.1-347 lb/(ft^2-hr). The latter value closely approaches commercially attractive rates. Run 5 of Table II illustrates results at the high feed rate of 347 lb/(ft^2-hr) under 3 atmospheres pressure. Allowing for the lower residence time, it is seen that the results are similar to those obtained at 1 atmosphere in the lower capacity operation of Run 4. The same high feed rate was demonstrated at 1.2 atmospheres pressure using a linear velocity of 2.67 fps at 65% of stoichiometric air. The results, not presented here, were quite similar to those of Run 5. No difficulties due to agglomeration of the bed solids were encountered in any of the work.

Effects of Variables

Figures 2, 3 and 4 show the effect of the variables on the distribution of carbon and sulfur in the product gas, melt, and fluo-solids. The reason that the distribution in the fluo-solids has to be taken into account is that the fluo-solids tend to trap and retain non-volatile solids (C, ZnS, and ZnO), and that a steady-state condition in the fluo-solids bed was not reached with respect to this retention. The carbon or sulfur retained in the bed, as obtained by difference on the plots, includes losses. However, analyses of the used fluo-solids confirm that the bulk of the sulfur and carbon not appearing in either the gas or melt was retained in the fluo-solids bed. The tendency of the fluo-solids bed to trap non-volatile solids provides for retention and better utilization of the combustibles. In addition, the bed acts as a thermal flywheel for maintaining ignition.

Figure 2 shows the effect of the percent of stoichiometric air on the distribution of carbon in the products, using the natural melt feed and the similar synthetic melt feed. With the natural melt feed there is a steady decrease of carbon burnout as the percent of stoichiometric air decreases, but burn-out still is quite good even at 54% of stoichiometric air. As the carbon burnout decreases, the carbon retained in the bed substantially increases. Carbon burnout does not decrease appreciably with reduction of percent stoichiometric air in the case of the synthetic melt feed. This may be due to a higher reactivity of the carbon black but more likely it is due to superior fluidization properties of the silica sand used as compared with the ZnO sinter used for the natural melt runs.

Figure 3 shows how, with a deficiency of air, the carbon burnout efficiency increases with increasing residence time. At constant residence time, increasing the pressure fro 1.0 to 3.1 atmospheres appears to increase somewhat the efficiency of carbon burnout.

Figure 4 illustrates how sulfur burnout drops abruptly from almost complete burnout at 90% or more of stoichiometric air to where only small amounts of sulfur are gasified at air inputs below about 80% of stoichiometric. Although some of the unburned ZnS is carried over into the melt, the majority is retained in the bed. With the synthetic melt feed, the sulfur burnout is less complete, whereas carbon burnout was more complete Possible reasons for this were given above. The results do indicate that, at some conditions, it is possible to produce a low-sulfur off-gas with as high as 80% of stoichiometric air.

Figure 5 shows that ammonia decomposition decreases quite rapidly and almost linearly as the percent of stoichiometric air is reduced below 100% at 2.4 seconds residence time. Ammonia can be destroyed either by oxidation according to reaction (4) or by thermal decomposition according to the following reaction:

$$ZnCl_2 \cdot NH_3 = ZnCl_2 + 1/2\ N_2 + 3/2\ H_2 \qquad (10)$$

When operating with approximately stoichiometric air, the oxidation reaction likely predominates, and decomposition is quite complete in 2.4 seconds residence time. With a deficiency of air, thermal decomposition by Reaction (10) probably predominates. Since thermal decomposition of ammonia is relatively slow, longer residence times and/or high temperatures are required to get efficient ammonia decomposition when operating with a deficiency of air. It is important that the ammonia content of the regenerated melt be low because ammonia inhibits the hydrocracking activity of the melt.

Results With the High-Carbon Feedstock

The results with the low-carbon feedstocks indicated that, by operating with a deficiency of air, a low-sulfur, low-Btu gas might be produced during the melt regeneration. Table III gives experimental examples of results with the high-carbon melt feed using a large deficiency of air, i.e., 44 to 59% of stoichiometric.

These results show that a low-sulfur fuel gas can be obtained by operating with 56% or less of the stoichiometric air at 1800°F and 6.25 seconds contact time. The Btu content of the gas goes up as the air i put is reduced, as expected. The highest heating value achieved in this work was 81 Btu/ft^3 at 44% of stoichiometric air input.

Two runs, 6 and 7, are shown in Table III wherein the residence time was decreased to 2.4 seconds with approximately the same air input as Run 8. A substantial increase in sulfur dioxide content of the gas and a decrease in carbon burnout efficiency was observed. Comparison of runs 6 and 7 show that increase of temperature from 1800 to 1900°F strongly increases the extent of NH_3 decomposition and also increases the Btu level of the gas. As with the lower-carbon melt, HCl appears in the effluent gas in an amount equivalent to 2 to 3 wt. % of the feed melt.

Effects of the Variables

Figures 6 and 7 show the distribution of carbon and sulfur, respectively, in the products as a function of percent stoichiometric air at residence times of 6.25 and 2.4 seconds. These distributions generally follow a similar pattern to that obtained with the low-carbon melts. Figure 8 shows the heating value of the offgas as a function of percent stoichiometric air at the residence times of 6.25 and 2.4 seconds. The main point brought out by Figures 6, 7, and 8 is that a minimum gas residence time in excess of 2.4 seconds is required to get efficient carbon burnout at 1800°F and to produce a substantially sulfur-free gas of relatively high heating value. The residence time required to achieve similar results is lower at a higher temperature as comparison of results in Table III with those in Figures 6, 7, and 8 show.

DISCUSSION

HCl in the Product Gas and Recovery

Steam generated in the combustion process hydrolyzes $ZnCl_2$ vapors to produce HCl by the reaction

$$ZnCl_2 + H_2O = ZnO + 2\ HCl \qquad (11)$$

The HCl formed is largely recovered by reversal of the hydrolysis reaction at the lower temperature of the $ZnCl_2$ condenser. There is sufficient total hydrogen in the low-carbon feed melt, for example, to potentially hydrolyze 74% of the $ZnCl_2$ in the feed if all of the hydrogen were oxidized to water. Reversal of the reaction in these studies was incomplete, and hence, significant amounts of HCl appeared in the product gas as shown in Tables II and III. The reasons for this are: (1) Relatively inefficient contact between the ZnO dust and HCl in the condenser, and (2) ZnO starvation in the condenser. The ZnO starvation was caused by retention of some ZnO in the fluo-solids bed.

Separate studies, not reported here,[5] have shown that with an efficient scrubber operated at 650-750°F much better HCl recovery can be obtained than was demonstrated in this work. The equilibrium constant for the hydrolysis reaction at 650 and 750°F was bracketed experimentally by studying the reaction from the H_2O side as well as the HCl side. The values obtained are:

$$K = \frac{(P_{HCl})^2}{P_{H_2O}} = \frac{650°F}{0.59 \times 10^{-4} \text{ to } 1.62 \times 10^{-4}} \quad \frac{750°F}{0.32 \times 10^{-3} \text{ to } 0.87 \text{ to } 10^{-3}}$$

This work indicates that if equilibrium had been reached at 650°F in the condenser with the gas generated in Run 2 of Table II, HCl in the effluent gas would be 0.63 wt % or lower (on melt), instead of the 2.8% actually observed.

Mechanism of Formation of Low-Sulfur Fuel Gas

The results above have shown that by operating with a relatively large deficiency of air, a low-sulfur fuel gas is produced providing sufficient residence times are employed. Large amounts of CO and H_2 are produced by incomplete combustion and also by secondary gasification of unburned carbon by CO_2 and H_2O. Undoubtedly, SO_2 is generated in the lower part of the fluo-solids bed (near the air inlet) by roasting of ZnS (Reaction 6). However, if sufficiently long vapor residence times are used, the following reactions tend to proceed to completion:

$$3\ H_2 + SO_2 = H_2S + 2\ H_2O \qquad K_{12} = (H_2S)(H_2O)^2/(H_2)^3(SO_2) = 6.3 \times 10^4 \text{ at } 1800°F \quad (12)$$

$$H_2S + ZnO = ZnS + H_2O \qquad K_{13} = (H_2O)/(H_2S) = 6.8 \times 10^2 \text{ at } 1800°F \quad (13)$$

$$3\ H_2 + SO_2 + ZnO = ZnS + 3\ H_2O \qquad K_{14} = (H_2O)^3/(H_2)^3(SO_2) = 4.3 \times 10^7$$

The equilibrium constant K_{12} was calculated from spectroscopic data of Gordon.[6] The value of K_{13} was obtained from the product of the equilibrium constants for Reactions (1) and (4). The equilibrium constant for Reaction (1) was obtained from experimental data of Kapustinskii[7] and that for Reaction (4) was calculated from available thermodynamic data on zinc compounds.[8] Extrapolation to 1800°F on a plot of log K vs 1/T was required to obtain K_{13}.

The ZnO trapped in the fluo-solids bed thus acts as a sulfur acceptor, and if equilibrium in Reaction (13) is established, the gas produced is almost completely free of sulfur. Thus, for example, if $P_{H_2O} = 5 \times 10^{-2}$ atm and $P_{H_2} = 5 \times 10^{-2}$ atm, then at equilibrium $P_{SO_2} = 2.3 \times 10^{-8}$ atm and $P_{H_2S} = 7.3 \times 10^{-5}$ atm.

Application of Results to a Commercial Process

In order to conduct the regeneration process adiabatically, it is necessary that the heats of combustion of the organic, NH_3, and ZnS impurities in the spent melt be sufficiently great to vaporize the melt and achieve the desired bed temperature. The operating temperature range would generally lie within the limits of about 1600-2100°F. The maximum temperature is dictated by the point at which defluidization occurs due to incipient sintering of the fluo-solids. The minimum temperature is dictated by the point at which adequate reaction kinetics prevail for carbon combustion and nitrogen and sulfur removal. In general, the preferred operating temperature is probably in the range of 1750-1950°F.

Figure 9 gives the adiabatic combustor temperature for several feed melts as a function of the percent of stoichiometric air and the melt carbon gasified. The input melt and air temperatures were assumed to be 800°F and 440°F, respectively, while product distributions obtained in actual runs were used in calculation of the heat and material balances. Extrapolation of the results of Figure 9 shows that at 100% stoichiometric air the feed melt must contain between 3.5 to 4.7% in order to remain within the preferred temperature limits. Somewhat higher carbon melts, i.e., up to about 6%, can be processed by lowering the preheat temperatures or by making a slight reduction in the amount of air used. Still higher carbon feeds require further lowering the percent of stoichiometric air or cooling of the combustor. Operation within the intermediate range of stoichiometric air (between 70 and 90%) has two drawbacks. First, the Btu content of the offgas is too low, and its sulfur content too high, for it to be useful as a fuel gas. Second, rejection of sulfur in a single-stage oxidation is incomplete.

Therefore, two types of operating regimes are of chief interest. The first is single-stage combustion with near-stoichiometric air using a feed containing 3.5-6.0% carbon. In this case substantially all of the impurities are burned out of the melt. By fine adjustment of the air input at about 90% of stoichiometric, a substantially oxygen-free gas containing sufficient CO can be generated to permit subsequent reduction of the SO_2 in the off-gas to elementary sulfur.

The second operating regime is a two-stage process that handles a relatively high-carbon melt and uses a deficiency of air, i.e., about 35-60% of stoichiometric, in order to stay within the operating temperature limits. In this type of process, a low-sulfur fuel gas is produced in the first stage and the sulfur is largely trapped as ZnS in the fluo-solids bed. This sulfur is rejected by a separate combustion operation where the trapped sulfur is removed by Reaction (6). The sulfur is liberated as a separate, concentrated SO_2 stream, from which it is relatively easy to recover elementary sulfur.

Acknowledgment

The sponsorship by the U.S. Office of Coal Research of this investigation is gratefully acknowledged.

Literature Cited

(1) Zielke, C. W., Struck, R. T., Evans, J. M., Costanza, C. P., Gorin, E., Ind. Eng. Chem. Process Design Develop. 5, 151 (1966).

(2) Ibid., 158 (1966).

(3) Struck, R. T., Clark, W. E., Dudt, P. J., Rosenhoover, W. A., Zielke, C. W., and Gorin, E., "Kinetics of Hydrocracking of Coal Extract with Molten Zinc Chloride Catalysts in Batch and Continuous Systems." To be presented before the Division of Fuel Chemistry, ACS, Atlantic City, N. J., Sept. 9, 1968.

(4) Obermiller, E. O., and Charlier, G. O., G.C. Method to appear in J. Gas Chrom.

(5) Summary Report I - Consol Synthetic Fuel Development, U. S. Office of Coal Research, Contract 14-01-0001-310, 1968.

(6) Gordon, A. R., J. Chem. Phys., 3, 336 (1935).

(7) Britzke, E. V., Kapustinskii, A. F., Vesselovskii, B. K., Z. Anorg. Allgem. Chem., 213, 65 (1933).

(8) Kitchener, J. A., Ignatowicz, S., Trans. Faraday Soc., 47, 1278 (1951).

TABLE I

Analysis of Melts Used

Composition	"Low" Carbon Natural Spent Melt	"High" Carbon Natural Spent Melt	Synthetic Melt
Wt %			
NH_3	1.56	1.35	1.37
C	5.42	8.76	5.78
org. H	0.25	0.44	--
org. N	0.17	0.16	0.13
org. S	0.05	0.07	0.08
$ZnCl_2$	84.27	80.55	84.77
ZnS	4.32	3.62	4.59
ZnO	0.46	1.37	0.70
H_2O	3.50	3.68	2.58

TABLE II

Results With Low-Carbon Natural Melt at Higher Air/Melt Ratios

Temperature = 1800°F

Run No.	1	2	3	4	5
% of Stoichiometric Air	115	108	90	77	74
Superficial Air Velocity, fps	0.41	0.38	0.42	0.42	1.05
Superficial Residence Time, sec	2.44	2.63	2.39	2.38	0.95
Pressure, psia	15.6	16.9	15.0	15.2	46
Melt Feed Rate, lb/(hr)(ft^2)	28.6	31.0	34.0	54.5	347
Results					
% NH_3 Burned to N_2 + H_2O	98	89	78	67	~ 50
% C Burned to CO + CO_2	95	91	89	86	87
% ZnS Burned to SO_2 + ZnO	100	100	91	28	29
HCl Produced, Wt % Feed Melt	3.3	2.0	2.8	3.5	2.4
Dry Exit Gas, Vol %					
SO_2	1.44	1.43	1.49	0.52	0.55
CO	2.00	2.62	3.57	4.77	5.76
O_2	2.57	2.57	0.23	0.05	0.00
H_2	0.05	0.08	0.06	0.55	1.84
Exit Gas - Heating Value					
Gross Btu/ft^3	6.6	8.7	11.7	17.0	24.5

TABLE III

Results With High-Carbon Natural Spent Melt

Run No.	6	7	8	9
% of Stoichiometric Air	58	59	56	44
Superficial Velocity, fps	0.41	0.42	0.16	0.16
Superficial Residence Time, sec	2.44	2.38	6.25	6.25
Temperature, °F	1800	1900	1800	1800
Pressure, psia	15.3	15.2	15.0	14.8
Melt Feed Rate, lb/(hr)(ft^2)	37.2	36.9	14.1	17.6
Fluo-Solids Used	← Mullite →			
	← 65x100 M →		← 100x150 M →	
Results				
% NH_3 Decomposed	28	70	52	63
% C Burned to CO + CO_2	72	75	84	78
% Inorganic S Burned to SO_2	28	24	0	1.5
HCl Produced, Wt % Feed Melt	2.6	2.9	3.2	2.0
Dry Exit Gas, Vol %				
CO_2	13.2	12.7	9.9	9.2
CO	6.2	6.9	10.8	13.4
H_2	7.8	7.8	7.8	11.7
SO_2	0.38	0.33	0.00	0.03
N_2	72.7	69.4	68.5	63.5
O_2	0.0	0.0	0.0	0.0
HCl	2.7	2.9	3.0	2.2
Dry Exit Gas Gross Heating Value, Btu/ft^3	35	47	60	81

FLUOSOLIDS COMBUSTION UNIT

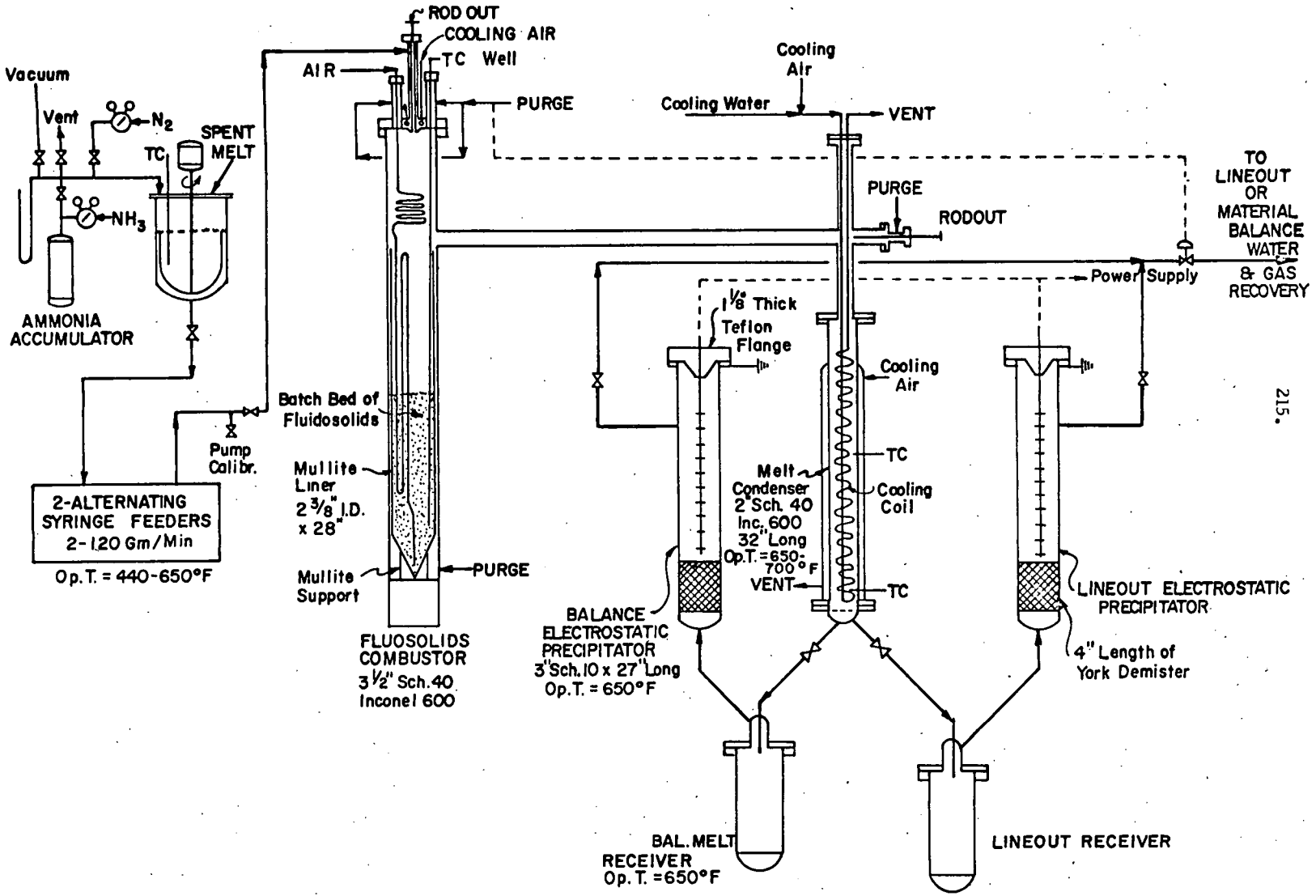

Figure 2

DISTRIBUTION OF CARBON FROM LOW-CARBON MELTS VS PERCENT OF STOICHIOMETRIC AIR

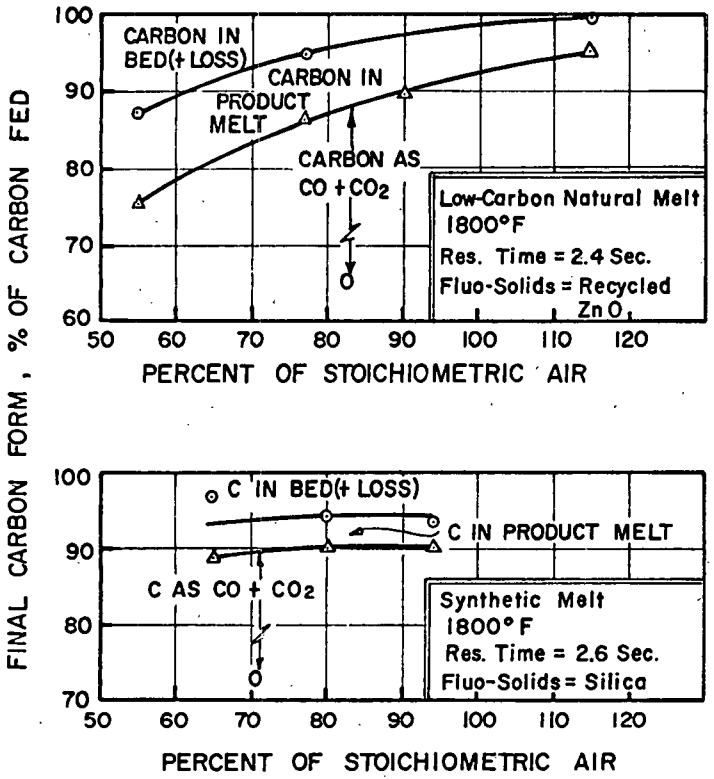

Figure 3

DISTRIBUTION OF CARBON FROM LOW-CARBON NATURAL MELTS VS RESIDENCE TIME

	Bed Height Inches	Press. Atm.	Fluidizing Velocity ft./sec.	% of Stoich. Air	Bed Solids
⊙	12	1.2	2.67	65	Mullite
⊕	12	3.1	1.05	76	
⊸	12	1.1	1.01	76	
⊡	16	1.1	1.01	73	
△	12	1.0	0.42	77	ZnO

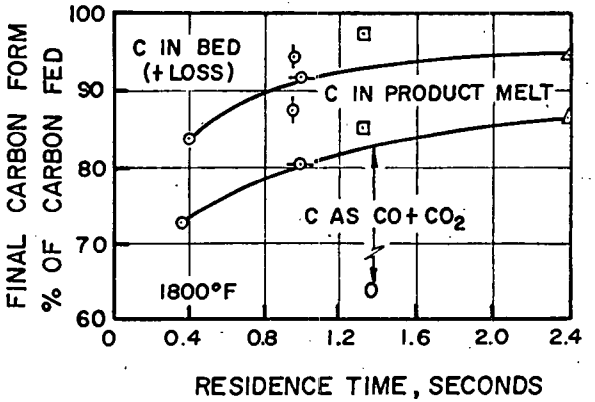

Figure 4

DISTRIBUTION OF SULFUR FROM LOW-CARBON MELTS

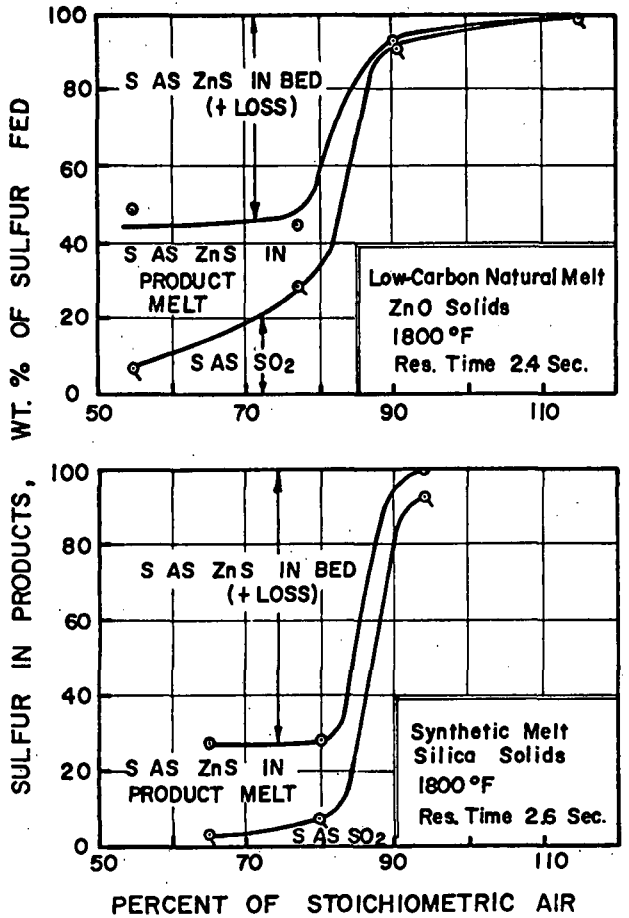

Figure 5

AMMONIA DECOMPOSITION VS PERCENT OF STOICHIOMETRIC AIR

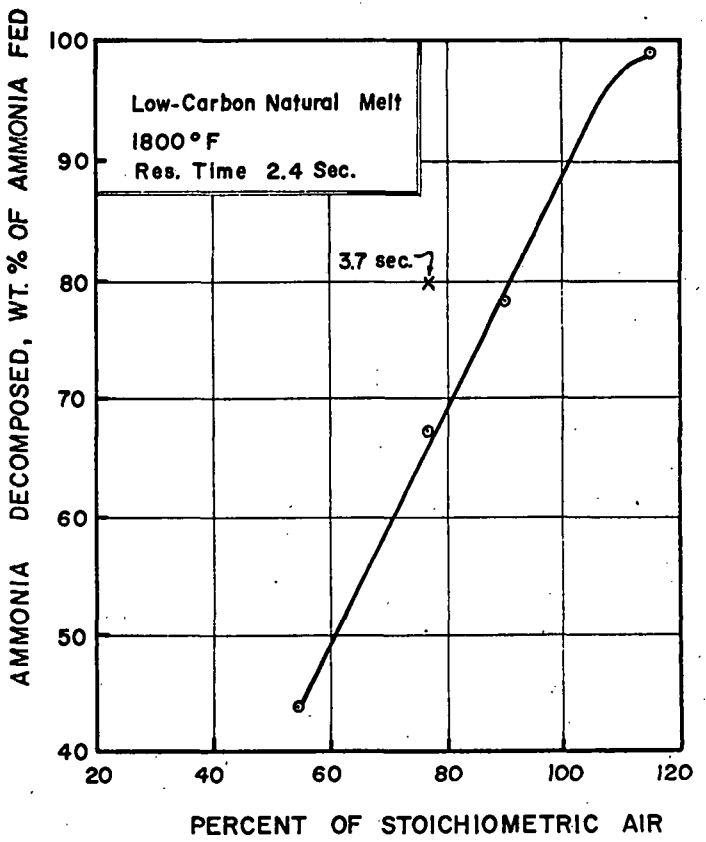

Figure 6

DISTRIBUTION OF CARBON FROM HIGH-CARBON NATURAL MELT

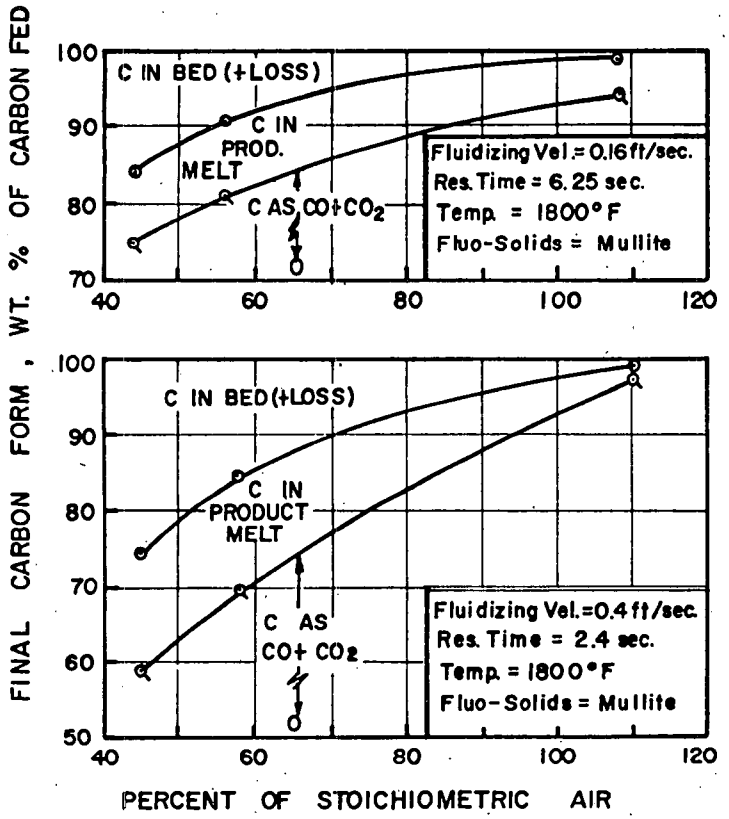

Figure 7

DISTRIBUTION OF SULFUR FROM HIGH-CARBON NATURAL MELT

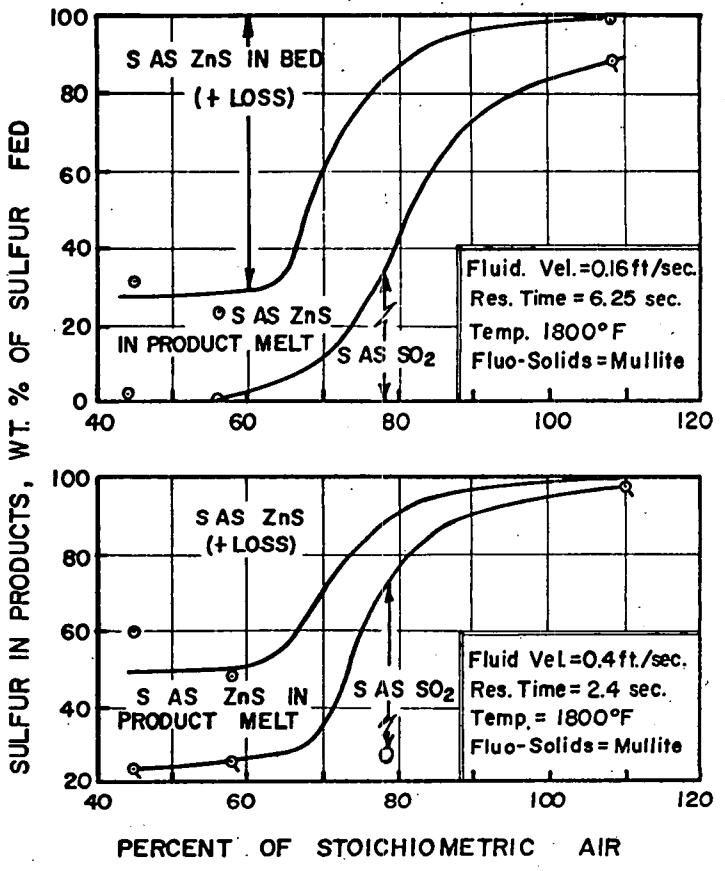

Figure 8

HEATING VALUE OF PRODUCT GAS VS PERCENT OF STOICHIOMETRIC AIR

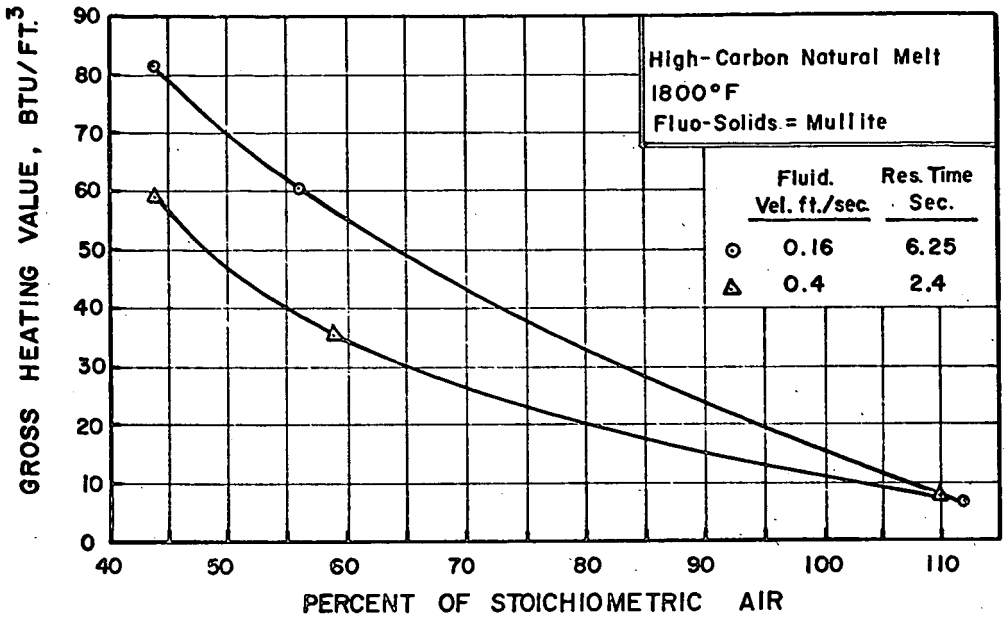

Figure 9

"ADIABATIC" COMBUSTOR TEMPERATURES FOR SEVERAL MELTS

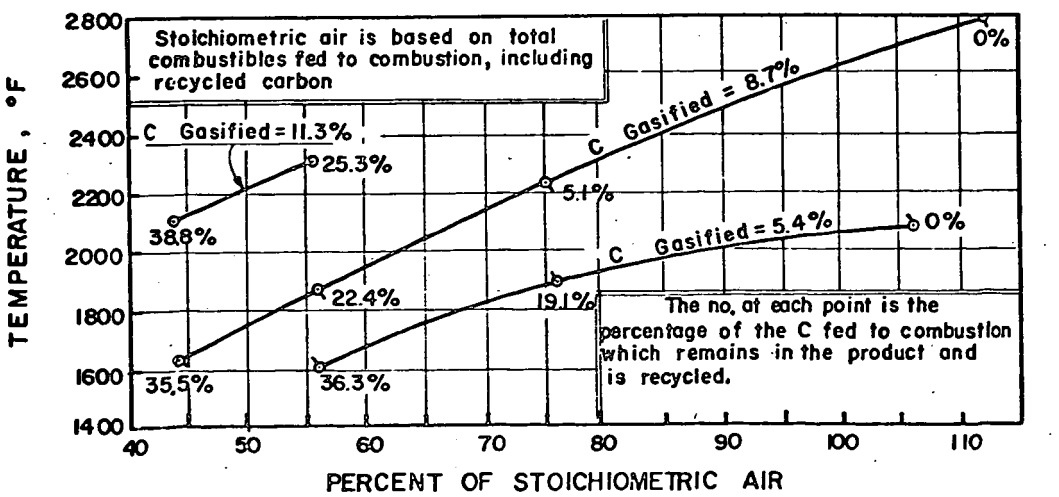

THE HYDROGENATION OF COAL WITH CARBON MONOXIDE AND WATER

Herbert R. Appell and Irving Wender

Pittsburgh Coal Research Center, Bureau of Mines,
U. S. Department of the Interior,
4800 Forbes Avenue, Pittsburgh, Pa. 15213

In 1921 Fischer[1] reported the use of carbon monoxide and water in coal dehydrogenation. The yields of ether-soluble material recovered (13 to 35%) were actually higher than those obtained with hydrogen at the same temperatures and pressures. Other investigators following this lead confirmed the results with coal,[2-4] but did not succeed in hydrogenating asphalt with carbon monoxide and water.[5] Although the early results looked promising, the relatively low conversions, the emphasis on a one step process for converting coal to gasoline, and the impact of the Fischer-Tropsch reaction caused the carbon monoxide plus water approach to coal hydrogenation to be ignored after 1925. This method of hydrogenation has been classified under hydrogenation with nascent hydrogen[6] because of the belief that activated hydrogen was being formed by the water-gas shift reaction.

The hydrogenation of coal with carbon monoxide and water was reinvestigated with the objective of preparing an oil which could then be converted to more volatile fuels by known hydrocracking techniques. Bituminous coal (Bruceton, hvab), a North Dakota lignite, and a Texas lignite, all -100 mesh, were used in this work. The bituminous coal and the North Dakota lignite were ball milled and stored under nitrogen. The Texas lignite powder had been stored in loosely capped cans for two years prior to use. The hydrogenations were conducted in a 500 ml stainless steel rocking autoclave. The extent of reaction was determined by extracting the product with benzene and weighing the dry residue. The percent conversion is 100 less the percent of benzene-insoluble residue (maf basis).

An equal weight of phenanthrene was used as a solvent in the runs with bituminous coal. Most of the work with lignite was conducted with an equal weight of 1:1 α-naphthol-phenanthrene as solvent. For purposes of comparison, several runs were made without a solvent.

RESULTS

The effects of temperature, pressure and time on the conversion of coal to benzene-soluble and volatile materials using carbon monoxide and water are shown in figures 1 to 4. The conversion increases with temperature, in the range investigated, for bituminous coal (figure 1). Conversions of bituminous coal are increased considerably by the phenanthrene solvent. About 10% of the solvent is hydrogenated, mainly to dihydrophenanthrene.

In the case of lignite (figure 2), the amount of conversion goes through a maximum between 375° and 400°C. The decrease in yield above 400°C is believed to be a result of conversion of some of the soluble product to insoluble high molecular weight material. Conversions of lignite are improved by a solvent but the effect is smaller than that observed with bituminous coal. In addition to hydrogenation of the phenanthrene, some of the α-naphthol is converted to naphthalene and tetrahydronaphthalene during the reaction.

The conversions of bituminous coal and lignite increase sharply with pressure up to about 1,000 psig initial pressure (figure 3). Above 1,000 psig the increases in conversion with increases in pressure are smaller.

A striking feature of the solubilization of lignite with carbon monoxide and water is the rapidity of the reaction (figure 4); conversion to benzene-solubles at the optimum conditions seems to be essentially complete in about 10 minutes. After the initial rapid reaction, the small amount of remaining solubilization may be masked by carbonization of some of the soluble product. Mass spectrometric analysis of the benzene soluble product taken at different times indicates that the rapid solubilization reaction is accompanied by a slow cracking reaction which leads to an increase in the lower molecular weight components of the product.

The reaction of lignite with hydrogen is slower. After 10 minutes of reaction, the solubilization is less than half that obtained with carbon monoxide and water. At longer residence times the extent of solubilization approaches, but does not reach, the value obtained with carbon monoxide and water.

The ultimate analysis and physical appearance of the benzene-soluble oil is very similar with either method of hydrogenation. The carbon monoxide and water undergo the water-gas shift reaction so that hydrogen is present during the reaction. At the completion of the lignite runs using carbon monoxide and water, the composition of the gas is usually within the limits: CO, 25-45%; CO_2, 35-50%; H_2, 15-25%; CH_4, 0.6-1.5%; and traces of higher paraffins and olefins.

The increase in hydrogen and the reduction in sulfur and oxygen contents during solubilization is shown in table 1. There is little, if any, reduction in the nitrogen. This run was conducted with more water and a higher carbon monoxide pressure than usual in order to obtain a high conversion without a solvent. The brown-black product was a pourable oil. In testing a number of lignites, the sulfur content of the benzene-soluble product averaged near 0.2%.

TABLE 1. Analysis of lignite and products

(1:1 Lignite-water, 2,000 psig initial CO pressure, 2 hr. 380°C)

	Lignite[1]	Benzene-soluble tar[2]	Residue
C	64.6	84.8	51.4
H	4.8	7.9	3.1
N	1.0	1.0	0.9
S	0.7	0.2	1.1
Ash	7.2	0.5	36.2
O	21.7	5.6	8.2
H/C mole ratio	0.89	1.1	0.7

[1] Burke County, North Dakota, -100 mesh, analysis water-free basis.
[2] Obtained in 87% conversion, maf basis.

Aged lignites were less reactive than freshly ball-milled lignite (table 2). An irreversible change occurs in the lignite on aging in air. The large decrease in reactivity obtained by heating powdered lignite at 105°C and the minor decrease obtained on drying under vacuum suggest that the deactivation is largely a result of oxidation of the lignite. A small increase in the conversion of a deactivated lignite can be obtained by increasing the amount of water used in the reaction. This procedure is generally applicable when a modest increase in the conversion of a low reactivity coal is desired.

TABLE 2. Solubilization of aged lignites (10 minutes at 380°C, 1,500 psig CO pressure)

Aging conditions	Water content,[4] percent	Conversion, percent
Fresh[1]	19	89
4 weeks in air[1]	13	77
105°C, 24 hr.,[1] in air	< 1	54
100°C, 0.5 hr., vacuum[1]	< 1	86
2 years in storage[2]	6	77
2 years in storage[2,3]	6	83

[1] North Dakota lignite.
[2] Texas lignite.
[3] 1:1 = water:lignite used in place of the standard 0.5:1 = water:lignite ratio.
[4] Determined in a stream of N_2 at 110°C. for 1 hour.

BIBLIOGRAPHY

1. F. Fischer and Hans Schrader, Brennstoff-Chem. 2 257 (1921).
2. H. I. Waterman and F. Kortland, Rec. trav. Chim. 43 258 (1924).
3. H. I. Waterman and F. Kortland, Rec. trav. Chim. 43 691 (1924).
4. H. I. Waterman and J. N. J. Perquin, Proc. Acad. Sci. Amsterdam, 27 132 (1924); C.A. 18 1903 (1924).
5. H. I. Waterman and F. Kortland, Rec. trav. Chim. 43 249 (1924).
6. W. Krönig "Die katalytische Druckhydriering von Kohlen Teern und Mineralölen." Springer-Verlag. Berlin 1950.

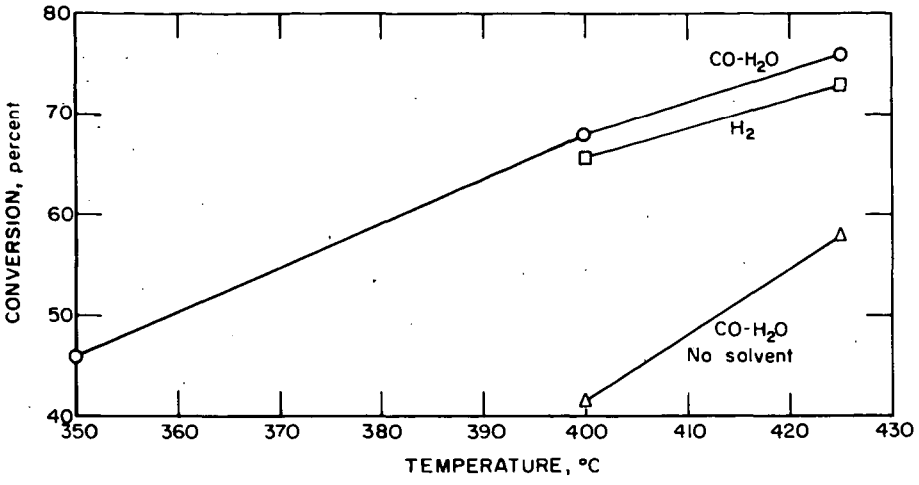

Figure 1.—Effect of temperature on bituminous coal conversion (2 hrs, 2,000 psig initial pressure, 1:1:0.5 = coal : phenanthrene : water).

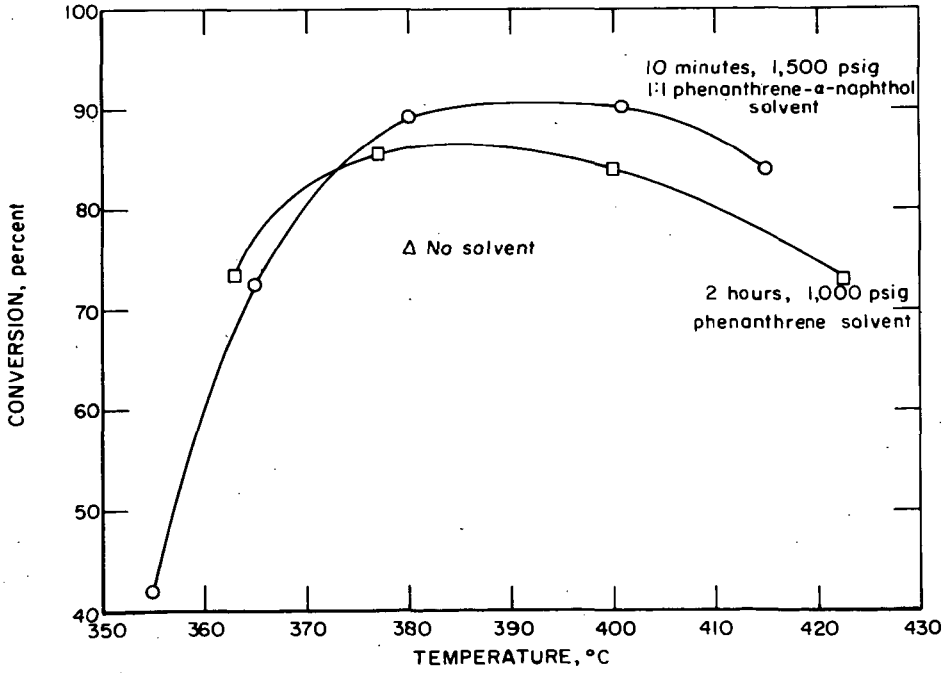

Figure 2.— Effect of temperature on lignite conversion (1:1:0.5 = coal : solvent : water).

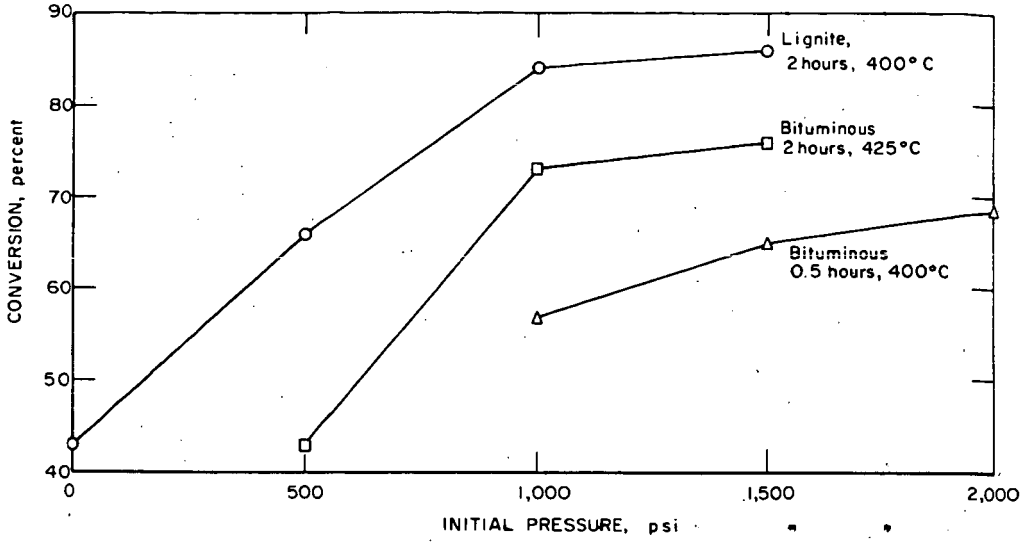

Figure 3.—Effect of pressure on coal conversion (1:1:0.5 = coal : phenanthrene : water)

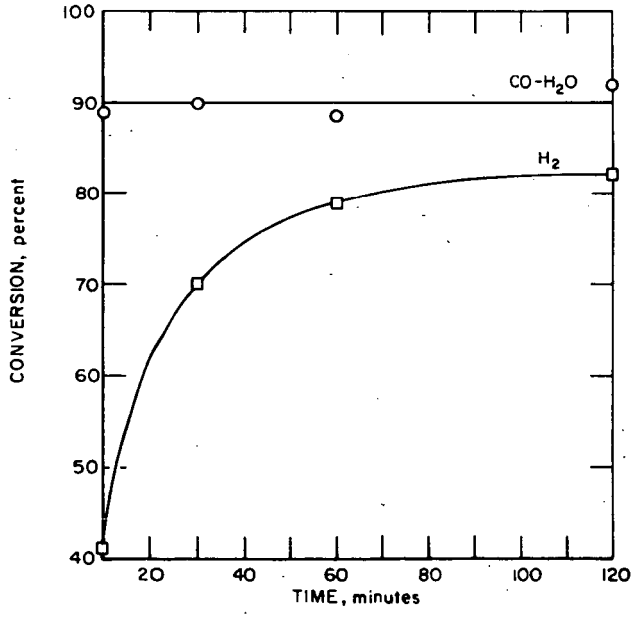

Figure 4—Effect of time on lignite conversion (1,500 psig initial pressure, 380° C).